

GEMS & GEMOLOGY

SUMMER 2020
VOLUME LVI

THE QUARTERLY JOURNAL OF THE GEMOLOGICAL INSTITUTE OF AMERICA



Naturally Colored Yellow and Orange Diamonds
New Technique for Separating Natural from
Laboratory-Grown Diamond
History of the Chivor Emerald Mine, Part II
Optical Whitening and Brightening of Pearls



p. 195



p. 255



p. 261



p. 269



p. 293



p. 312

EDITORIAL

193 Yellow and Orange Diamonds, New Identification Techniques, and the Chronicles of Chivor

Duncan Pay

FEATURE ARTICLES

194 Naturally Colored Yellow and Orange Gem Diamonds: The Nitrogen Factor

Christopher M. Breeding, Sally Eaton-Magaña, and James E. Shigley

Presents the four major groups of defects responsible for the color in nearly all yellow and orange diamonds.

220 Separation of Natural from Laboratory-Grown Diamond Using Time-Gated Luminescence Imaging

Colin D. McGuinness, Amber M. Wassell, Peter M.P. Lanigan, and Stephen A. Lynch

Researchers from De Beers Group Technology present a technique that expands on the surface luminescence used in the DiamondView instrument to provide additional imaging information and quickly distinguish colorless or near-colorless natural diamond from laboratory-grown diamond.

230 History of the Chivor Emerald Mine, Part II (1924–1970): Between Insolvency and Viability

Karl Schmetzer, Gérard Martayan, and Andrea R. Blake

Chronicles developments at the Chivor emerald mine in Colombia between 1924 and 1970, based on archival records.

258 Optical Whitening and Brightening of Pearls: A Fluorescence Spectroscopy Study

Chunhui Zhou, Tsung-Han Tsai, Nicholas Sturman, Nanthaporn Nilpetploy, Areeya Manustrong, and Kwanreun Lawanwong

Presents a study that suggests optically brightened pearls can be consistently separated from non-brightened pearls using fluorescence spectroscopy.

266 Hydrogen and Oxygen Stable Isotope Ratios of Dolomite-Related Nephrite: Relevance for Its Geographic Origin and Geological Significance

Kong Gao, Ting Fang, Taijin Lu, Yan Lan, Yong Zhang, Yuanyuan Wang, and Yayun Chang

Examines the effectiveness of hydrogen and oxygen isotopes in discriminating dolomite-related nephrites from the four most important occurrences worldwide.

REGULAR FEATURES

281 Lab Notes

Cat's-eye andradite • Quench-crackled dyed blue chalcedony resembling Larimar • Irradiated blue diamond with interesting DiamondView image • Multiple radiation stains suggest interesting geological residency • Hemimorphite resembling Paraíba tourmaline • Exceptional purple Montana sapphire • Negative crystal containing a mobile CO₂ bubble in blue sapphire heated with pressure • Pink Mozambique sapphire • HPHT-processed CVD lab-grown diamonds with low color grades • HPHT lab-grown pink diamond with unstable color

292 G&G Micro-World

Böhmite in corundum • Chabazite in Ethiopian opal • Fluorophlogopite in Burmese spinel • Unusually shaped rutile crystal inclusions in Russian emerald • Sapphire with negative crystal containing mobile graphite daughter crystal • Windmills in rare mineral sphalerite • Trapiche-like pattern in emerald from Pakistan • Quarterly Crystal: Pyrite in quartz

298 Gem News International

Purplish pink diasporite reportedly from Afghanistan • Fossil ivory update with Lee Downey • The "Fragility of the Eternal" kunzite: Origin, cutting, and identification • Petrified woods in the Russian Far East: Gemology and origin • Portrait of a Paraíba rough • "Rhodotrolite," a new gem material from Indonesia • Field trip to Crater of Diamonds, USA • Greenish blue glass imitating gem silica • Marble imitation of jadeite rough

Editorial Staff

Editor-in-Chief

Duncan Pay

Managing Editor

Stuart D. Overlin
soverlin@gia.edu

Associate Editor

Brooke Goedert

Technical Editors

Tao Z. Hsu
tao.hsu@gia.edu
Jennifer Stone-Sundberg
jstone@gia.edu

Editors, Lab Notes

Thomas M. Moses
Shane F. McClure

Editors, Micro-World

Nathan Renfro
Elise A. Skalwold
John I. Koivula

Editors, Gem News

Emmanuel Fritsch
Gagan Choudhary
Christopher M. Breeding

Assistant Editor

Erin Hogarth

Contributing Editors

James E. Shigley
Raquel Alonso-Perez
Donna Beaton

Editor-in-Chief Emeritus

Alice S. Keller

Customer Service

Martha Erickson
(760) 603-4502
gandg@gia.edu

Production Staff

Creative Director

Faizah Bhatti

Production and Multimedia Specialist

Juan Zanahuria

Photographer

Robert Weldon

Photo/Video Producer

Kevin Schumacher

Illustrator

Russel Samson

Multimedia Associate

Christopher Bonine

Video Production

Larry Lavitt
Pedro Padua
Albert Salvato

Editorial Review Board

Ahmadjan Abduriyim

Tokyo, Japan

Timothy Adams

San Diego, California

Edward W. Boehm

Chattanooga, Tennessee

James E. Butler

Washington, DC

Alan T. Collins

London, UK

Sally Eaton-Magaña

Carlsbad, California

John L. Emmett

Brush Prairie, Washington

Emmanuel Fritsch

Nantes, France

Eloïse Gaillou

Paris, France

Al Gilbertson

Carlsbad, California

Gaston Giuliani

Nancy, France

Lee A. Groat

Vancouver, Canada

Yunbin Guan

Pasadena, California

Richard W. Hughes

Bangkok, Thailand

Jaroslav Hyršl

Prague, Czech Republic

Dorrit Jacob

Sydney, Australia

A.J.A. (Bram) Janse

Perth, Australia

Mary L. Johnson

San Diego, California

Stefanos Karamelas

Basel, Switzerland

Lore Kiefert

Lucerne, Switzerland

Ren Lu

Wuhan, China

Thomas M. Moses

New York, New York

Aaron Palke

Carlsbad, California

Ilene Reinitz

Chicago, Illinois

Nathan Renfro

Carlsbad, California

Benjamin Rondeau

Nantes, France

George R. Rossman

Pasadena, California

Andy Shen

Wuhan, China

Guanghai Shi

Beijing, China

James E. Shigley

Carlsbad, California

Elisabeth Strack

Hamburg, Germany

Nicholas Sturman

Bangkok, Thailand

Fanus Viljoen

Johannesburg,
South Africa

Wuyi Wang

New York, New York

Christopher M. Welbourn

Reading, UK

Chunhui Zhou

New York, New York

J.C. (Hanco) Zwaan

Leiden, The Netherlands

Subscriptions

Copies of the current issue may be purchased for \$29.95 plus shipping. Subscriptions are \$79.99 for one year (4 issues) in the U.S. and \$99.99 elsewhere. Canadian subscribers should add GST. Discounts are available for renewals, group subscriptions, GIA alumni, and current GIA students. To purchase print subscriptions, visit store.gia.edu or contact Customer Service. For institutional rates, contact Customer Service.

Database Coverage

Gems & Gemology's impact factor is 1.844, according to the 2017 Thomson Reuters Journal Citation Reports (issued July 2018). *G&G* is abstracted in Thomson Reuters products (Current Contents: Physical, Chemical & Earth Sciences and Science Citation Index—Expanded, including the Web of Knowledge) and other databases. For a complete list of sources abstracting *G&G*, go to gia.edu/gems-gemology, and click on "Publication Information."

Manuscript Submissions

Gems & Gemology, a peer-reviewed journal, welcomes the submission of articles on all aspects of the field. Please see the Author Guidelines at gia.edu/gems-gemology or contact the Managing Editor. Letters on articles published in *G&G* are also welcome. Please note that Field Reports, Lab Notes, Gem News International, Micro-World, Diamonds from the Deep, and Charts are not peer-reviewed sections but do undergo technical and editorial review.

Copyright and Reprint Permission

Abstracting is permitted with credit to the source. Libraries are permitted to photocopy beyond the limits of U.S. copyright law for private use of patrons. Instructors are permitted to reproduce isolated articles and photographs/images owned by *G&G* for noncommercial classroom use without fee. Use of photographs/images under copyright by external parties is prohibited without the express permission of the photographer or owner of the image, as listed in the credits. For other copying, reprint, or republication permission, please contact the Managing Editor.

Gems & Gemology is published quarterly by the Gemological Institute of America, a nonprofit educational organization for the gem and jewelry industry.

Postmaster: Return undeliverable copies of *Gems & Gemology* to GIA, The Robert Mouawad Campus, 5345 Armada Drive, Carlsbad, CA 92008.

Our Canadian goods and service registration number is 126142892RT.

Any opinions expressed in signed articles are understood to be opinions of the authors and not of the publisher.

About the Cover

Naturally yellow and orange diamonds, both of which are colored by nitrogen defects, are the subject of the lead article in this issue. Orange diamonds are a rarity of nature, ranging from subtle hues to vivid intensities of color. The rectangular diamond shown on the cover has a Fancy Vivid orange color and weighs 1.32 ct. The oval is a Fancy pinkish orange, internally flawless diamond weighing 2.48 ct. Photo by Robert Weldon/GIA; courtesy of Christian Tse.

Printing is by L+L Printers, Carlsbad, CA.

GIA World Headquarters The Robert Mouawad Campus 5345 Armada Drive Carlsbad, CA 92008 USA

© 2020 Gemological Institute of America

All rights reserved.

ISSN 0016-626X



Yellow and Orange Diamonds, New Identification Techniques, and the Chronicles of Chivor



Welcome to the Summer *Gems & Gemology*! This issue is packed with informative contents, including the characteristics of yellow and orange diamonds, new gem identification techniques, and the colorful history of the Chivor emerald mine.

In the world of fancy-color diamonds, yellow diamonds are by far the most common while those with an unmodified orange hue are among the very rarest (kudos to Robert Weldon for capturing them on the cover). Both yellow and orange diamonds owe their color to nitrogen-related defects. In the lead article, a GIA team led by Christopher M. Breeding and Sally Eaton-Magaña presents the last in their series

“In the world of fancy-color diamonds, yellow diamonds are by far the most common while those with an unmodified orange hue are among the very rarest.”

documenting the gemological and spectroscopic properties of fancy-color diamonds.

Next, Colin McGuinness and colleagues present a luminescence imaging technique developed by De Beers Group Technology that can quickly and easily distinguish colorless and near-colorless natural diamond from laboratory-grown diamond. One marker can identify more than 99% of natural type Ia and type IIa diamond. A pair of newly developed instruments expand on the technology of the DiamondView instrument introduced by De Beers a quarter of a century ago.

In the third article, Karl Schmetzer and coauthors conclude a sweeping two-part series chronicling the Chivor emerald mine in Colombia. This article examines events from 1924 to 1970, when the mine was principally owned by an American firm. While the early era was marked by stock market speculation and scandal, there were also highly productive periods at the fabled mine.

Optical brightening agents for pearls, which are separate from bleaching and *maeshori* treatments, are the topic of the fourth article. A team of GIA researchers led by Chunhui Zhou provides a fluorescence spectroscopy technique for confidently separating optically brightened pearls from non-brightened pearls.

In the final article, a team of researchers led by Kong Gao of NGTC in China provide a means of discriminating the geographic origin of dolomite-related nephrite from the four most important sources worldwide. This determination relies on hydrogen and oxygen stable isotope ratios. Isotope analysis is an emerging method in gemological research.

As always, our regular columns offer an illuminating array of insights. Highlights of the *Lab Notes* section include an exceptional purple sapphire from Montana, a vivid blue hemimorphite cabochon resembling Paraíba tourmaline, and interesting observations on an irradiated blue diamond and a rough diamond crystal with irradiation staining. *Micro-World* reveals rare and breathtaking observations from the inner landscapes of gemstones, including what is believed to be the first reported inclusion of fluorophlogopite in spinel (or any other gem material). In *Gem News International*, you'll find a characterization of purplish pink diasporite reportedly from a new deposit in Afghanistan, a look at the cutting and identification of the world's largest faceted kunzite, a study of petrified woods from the Russian Far East, and much more.

On a final note, the *G&G* Facebook group (www.facebook.com/groups/giagemsgemology) is now more than 10,000 members strong. We thank you for your participation and your continued interest in the journal.

Duncan Pay | Editor-in-Chief | dpay@gia.edu

NATURALLY COLORED YELLOW AND ORANGE GEM DIAMONDS: THE NITROGEN FACTOR

Christopher M. Breeding, Sally Eaton-Magaña, and James E. Shigley

Natural yellow gem diamonds are the most common of the fancy-color diamonds, while orange diamonds are among the rarest when they have unmodified hues. Both categories owe their coloration to atomic-level lattice defects associated with nitrogen impurities in the diamond structure. Four major groups of defects are responsible for the color in nearly all yellow and orange diamonds: cape defects (N3 and associated absorptions), isolated nitrogen defects, the 480 nm visible absorption band, and H3 defects. Nitrogen-bearing diamonds are thought to incorporate isolated nitrogen during growth by substitution for carbon, meaning that natural diamonds start out with yellow to orange color. However, only the very rare type Ib diamonds maintain that original color. With time at high temperatures deep in the earth, the nitrogen atoms in most diamonds aggregate, resulting in either near-colorless stones or yellow diamonds colored by cape defects. Yellow and orange diamonds can be grown in a laboratory or created by color treatments, so a thorough understanding of the defects responsible for color in the natural stones is critical for identification. Yellow diamonds serve as the best ambassador to the colored diamond world due to their abundance and may be the only colored diamond many people will ever see in a jewelry store.

Among fancy-color diamonds, those with saturated blue, green, and red colors are the rarest and generally the most highly valued. Over the last decade, however, diamonds with pure hues in these colors have made up less than one-tenth of one percent of all diamonds examined at GIA, making them virtually unattainable in the marketplace. In recent issues of *Gems & Gemology*, we have documented the gemological and spectroscopic properties of the rarest of fancy-color diamonds ranging from pink-to-red, blue, and green to the more unusual white and black. This article will address the most common colored diamonds, those with yellow hues, while also examining their much rarer orange cousins (figure 1). This is the last of the fancy color groups in this series, and a brief summary of all the colored diamond groups is provided at the end of the article.

Yellow and orange diamonds owe their color primarily to nitrogen impurities that are incorporated

in the diamond lattice during growth deep in the earth. Nitrogen is the most common impurity in natural diamond due to the very similar atomic radii of nitrogen and carbon atoms (155 and 170 picometer Van der Waals radii, respectively) as well as the relative abundance of nitrogen in the growth environ-

In Brief

- Among natural-color diamonds, those with a yellow hue are the most common.
- Diamonds with unmodified orange hues are among the rarest of colored diamonds.
- Yellow and orange diamonds owe their color primarily to nitrogen impurities.
- Identification of treatment in yellow and orange diamonds requires careful evaluation of the defects responsible for the color.

ment. If nitrogen is present when diamond grows, it will inevitably be incorporated. Nitrogen is the sixth most abundant element in the universe and accounts for more than 75% of the earth's atmosphere (Bebout

See end of article for About the Authors and Acknowledgments.

GEMS & GEMOLOGY, Vol. 56, No. 2, pp. 194–219,

<http://dx.doi.org/10.5741/GEMS.56.2.194>

© 2020 Gemological Institute of America



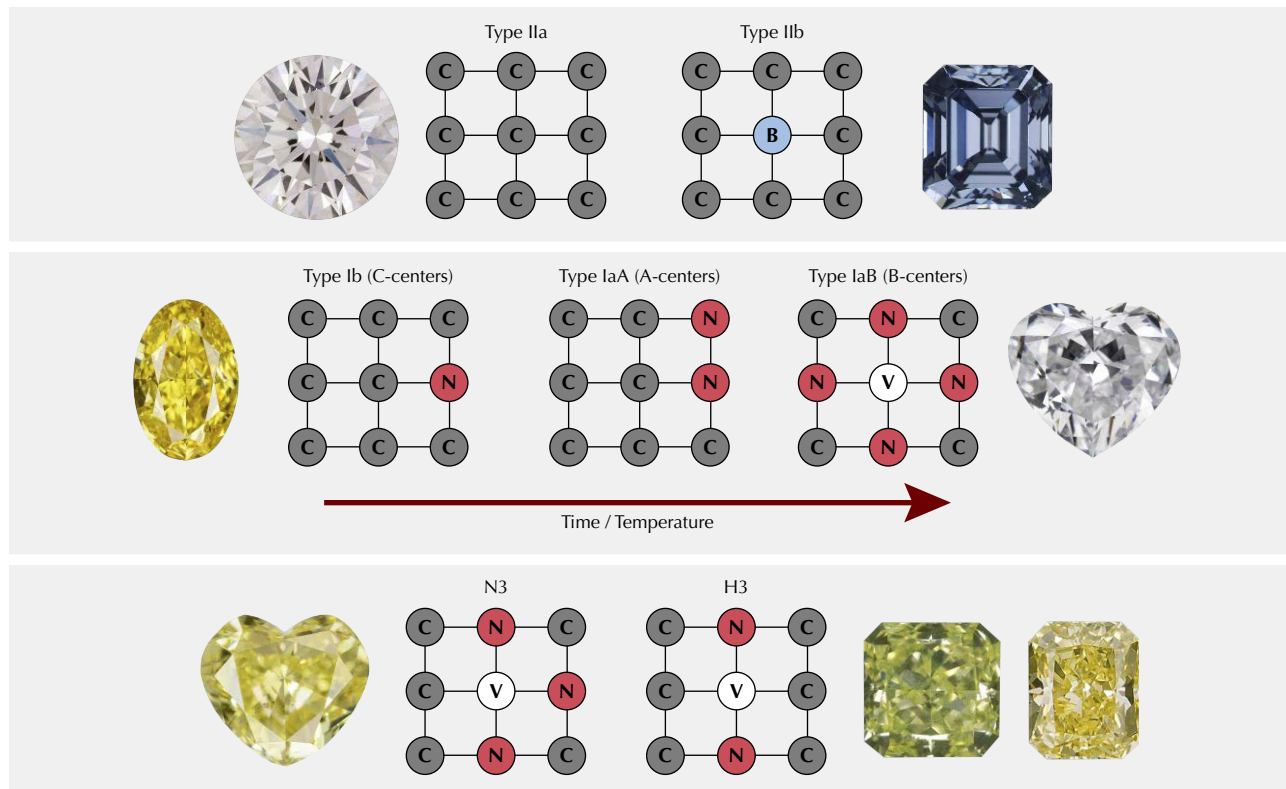
Figure 1. Yellow is the most common of the fancy-color diamonds, and its close relative orange is among the rarest. Photos by GIA staff.

et al., 2013). While the amount of nitrogen in the earth's mantle is significantly lower than that, about

98% of natural gem diamonds recovered (both colorless and fancy-color) are type Ia, meaning they contain FTIR-measurable concentrations of nitrogen impurities, thus proving that nitrogen is present in most diamond growth environments.

Nitrogen can exist as single isolated atoms substituting for carbon (i.e., C-centers, single substitutional nitrogen, or type Ib), aggregated groupings of atoms in pairs or fours (i.e., A-centers or type IaA, and B-centers or type IaB), or as more complex defects (e.g., N₃, H₂, H₃, H₄, and NV) (figure 2; see Collins, 1997, 1999, 2001 and Breeding and Shigley, 2009 for more information). Some of these nitrogen defects cause diamond to absorb light in the visible range to cause color (C-centers, N₃, H₃, and NV) while others produce no color at all in diamond but exhibit characteristic infrared absorptions (A- and B-centers). Simply having nitrogen present in the diamond lattice is not enough to produce a beautiful and rare fancy-color yellow or orange diamond. The nitrogen must exist in high enough concentrations and be configured in a way that selectively absorbs light toward the blue end of the visible spectrum substantially enough to pro-

Figure 2. Atomic lattice defects cause different colors in diamond. Their configuration makes a significant difference in the color. Photos by GIA staff.



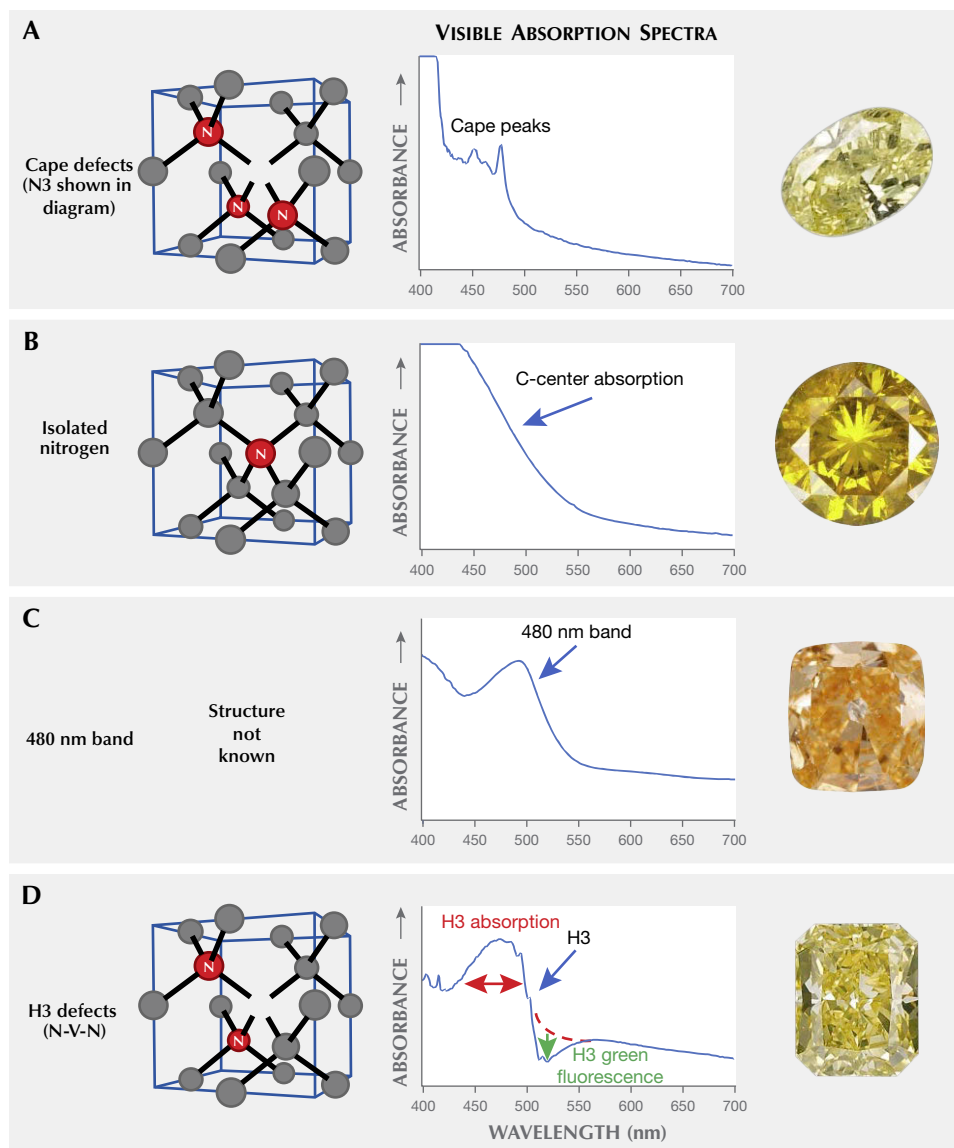


Figure 3. Yellow and orange diamonds are colored by four main mechanisms: cape defects, isolated nitrogen, the 480 nm band, and H3 defects. Photos by GIA staff.

duce yellow or orange color. However, the defects that are responsible for yellow and orange color are not always the same. Most natural yellow gem diamonds are colored by either the N3 defect and its associated absorptions (collectively termed “cape” diamonds by gemologists), or by C-centers (figure 3, A and B). Other color centers such as the 480 nm visible absorption band, H3, and H-related defects occasionally contribute to the color components in yellow diamonds as well (figure 3, C and D). Fancy orange diamonds, however, are nearly always colored by the 480 nm visible absorption band or by C-centers (figure 3, C and B). Orange color is also created occasionally as a primary hue in diamonds colored by the H3 defect in combination with a 550 nm visible absorption band or by nitrogen-vacancy defects.

During the last decade, GIA has examined several hundred thousand naturally colored diamonds with yellow or orange hue components, more than two-thirds of which had pure, unmodified yellow hues. In stark contrast to yellow diamonds, which are by far the most common fancy color, less than one-tenth of a percent of the stones examined over the same period had pure, unmodified orange hues. To our knowledge, data from such a quantity of yellow and orange diamonds has never before been compiled in a publication. As with the previous articles in this series (Breeding et al., 2018; Eaton-Magaña et al., 2018a, 2018b, 2019), our goal is to provide a detailed account of the gemological and spectroscopic characteristics of natural yellow and orange diamonds colored by different nitrogen-related defects.

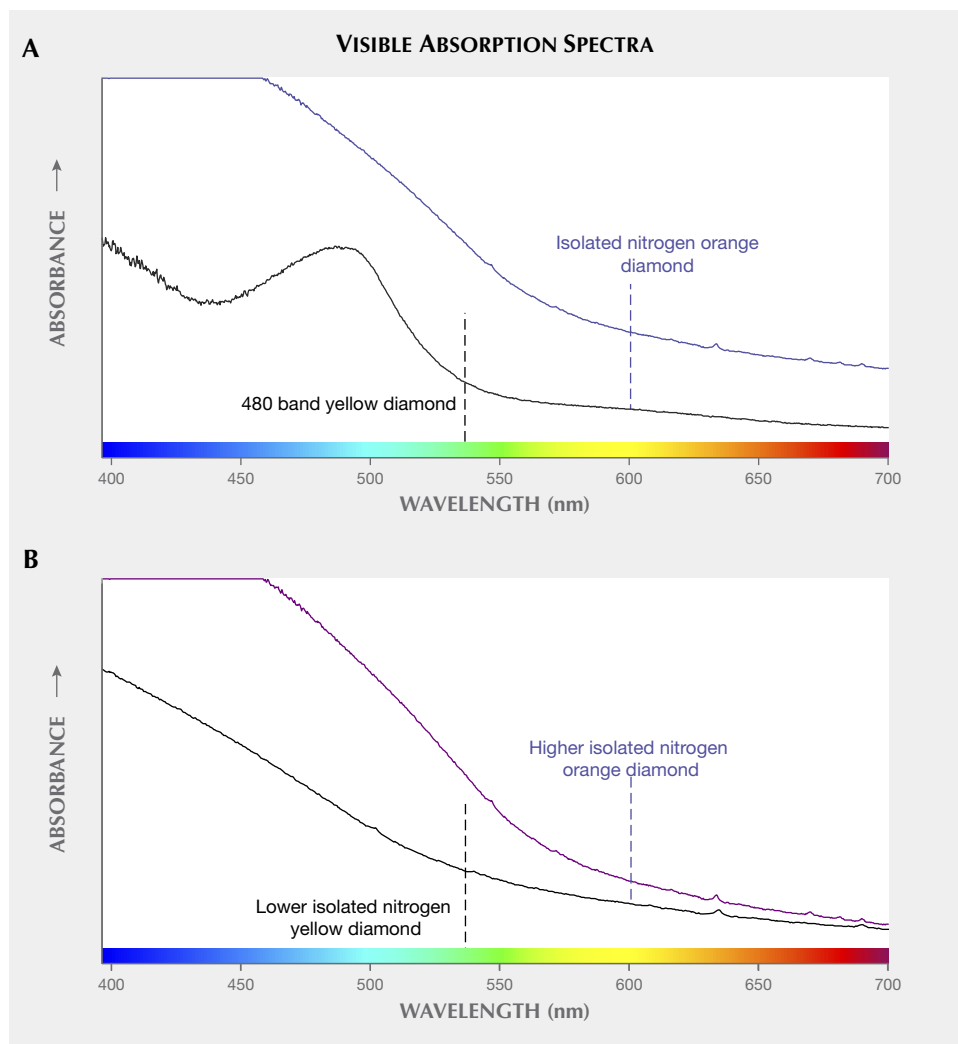


Figure 4. Each particular defect absorption determines the diamond color. A: If the absorption extends to ~600 nm, an orange color is seen; otherwise, most nitrogen color centers produce yellow color. B: Different concentrations of the same defect can generate yellow or orange color.

For the spectroscopic and abundance evaluations, we used a random, representative sampling of 500 diamonds, including both yellow and orange stones. For spectra collection details, please see table S-1 in Breeding et al. (2018). This article is not intended to be a comprehensive review of nitrogen in gem diamond. Instead, it is aimed at helping those in the diamond trade to better understand these beautiful, more common, fancy yellow-colored gems that are far more likely to cross their desks than many of the ultra-rare colored diamonds represented in the previous articles in this series.

CAUSE OF COLOR

Yellow and orange diamonds are closely linked by their dependence on nitrogen-related defects to produce their colors. In fact, the main difference between the two colors is a slight shift in the transmission window in the visible spectrum. Both orange and yellow

bodycolors in diamond are produced by a combination of all transmitted visible light above a certain wavelength. Yellow color is seen when most of the nitrogen-related absorptions occur primarily in the blue part of the visible spectrum at wavelengths less than ~510 nm, whereas orange color is seen when the absorptions extend to ~600 nm (figure 4A). Different defects absorb slightly different energy parts of the visible spectrum, meaning that the main defects responsible for yellow color are somewhat different than those for orange color. Of course, the concentration of each defect can range from low to high, and thus the absorption band can shift in wavelength location (figure 4B), and other defects due to plastic deformation may impact the color as well (Hainschwang et al., 2013). This means that the color produced depends not only on the defects present but also their abundance. For example, low concentrations of nitrogen defects can produce pale yellow color, but higher con-

TABLE 1. Mechanisms of yellow and orange color in diamond.

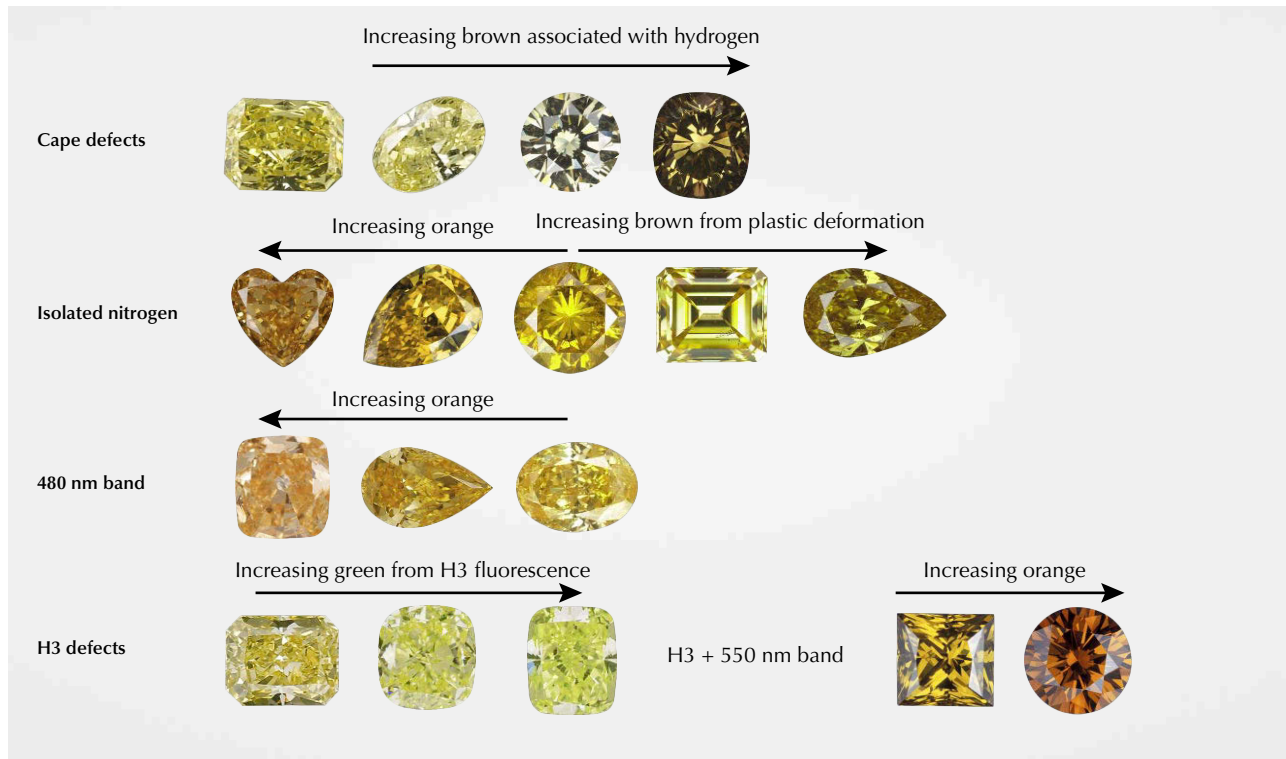
Cause of color	Defect(s) responsible	Most common colors	Geological formation	Key gemological observations
Cape defects	N3, N2 (478 nm), 451 nm, 463 nm	Yellow, brownish yellow	Aggregation of N over time in mantle	Strong blue fluorescence; cape lines in spectroscope
Isolated nitrogen	C-centers	Yellow, orangy yellow, orange	Incorporated at growth	Oriented needle inclusions
480 nm band	480 nm visible absorption band	Yellowish orange, orange, yellow	Unknown	Platy inclusions; yellow or orange fluorescence
H3 defects	H3, 550 nm absorption band	Yellow, greenish yellow, brownish orange	Heating in mantle (H3); plastic deformation (550 nm)	Localized or dispersed green fluorescence with focused lighting; brown graining

centrations can increase the overall absorption and thus increase the amount of yellow color and occasionally shift the transmission window into the orange region (figure 4B). Here we discuss the color centers in order of abundance for fancy yellow diamonds. The order of importance for orange diamonds is slightly different and noted in each section below. Table 1 provides a summary of each of the major groups.

“Cape” Defects. The majority of fancy yellow diamonds seen at GIA over the last decade (~74%) are colored primarily by a combination of absorptions from the N3 defect (three nitrogen atoms adjacent to

a vacancy; ZPL [zero phonon line] = 415 nm) and its associated absorptions at 451, 463, and 478 nm (N2 defect; Davies, 1981) (figure 3A). These absorption features are associated with “cape” diamonds because they can be seen as a pattern of sharp absorption lines when the diamonds are viewed with a gemological spectroscope. The term “cape” was originally used to refer to pale to deeply colored yellow stones derived from the former Cape Province in South Africa, which was well known for its yellow diamonds (Bruton, 1971; Liddicoat, 1993; King et al., 2005). The term now refers to diamonds from any location with color saturations typically in the light yellow range that are colored by the N3-related ab-

Figure 5. Each of the four groups of color mechanisms for yellow and orange diamonds shows a slightly different range in hues. Photos by GIA staff.



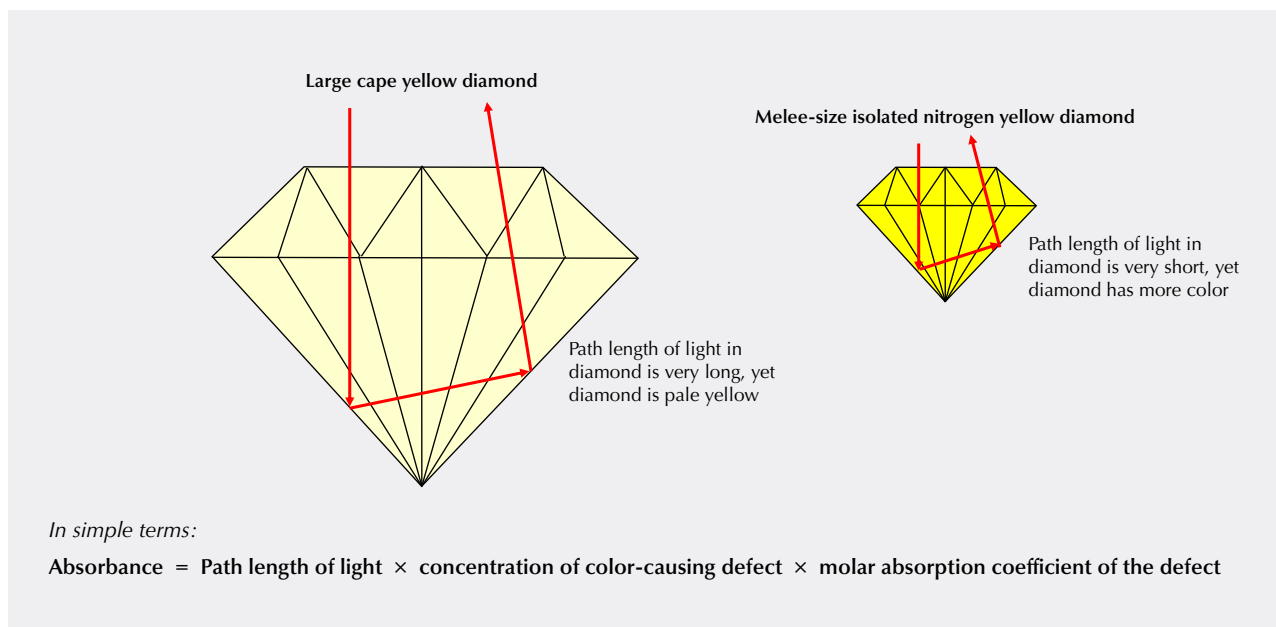


Figure 6. The color of a diamond is controlled by the light that is absorbed and transmitted. Absorbance is a product of the path length of light, the concentration of defects, and the absorption properties of the defects. C-centers are much more efficient absorbers than cape defects, and thus most small yellow diamonds are colored by C-centers.

sorptions listed above (figure 5). We will collectively refer to these N3-related absorptions as cape defects in this article. The cape defects are also responsible for the slight amount of color in most diamonds in the D-to-Z range of the GIA color grading scale (some D-to-Z diamonds have brownish tints from plastic deformation instead of nitrogen impurities; King et al., 1994, 2005, 2008). Cape defects are largely assumed to be relatively weak light absorbers, meaning that it takes high concentrations of the defects (or longer path lengths of light travel, as with larger faceted diamonds) to produce a saturated yellow color (figure 6). For G-color and N-color diamonds of the same size and cut, for example, the N color will have significantly more cape defects. Similarly, a fancy yellow cape diamond of the same size and cut will have a higher concentration of the defects. Orange color is usually not produced by cape defects.

In about 15% of the yellow diamonds colored by cape defects, we observed significant absorption contributions from hydrogen-related defects (see Breeding et al., 2018, for details on H-related defects). Often the yellow diamonds with substantial hydrogen showed brown or green color components from the combination of absorptions from nitrogen and hydrogen-related impurities (figure 5).

Isolated Nitrogen. Single isolated atoms of nitrogen substituting for carbon in the diamond lattice (figures

2 and 3B; C-centers) are the second most common cause of color in natural yellow diamonds, comprising just over 13% of the stones evaluated. C-centers are very strong absorbers, requiring concentrations of only a few parts per million (ppm) of isolated nitrogen atoms to produce strong yellow color (Collins, 1982, 2001; Hainschwang et al., 2013) (figure 6). These diamonds are often referred to as “true canaries” in the industry and are popular in the diamond trade (Liddicoat, 1976; Collins, 1980; Wang and Poon, 2018). While the yellow diamonds analyzed for this study were primarily larger than melee sizes, it should be mentioned that nearly all melee-sized natural diamonds (<0.20 ct) with Fancy yellow or more intense color grades are colored by C-centers due to their very strong light absorption. The short absorption path length in a melee stone requires that C-centers be present to produce yellow color, as cape defects are significantly weaker absorbers and cannot produce much yellow color over very short path lengths (again, see figure 6). C-centers are rare in natural diamond, as they are typically destroyed by combining with other C-centers to form pairs of nitrogen atoms (A-centers) during the normal nitrogen aggregation process that occurs over geologic time during residence deep in the earth (figure 2; Anderson, 1961; Davies, 1970). While C-centers produce strong yellow color in diamond, A-centers produce no color at all. Higher concentrations of C-centers can produce deeper yellow colors (though



Figure 7. When gently heated, diamonds colored by a 480 nm band will temporarily change color to a more orangy hue. Photos by Wuyi Wang.

not always) and orangy components to the diamond hue as well (figure 5). C-centers, in conjunction with plastic deformation (Hainschwang et al., 2013), are the most common cause of primary orange color components in diamond.

480 nm Visible Absorption Band. One of the more interesting mechanisms for producing yellow color in diamond is a broad absorption band centered at ~480 nm in the visible spectrum (figure 3C). The makeup and structure of the 480 nm band is not well understood by scientists. Our observations indicate that it is almost always associated with both A-centers (nitrogen pairs) and very low concentrations of C-centers. The defect has been attributed by some authors to substitutional oxygen atoms in the diamond lattice based primarily on modeling results (Gali et al., 2001; Shiryayev et al., 2010). Based on a decade of GIA data, the broad absorption is responsible for the color in ~5% of yellow diamonds. Among diamonds with orange hue components, the 480 nm band is the second most common cause of color. However, for diamonds with pure (unmodified) orange hues, this feature is responsible for the color in ~86% of these ultra-rare and highly valued stones. The absorption band at 480 nm also has thermochromic properties, meaning the colors are affected by temperature changes. When a diamond with this feature is heated to 400°–500°C, the absorption band typically broadens and creates a temporary color change to more orangy hues (figure 7). This effect also contributes to the color change in

chameleon diamonds (Hainschwang et al., 2005; Breeding et al., 2018), which always exhibit the 480 nm band (Scarratt, 1984; Fritsch et al., 2007b).

H3 Defects. The H3 defect is the next most common cause of color in yellow diamonds. H3 is an uncharged defect consisting of two nitrogen atoms adjacent to a vacancy in the diamond lattice with a ZPL at 503.2 nm (Collins, 1982, 2001; Shigley and Breeding, 2013b, and references therein; figure 3D). H3 absorption can, by itself, produce yellow color and does so in about 2% of our spectroscopic sample set (figure 5). H3 also has a luminescence component that produces green fluorescence to ultraviolet (UV) and visible light (again, see figure 3). As discussed in Breeding et al. (2018), if the H3 concentration is high enough and the A-center concentration is relatively low (to avoid fluorescence quenching), H3 can produce visibly green diamonds (Collins, 2001; Breeding et al., 2018). However, when A-center concentrations are higher, H3 will produce yellow or greenish yellow diamonds.

H3 also frequently combines with plastic deformation-related defects such as the 550 nm absorption band (discussed in Eaton-Magaña et al., 2018b, as the main cause of color in pink diamonds) to produce more orangy yellow to orange colors, as we see in ~4% of the samples surveyed (figures 3 and 5). In fact, this combination of absorptions due to H3 and the 550 nm band is the only other significantly occurring mechanism to produce diamonds with primary orange hues.

OCCURRENCE AND FORMATION

Diamonds grow deep in the earth's mantle, and by the time they are in a faceted form they generally have no remaining unique characteristics from the geographic region (i.e., country of origin) in which their kimberlites came to the earth's surface. Nonetheless, certain mines or regions have produced many of the blue (Cullinan mine, South Africa), green (Brazil and Guyana), and pink to red diamonds (Argyle mine, Australia; Lomonosov mine, Russia; Smit and Shor, 2017; Breeding et al., 2018; Eaton-Magaña et al., 2018a, 2018b). This correlation has more to do with the unique geological environment required to produce those colors. For example, most blue diamonds require a source of boron (uncommon in the earth's mantle) and are thought to grow much deeper in the earth than most other diamonds (Smith et al., 2018). Pink to red diamonds require extensive plastic deformation, while green diamonds usually require extensive residence time in near-surface alluvial settings with the presence of radioactive fluids.

The prevalence of nitrogen in the earth, and diamond's affinity for nitrogen, means that most areas of diamond formation have readily available nitrogen that will be incorporated during diamond growth. The main factor that controls whether nitrogen-bearing diamonds are yellow tends to be how long they reside at high temperatures deep in the earth (to allow nitrogen atoms to aggregate), which has little to do with geographic regions where kimberlites erupt (figure 8). Consequently, fancy-color natural yellow and orange diamonds are recovered in nearly all mining areas around the world. A few localities are well known for producing high-quality fancy-color yellow diamonds of different types. Type Ia cape diamonds were named for their occurrences in South Africa, and the Ellendale mine in Australia has been a very important source for these types of fancy yellow diamonds (Smit, 2008). Type Ib yellow diamonds (containing C-centers) are relatively rare because most diamonds stay at depth in the earth at high temperatures for prolonged periods of time,

Figure 8. Some color centers are created during diamond growth in the mantle, while others are acquired after long residence times at high temperatures or during plastic deformation that might occur due to mantle flow or during initial stages of transport in kimberlite.





Figure 9. Famous orange diamonds include *The Orange* (top, 14.82 ct; courtesy of Christie's) and *the Pumpkin* (bottom, 5.54 ct) photo by Shane F. McClure). Middle row, left to right: Well-known yellows include the *Arctic Sun* (30.54 ct; photo by Jae Liao), the *Tiffany Yellow* (128.54 ct; photo by Carlton Davis), and the *Incomparable* (407.78 ct; photo by Jae Liao). Composite image, photos not to scale.

causing preexisting C-centers to aggregate to A- and B-centers. A few locations, however, such as the Ekati and Diavik mines in Canada and the Zimmi deposit in Sierra Leone, are well known for their unusually large type Ib yellow diamonds (Shigley and Breeding, 2013a; Smit et al., 2016, 2018).

Many very large and famous yellow and orange diamonds have been unearthed and sold for strong prices at auction (figure 9). One of the largest yellow diamonds is the 407.48 ct Fancy Deep brownish yellow (and Internally Flawless) Incomparable diamond, discovered in the Congo. Other famous yellow diamonds include the 128.54 ct Tiffany Yellow (South Africa), the 132.27 ct Florentine (India), the 127 ct Sun of Africa (South Africa), the 101.29 ct Allnatt (likely South Africa), the 30.54 ct Arctic Sun (Canada), and the 4.25 ct Kahn Canary (Arkansas, United States) (Thompson, 2004; Manutchehr-Danai, 2013; <http://famousdiamonds.tripod.com>). Orange

diamonds are considerably rarer than yellows, particularly unmodified pure orange hues, but a few famous ones exist. The largest is *The Orange*, a Fancy Vivid orange diamond of unknown origin weighing 14.82 ct that sold at auction in 2013 for ~US\$2.4 million per carat, a record price at the time (DeMarco, 2013). Another well-known orange diamond is *the Pumpkin*, a 5.54 ct Fancy Vivid orange stone from the Central African Republic purchased the day before Halloween in 1997 for US\$1.3 million (Goldberg, 2015).

GEMOLOGICAL OBSERVATIONS

Fancy yellow and orange diamonds have a few distinctive features that can be seen under magnification with a gemological microscope (table 1 and figure 10). As there are different mechanisms for producing yellow and orange colors, the various groups have somewhat differing characteristics.

Cape Defects. Cape yellow diamonds tend to have even color distributions and often contain crystal inclusions, much like colorless and near-colorless diamonds. Generally, there is nothing unique about cape diamonds under magnification. Those with significant hydrogen-related defects will sometimes contain finely dispersed particle clouds (figure 10D) that may be zoned in a way that creates a cross-like appearance (Wang and Mayerson, 2002; Rondeau et al., 2004). The cape absorption features (415, 451, 463, and 478 nm) can often be seen as dark lines in a handheld or desk-model spectroscope, and their fluorescence tends to be remarkably consistent, with a moderate to strong blue or yellow reaction to long-wave UV (365 nm) and a weak to moderate yellow to orange reaction to short-wave UV (254 nm) light.

Isolated Nitrogen. Type Ib yellow and orange diamonds often show more distinctive gemological fea-

tures than the other groups. Under magnification, it is common to see somewhat dense clouds of particle inclusions or groupings of oriented needles in diamonds colored by isolated nitrogen (figure 10, A and B). These clouds and needles are often in particular zones of yellow or orange color that indicate the distribution of C-centers in a diamond. With the spectroscope, only a strong general absorption in the blue end of the spectrum can usually be seen. These diamonds also show rather consistent fluorescence reactions. To both long-wave and short-wave UV, type Ib diamonds are typically inert. If they show any fluorescence, it is usually weak orange, yellow, or green.

480 nm Visible Absorption Band. Yellow and orange diamonds colored by the 480 nm band tend to be variable when viewed in the microscope. Quite often the color looks uniform in faceted stones, but there are subtle zones of yellow or orange intermixed with

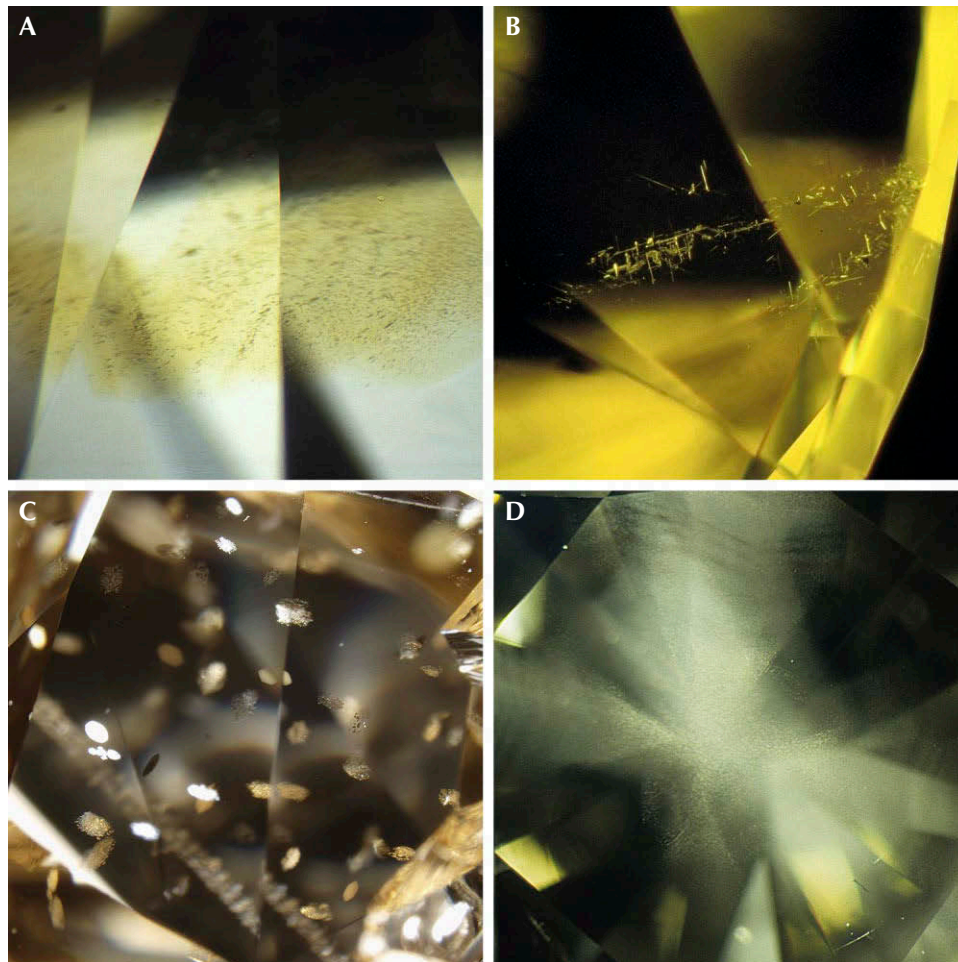


Figure 10. Some yellow and orange diamond groups show distinctive inclusions such as color-zoned particle clouds (A) and oriented needles (B) in type Ib diamonds, oriented platy inclusions in 480 nm band diamonds (C), and patterned clouds in cape diamonds with hydrogen (D). Photomicrographs by GIA staff. Field of view 3.0 mm (A), 3.5 mm (B), 2.5 mm (C), and 5.0 mm (D).

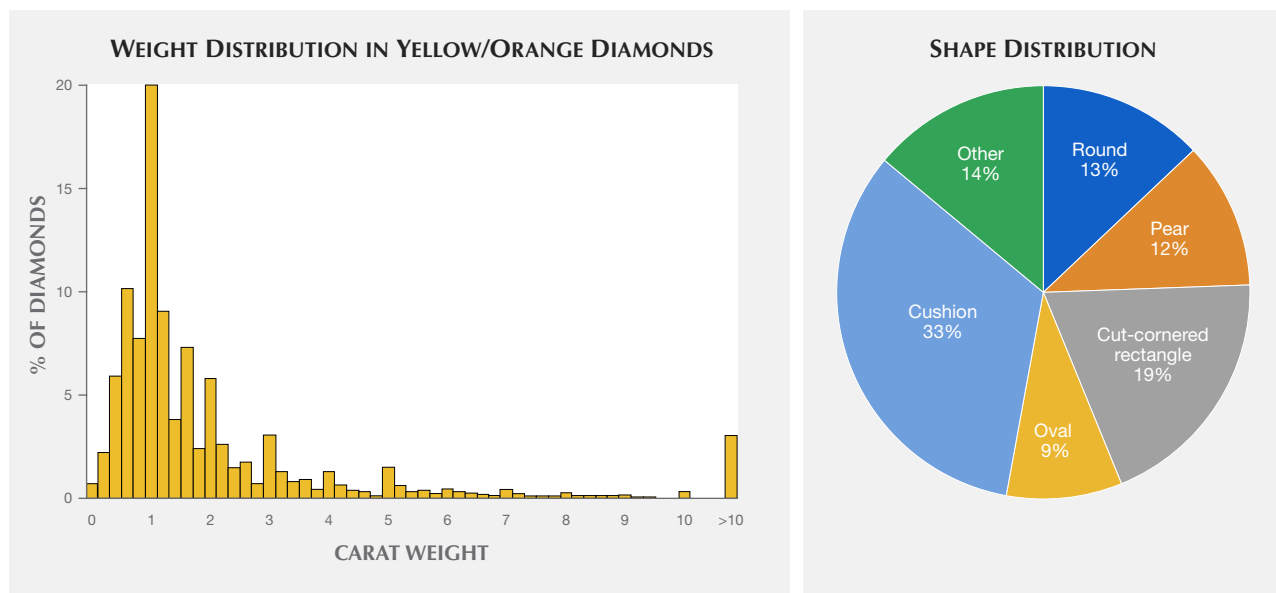


Figure 11. Most yellow and orange diamonds seen at GIA have weighed between one and two carats and been faceted into cushion or cut-cornered rectangle shapes.

near-colorless diamond that only show well from fluorescence differences. Diamonds in this group are commonly very included and sometimes show platy oriented groups of inclusions that are somewhat distinctive (figure 10C). A broad absorption band from 450 to 500 nm can often be seen as a dark patch in the spectroscope. The fluorescence from 480 nm band diamonds is very distinctive, with moderate to strong yellow or orangy yellow reactions to long-wave UV and weak to moderate yellow reactions to short-wave UV. These diamonds may phosphoresce a weak to moderate yellow after the short-wave UV lamp is turned off.

H3 Defects. Yellow diamonds colored by the H3 defect can show a range of gemological properties. There are no characteristic inclusions, and color distribution may be uniform or consist of yellow banding. Under fiber-optic illumination in the microscope, these bands (or random areas within the stone) may show green luminescence from the H3 defect. With the spectroscope, a broad absorption from H3 can be seen at wavelengths < 500 nm and, if the stone is cooled with a spray refrigerant or in liquid nitrogen, the ZPL at 503.2 nm may be discernible with a spectroscope. The fluorescence reactions of H3-dominated diamonds tend to be green to both long-wave and short-wave UV. For orange diamonds colored by a combination of H3 and the 550 nm band, most of the features are the same. However,

brown grainlines caused by plastic deformation with localized green luminescence from H3 may occasionally be visible with the microscope. The green luminescence is not usually strong or widely distributed enough to affect the bodycolor.

LABORATORY SUBMISSIONS AND GRADING

Of the yellow and orange diamonds submitted to GIA over nearly a decade, 40% were in the one- to two-carat size range (figure 11, left). The overall size distribution included 29% weighing less than one carat and 28% weighing from two to ten carats. About 3% of the stones exceeded 10 ct. Unlike D-to-Z diamonds, where round shapes are most common, the yellow and orange diamonds were most often cut into cushions (33%) or cut-cornered rectangles (19%) (figure 11, right). Rounds (13%), pears (12%), and ovals (9%) were the next most common shapes. Clarity grades covered the entire grading range, and no discernible trends were noted.

The color grade distribution was strongly skewed toward unmodified yellow hues (~79%), followed by greenish yellows with occasional gray or brown components (~9%), combinations of orange and yellow with occasional brown components (i.e., orange-yellow, yellowish orange, brownish orangy yellow, etc.; ~6%), brownish yellows (~5%), brown-oranges (~1%), and finally the extremely rare unmodified orange hues (0.05%). In addition, the color saturation was strongly skewed toward Fancy Light and greater,

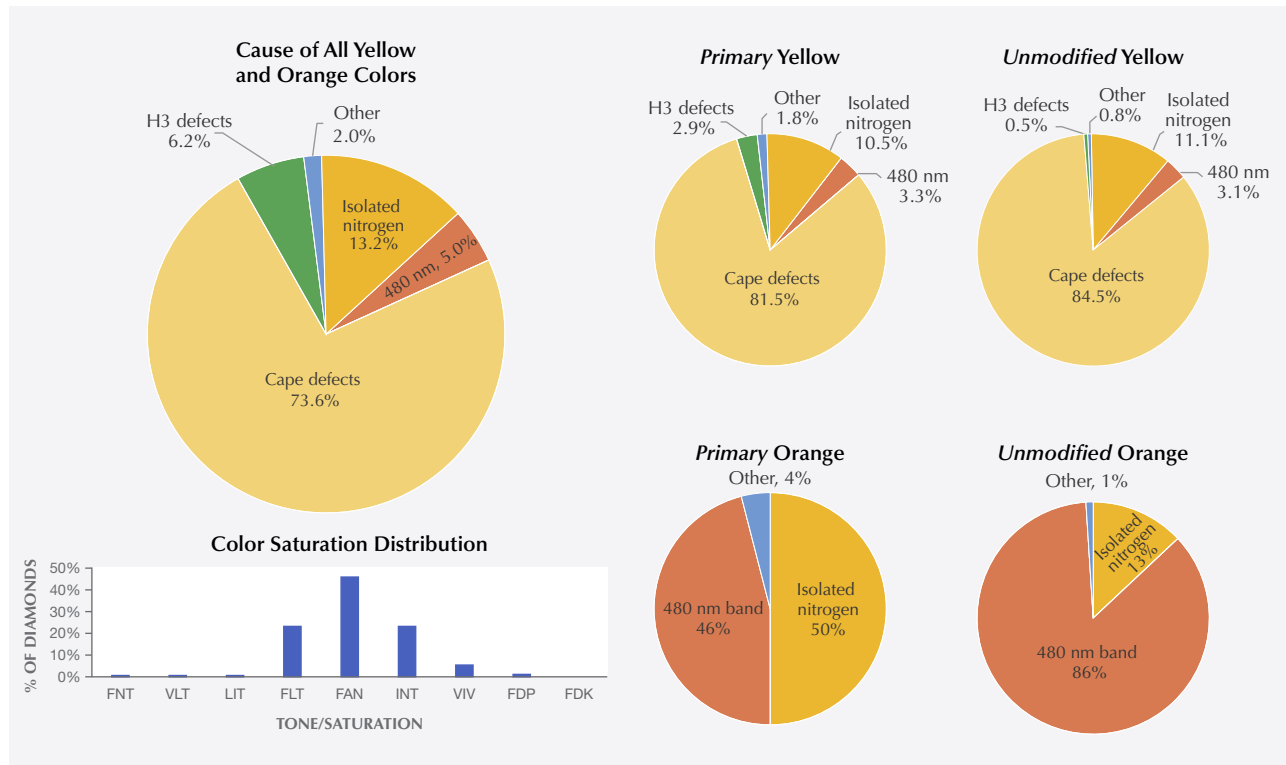
with Fancy the most common. The reason for this skew is that yellow diamonds with unmodified hues in the Faint, Very Light, and Light ranges are classified on the D-to-Z grading scale and are therefore not included in this dataset (King et al., 1994, 2008).

As mentioned earlier, a random sampling of 500 natural yellow and orange diamonds was examined to assess the causes of color (figure 12). From these data we see that cape defects (sometimes including hydrogen) accounted for almost three-quarters of the stones (73.6%; figure 12). Isolated nitrogen was the coloring agent in 13.2%, followed by H3 (sometimes including 550 nm plastic deformation band) at 6.2%, the 480 nm visible absorption band at 5%, and a few oddities making up the final 2%. While these data describe the various causes of color in the group as a whole, they are significantly skewed toward the much higher population of yellow diamonds. Interesting characteristics can be seen by comparing the causes of color in stones with yellow or orange as the primary color component (e.g., “brownish orangy yellow” would be primarily yellow, while “brownish

yellowish orange” would be primarily orange and “orange” alone would be termed as an unmodified hue here) to the distribution of the unmodified yellow and orange hues. Among the primarily yellow diamonds, ~81.5% were colored by cape defects (sometimes including hydrogen), ~10.5% by isolated nitrogen (or type Ib), 3.3% by the 480 nm band, and ~3% by H3 (with or without the 550 nm band; figure 12). Stones with unmodified yellow hues had a very similar distribution of defects, with ~84.5% capes, ~11% isolated nitrogen, ~3% 480 nm band, ~0.5% H3, and a few oddities (figure 12).

The 500-stone data set was largely composed of yellow diamonds, so in order to similarly evaluate the primary and unmodified orange diamonds, data from GIA’s nearly decade-long intake of orange diamonds (both primary and unmodified, more than 13,000 stones) were screened for color origin. Orange diamonds, however, show a marked difference between those with primary and unmodified orange hues. The causes of color in orange diamonds with additional color components are nearly evenly dis-

Figure 12. Cape defects are by far the most common cause of fancy yellow color in diamond, including unmodified yellow hues. Isolated nitrogen is the most common producer of orange hue components, though 480 nm bands dominate the unmodified oranges.



tributed between isolated nitrogen (~50%) and the 480 nm visible absorption band (46%), with the remainder (4%) consisting mostly of stones with H3 and plastic deformation and a few colored by NV centers (figure 12). Orange diamonds with pure, unmodified hues are extremely rare (< 200 seen at GIA in the last decade) and strikingly consistent in their cause of color, with ~86% from 480 nm bands, ~13% from isolated nitrogen, and less than 1% from other mechanisms (again, see figure 12). From these data, it is apparent that some unique aspect of the 480 nm visible absorption band contributes to a purer, unmodified orange hue.

ABSORPTION SPECTROSCOPY

Absorption spectroscopy is a powerful tool for examining colored diamonds. This nondestructive method directly measures the major impurities in the diamond lattice (infrared absorption, measured at room temperature) as well as defects that are responsible for color (visible absorption, measured at ~77 K, i.e., liquid nitrogen temperature). Each of the different causes of color in yellow and orange diamonds has characteristic features that can be identified using absorption spectroscopy. Here we present representative spectra from each of the groups to illustrate the differences.

Infrared Absorption (FTIR). Natural fancy-color yellow diamonds colored by cape defects have remarkably consistent FTIR spectra, regardless of color. All of these diamonds are type Ia with extremely high concentrations of nitrogen impurities (often >1000 ppma total nitrogen) that cannot be fully resolved by the detectors of FTIR instruments (i.e., the absorption peaks exceed the vertical scale of the graph; figure 13). Both A-centers (1282 cm^{-1}) and B-centers (1175 cm^{-1}) are present, but usually no C-centers (1130 and 1344 cm^{-1}) can be detected, which is typical of most type Ia diamonds. This is a product of the natural aggregation process where C-centers (isolated N) aggregate to A-centers (paired N) and finally to B-centers (four N and a vacancy) with enough time at high temperatures inside the earth (figure 2; Anderson, 1961; Davies, 1970). Cape diamonds also have strong platelet peaks (variable position from ~1360 to 1375 cm^{-1} ; Allen and Evans, 1981; Breeding and Shigley, 2009), as well as a series of three broad infrared absorptions at ~1490, 1525, and 1550 cm^{-1} that occur almost exclusively in diamonds with cape defects (figure 13A). In most fancy-color yellow cape

diamonds, two additional relatively broad FTIR absorptions can usually be seen at 1430 and 1450 cm^{-1} ; these are always proportional to each other in intensity. The 1450 cm^{-1} feature has a peak position very similar to that of the H1a interstitial radiation-related defect (Collins, 1982; Zaitsev, 2003), but in cape diamonds the feature is broader and unrelated to radiation exposure. For cape diamonds with hydrogen impurities, a peak at 3107 cm^{-1} (three nitrogen atoms adjacent to a vacancy with a hydrogen atom; Goss et al., 2014; figure 13A) and related modes at 1405 and 4495 cm^{-1} are ubiquitous and generally vary in intensity with hydrogen content.

Yellow and orange diamonds colored by isolated nitrogen always show the related features at 1344 and ~1130 cm^{-1} , but otherwise the FTIR spectra are somewhat variable. These occur as type Ib diamonds dominated by C-center absorption, type IaA + Ib diamonds with a combination of A-center and C-center absorptions (figure 13B), or diamonds dominated by A-aggregates with trace concentrations of C-centers. Because C-centers are such strong absorbers, it only takes a few ppm to produce strong yellow color. Consequently, the amount of isolated nitrogen is often quite low in both types (usually <100 ppma; concentrations calculated using a modified version of a deconvolution spreadsheet provided by Dr. David Fisher of DTC Research Center, Maidenhead, UK; Boyd et al., 1994, 1995). Very special geological conditions that are not completely understood are required for C-centers to be preserved at all in natural diamonds. A-center concentration ranges from a few ppma to a few thousand ppma and may be higher or lower than the C-center concentration in different samples. Additional FTIR absorptions of unknown structure at 1353, 1358, 1363, and 1373 cm^{-1} commonly occur in yellow and orange diamonds with isolated nitrogen (figure 13B). Weak H1b (4935 cm^{-1}) absorption also occurs in many type Ib diamonds. Hydrogen absorptions similar to those in cape diamonds sometimes occur, as well, along with a series of tiny peaks in the 3000–3500 cm^{-1} range that are hydrogen-related and seem to correlate with a defect described as the Y-center (Hain-schwang et al., 2012). We have only observed these 3000–3500 cm^{-1} features in diamonds with isolated nitrogen. Finally, plastic deformation often occurs in yellow type Ib diamonds and is represented by “amber center” absorptions (usually occurring at 4165, 4110, or 4065 cm^{-1} ; Massi et al., 2005), especially in brownish yellow stones or those with an olive greenish hue.

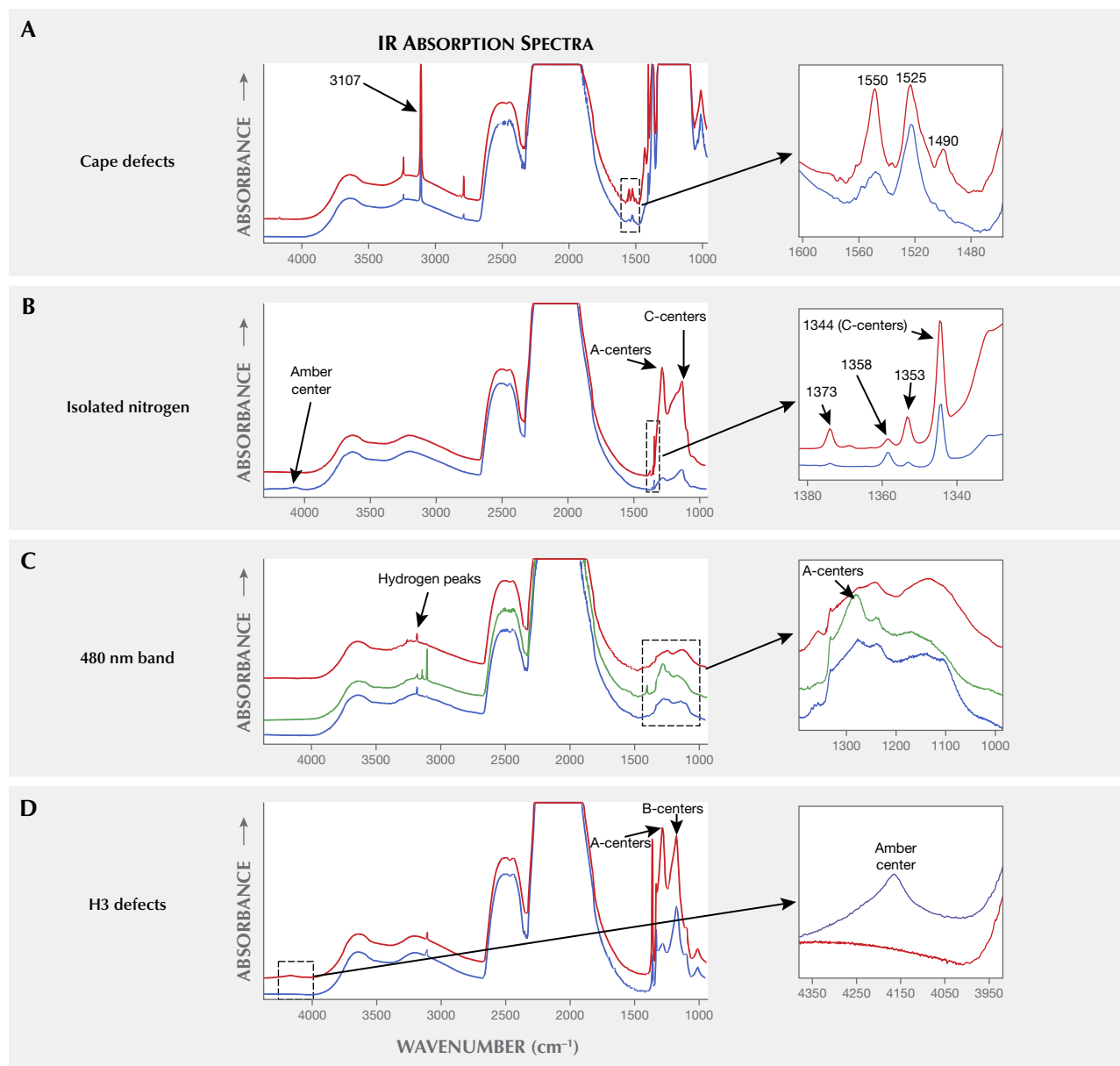


Figure 13. Each group of color mechanisms for yellow and orange diamonds has a few distinctive IR absorption spectral features. Spectra are offset vertically for clarity.

Yellow and orange diamonds colored by a 480 nm visible absorption band are nearly always type Ia and usually have low to moderate concentrations of A-centers, but sometimes they show very irregular and distorted one-phonon regions in the infrared spectrum that are not well understood (figure 13C). In some samples, trace concentrations of C-centers can also be detected. Hydrogen impurities are variable, but when present, they occur with the same peaks mentioned above for isolated nitrogen yellows.

Yellow diamonds colored by H3 defects are quite variable in their FTIR spectra. H3 absorbs and emits

light (luminesces) simultaneously. Diamonds colored by H3 are always type Ia with variable proportions of A- and B-centers (figure 13D). For greenish yellow stones, the total nitrogen, as well as the A-center concentration, is always relatively low to allow the H3 green luminescence to be seen along with the yellow from absorption. In H3-dominated yellow diamonds with high A-center concentrations (saturated), the green luminescence from H3 is completely quenched (Collins, 1982, 2001), leaving only the yellow color from H3 absorption. Similar to cape diamonds, the platelet, 1430 cm^{-1} , and 1450 cm^{-1} fea-

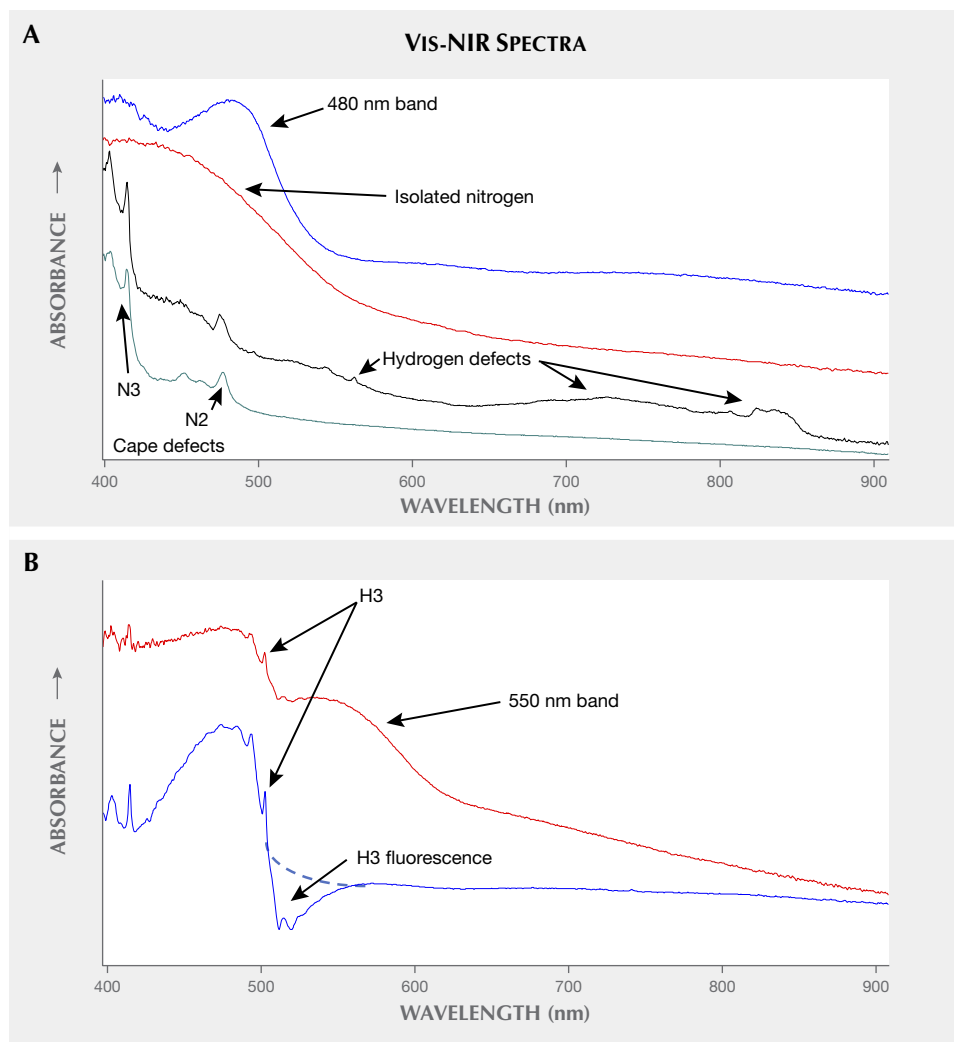


Figure 14. Each group of color mechanisms for yellow and orange diamonds has characteristic Vis-NIR absorptions that produce color. Diamond spectra can include multiple causes of color, which can create variations on their normally produced colors. For example, spectra with cape features can include hydrogen defects and H3 spectra can include the 550 nm absorption band. Spectra are offset vertically for clarity.

tures as well as occasional H-related features are seen in all H3 diamonds. In contrast, brownish yellow and orange diamonds colored by the combination of H3 and a 550 nm visible absorption band are extremely consistent as type IaA diamonds with moderate amounts of total nitrogen, a weak platelet peak, and the presence of amber centers (Massi et al., 2005; Eaton-Magaña et al., 2018b) that mark the plastic deformation related to the 550 nm band.

Ultraviolet-Visible/Near-Infrared Absorption (UV-Vis-NIR). Much like their FTIR spectra, the UV-Vis-NIR spectra of natural yellow diamonds colored by cape defects are extremely consistent, with the N3 ZPL (Collins, 1982, 2001; Zaitsev, 2003; Shigley and Breeding, 2013b) at 415 nm, a related broad absorption band to shorter wavelengths, as well as the other N3-related cape absorption features at (listed in order of intensity) 478 (N2), 451, 463, 435, and 426 nm (fig-

ure 14A). The last three cape peaks listed only appear with increasing saturation of the yellow color. The observed yellow color comes primarily from the absorptions from N2 and the 451 nm band, with only minor contribution from the N3 itself, but all the cape peaks are proportional in intensity to N3. If hydrogen-related defects are present, two broad asymmetric bands centered at ~730 and ~836 nm often occur along with a smaller peak at 563 nm (figure 14A), causing the color to have brownish or greenish components.

UV-Vis-NIR absorption in yellow and orange diamonds primarily colored by isolated nitrogen is quite different. A very strong absorption by C-centers occurs in the UV range at ~270 nm (Jones et al., 2009) (not shown). Even with a few ppm of C-centers, the absorption is so strong that the absorption "tail" extends into the visible range, creating an absorption continuum to ~510 nm in yellow hues and ~600 nm in orange-hued

type Ib diamonds (figure 14A). This gradually increasing absorption toward the UV is the only feature seen in the UV-Vis-NIR spectra of most of these diamonds.

Yellow and orange diamonds colored by the 480 nm band show the so-named broad absorption centered at roughly 480 nm (figure 14A) along with another broad absorption at 370 nm and a much weaker band at 427 nm (not shown). Occasionally a weak N3 peak at 415 nm can also be seen. The intensity and, to some extent, the shape of the 480 nm band are variable and do not always correlate with the intensity of yellow or orange color. More notably, the 480 nm absorption extends only to ~550 nm in nearly all of these stones, even in the orange fancy-color diamonds. Absorption color calculations indicate that the resulting color should be mostly yellow in all cases, strongly suggesting that the luminescence discussed in the next section accounts for part of the color in the orange stones (Titkov et al., 2015).

H3-dominated yellow diamonds produce relatively simple UV-Vis-NIR absorptions with the H3 ZPL at 503.2 nm (Collins, 1982, 2001; Shigley and Breeding, 2013b) and its related absorption band to shorter wavelengths as their major feature (figure 14B). When plastic deformation is also present, a broad 550 nm band and an underlying increase in overall absorption toward the UV caused by vacancy clusters accompany the H3 absorptions to extend the absorption edge to ~620 nm and produce brownish orange hues (figure 14B). Often, weak 535.8 nm and H2 (986 nm) absorption peaks are also seen in these diamonds.

LUMINESCENCE SPECTROSCOPY AND IMAGING

In addition to absorbing energy, many defects also emit light (or luminesce) when exposed to certain wavelengths of light. The two major forms of luminescence used in gemology are referred to as photoluminescence and fluorescence, typically depending on whether a laser or UV lamp is used for excitation and whether the collection occurs at liquid nitrogen or room temperature.

Photoluminescence (PL). PL is a very sensitive, non-destructive analytical technique that involves exposing a diamond to light of known energy (i.e., with a wavelength in the UV, visible, or infrared range) and measuring any new light that is given off as a result of atomic-level interactions within the diamond. PL

analysis is usually performed with the sample at liquid nitrogen temperature (~77 K) and can detect diamond defects as low as a few parts per billion (ppb) (Eaton-Magaña and Breeding, 2016). Each cause of color in yellow and orange diamonds shows a few distinctive features in the PL spectra.

Natural yellow cape diamonds consistently exhibit a number of PL peaks including 415 (N3), 496 (H4), 503.2 (H3), 508, 535, 604, 660, 700, 787, 911, 933, and 952 nm. Besides the strong N3 at 415 nm that contributes to the cape absorption that causes the yellow color, the most prominent tend to be the 700 and 787 nm features, which have been attributed to nickel, nitrogen, and likely hydrogen impurities (Fritsch et al., 2007a; figure 15A). In cape diamonds with abundant hydrogen, these two peaks tend to be very strong, and the NE8 Ni-N defect (Yelisseyev and Kanda, 2007) consistently appeared at 793 nm.

For yellow and orange diamonds colored by isolated nitrogen, the following PL peaks are often detected: 503.2 (H3), 525, 565.8, 575 (NV⁰), 578, 604, 637 (NV⁻), 689, 698, 805, 830, 904, 953, and 986 nm (H2). Of these, the most significant are the NV centers at 575 and 637 nm (figure 15B) and the H2 defect at 986 nm. The abundance of C-centers, which are electron donors, tends to provide extra electrons to adjacent defects to make them negatively charged (Collins, 1982, 2001). In type Ib diamonds under 514 or 532 nm laser excitation, the 637 (NV⁻)/575 (NV⁰) ratio is almost always >1, and the H2 defect (two nitrogen atoms adjacent to a vacancy in a negative charge state) is ubiquitous due to the available electrons.

PL spectra from 480 nm band stones are noticeably different from those exhibited by the other groups. Between 550 and 700 nm, nearly a hundred small PL peaks are sometimes observed with 488 nm laser excitation. Overall, the following peaks are commonly seen: 589, 592, 616, 619, 678, 683, 693, 709, 723, 799, 807, 817, 883/885, and 904 nm. Of these, the 799 and 883/885 nm doublet are most noteworthy. The 799 nm peak occurs in all 480 nm band diamonds evaluated, and the 883/885 nm doublet is the well-studied 1.4 eV Ni center (Yelisseyev and Kanda, 2007). More significant seems to be the broad luminescence band in the red end of the spectrum, centered at ~670–700 nm, when a blue or green laser is used for excitation of some 480 nm band diamonds (figure 15C; first described in Collins and Mohammed, 1982). This band signifies red luminescence to visible light (from laser excitation in this case) that likely plays a role in the color of some orange diamonds. As discussed in the UV-Vis-

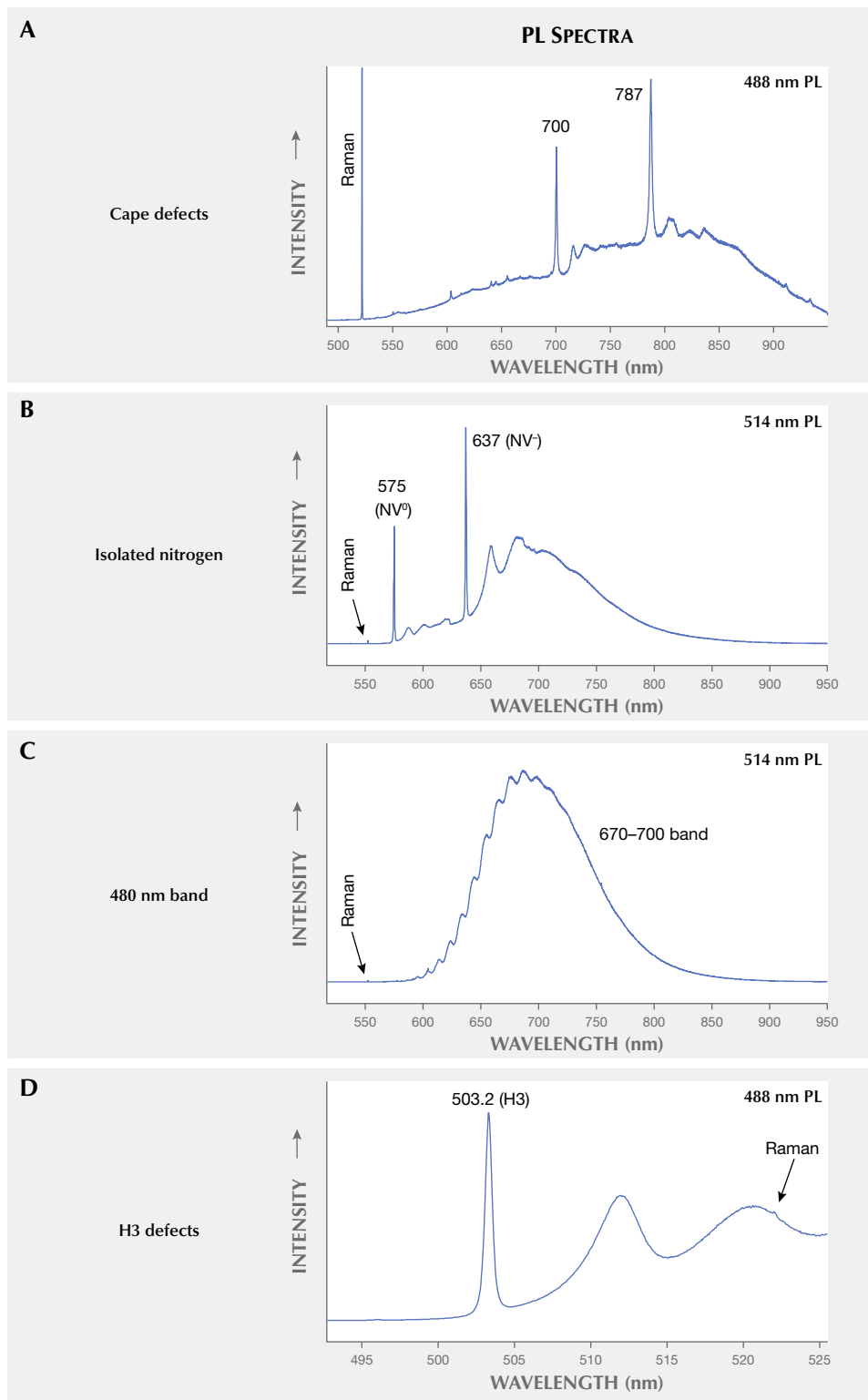


Figure 15. Each group of color mechanisms for yellow and orange diamonds has a few distinctive PL emission features.

NIR section earlier, 480 nm band absorption alone produces only yellow color. However, the combination of that absorption and this red luminescence is likely the cause of orange color in the majority of the

world's most beautiful orange diamonds (Titkov et al., 2015).

Yellow diamonds colored by H3 and orange diamonds colored by the combination of H3 and the 550

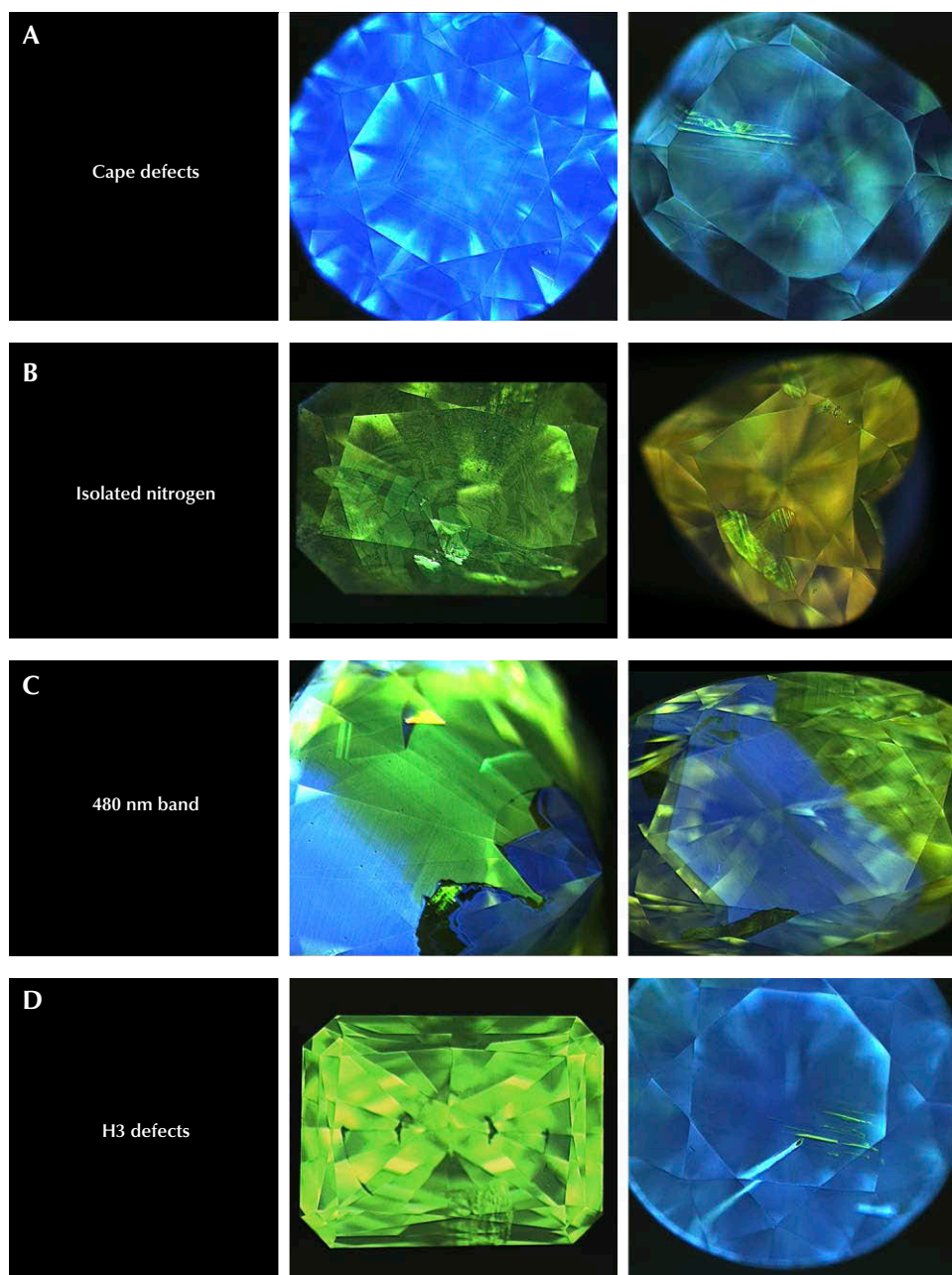


Figure 16. Each group of color mechanisms for yellow and orange diamonds displays different aspects of their fluorescence colors or patterns under deep-UV excitation. Diamond-View images by GIA staff.

nm plastic deformation band both show relatively similar PL spectra, with emissions at 496 (H4), 503.2 (H3), 535.8, 575 (NV⁰), 637 (NV⁻), 657, 700, 741 (GR1), 804, 812, 953, and 986 (H2). Apart from the very strong H3 PL peak (figure 15D), the only other notable observation was that the 535.8 nm peak was often much larger in stones with the 550 nm visible absorption band (not shown).

Deep-UV Fluorescence. Earlier in the gemological observations section, we discussed the fluorescence reactions of each group to standard short-wave and

long-wave UV light. Here we further examine the deep-UV (<230 nm excitation) fluorescence reactions of the groups observed using a DiamondView instrument. Due to the extreme absorption of UV at these and shorter wavelengths by diamond, this high-energy excitation only stimulates fluorescence from the surface of a diamond, thus providing a highly resolved image of fluorescence distribution within different diamond growth events and sectors (Welbourn et al., 1996).

Cape diamonds mostly show strong blue fluorescence to deep UV (due to N3 defects), often with dis-



Figure 17. Orange and yellow diamonds can occur naturally, be grown in a laboratory, or result from the treatment of off-color natural diamonds. Photos by GIA staff.

tinctive growth bands forming multiple rectangles within each other from octahedral growth (figure 16A). Occasionally a thin, bright green band of fluorescence from localized H3 defects is observed following the growth pattern in some areas. Hydrogen content has little effect on the deep-UV fluorescence.

Yellow and orange type Ib diamonds often have irregular deep-UV fluorescence patterns, seemingly suggesting more chaotic, possibly unstable growth environments recording periods of diamond growth and resorption. These images show variable patterns of green (H3), orange (NV⁰), or pink to red (NV⁻) fluorescence or some combination of those (figure 16B). Oftentimes the red or green fluorescence follows lines of plastic deformation within the diamonds, suggesting that some of the fluorescence was created after diamond growth during deformation. Overall fluorescence in type Ib diamonds is relatively low in intensity to deep UV.

Diamonds colored by the 480 nm band tend to be even more irregular. Deep-UV imaging shows dark blue (N3), light blue (unknown defect), greenish yellow (correlated with the 480 nm band), and occasionally green (H3) fluorescence. Inert areas between

other fluorescence colors are common as well (figure 16C). These textures suggest multiple stages of diamond growth under different conditions with different defects incorporated. Their irregular patterns are markedly similar to chameleon diamonds, which also exhibit the 480 nm band (Scarratt, 1984; Hain-schwang et al., 2005; Fritsch et al., 2007b), suggesting a genetic link.

H3-dominated yellow diamonds show very strong green fluorescence (H3) that appears uniform or is isolated to lines of plastic deformation (figure 16D). Blue fluorescence (N3) is common as well, especially in stones with localized green fluorescence. Most of the orange diamonds with H3 and 550 nm bands show the green fluorescence associated with H3 very localized along the plastic deformation slip planes.

IDENTIFICATION CONCERNS

Identification of fancy-color diamonds involves determining whether a stone grew in the earth or in a laboratory, and whether the color we see is natural or has been artificially created by treatment. Yellow diamonds (and those with orange hue components) can easily be created in a laboratory using the high-pres-

sure, high-temperature (HPHT) growth method (figure 17). As mentioned above, nitrogen is extremely abundant in the atmosphere and thus readily available in an HPHT growth chamber unless strict measures are taken to remove it. Under normal conditions of growth, most HPHT lab-grown diamonds are yellow to orange in color depending on how much nitrogen gets incorporated as C-centers. These mostly type Ib diamonds show typical features related to their growth in a laboratory such as color zoning that follows cuboctahedral growth patterns, particle clouds, metallic flux inclusions, and a lack of birefringence (direct measurement of lattice strain) under cross-polarized magnification (Eaton-Magaña et al., 2017, and references therein). Natural yellow and orange diamonds colored by C-centers have absorption spectra similar to those of their lab-grown counterparts but can usually be separated by the presence of natural inclusions, uniform to irregular color zoning, wispy clouds, and a distinct strain pattern. On rare occasions, both HPHT lab-grown and natural yellow diamonds can be type Ia with traces of isolated nitrogen, but the same separation criteria apply and lab-grown diamonds generally do not have cape defects in visible absorption. Chemical vapor deposition (CVD) methods can be used to grow yellow diamonds with isolated nitrogen, but it is rarely done and most of the products lack the color saturation of HPHT-grown samples (Kitawaki et al., 2015; Eaton-Magaña and Shigley, 2016). CVD-grown diamonds can occasionally have orange hue components if subjected to post-growth irradiation and annealing treatments to create relatively low concentrations of NV centers.

Determining whether the yellow or orange color in an earth-grown gem diamond is natural or artificially produced through treatment is a more challenging endeavor. Cape-related defects, as a group, cannot be added or removed through any known commercial treatment, so their presence is generally a good indicator that the diamond naturally exhibited some yellow color. However, it is relatively easy to create H3 defects through artificial irradiation and annealing treatment that absorbs blue light to create yellow color (figure 17). This can be done on an off-color brown diamond to make it yellow or even on a pale yellow cape diamond to intensify the color. Natural radiation exposure and heating in the earth can have similar effects, making the separation even more difficult. Extreme amounts of irradiation and annealing can turn most nitrogen-bearing diamonds to an orange to brown color, but this degree of treatment is easily spotted using absorption spectroscopy. Another form

of color enhancement that is harder to detect is HPHT treatment of type I diamonds. At pressures and temperatures higher than those in the earth where most diamonds grow, HPHT treatment can cause the creation of H3 defects as well as the breakup of aggregated nitrogen into isolated nitrogen (Collins, 2001). Both H3 and these newly created C-centers will give a diamond a yellow color (again, see figure 17). If the starting material is a cape diamond, the addition of C-centers during treatment can produce an orange color. HPHT treatment may produce graphitized feathers or inclusions or frosted facets that are not properly repolished afterward. Irradiation and annealing treatments may leave yellow or orange color zones near the culet. However, it is often impossible to geologically identify these types of treatments, and all fancy-color diamonds should be sent to a laboratory for conclusive determination of color origin.

UNUSUAL EXAMPLES

Yellow diamonds are the most common of the fancy-color diamonds and are dominated by the groups of color-causing defects described here. As with anything in nature, though, there are a few examples of unusual yellow diamonds that do not perfectly fit the categories. In our previous colored diamond articles, we have presented a few odd samples in this section. Here we will discuss two other ways to produce yellow color involving isolated nitrogen: type IaB yellow diamonds colored by isolated nitrogen and growth-zoned yellow diamonds with type Ia cores and type Ib rims.

For most natural diamonds, the aggregation path from C-centers to A-centers to B-centers is a one-way route that usually progresses to some point with a combination of A- and B-centers. The transformation from A- to B-centers is the point at which most N3 defects are created in nature, and thus most cape diamonds fall somewhere therein. We have already discussed the unlikelihood of preserving C-centers in natural yellow diamonds, but not in the more maturely aggregated type IaB diamonds. Occasionally GIA receives a Fancy to Fancy Intense yellow diamond that is type IaB with extremely weak C-center absorption and no cape defects. These unusual stones are bothersome, as B-aggregates of nitrogen should not coexist naturally with C-centers. It is common to disaggregate some nitrogen aggregates during HPHT treatment (~2000°C, 6 GPa; Dobrinets et al., 2013) to form new C-centers, but these conditions do not seem feasible for natural diamond-forming environments, and the presence of B-centers with C-centers

in an FTIR spectrum usually arouses suspicion that treatment is involved. However, there are a handful of naturally intense yellow diamonds that are highly aggregated (mostly type IaB), but still have enough traces of C-centers to produce their saturated colors, perhaps indicating very rare, HPHT-like conditions in the earth. These diamonds usually have small feathers on their natural surfaces from movement in an alluvial environment and contain PL features indicating they are naturally colored, despite similarities with HPHT-treated yellow diamonds.

Another unusual group of yellow fancy-color diamonds seen at GIA and by Hainschwang et al. (2006) displayed FTIR spectra with A-, B-, and C-centers that normally do not exist naturally. However, the diamonds seen at GIA were sourced from the Ekati mine in Canada and were known to have never been treated (Lai et al., 2019). After breaking a couple of the melee-sized rough diamonds, we discovered they consisted of near-colorless cores and yellow rims from two different episodes of diamond growth (figure 18). FTIR analysis is a bulk measurement technique, meaning the spectrum recorded is an average of all of the path lengths within the diamond through which the infrared beam passes. Thus, a diamond like this will show both the A- and B-centers from the core along with the C-centers from the rim in the same spectrum. Occasionally at GIA, we see larger faceted yellow gem diamonds with only small amounts of yellow color concentrated near the surface (enough to achieve a Fancy color grade) and the remainder of the stone is colorless. We refer to these as “yellow-skin” diamonds, but their FTIR spectra

are often more indicative of a treated-color diamond due to the mixed sampling. These diamonds represent the larger version of the melee-sized Ekati stones that have had much of their yellow outer rim removed during faceting. With careful examination, gemologists can conclusively identify these diamonds as natural, but they are definitely unusual.

COMPARISON OF ALL FANCY-COLOR DIAMONDS

This article completes the fancy-color portion of this series in *Gems & Gemology*. The final article will look principally at colorless diamonds and the rest of the D-to-Z scale. We wish to conclude this exploration of fancy-color natural diamonds by providing a brief summary and comparison of all five diamond color groups: green (Breeding et al., 2018), blue/gray/violet (Eaton-Magaña et al., 2018a), pink/purple/red/brown (Eaton-Magaña et al., 2018b), white/black (Eaton-Magaña et al., 2019) and yellow/orange (this article). Table 2 lists the major causes of color in descending order of abundance within each of the color groups in the diamonds seen at GIA.

CONCLUSIONS

Yellow and orange are the largest group of fancy-color diamonds and owe their color to four major causes associated with nitrogen impurities: cape defects, isolated nitrogen, the 480 nm visible absorption band, and H3 defects (table 1). Cape defects are by far the most important color-producing mechanism for yellow diamonds, accounting for nearly three-quarters of the dia-

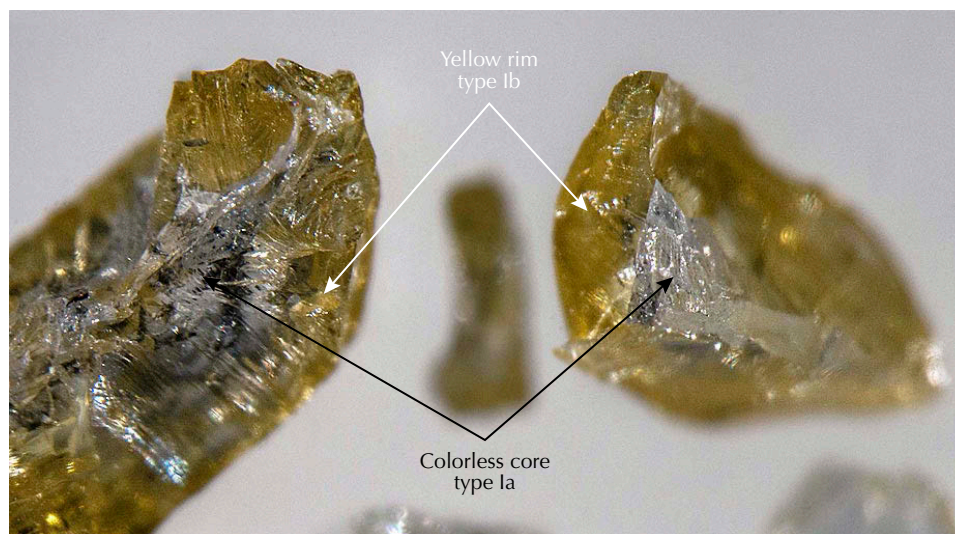


Figure 18. Small yellow diamonds (~0.02 ct each) from the Ekati mine in Canada show colorless type Ia cores, surrounded by yellow type Ib rims. IR absorption spectra from these stones suggest the simultaneous presence of A-, B-, and C-centers due to mixing of both zones during spectra collection. Photo by Mei Yan Lai.



Figure 19. Intensely colored orange and yellow gem diamonds are rare and beautiful, both in appearance and complexity of their origin of color. Left: A 4.08 ct Fancy Vivid orange diamond auctioned by Sotheby's Hong Kong in April 2016. Courtesy of Sotheby's. Right: A yellow and white diamond necklace by Chatila containing a 54.29 ct cushion-cut Fancy Intense yellow diamond. Photo by Robert Weldon.

monds evaluated, while isolated nitrogen and the 480 nm band are most important for orange stones. Yellow and orange diamonds are recovered from almost all diamond mines worldwide, but South Africa and the Central African Republic have produced some of the most famous and valuable examples. Yellow and yellowish orange lab-grown diamonds are easy to produce by the HPHT growth method, and diamond color treatments routinely create yellow and orange colors by creating

H3 or isolated nitrogen defects through HPHT treatment or artificial irradiation and annealing. Cape defects (as a group) and the 480 nm band, however, are usually not present in lab-grown diamonds. Yellow diamonds are the only natural colored diamonds many people will ever encounter and serve as an important representative for the fancy-color diamond trade, while orange diamonds with unmodified hues are among the rarest of all fancy-color diamonds (figure 19).


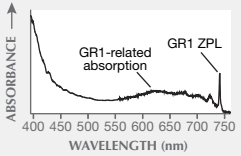

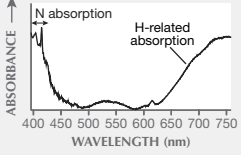

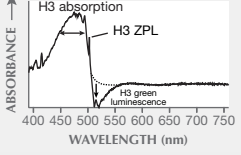

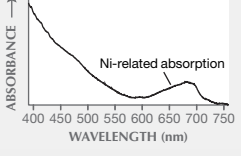

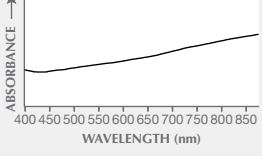

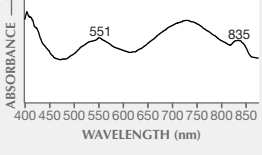

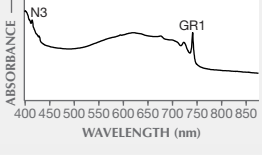

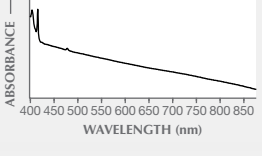

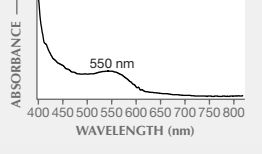
ABOUT THE AUTHORS


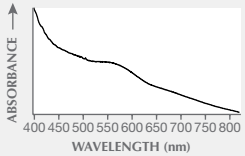

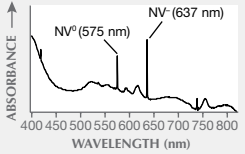


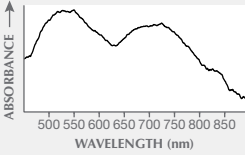

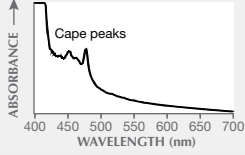

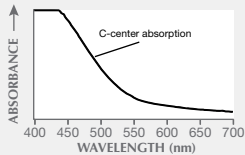

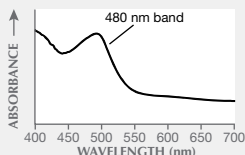

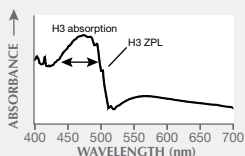
Dr. Breeding is a senior manager of analytics, Dr. Eaton-Magaña is a senior manager of diamond identification, and Dr. Shigley is a distinguished research fellow, at GIA in Carlsbad, California.

ACKNOWLEDGMENTS

The authors thank GIA's Tom Moses and John King for constructive comments on early versions of the article. GIA's Claudia Jannucci and Judy Colbert provided valuable assistance with images of famous diamonds.

TABLE 2. Causes of color within each major fancy-color diamond group in this G&G series (based on stones submitted to GIA labs).

	Cause of color	Percentage of diamonds affected within color class ^a	Representative example of color ^b	Representative Vis-NIR spectrum
Green (Breeding et al., 2018)	GR1	62%		
	Hydrogen defects	36%		
	H3	29%		
	Nickel	1%		
Blue/Gray/Violet (Eaton-Magaña et al., 2018a)	Boron	36%		
	Hydrogen defects	31%		
	GR1	27%		
	Micro-inclusions	7%		
Pink/Purple/Red/Brown (Eaton-Magaña et al., 2018b)	550 nm absorption band	99.5%		

	Cause of color	Percentage of diamonds affected within color class ^a	Representative example of color ^b	Representative Vis-NIR spectrum
Pink/Purple/Red/Brown (Eaton-Magaña et al., 2018b)	Brown absorption continuum	31%		
	NV centers	0.5%		
Fancy White/Black (Eaton-Magaña et al., 2019)	Nano-inclusions to micro-inclusions	White: 100% Black: 99.2%		N/A
	Very high defect concentrations	Black: 0.8%		
Yellow/Orange (this article)	Cape defects	74%		
	Isolated nitrogen	13%		
	480 nm band	0.5%		
	H3 defects	6%		

^aSome diamonds are affected by more than one cause of color (for example, a green diamond may be colored both by the CR1 defect and H3 green fluorescence); therefore, percentages within each color class may sum to greater than 100%.

^bDiamonds with relatively saturated color are included here as examples; however, a significant quantity in each class show lighter colors.

REFERENCES

- Allen B.P., Evans T. (1981) Aggregation of nitrogen in diamond, including platelet formation. *Proceedings of the Royal Society of London A*, Vol. 375, No. 1760, pp. 93–104, <http://dx.doi.org/10.1098/rspa.1981.0041>
- Anderson B.W. (1961) Nitrogen in diamond. *The Gemmologist*, Vol. 30, No. 355, pp. 21–22.
- Bebout G., Fogel M., Cartigny P. (2013) Nitrogen: Highly volatile yet surprisingly compatible. *Elements*, Vol. 9, pp. 333–338, <http://dx.doi.org/10.2113/gselements.9.5.333>
- Boyd S.R., Kiflawi I., Woods G.S. (1994) The relationship between infrared absorption and the A defect concentration in diamond. *Philosophical Magazine B*, Vol. 69, No. 6, pp. 1149–1153, <http://dx.doi.org/10.1080/01418639408240185>
- (1995) Infrared absorption by the B nitrogen aggregate in diamond. *Philosophical Magazine B*, Vol. 72, No. 3, pp. 351–361, <http://dx.doi.org/10.1080/13642819508239089>
- Breeding C.M., Shigley J.E. (2009) The “type” classification system of diamonds and its importance in gemology. *G&G*, Vol. 45, No. 2, pp. 96–111, <http://dx.doi.org/10.5741/GEMS.45.2.96>
- Breeding C.M., Eaton-Magaña S., Shigley J.E. (2018) Natural-color green gem diamonds: A beautiful conundrum. *G&G*, Vol. 54, No. 1, pp. 2–27, <http://dx.doi.org/10.5741/GEMS.54.1.2>
- Bruton E. (1971) *Diamonds*. Chilton Book Co., Radnor, PA, 273 pp.
- Collins A.T. (1980) Spectroscopic investigation of a canary yellow diamond. *Journal of Gemmology*, Vol. 17, No. 4, pp. 213–222.
- (1982) Colour centres in diamond. *Journal of Gemmology*, Vol. 18, No. 1, pp. 37–75.
- (1997) The electronic and optical properties of diamond. In A. Paoletti and A. Tucciarone, Eds., *The Physics of Diamond*. Course 135, *Proceedings of the International School of Physics*, IOS Press, Amsterdam, p. 273.
- (1999) Things we still don't know about optical centres in diamond. *Diamond and Related Materials*, Vol. 8, No. 8-9, pp. 1455–1462, [http://dx.doi.org/10.1016/S0925-9635\(99\)00013-8](http://dx.doi.org/10.1016/S0925-9635(99)00013-8)
- (2001) The colour of diamond and how it may be changed. *Journal of Gemmology*, Vol. 18, No. 1, pp. 341–359.
- Collins A.T., Mohammed K. (1982) Optical studies of vibronic bands in yellow luminescing natural diamonds. *Journal of Physics C: Solid State Physics*, Vol. 15, No. 1, pp. 147–158, <http://dx.doi.org/10.1088/0022-3719/15/1/012>
- Davies G. (1970) Aggregation of nitrogen in diamond. *Nature*, Vol. 228, No. 5273, p. 758, <http://dx.doi.org/10.1038/228758a0>
- (1981) The origin of the N₂ absorption band in natural yellow diamonds. *Portugaliae Physica*, Vol. 13, No. 3/4, pp. 241–261.
- DeMarco A. (2013) 14.82-carat orange diamond sells for a world record \$35.5 million. *Forbes.com*, <https://www.forbes.com/sites/anthonydemarco/2013/11/12/14-82-carat-orange-diamond-sells-for-a-world-record-35-5-million/#5919e3c61657>
- Dobrinets I.A., Vins V.G., Zaitsev A.M. (2013) *HPHT-Treated Diamonds: Diamonds Forever*. Springer, Heidelberg.
- Eaton-Magaña S.C., Breeding C.M. (2016) An introduction to photoluminescence spectroscopy for diamond and its applications in gemology. *G&G*, Vol. 52, No. 1, pp. 2–17, <http://dx.doi.org/10.5741/GEMS.52.1.2>
- Eaton-Magaña S., Shigley J.E. (2016) Observations on CVD-grown synthetic diamonds: A review. *G&G*, Vol. 52, No. 3, pp. 222–245, <http://dx.doi.org/10.5741/GEMS.52.3.222>
- Eaton-Magaña S., Shigley J.E., Breeding C.M. (2017) Observations on HPHT-grown synthetic diamonds: A review. *G&G*, Vol. 53, No. 3, pp. 262–284, <http://dx.doi.org/10.5741/GEMS.53.3.262>
- Eaton-Magaña S., Breeding C.M., Shigley J.E. (2018a) Natural-color blue, gray, and violet diamonds: Allure of the deep. *G&G*, Vol. 54, No. 2, pp. 112–131, <http://dx.doi.org/10.5741/GEMS.54.2.112>
- Eaton-Magaña S., Ardon T., Smit K.V., Breeding C.M., Shigley J.E. (2018b) Natural-color pink, purple, red, and brown diamonds: Band of many colors. *G&G*, Vol. 54, No. 4, pp. 352–377, <http://dx.doi.org/10.5741/GEMS.54.2.352>
- Eaton-Magaña S., Ardon T., Breeding C.M., Shigley J.E. (2019) Natural-color fancy white and fancy black diamonds: Where color and clarity converge. *G&G*, Vol. 55, No. 3, pp. 320–337, <http://dx.doi.org/10.5741/GEMS.55.3.320>
- Fritsch E., Hainschwang T., Massi L., Rondeau B. (2007a) Hydrogen-related optical centers in natural diamond: An update. *New Diamond and Frontier Carbon Technology*, Vol. 17, No. 2, pp. 63–89.
- Fritsch E., Massi L., Rossman G.R., Hainschwang T., Jobic S., Dessapt R. (2007b) Thermochromic and photochromic behavior of “chameleon” diamonds. *Diamond and Related Materials*, Vol. 16, No. 2, pp. 401–408, <https://doi.org/10.1016/j.diamond.2006.08.014>
- Gali A., Lowther J.E., Deak P. (2001) Defect states of substitutional oxygen in diamond. *Journal of Physics: Condensed Matter*, Vol. 13, No. 50, pp. 11607–11613, <http://dx.doi.org/10.1088/0953-8984/13/50/319>
- Goldberg W. (2015) Famous Diamonds – Part 3: The Pumpkin diamond (<http://www.williamgoldberg.com/house-of-goldberg/2015/11/famous-diamonds-part-3-the-pumpkin-diamond/>) [Accessed Feb. 28, 2020]
- Goss J.P., Briddon P.R., Hill V., Jones R., Rayson M.J. (2014) Identification of the structure of the 3107 cm⁻¹ H-related defect in diamond. *Journal of Physics: Condensed Matter*, Vol. 26, No. 14, pp. 1–6, <http://dx.doi.org/10.1088/0953-8984/26/14/145801>
- Hainschwang T., Simic D., Fritsch E., Deljanin B., Woodring S., DelRe N. (2005) A gemological study of a collection of chameleon diamonds. *G&G*, Vol. 41, No. 1, pp. 20–35, <http://dx.doi.org/10.5741/GEMS.41.1.20>
- Hainschwang T., Notari F., Fritsch E., Massi L. (2006) Natural, untreated diamonds showing the A, B and C infrared absorptions (“ABC diamonds”), and the H₂ absorption. *Diamond and Related Materials*, Vol. 15, pp. 1555–1564, <http://dx.doi.org/10.1016/j.diamond.2005.12.029>
- Hainschwang T., Fritsch E., Notari F., Rondeau B. (2012) A new defect center in type Ib diamond inducing one phonon infrared absorption: The Y center. *Diamond and Related Materials*, Vol. 21, pp. 120–126, <http://dx.doi.org/10.1016/j.diamond.2011.11.002>
- Hainschwang T., Fritsch E., Notari F., Rondeau B., Katruscha A. (2013) The origin of color in natural C center bearing diamonds. *Diamond and Related Materials*, Vol. 39, pp. 27–40, <http://dx.doi.org/10.1016/j.diamond.2013.07.007>
- Jones R., Goss J.P., Briddon P.R. (2009) Acceptor level of nitrogen in diamond and the 270-nm absorption band. *Physical Review B*, Vol. 80, No. 3, Article 033205, <http://dx.doi.org/10.1103/PhysRevB.80.033205>
- King J.M., Moses T.M., Shigley J.E., Liu Y. (1994) Color grading of colored diamonds in the GIA Gem Trade Laboratory. *G&G*, Vol. 30, No. 4, pp. 220–242, <http://dx.doi.org/10.5741/GEMS.30.4.220>
- King J.M., Shigley J.E., Gelb T.H., Guhin S.S., Hall M., Wang W. (2005) Characterization and grading of natural-color yellow diamonds. *G&G*, Vol. 41, No. 2, pp. 88–115, <http://dx.doi.org/10.5741/GEMS.41.2.88>
- King J.M., Geurts R.H., Gilbertson A.M., Shigley J.E. (2008) Color grading “D-to-Z” diamonds at the GIA Laboratory. *G&G*, Vol. 44, No. 4, pp. 296–321, <http://dx.doi.org/10.5741/GEMS.44.4.296>
- Kitawaki H., Hisanaga M., Yamamoto M., Emori K. (2015) Type Ib yellow to brownish yellow CVD synthetic diamonds seen at CGL. *Journal of Gemmology*, Vol. 34, No. 7, pp. 594–604.
- Lai M.Y., Stachel T., Breeding C.M., Stern R. (2019) Yellow diamonds with colourless cores – evidence for episodic diamond growth beneath Chidliak and the Ekati mine, Canada. *Mineralogy & Petrology*, Vol. 114, No. 2, pp. 91–103, <http://dx.doi.org/10.1007/s00710-020-00693-0>
- Liddicoat R.T. (1976) True canary. *G&G*, Vol. 15, No. 8, p. 235.

- Liddicoat R.T., Ed (1993) *The GIA Diamond Dictionary*. Gemological Institute of America, Santa Monica, CA, 275 pp.
- Manutchehr-Danai M. (2013) *Dictionary of Gems and Gemology*. Springer Science & Business Media, p. 186.
- Massi L., Fritsch E., Collins A.T., Hainschwang T., Notari F. (2005) The "amber centres" and their relation to the brown colour. *Diamond and Related Materials*, Vol. 14, No. 10, pp. 1623–1629, <http://dx.doi.org/10.1016/j.diamond.2005.05.003>
- Rondeau B., Fritsch E., Guiraud M., Chalain J.-P., Notari F. (2004) Three historical 'asteriated' hydrogen-rich diamonds: Growth history and sector-dependent impurity incorporation. *Diamond and Related Materials*, Vol. 13, No. 9, pp. 1658–1673, <http://dx.doi.org/10.1016/j.diamond.2004.02.002>
- Scarratt K. (1984) "Chameleon diamonds." *Journal of Gemmology*, Vol. 19, No. 2, pp. 98–100.
- Shigley J.E., Breeding C.M. (2013a) Gem News International: Bright yellow diamonds from Sierra Leone. *G&G*, Vol. 49, No. 4, pp. 259–260.
- (2013b) Optical defects in diamond: A quick reference chart. *G&G*, Vol. 49, No. 2, pp. 107–111, <http://dx.doi.org/10.5741/GEMS.49.2.107>
- Shiryaev A.A., Wiedenbeck M., Hainschwang T. (2010) Oxygen in bulk monocrystalline diamonds and its correlations with nitrogen. *Journal of Physics: Condensed Matter*, Vol. 22, No. 4, 6 pp., <http://dx.doi.org/10.1088/0953-8984/22/4/045801>
- Smit K.V. (2008) Diamond formation in craton margin settings: Mesoproterozoic age of Ellendale peridotitic diamonds (Western Australia). Master's thesis, University of Cape Town, South Africa.
- Smit K.V., Shor R. (2017) Geology and development of the Lomonosov diamond deposit, northwestern Russia. *G&G*, Vol. 53, No. 2, pp. 144–167, <http://dx.doi.org/10.5741/GEMS.53.2.144>
- Smit K.V., D'Haenens-Johansson U.F.S., Howell D., Loudin L.C., Wang W. (2018) Deformation-related spectroscopic features in natural type Ib-IaA diamonds from Zimmi (West African craton). *Mineralogy and Petrology*, Vol. 112, Supp. 1, pp. 243–257, <http://doi.org/10.1007/s00710-018-0587-6>
- Smit K.V., Shirey S.B., Wang W. (2016) Type Ib diamond formation and preservation in the West African lithospheric mantle: Re-Os age constraints from sulphide inclusions in Zimmi diamonds. *Precambrian Research*, Vol. 286, pp. 152–166, <http://dx.doi.org/10.1016/j.precamres.2016.09.022>
- Smith E.M., Shirey S.B., Richardson S.H., Nestola F., Bullock E.S., Wang J., Wang W. (2018) Blue boron-bearing diamonds from Earth's lower mantle. *Nature*, Vol. 560, No. 7716, pp. 84–87, <http://dx.doi.org/10.1038/s41586-018-0334-5>
- Thompson R. (2004) The Tiffany Yellow. Famous, Historic and Notable Diamonds. <http://famousdiamonds.tripod.com/tiffanyyellowdiamond.html>
- Titkov S.V., Mineeva R.M., Zudina N.N., Sergeev A.M., Ryabchikov I.D., Shiryaev A.A., Speransky A.V., Zhikhareva V.P. (2015) The luminescent nature of orange coloration in natural diamonds: optical and EPR study. *Physics and Chemistry of Minerals*, Vol. 42, No. 2, pp. 131–141, <http://dx.doi.org/10.1007/s00269-014-0705-x>
- Wang W., Mayerson W. (2002) Symmetrical clouds in diamond – the hydrogen connection. *Journal of Gemmology*, Vol. 28, No. 3, pp. 143–152.
- Wang W., Poon T. (2018) Canary yellow diamonds. *G&G*, Vol. 54, No. 3, pp. 262–263.
- Welbourn C.M., Cooper M., Spear P.M. (1996) De Beers natural versus synthetic diamond verification instruments. *G&G*, Vol. 32, No. 3, pp. 156–169, <http://dx.doi.org/10.5741/GEMS.32.3.156>
- Yelissev A., Kanda H. (2007) Optical centers related to 3d transition metals in diamond. *New Diamond and Frontier Carbon Technology*, Vol. 17, pp. 127–178.
- Zaitsev A.M. (2003) *Optical Properties of Diamond: A Data Handbook*. Springer-Verlag, Berlin.

For online access to all issues of GEMS & GEMOLOGY from 1934 to the present, visit:

gia.edu/gems-gemology



SEPARATION OF NATURAL FROM LABORATORY-GROWN DIAMOND USING TIME-GATED LUMINESCENCE IMAGING

Colin D. McGuinness, Amber M. Wassell, Peter M.P. Lanigan, and Stephen A. Lynch

A technique that expands on the surface luminescence imaging used in the DiamondView instrument has been developed at De Beers Group Technology, Maidenhead, UK. This provides an additional level of imaging information by way of separating prompt and delayed surface luminescence. The technique has the added benefit of quickly and easily distinguishing colorless or near-colorless natural diamond from laboratory-grown diamond. It can be applied when the identification of natural diamond is required in the study of single stones, multiples in batches, set jewelry, or in a fully automated process. The prompt and delayed luminescence characteristics of natural diamond are compared with a range of chemical vapor deposition (CVD) and high-pressure, high-temperature (HPHT) synthetic diamonds. Of significant interest are some of the less common CVD synthetic samples that have been observed in recent years. This article will summarize the luminescence observed in different diamond types, discuss its spectral characteristics, and serve as a useful reference when interpreting such luminescence images.

The task of identifying a diamond will typically fall to a diamond appraiser, grader, or gemologist while preparing a grading certificate or appraisal. Whether a diamond is natural or lab-grown is a key factor in its market value and is of paramount importance to the gemologist. Many characteristics can be used to distinguish between natural and synthetic diamond, but the inherent variability in the properties of natural and synthetic diamond can make such a task difficult.

A useful and proven characteristic is the emission of luminescence when a diamond is excited by a source of ultraviolet energy. Typically, a gemologist would utilize an ultraviolet lamp with excitation wavelengths of 365 nm (long-wave ultraviolet, LWUV) or 254 nm (short-wave ultraviolet, SWUV), which correspond to the emission lines of a low-pressure mercury-vapor lamp. In this application, “fluorescence” would be observed during ultraviolet excitation, while “phosphorescence” may be observed when the excitation is removed.

The De Beers DiamondView instrument (Spear and Welbourn, 1994; Welbourn et al., 1996) was de-

signed to authenticate natural diamonds and synthetic diamonds. It allows a more sophisticated observation to be made by way of a shorter wavelength excitation of <225 nm corresponding to the primary absorption edge and only exciting around 1-micron depth of material, such that observed luminescence

In Brief

- Correctly identifying natural versus laboratory-grown diamond is important for its market value and maintaining consumer confidence.
- A time-gated imaging technique has been developed at De Beers Group Technology to allow easy separation of colorless/near-colorless natural and synthetic diamond.
- A blue delayed luminescence can be used as a specific marker for identification of >99% of natural type IIa and type Ia diamond.

can be considered as produced at the surface. Studies have shown (Martineau et al., 2004) that such luminescence imaging techniques can provide very useful information for identifying all synthetic diamond types. That article reported the identification of all CVD synthetics under study using DiamondView

See end of article for About the Authors and Acknowledgments.

GEMS & GEMOLOGY, Vol. 56, No. 2, pp. 220–229,

<http://dx.doi.org/10.5741/GEMS.56.2.220>

© 2020 Gemological Institute of America



Figure 1. The De Beers SYNTHdetect, an instrument designed for screening of colorless to near-colorless diamonds of all cuts mounted in jewelry. Loose stones can also be screened with no lower size limit. The dimensions of the instrument are 31.0 cm wide × 34.0 cm deep × 45.8 cm high. A range of jewelry holders and a flat sample tray are included. Photo by Danny Bowler/De Beers Group Industry Services.



Figure 2. The De Beers AMS2, an instrument for automated screening of small colorless to near-colorless diamonds for potential synthetics and simulants at rates of up to 3,600 samples/hour. The size range is 0.003–0.20 ct for round brilliants and 0.01–0.20 ct for all other cuts. The instrument measures 31.5 cm wide × 40.0 cm deep × 55.0 cm high. Photo by Danny Bowler/De Beers Group Industry Services.

imaging, with techniques such as X-ray topography providing supporting evidence in more challenging cases. More recently, a set of color emission filters has been included with the DiamondView instrument to assist with some of the more challenging silicon-doped CVD synthetics that exhibit a degree of luminescence toward the red end of the spectrum, normally swamped by blue dislocation luminescence (Martineau, 2017).

To help negate the need for further time-consuming and expensive investigation, and to assist less experienced gemologists, the imaging technique employed by the DiamondView has been extended by way of hardware synchronization of the light source and camera (Smith et al., 2017), allowing camera exposures to be controlled relative to the lamp pulse with microsecond accuracy. As the temporal characteristics of diamond luminescence can be complex and the distinction between fluorescence and phosphorescence is not always clear, we use the term *prompt luminescence* to describe luminescence recorded at the same time as the lamp pulse, with *delayed luminescence* recorded after the lamp pulse.

There have been numerous “time-resolved” methods used to study the complex temporal nature of diamond luminescence. These methods can in-

clude time-gated luminescence (Khong et al., 1994; Lindblom et al., 2003; Lipatov et al., 2007), single-photon counting (Thomaz and Davies, 1978), and time-correlated single-photon counting (TCSPC) (Li-angaudas et al., 2009; Jones et al., 2020), to name a few. The method described in this article can be used to positively identify a natural type IIa or type Ia colorless diamond by accurately imaging a weak delayed luminescence having peak emission at 455 nm and a characteristic unquenched decay constant of 8.8 ms. An example of a quenched (i.e., a decrease in the luminescence efficiency and a reduction of the measured decay time) luminescence decay, which has been observed in type IIa and type Ia natural diamonds, will be shown for comparison. The absence of the blue delayed luminescence, quenched or unquenched, would indicate that a sample may be type IIb natural, unusual type Ia natural, synthetic, or simulant and would require further testing to verify its origin. The De Beers Group screened many millions of individual colorless diamonds to verify this concept, and it is this principle that is used in both the De Beers SYNTHdetect jewelry screening instrument and the second version of the Automated Melee Screener (AMS2) (figures 1 and 2) (Martineau and McGuinness, 2018).

More recently, this technique has identified a previously unknown green luminescence feature at 499 nm (Wassell et al., 2018) observable in lab-grown diamonds obtained from Gemesis Inc. (now Pure Grown Diamonds) and in silicon-containing samples sourced by Element Six that had undergone post-growth annealing.

MATERIALS AND METHODS

A selection of colorless/near-colorless natural and lab-grown polished diamond samples were chosen for this study, the details of which are listed in table 1. The samples are not an exhaustive set but were chosen to demonstrate the wide range of prompt and delayed luminescence characteristics that can be observed, and to provide a useful reference source for operators interpreting output from the SYNTHdetect instrument.

Microsecond time-gated imaging was carried out using a Teledyne Dalsa Genie Nano C2050 area-scan CMOS camera. Above-diamond band-gap excitation was provided by a Hamamatsu Photonics L7685 xenon flash lamp spectrally filtered to 190–227 nm output, with a temporal pulse width of 2.9 μ s at full width half maximum. The camera and flash lamp were synchronized using the camera's internal timer, with the flash lamp signal offset by 11 μ s with respect to the timer to account for the difference in latency between the two devices. Images shown represent an average of 20 individual captures. These images are at 1.5 \times magnification as opposed to 0.25 \times in SYNTHdetect for the purposes of this publication.

TABLE 1. Diamond samples from this study.

Sample	Description	Shape and Cutting Style
D1	Type IIa natural	Round brilliant
D2	Green-fluorescing type Ia natural	Round brilliant
D3	Unusual natural	Round brilliant
D4	Weak type IIb natural	Round brilliant
C1	As-grown nitrogen-containing CVD	Round brilliant
C2	CVD of Chinese origin	Round brilliant
C3	Gemesis CVD synthetic	Modified square brilliant
C4	Diamond Foundry CVD	Round brilliant
C5	CVD of unknown origin	Round brilliant
S1	Typical HPHT synthetic	Round brilliant

Room-temperature spectral data was collected by an Andor iStar DH320T-18U-E3 intensified CCD camera via a Horiba iHR-320 spectrometer, with excitation from the same source as the imaging setup. Synchronization with the flash lamp and camera was supplied by two externally generated pulsed signals offset in a similar way to the imaging setup. To record prompt luminescence, the intensifier delay was set to zero, with emission integrated over a 5 μ s gate. To record delayed luminescence, the intensifier delay was set to 100 μ s or more, with emission integrated over a chosen gate. Here, 40 accumulations were averaged. A simplified diagram illustrating the principle of time-gated luminescence is shown in figure 3.

Selected room-temperature delayed luminescence decay data was collected by a Horiba Jobin Yvon IBH TBX-04 thermoelectrically cooled photomultiplier

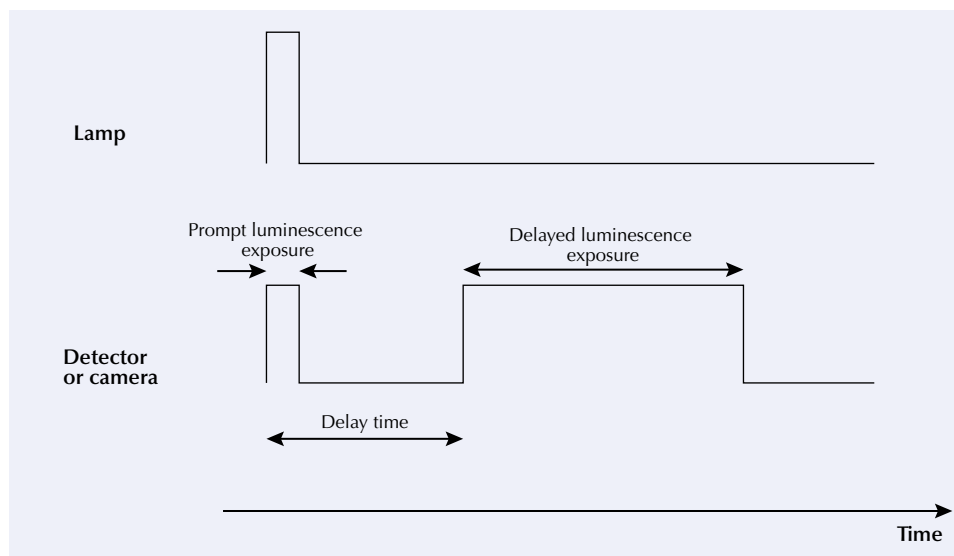


Figure 3. Simplified diagram of time-gated luminescence. To acquire a delayed spectrum or a delayed image, the detector or camera is activated after a delay, which ensures that the prompt luminescence has decayed almost to zero. Switching the detector or camera on and off is analogous to the opening and closing of a gate. To detect the prompt luminescence, and reject the delayed luminescence, the detector is turned on only when the lamp is on.

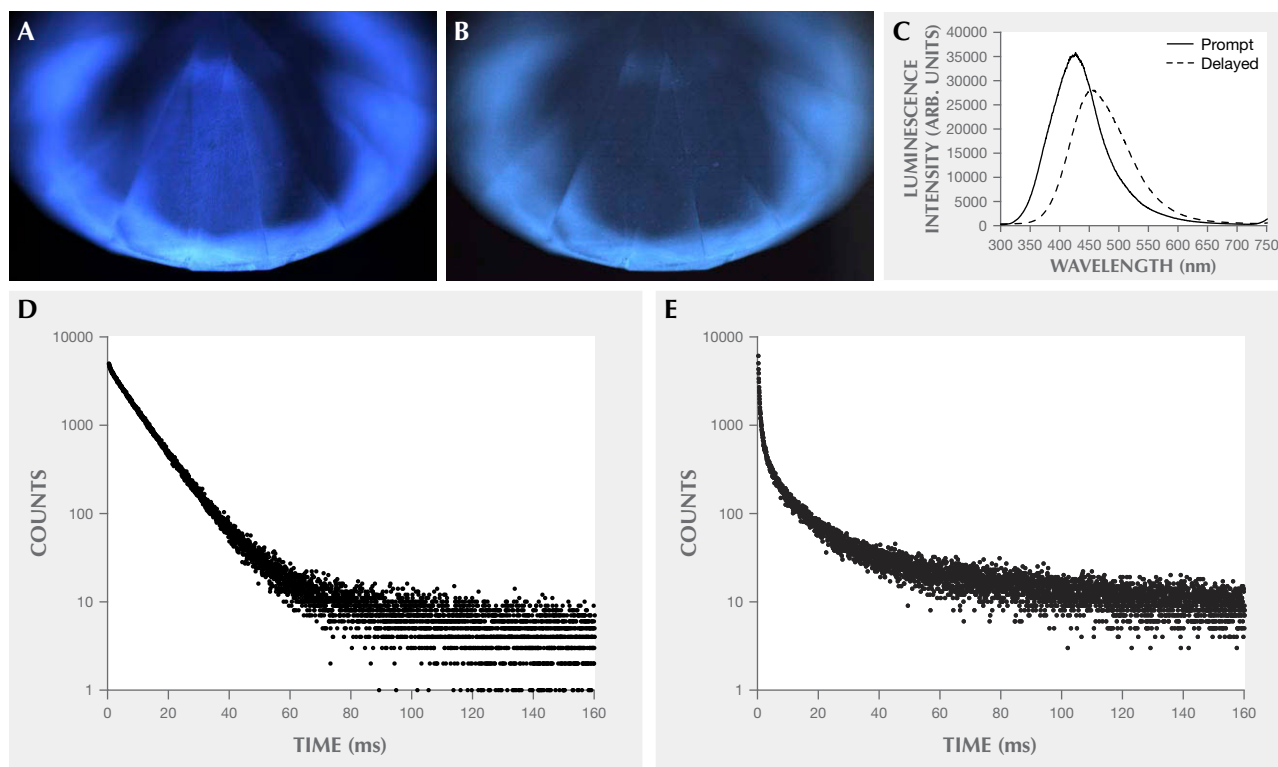


Figure 4. A: CMOS image of sample D1 showing the spatial distribution of the prompt blue dislocation-related luminescence signal exhibited by a typical type IIa natural diamond. B: CMOS image showing the delayed luminescence signal exhibited. Recorded with a delay of 100 μ s after the rising edge of the UV pump pulse and integrated for 30 ms. C: Prompt (peak at 435 nm) and delayed (peak at 455 nm) luminescence recorded for sample D1. Delayed luminescence was recorded with a delay of 100 μ s after the rising edge of the UV pump pulse and integrated for 30 ms. D: Delayed luminescence decay profile of sample D1. In this example, the decay is unquenched and can be fitted to a simple monoexponential function with decay constant 8.8 ms. Type Ia natural diamonds may also show unquenched decays. E: Example of a quenched decay seen in type IIa and type Ia natural diamonds. It would not be possible to distinguish this from an unquenched example using the imaging setup. At the time of this writing, it is not fully understood what processes would contribute to a quenching of this delayed luminescence.

module via a Horiba iHR320 spectrometer with excitation as above. Detector and flash lamp were triggered simultaneously, with channels recording both prompt and delayed luminescence in each time sweep of the multichannel analyzer. The time spacing of the channels was selected to suit the decay time being measured. After the data were accumulated, the channels recording prompt luminescence were rejected.

RESULTS

Natural Diamonds. The luminescence characteristics of a typical type IIa natural diamond are shown in the figure 4 set. The prompt luminescence (figure 4A) is dominated by blue luminescence from dislocations and is identical to that seen in the Diamond-

View instrument. The delayed luminescence (figure 4B) cannot be observed in DiamondView images due to the weak nature of the luminescence and the fact that it is masked by the prompt dislocation luminescence. It can be seen from the imaging that the blue delayed luminescence is not related to the blue dislocation prompt luminescence. The spectral data (figure 4C) and decay data (figure 4D) also show that it does not arise from N3 defect fluorescence. Figure 4E is an example of quenched blue delayed luminescence decay and is shown for comparison with the unquenched decay of sample D1. This blue delayed luminescence is the specific marker used by AMS2 and SYNTHdetect as a positive identifier of natural diamond, as it is not seen in synthetic diamonds.

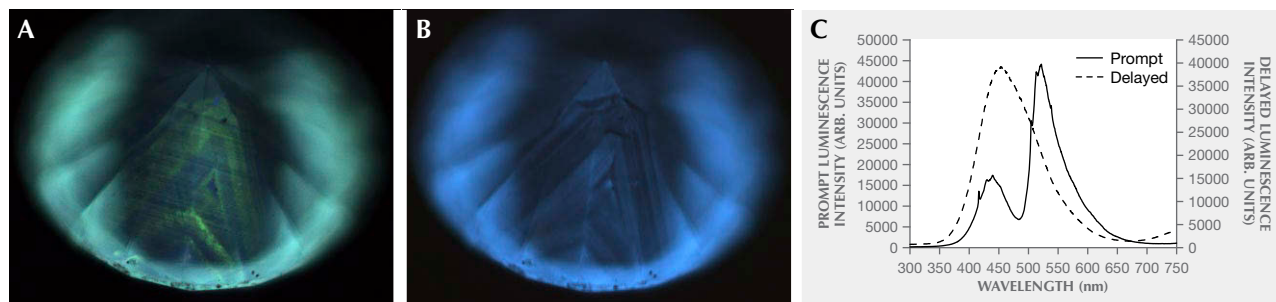


Figure 5. A: CMOS image of sample D2 showing the prompt green luminescence related to the H3 defect in type Ia natural diamond. Underlying prompt blue luminescence attributed to the N3 defect is also observed. B: CMOS image showing the blue delayed luminescence signal. In this case, structure is observed in the delayed luminescence signal, similar to the prompt luminescence signal. C: Prompt and delayed (peak at 455 nm) luminescence recorded for sample D2 showing green prompt luminescence. Delayed luminescence recorded with a delay of 100 μ s after the rising edge of the UV pump pulse and integrated for 30 ms.

This was confirmed in tests by De Beers Group on over 20 million individual colorless diamonds. In addition, the Diamond Producers Association ASSURE program found that less than 1% of natural diamonds do not exhibit this luminescence and would be referred for further testing (Dupuy and Phillips, 2019). At the time of writing, the origin of this luminescence is not fully understood.

The diamond in figure 5A is a predominantly “green-fluorescing” example where the green prompt luminescence is attributed to the H3 defect and the blue to the N3 defect, as shown by the spectral data in figure 5C. The spectral data further show that the delayed luminescence is not related to N3 defect fluorescence, although the delayed luminescence image (figure 5B) shows that it is predominantly in the same spatial region of the stone as the N3 luminescence, which may suggest it is related to higher aggregated states of nitrogen such as B-centers.

Diamond D3 is a slightly more unusual natural diamond in that it exhibits blue prompt luminescence (figure 6A) and a blue/green delayed luminescence (figure 6B). The green delayed luminescence component is due to the H3 defect (figure 6D). This phenomenon has been reported previously and attributed to the population of triplet states within the defect (Pereira and Monterio, 1991). In this sample, the spectral data also show a small contribution of H3 in the prompt luminescence. By extending the delay from 100 μ s to 2 ms (figure 6C), it can be seen that the delayed green luminescence from H3 decays much faster than the blue delayed luminescence used to identify natural diamond. Therefore, in examples such as these, increasing the camera

delay time from the microsecond range to the millisecond range reduces the fast-decaying green components, allowing the underlying blue luminescence to be observed—a feature that is available to users of the SYNTHdetect instrument. Extensive testing by De Beers indicates that ~0.5% of natural diamonds would exhibit luminescence properties such as this.

The figure 7 set illustrates a typical example of a colorless weak type IIb natural diamond, sample D4. This would show turquoise-colored long-lived delayed luminescence in the DiamondView. In figure 7A, the underlying blue dislocation prompt luminescence can be clearly seen as the long-lived turquoise delayed luminescence shown in figure 7B is gated out. This prompt luminescence would be nearly impossible to observe in the DiamondView due to the unsynchronized nature of the lamp and camera and the strong long-lived delayed luminescence, which would quickly mask the blue prompt luminescence. Indeed, a continual live feed of this prompt luminescence image is not possible in the DiamondView. Figure 7C illustrates the spectral profile, with the peak of the prompt luminescence at 425 nm and the peak of the delayed luminescence at 480 nm commonly seen in such diamonds. Due to the high resolution and higher magnification of these images, it is possible to identify this as natural diamond from the dislocation patterns in the prompt luminescence. However, in a lower-magnification system such as the SYNTHdetect, which is designed to look at an ensemble of diamonds in jewelry, the dislocation patterns may not be visible and such a diamond would need to be referred for further testing. This is due to the potential

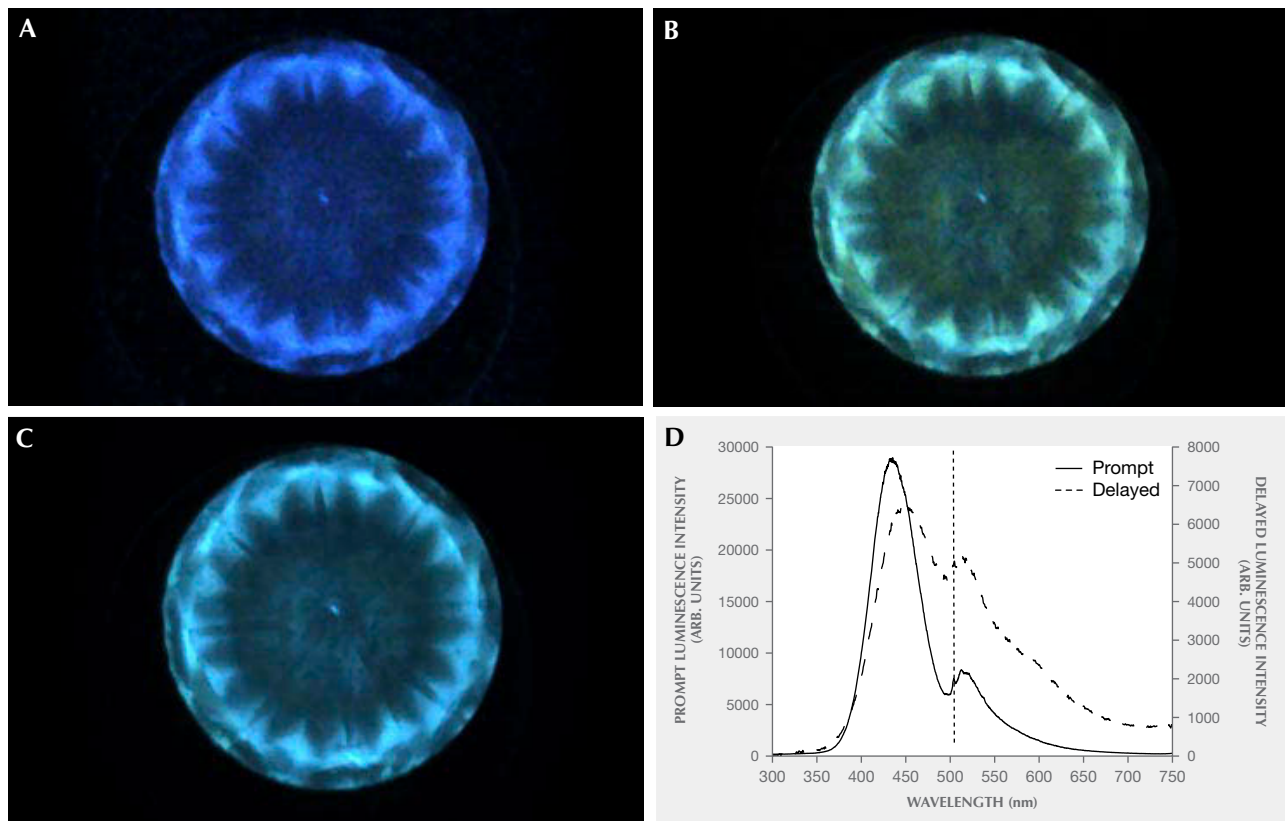
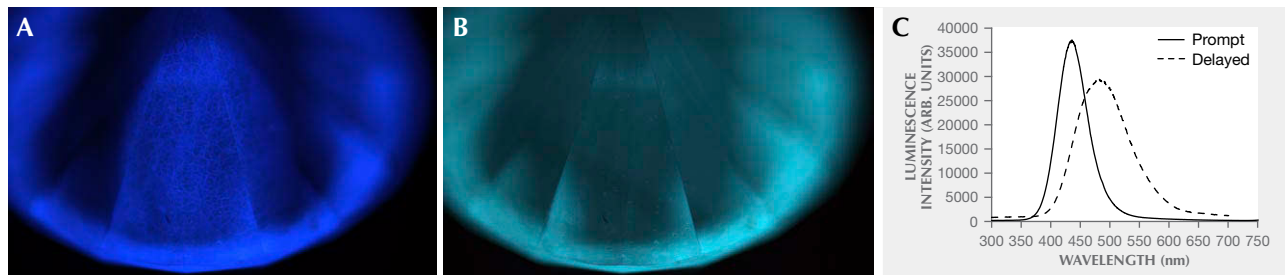


Figure 6. A: CMOS image of sample D3 showing the prompt luminescence from a slightly more unusual natural diamond. B: CMOS image of sample D3 showing a more unusual blue/green delayed luminescence signal in a natural diamond. Recorded with a delay of 100 μ s after the rising edge of the UV pump pulse and integrated for 30 ms. C: CMOS image showing the delayed luminescence recorded with a longer delay of 2 ms after the rising edge of the UV pump pulse and integrated for 30 ms. The green luminescence component has decayed. D: Prompt and delayed luminescence recorded for sample D3 showing both blue and green delayed luminescence. Delayed luminescence, recorded with a delay of 100 μ s after the rising edge of the UV pump pulse and integrated for 30 ms, corresponds to figure 6B. The dotted line at 503 nm indicates the H3 zero-phonon line common to prompt and delayed luminescence.

for certain synthetic types to produce prompt blue luminescence and delayed turquoise luminescence.

CVD Synthetic Diamonds. Sample C1 is a typical as-grown CVD synthetic diamond that displays or-

Figure 7. A: CMOS image of sample D4 showing the spatial distribution of the prompt blue dislocation-related luminescence signal exhibited by a typical type IIb natural diamond. B: CMOS image showing the delayed luminescence signal exhibited. Recorded with a delay of 100 μ s after the rising edge of the UV pump pulse and integrated for 30 ms. C: Prompt and delayed (peak at 480 nm) luminescence recorded for sample D4. Delayed luminescence recorded with a delay of 100 μ s after the rising edge of the UV pump pulse and integrated for 30 ms.



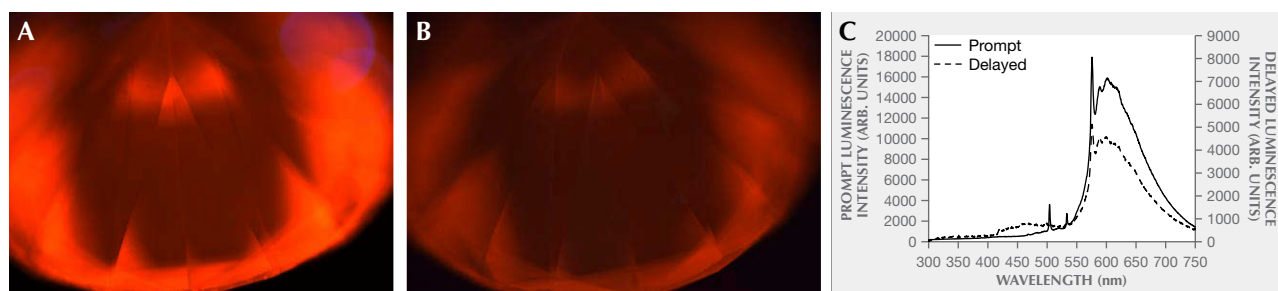


Figure 8. A: CMOS image of sample C1 showing the prompt luminescence from a typical as-grown CVD synthetic diamond. B: CMOS image showing the delayed luminescence signal exhibited. Recorded with a delay of 100 μ s after the rising edge of the UV pump pulse and integrated for 60 ms. C: Prompt and delayed luminescence recorded for sample C1. Delayed luminescence recorded with a delay of 100 μ s after the rising edge of the UV pump pulse and integrated for 60 ms.

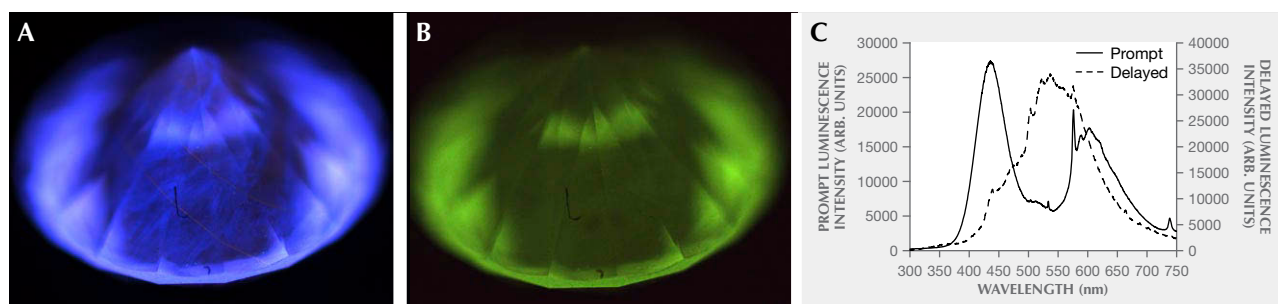
ange prompt luminescence (figure 8A), primarily from the NV⁰ defect (figure 8C). An interesting effect noticed in this type of diamond is the delayed orange luminescence (figure 8B). Spectral analysis shows that this also originates from the NV⁰ defect. It can be concluded that the NV⁰ defect can experience emission from spin-forbidden transitions in a way similar to the H3 defect (Pereira and Monterio, 1991), although this discussion is beyond the scope of this article.

Diamond C2 is a commercially available CVD synthetic made in China. Figure 9A shows blue dislocation luminescence with discrete narrow bands and a weak general underlying red luminescence. Spectral data in figure 9C shows that the red prompt luminescence is predominantly from the NV⁰ defect. The delayed green luminescence in this example (figure 9B) is due to the H3 defect. Delayed luminescence from the H3 defect has been discussed for the natural diamond D3 (again, see figure 6). It is also a

good indication that this synthetic diamond has undergone post-growth annealing, as this delayed luminescence has been previously observed in such samples that have undergone annealing at around 1700°C (Wassell et al., 2018).

Sample C3 is a commercially available CVD synthetic diamond from Gemesis that has been reported previously (Wassell et al., 2018). At first glance, the delayed luminescence CMOS image (figure 10B) appears very similar to that of sample C2 in figure 9. However, the spectral data highlight that this luminescence, although similar in color, originates from an entirely different defect, with a zero-phonon line at 499 nm (figure 10C). This defect has been shown to be generated by post-growth annealing at around 1700°C. This sample is of interest in diamond verification, as it exhibits blue prompt luminescence from dislocation patterns in local regions (figure 10A) and could be incorrectly identified as a type IIa natural by a low-magnification system or an instru-

Figure 9. A: CMOS image of sample C2 showing the prompt luminescence from a commercially available CVD synthetic of Chinese origin. B: CMOS image showing the delayed luminescence signal exhibited. Recorded with a delay of 100 μ s after the rising edge of the UV pump pulse and integrated for 60 ms. C: Prompt and delayed luminescence recorded for sample C2. Delayed luminescence recorded with a delay of 100 μ s after the rising edge of the UV pump pulse and integrated for 60 ms.



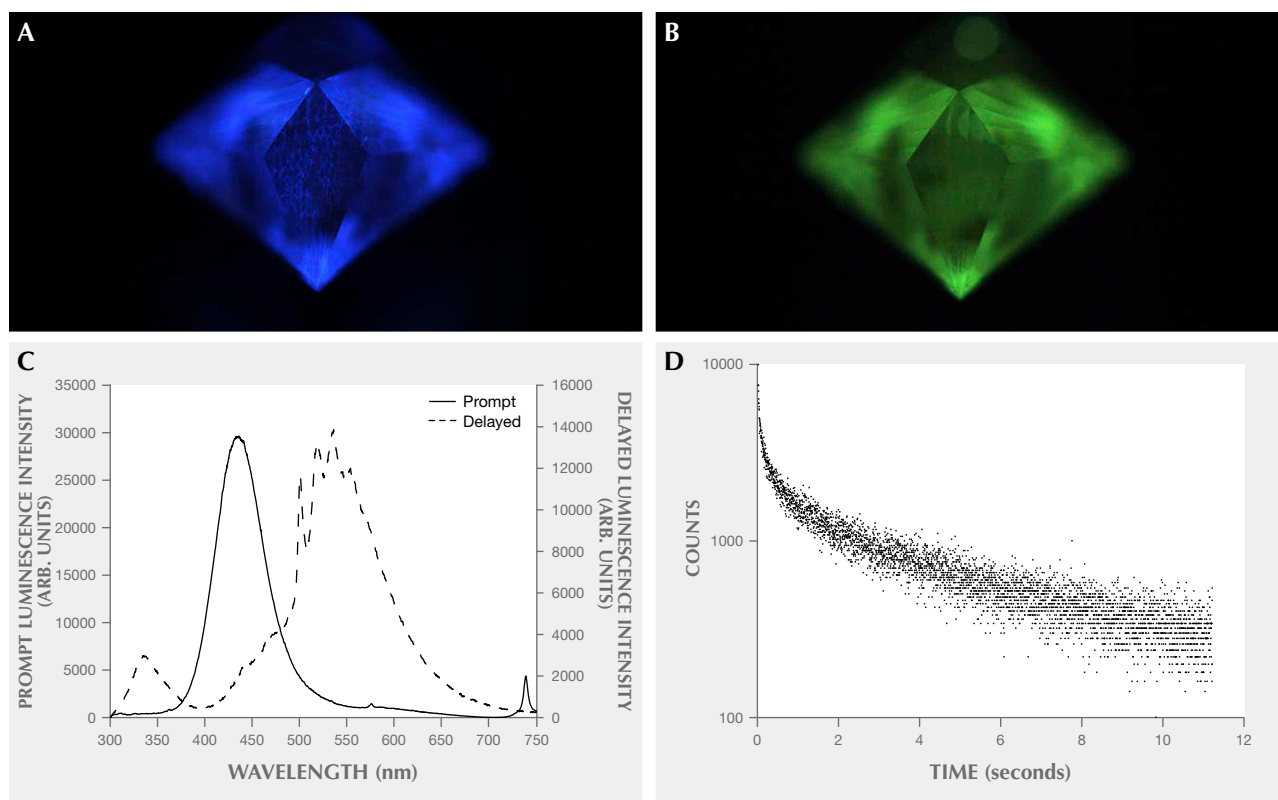


Figure 10. A: CMOS image of sample C3 showing the spatial distribution of the prompt blue luminescence signal for a commercially available Gemesis CVD synthetic. B: CMOS images of the delayed 499 nm luminescence signal, with a delay of 100 μ s after the rising edge of the UV pump pulse and integrated for 60 ms. C: Prompt and delayed (499 nm ZPL) luminescence recorded for sample C3. Delayed luminescence recorded with a delay of 100 μ s after the rising edge of the UV pump pulse and integrated for 60 ms. D: Delayed luminescence decay profile of a blue-fluorescing Si-containing CVD synthetic. In this example, the decay is complex and non-exponential. An average decay time of \sim 1 sec is observed.

ment with a low-resolution camera where blue fluorescence is used as a natural identifier. Figure 10D shows the delayed luminescence decay profile for the 499 nm feature. It should not be assumed, however, that this observed decay is the decay profile for the 499 nm feature in general. Rather, it is the decay profile of the 499 nm feature in this sample. It was also suggested by Wassell et al. (2018) that prompt luminescence of 499 nm could not be ruled out due to swamping by blue prompt luminescence.

A commercially available CVD synthetic diamond from Diamond Foundry (sample C4) shows both a green prompt and green delayed luminescence (figures 11A and 11B). Again, this could be attributed to the H3 defect, but spectral data (figure 11C) show that this is a result of the 499 nm feature in both prompt and delayed luminescence.

Sample C5 is a commercially available CVD diamond of unknown origin. Figure 12A shows growth bands roughly perpendicular to the growth direction

in the prompt luminescence, consistent with CVD synthesis. The spectral data presented in figure 12C show that this luminescence is predominantly from the 499 nm feature with components at 575 nm (the NV⁰ defect) and at 415 nm (the N3 defect), although this level of imaging does not show these defects in specific localized areas. Interestingly, the delayed luminescence seen in figure 12B does not show as prominent growth band patterns, suggesting the delayed turquoise luminescence does not form these patterns in the same way as the prompt luminescence. The spectral data show that the delayed luminescence is dominated by the broad turquoise feature with only a small level of the 499 nm feature visible. This sample also indicates that the 499 nm feature can experience both prompt and delayed emission.

HPHT Synthetic Diamond. Sample S1 is an example of a typical commercially sourced HPHT syn-

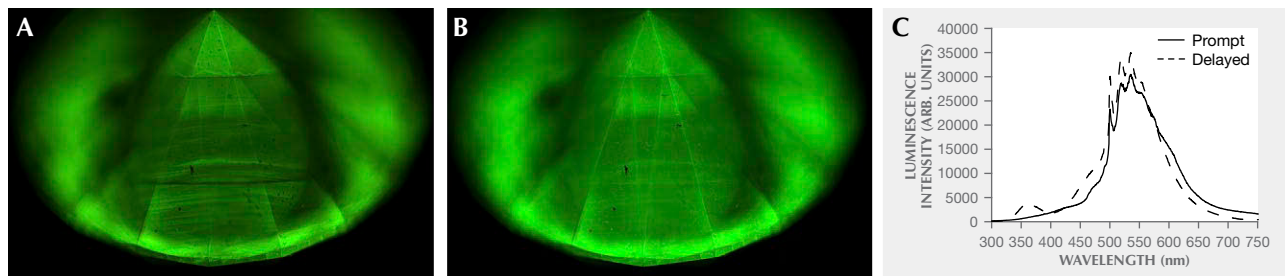


Figure 11. A: CMOS image of sample C4 showing prompt green luminescence from the 499 nm feature for a commercially available Diamond Foundry CVD synthetic. B: CMOS image of the delayed 499 nm luminescence signal, with a delay of 100 μ s after the rising edge of the UV pump pulse and integrated for 60 ms. C: Prompt and delayed luminescence recorded for sample C4. Delayed luminescence recorded with a delay of 100 μ s after the rising edge of the UV pump pulse and integrated for 60 ms.

thetic diamond. The delayed luminescence (figure 13B) is identical to the strong long-lived luminescence that would be observed in the DiamondView. This long-lived luminescence is understood and has been reported as being interpretable in terms of a donor-acceptor recombination model (Watanabe et al., 1997). Of interest here is the prompt luminescence (figure 13A), which is a weak green/red and would normally be obscured by the long-lived luminescence in the DiamondView. This luminescence could be due to the presence of metal ions in the solvent catalyst. However, the prompt luminescence spectrum shown in figure 13C, along with the delayed luminescence, is broad and featureless at room temperature and gives little in the way of information.

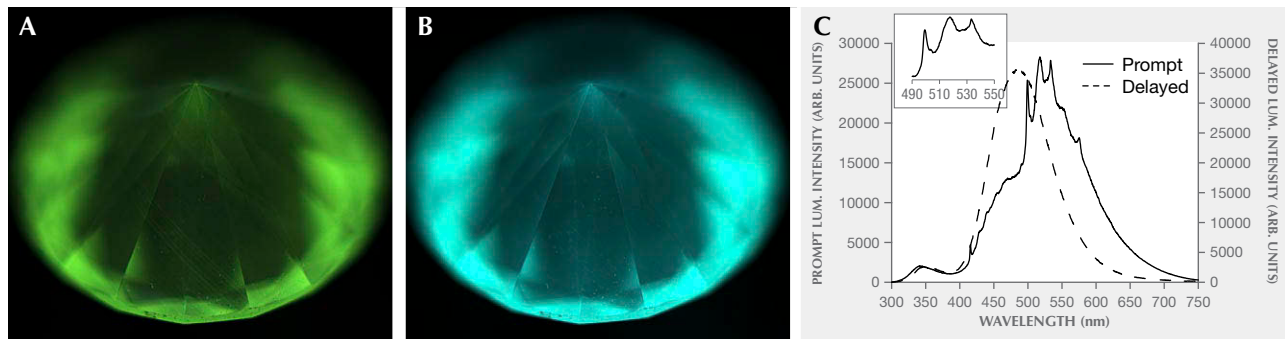
This weak green prompt luminescence and strong long-lived turquoise luminescence are typical of many HPHT synthetics. They can be used as an iden-

tifying feature, as this combination of luminescence features have not been seen in natural diamond.

CONCLUDING COMMENTS

Diamond screening is becoming increasingly challenging, and organizations other than gemological laboratories, such as independent jewelers, auction houses, and pawnbrokers, are charged with this important task. Not only are more sophisticated techniques required to assist with this challenge, but the equipment must not be so complex to use and difficult to understand that diamond screening becomes an overly time-consuming and inefficient task. In this article, a selection of natural and lab-grown polished colorless diamonds has been studied using deep-UV excitation where the recording of the luminescence is synchronized with the excitation source, allowing a time-gated measurement. This technique provides a useful additional level of verification when screening

Figure 12. A: CMOS image of sample C5 showing the spatial distribution and growth bands perpendicular to the growth direction in the prompt green luminescence signal exhibited by a commercially available CVD synthetic diamond. B: CMOS image showing the delayed turquoise-colored luminescence signal exhibited. The growth patterns in the prompt luminescence are less prominent here. C: Prompt and delayed luminescence recorded for sample C5. Delayed luminescence recorded with a delay of 100 μ s after the rising edge of the UV pump pulse and integrated for 60 ms. The inset zooms in on the region of the 499 nm ZPL.



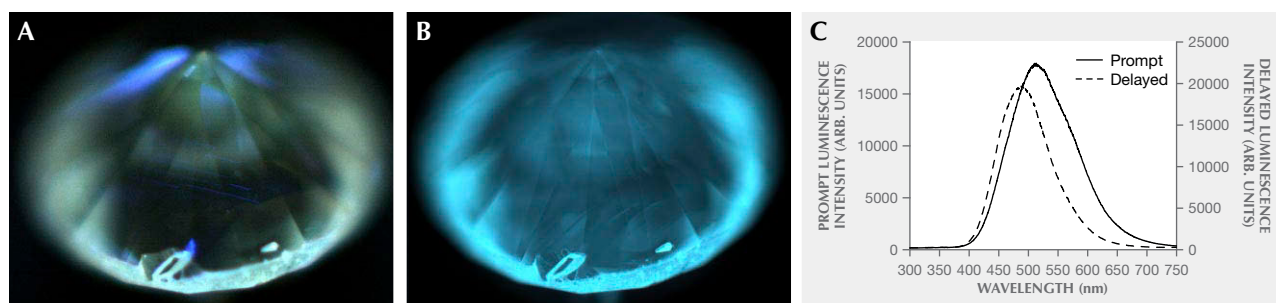


Figure 13. A: CMOS image of sample S1 showing a prompt green/red luminescence from a typical colorless HPHT synthetic diamond. B: CMOS image of sample S1 showing the delayed luminescence from a typical colorless HPHT synthetic—normally attributed to the presence of boron. C: Prompt (peak ~513 nm) and delayed (peak ~480 nm) luminescence recorded for sample S1. Delayed luminescence recorded with a delay of 100 μ s after the rising edge of the UV pump pulse and integrated for 10 ms.

for challenging synthetics such as blue-fluorescing CVD synthetics. Although the examples contained in this article are not an exhaustive list, they should

serve as a useful reference guide and knowledge base for all SYNTHdetect users when studying individual samples or screening challenging examples.

ABOUT THE AUTHORS

Dr. McGuinness is a senior scientist, and Dr. Lanigan is a research scientist, at De Beers Group Technology, Maidenhead, Berkshire, United Kingdom. Ms. Wassell is a doctoral student, and Dr. Lynch is associate dean of research, at the School of Physics & Astronomy, Cardiff University, Cardiff, United Kingdom.

ACKNOWLEDGMENTS

The authors would like to thank Mr. Hugh Leach at De Beers Group Technology for mechanical engineering and instrument development effort, and to the team at Element Six whose samples were used extensively in the development of this technique.

REFERENCES

- Dupuy H., Phillips J.C. (2019) Selecting a diamond verification instrument based on the results of the Assure program: An initial analysis. *Journal of Gemmology*, Vol. 36, pp. 606–619.
- Jones D.C., Kumar S., Lanigan P.M.P., McGuinness C.D., Dale M.W., Twitchen D.J., Fisher D., Martineau P.M., Neil M.A.A., Dunsby C., French P.M.W. (2020) Multidimensional luminescence microscope for imaging defect colour centres in diamond. *Methods and Applications in Fluorescence*, Vol. 8, No. 1, 014004, <http://dx.doi.org/10.1088/2050-6120/ab4eac>
- Khong Y.L., Collins A.T., Allers L. (1994) Luminescence decay time studies and time-resolved cathodoluminescence spectroscopy of CVD diamond. *Diamond and Related Materials*, Vol. 3, No. 7, pp. 1023–1027, [http://dx.doi.org/10.1016/0925-9635\(94\)90112-0](http://dx.doi.org/10.1016/0925-9635(94)90112-0)
- Liaugaudas G., Collins A.T., Suhling K., Davies G., Heintzmann R. (2009) Luminescence-lifetime mapping in diamond. *Journal of Physics: Condensed Matter*, Vol. 21, No. 36, 364210, <http://dx.doi.org/10.1088/0953-8984/21/36/364210>
- Lindblom J., Hölsä J., Papunen H., Häkkinen H., Mutanen J. (2003) Differentiation of natural and synthetic gem-quality diamonds by luminescence properties. *Optical Materials*, Vol. 24, No. 1-2, pp. 243–251, [http://dx.doi.org/10.1016/S0925-3467\(03\)00130-7](http://dx.doi.org/10.1016/S0925-3467(03)00130-7)
- Lipatov E.I., Lisitsyn V.M., Oleshko V.I., Tarasenko V.F. (2007) Spectral and kinetic characteristics of the pulsed cathodoluminescence of a natural IIa-type diamond. *Russian Physics Journal*, Vol. 50, No. 1, pp. 52–57, <http://dx.doi.org/10.1007/s11182-007-0005-8>
- Martineau P.M. (2017) The 68th Diamond Conference. University of Warwick, T2.1, July 10–13.
- Martineau P.M., McGuinness C.D. (2018) De Beers consumer confidence technical research and diamond verification instruments. *Diamonds – Source to Use Conference 2018*, Southern African Institute of Mining and Metallurgy, Johannesburg, June 11–13, pp. 35–44.
- Martineau P.M., Lawson S.C., Taylor A.J., Quinn S.J., Evans D.J.F., Crowder M.J. (2004) Identification of synthetic diamond grown using chemical vapor deposition (CVD). *G&G*, Vol. 40, No. 1, pp. 2–25, <http://dx.doi.org/10.5741/GEMS.40.1.2>
- Pereira E., Monterio T. (1991) Delayed luminescence of the H₃ centre in diamond. *Journal of Luminescence*, Vol. 48-49, pp. 814–818, [http://dx.doi.org/10.1016/0022-2313\(91\)90248-T](http://dx.doi.org/10.1016/0022-2313(91)90248-T)
- Smith J.G.C., McGuinness C.D., Fisher D. (2017) Luminescence measurements in diamond. Patent Application WO/2017/001835
- Spear P.M., Welbourn C.M. (1994) Distinguishing natural from synthetic diamond. Patent Application WO/83/00389A1
- Thomaz M.F., Davies G. (1978) The decay time of N3 luminescence in natural diamond. *Proceedings of the Royal Society A*, Vol. 362, No. 1710, pp. 405–419, <http://dx.doi.org/10.1098/rspa.1978.0141>
- Wassell A.M., McGuinness C.D., Hodges C., Lanigan P.M.P., Fisher D., Martineau P.M., Newton M.E., Lynch S.A. (2018) Anomalous green luminescent properties in CVD synthetic diamonds. *Physica Status Solidi A*, Vol. 215, No. 22, 1800292, <http://dx.doi.org/10.1002/pssa.201800292>
- Watanabe K., Lawson S.C., Isoya J., Kanda H., Sato Y. (1997) Phosphorescence in high-pressure synthetic diamond. *Diamond and Related Materials*, Vol. 6, No. 1, pp. 99–106, [http://dx.doi.org/10.1016/S0925-9635\(96\)00764-9](http://dx.doi.org/10.1016/S0925-9635(96)00764-9)
- Welbourn C.M., Cooper M., Spear P.M. (1996) De Beers natural versus synthetic diamond verification instruments. *G&G*, Vol. 32, No. 3, pp. 156–169, <http://dx.doi.org/10.5741/GEMS.32.3.156>

HISTORY OF THE CHIVOR EMERALD MINE, PART II (1924–1970): BETWEEN INSOLVENCY AND VIABILITY

Karl Schmetzer, Gérard Martayan, and Andrea R. Blake

The history of the Chivor emerald mine in Colombia is a saga with countless twists and turns, involving parties from across the globe. Indigenous people initially exploited the property, followed by the Spanish in the sixteenth and seventeenth centuries, before abandonment set in for 200 years. The mine was rediscovered by Francisco Restrepo in the 1880s, and ownership over the ensuing decades passed through several Colombian owners and eventually to an American company, the Colombian Emerald Syndicate, Ltd., with an intervening but unsuccessful attempt by a German group organized by Fritz Klein to take control. With the Colombian Emerald Syndicate succumbing to bankruptcy in 1923, the property was sold and then transferred in 1924 to another American firm, the Colombia Emerald Development Corporation. Under the new ownership, stock market speculation played a far more prominent role in the story than actual mining. Nonetheless, periods of more productive mining operations did take place under managers Peter W. Rainier and Russell W. Anderton. Yet these were not enough to prevent the company, renamed Chivor Emerald Mines, Inc. in 1933, from entering insolvency in 1952 and being placed into receivership. Leadership by Willis Frederick Bronkie enabled the firm to regain independence in 1970 and shortly thereafter to be sold in a series of transactions, with Chivor gradually being returned to Colombian interests.

Many legends are told about the history of the Chivor emerald mine.¹ The story begins with the sporadic working of the Colombian mine by indigenous people before being sought out by Spanish conquistadores in the first half of the sixteenth century. The property was exploited by the Spanish in the sixteenth and seventeenth centuries and then forgotten in the jungle for a period of more than two centuries after 1672. Schmetzer et al. (2020) chronicled the first part of the modern era commencing after the 200-year break, covering from 1880 to 1925. During that interval, Colombian miner Francisco Restrepo searched for and rediscovered the mine, and mining titles were granted to him and his associates in 1889. Through a series of transactions, the mining titles and land in the area came under the ownership of the *Compañía de las Minas de Esmeraldas de Chivor*, a Colombian entity in which Restrepo

was involved. Only intermittent operational activities took place until 1912, when the German gem cutter and merchant Fritz Klein joined Restrepo with an increased focus on the operational side. Early mining by Restrepo and Klein yielded several finds promising enough for them to travel to Germany together in 1913 to seek investors (figure 1). Further work was curtailed one year later, however, when Restrepo died in 1914 and Klein, who had hoped to purchase the mine with German funding, was thwarted by the outbreak of World War I.

When hostilities ended, Klein sought to recommence his efforts to buy the mine in 1919, but an American corporation, the Colombian Emerald Syndicate, Ltd., had in the interim obtained an option to purchase the mine. That option was exercised, and the mine was sold in December 1919 to two key representatives of the American group, Wilson E. Griffiths and Carl K. MacFadden. On behalf of the Colombian Emerald Syndicate, mining operations

See end of article for About the Authors and Acknowledgments.

GEMS & GEMOLOGY, Vol. 56, No. 2, pp. 230–257,

<http://dx.doi.org/10.5741/GEMS.56.2.230>

© 2020 Gemological Institute of America

¹See, e.g., Peretti and Falise, 2018.

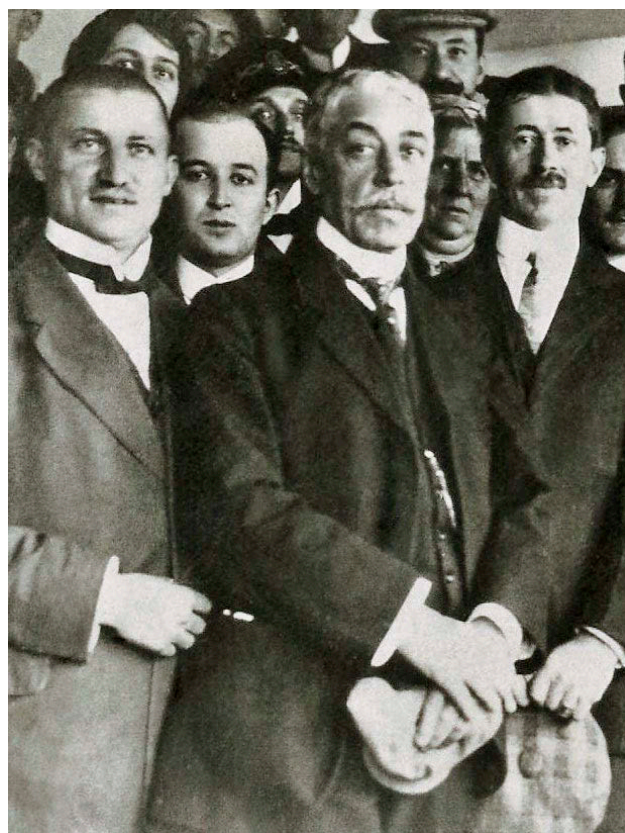


Figure 1. Portrait of the Colombian miner Francisco Restrepo Escobar (center) in 1913. Restrepo is credited with rediscovery of the Chivor emerald mines in the 1880s, after two centuries of abandonment. He later traveled to Germany with Fritz Klein to seek investors for the project, returning to Colombia in 1913 by ship. Klein followed aboard another ship somewhat later. Photo with passengers and crew members, most likely of the President Lincoln returning from Germany to Colombia via New York; courtesy of Eduardo Restrepo Ortega.

were conducted from 1919 to 1924 under the alternating leadership of the English miner and entrepreneur Christopher Ernest Dixon, who had lived in Colombia since the late 1880s, and Klein (figure 2), who served two terms of several months each under contracts with the new owners. Although both Dixon and Klein reported good production, the financial situation of the company nonetheless deteriorated, and an involuntary bankruptcy petition was filed against the Colombian Emerald Syndicate in

²See, e.g., Weldon et al., 2016.

³*Tic-Polonga* was published in the United States in 1953 and in the United Kingdom in 1954. The 1954 edition was consulted for purposes of this study, and references henceforth will be to that publication.

1923. The Chivor mine was sold in 1924, and it is here that the present paper, Part II, picks up the tale.

The following decades of Chivor's operational history were dominated by three key mine managers or administrators, Peter W. Rainier (1890–1945), Russel W. Anderton (1909–1982), and Willis Frederick Bronkie (1912–1979).² Both Rainier (*Green Fire*, 1942) and Anderton (*Tic-Polonga*, 1953, 1954)³ published books recounting their adventures, and Bronkie's successful management was the subject of several reports, including those by Johnson (1959, 1961). These publications, however, fall short of fully elucidating the mine's modern development, and the shortcomings are analogous to those faced in Part I with Klein's work (1941, 1951). For example, Rainier's account provided few actual dates, and Anderton likewise of-

Figure 2. Portrait of the German gem merchant Fritz Klein, who cooperated with Restrepo at Chivor from 1912 to 1914. Klein was subsequently engaged in the early 1920s to serve as head of mining operations for the new American owners of the property. Later he established his own company in Germany, focused on the emerald trade, and he also worked for the Colombian government. Photo 1937; courtesy of Carola Kroll.



ferred little to contextualize the timeline. Consequently, the present authors sought to fill existing gaps and present a comprehensive survey through reliance on contemporaneous primary documents and references. This second installment focuses on an overview of the half-century after the bankruptcy of the Colombian Emerald Syndicate, from 1924 to 1970. Following brief interim transactions in 1924, Chivor was owned throughout this period by a single American entity, operating first under the name Colombia Emerald Development Corporation and from 1933 as Chivor Emerald Mines, Inc. A summary of the main events is given in table 1.

SOURCES

The search for contemporaneous materials spanned South America, North America, and Europe (i.e., Colombia, the United States, and the United Kingdom). The primary documents found were compared with the known literature on the topic. Full citations for the principal existing publications consulted are

In Brief

- From 1924 to 1970, the Chivor emerald mine was under the ownership principally of a single American firm, operating first as the Colombia Emerald Development Corporation and then as Chivor Emerald Mines, Inc.
- The early years of that period were dominated by stock market speculation and scandal, featuring in particular the manipulations of Frederick Lewisohn and George Graham Rice.
- More productive operational stretches followed with Peter W. Rainier and Russell W. Anderton managing the mine, but insolvency and receivership nonetheless ensued in 1952.
- Leadership by Willis Frederick Bronkie eventually enabled the company to exit receivership in 1970 and to be sold, returning Chivor to Colombian interests.

summarized in the reference list. Other primary documents, such as governmental and judicial reports and decrees that may appear in broader compendiums, certain trade periodicals, archived contracts, business records, newspaper articles, personal correspondence, etc., are identified to the extent feasible in the footnotes, along with brief citations to publications included in the reference list.

Colombian materials were found in the form of government publications printed, typically anonymously, in the “Diario Oficial (Colombia),” in the “Gaceta Judicial (Colombia)” of the Corte Suprema de Justicia (Supreme Court), and in the reports of ministries or other government offices, especially in the series “Memoria del Ministro de Minas y Petróleos al Congreso.” These included legislative texts, decrees, governmental or judicial pronouncements, and statements on petitions and complaints. The Archivo General de la Nación (Colombia) in Bogotá further proved to be a repository of files collecting correspondence, notarial acts (*escrituras*), and attachments reflecting mine title transfers, sales of shares between various shareholders, and agreements shedding light on the ongoing fluctuations in Chivor ownership and related events.⁴

Governmental collections of a similarly useful nature were found in the United Kingdom. Particularly apposite was correspondence and associated materials archived at the Royal Academy of Music, London, where the legacy of Peter Rainier’s sister Priaulx is preserved.

Relevant information was also found in periodicals, largely from American publishers, concerning mining and the mining industry, such as the *Engineering and Mining Journal*, *Minerals Yearbook*, or *Mineral Trade Notes*. Financial sector periodicals were equally pertinent, and publications of U.S. universities yielded material on alumni who went on to work as mining engineers or geologists at Chivor.

Even online resources added to the available contemporaneous data. Noteworthy in this regard were digitized compilations of records detailing transit of persons, such as passenger lists maintained by the United States Immigration Office in New York. Those records detailed information that could incorporate departures and arrivals through national borders, starting points, destinations, and, most importantly, specific dates to help establish or corroborate event time frames. Similarly insightful were digital archives of newspapers across the United States, which enabled a view of events as presented to the public.

Finally, personal information obtained from eyewitnesses such as Peter Rainier, Jr., Manuel J. Marcial,

⁴Most germane at the Archivo General de la Nación (Colombia) in Bogotá, were several notarial acts (*escrituras*) designated herein by escritura number and date. Likewise instructive was the file “Joaquín Daza B.,” Volume “Propuestas Minas 99,” Ministerio de Industrias, Departamento de Minas y Petróleos, which contained documents covering 1929 to 1954 and detailing mine boundaries and history.

TABLE 1. History of Chivor, 1924–1970.

Date	Events in Colombia and the United States
March 1924	The “Chivor Emerald Corporation” is incorporated under the laws of the State of Delaware
August 1924	The mining titles for Chivor 1 and 2 and land in the region are sold to the “Chivor Emerald Corporation” in a bankruptcy sale
November 1924	The “Colombia Emerald Development Corporation” is incorporated in Delaware by three individuals associated with various mining companies owned by the Lewisohn family; E.J. MacNamara serves as president
Winter 1924	Ownership of Chivor 1 and 2 and the related land is transferred to the “Colombia Emerald Development Corporation” in exchange for stock
1925–1926	A large block of shares in the “Colombia Emerald Development Corporation” is transferred from F. Lewisohn to G.G. Rice and then aggressively marketed by G.G. Rice
1925–Spring 1926	W. Burns leads mining operations at Chivor
May 1926	C. Mentzel succeeds W. Burns as head of mining operations at Chivor
1926–1928	Legal proceedings implicating F. Lewisohn, E.J. MacNamara, and G.G. Rice in allegations of fraud and stock market manipulation take place in New York
1927	P.W. Rainier replaces C. Mentzel as the mining engineer overseeing operations at Chivor
December 1929	J. Daza instigates a legal dispute over ownership and control of the Chivor mines, referred to as the <i>Joaquín Daza</i> case
February 1930	P.W. Rainier presents a study describing the Chivor mining operations at a conference in New York
April–August 1930	Geologist V.A. Gilles evaluates the Chivor mine
August 1930	R.E. Sylvester joins P.W. Rainier at Chivor as an assistant
1930	The “Colombia Emerald Development Corporation” sustains a drastic loss for the year on mining operations at Chivor
1931–1957	Attorney F.P. Pace serves the “Colombia Emerald Development Corporation” and “Chivor Emerald Mines, Inc.” in multiple roles, including president in 1947, subsequent to W.J. Cowan’s tenure
January–February 1931	The Chivor mine is inspected in connection with the <i>Joaquín Daza</i> case by Colombian officials together with P.W. Rainier, R.E. Sylvester, and J. Daza; later security problems arise at the mine
October 1931	R.E. Sylvester returns to New York at the end of his tenure at Chivor; P.W. Rainier travels separately to New York to meet with the mine owners
By early 1932–1947	The Chivor mine is largely dormant after being reported as closed, with little documented operational activity beyond illegal mining and some work under lease to a Colombian company
September 1933	The name of the “Colombia Emerald Development Corporation” changes to “Chivor Emerald Mines, Inc.”
1936–1940	Records reflect that banker R.E. Henry was serving as president of “Chivor Emerald Mines, Inc.,” with E.J. MacNamara’s term having ended at some point after 1932
1937–1940/1941	Records reflect that the Chivor mine was being leased to the “Compañía de Esmeraldas de Colombia” and/or being operated with E. Fernández as the mine administrator
Early to mid-1940s	W.J. Cowan holds the position of president for “Chivor Emerald Mines, Inc.”
January 1941	Chivor is evaluated again by Colombian officials in connection with the <i>Joaquín Daza</i> case, with a continued focus on mine boundaries, leading to a report by N. Rosso
April 1944	P.W. Rainier considers returning to Chivor when approached by the mine owners about a possible consulting position, but no further steps are taken, and the mine remains inactive
1947	F.P. Pace replaces W.J. Cowan as president. In 1947, 1948, and 1950, Pace travels to Colombia to restart and supervise mining operations on behalf of “Chivor Emerald Mines, Inc.”; local control in Colombia is placed under a series of managers
Early 1950–Fall 1950	R.W. Anderton serves as head of mining operations at Chivor
Late 1950/early 1951	A dispute ensues between U.S. and Colombian associates, and the situation at the mine is characterized by lawlessness, with all production being sold on the black market
By February 1952	Insolvency proceedings commence in Bogotá and result in “Chivor Emerald Mines, Inc.,” being placed in receivership
1952–1970	The Chivor mine is operated under receivership
1952–1953	R.W. Anderton returns to Colombia and again serves in a management capacity at Chivor
January 1955–September 1957	W. de Freitas serves as receiver and P.P. Patiño as mine inspector at Chivor
1957	F.P. Pace dies; O.J. Troster of New York becomes involved, serving as a director and secretary of “Chivor Emerald Mines, Inc.”
1960s (or before)	G.D. Besler serves as president of “Chivor Emerald Mines, Inc.”
October 1957–circa 1969/1970	W.F. Bronkie is named receiver of “Chivor Emerald Mines, Inc.,” and simultaneously serves as mining engineer supervising operations at Chivor, working in conjunction with Spanish mine manager E. Muñoz by the mid-1960s
1960s	W.F. Bronkie’s business approach expands to incorporate buying emeralds on the open market in Colombia and selling rough and faceted stones to international customers, as well as operating jewelry retail shops in Colombia and elsewhere
1968	The press reports that W.F. Bronkie intends to file documentation that will set in motion a process to end the receivership
1970	The receivership is lifted, and as of the year of the transition, American attorney R.S. Pastore is serving as receiver, N.R. Merriam as general manager, and J. Rodríguez as mine manager
After 1970	Ownership of Chivor is gradually transferred to Colombian stakeholders

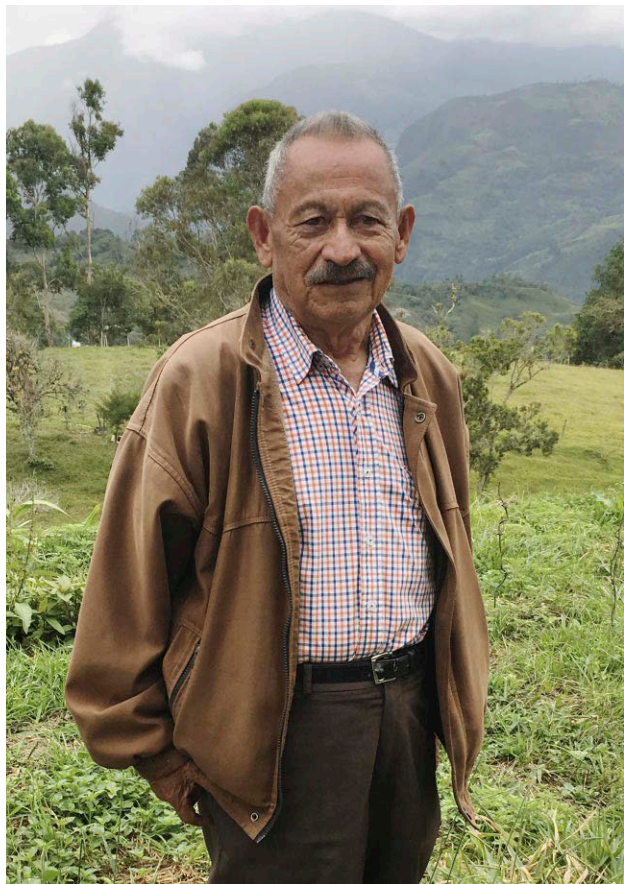


Figure 3. Personal recollections regarding the history of the Chivor emerald mine were obtained from eyewitnesses such as don Alfonso Montenegro. Montenegro, a miner presently residing in the small town of Macanal, not far from Chivor, began working at the mine in 1955 at the age of 12 under the receivership of Walter de Freitas, and he continued to serve under Freitas's successor Willis Frederick Bronkie. Photo by Gérard Martayan, December 2018.

don Alfonso Montenegro (figure 3), Renata de Jara, Gonzalo Jara, and Robert E. Friedmann, was invaluable in achieving the aims of this study.

CHIVOR AS A SUBJECT OF STOCK MARKET SPECULATION (1924–1927)

To recap the period from 1924 to 1925 bridging Parts I and II of this study, the mining titles for Chivor 1 and 2 and the related land ownership were sold in a bankruptcy sale on or about August 23, 1924, to the recently formed Chivor Emerald Corporation.⁵ The price paid was only US\$7,800 to \$8,000, depending

on the report consulted,⁶ which did not even cover liabilities in the range of \$45,000 of the former owner, the Colombian Emerald Syndicate (see part one of this article).⁷ The Chivor Emerald Corporation had been incorporated on March 6, 1924, under the laws of the State of Delaware, by Samuel C. Wood, Harry C. Hand, and Raymond J. Gorman.⁸ The stated corporate purpose was to “mine and prepare for market emeralds, diamonds.”⁹ The three named individuals served as registrants of numerous corporations across a spectrum of industries in the 1920s (e.g., motion pictures, radio accessories, petroleum, and rubber), operating via a business model that acquired bankrupt or troubled companies (or their assets) and resold them after improvement in the price.¹⁰

Another new entity, the Colombia Emerald Development Corporation, was then incorporated on November 7, 1924, likewise in the state of Delaware, by Edmund J. MacNamara (1874–?), Ernest W. Brown, and William B. Anderson.¹¹ The intended business was “to mine, manufacture and deal in precious stones, emeralds, rubies, diamonds, jades and garnets.”¹² The Chivor claims and land were transferred to that company in late 1924 in exchange for stock.¹³ The Chivor Emerald Corporation thereafter served merely as a holding company, owning approximately 40 percent of the capital stock in the Colombia Emerald Development Corporation but no other assets.¹⁴

⁵*The Cumulative Daily Digest of Corporation News*, No. 3 (1924), pp. 150, 161. This entity should not be conflated with an unrelated Canadian company of the same name that was active at Chivor decades later in the 1990s.

⁶*The Brooklyn Daily Eagle*, January 9, 1927, p. 22; *The New York Times*, January 9, 1927; *The Bridgeport Telegram*, January 10, 1927, p. 5; *The Tribune* (Coshocton, Ohio), January 10, 1927, p. 4; *The New York Times*, January 28, 1927; *The New York Times*, February 20, 1927; *Jewelers' Circular*, 94, No. 4 (1927), p. 61; *Chicago Tribune*, February 27, 1927, p. 40.

⁷Robert D. Fisher *Manual of Valuable and Worthless Securities*, 6 (1938), p. 227.

⁸State of Delaware, Department of State, Division of Corporations, Entity Details; *The Morning News*, March 7, 1924, p. 11.

⁹*The Morning News*, March 7, 1924, p. 11.

¹⁰*The Morning News*, November 15, 1923, p. 9; *The Morning News*, April 14, 1925, p. 11; *The Morning News*, July 1, 1925, p. 9; *Arizona Republic*, March 13, 1929, p. 4.

¹¹State of Delaware, Department of State, Division of Corporations, Entity Details; *The Morning News*, November 8, 1924, p. 13; *The Philadelphia Inquirer*, November 10, 1924, p. 33; *The Cumulative Daily Digest of Corporation News*, No. 4 (1924), p. 222; Winkler, 1928.

¹²*The Philadelphia Inquirer*, November 10, 1924, p. 33.

¹³*The Cumulative Daily Digest of Corporation News*, No. 4 (1924), pp. 209, 222; Winkler, 1928; Rainier, 1929, 1931.

¹⁴Robert D. Fisher *Manual of Valuable and Worthless Securities*, 11 (1946), p. 149.

Per available evidence, the two firms were headquartered together in New York City and generally controlled by a common group of individuals,¹⁵ with the Colombia Emerald Development Corporation apparently established to take over and carry on the emerald business as the operating enterprise. Registration of the two companies in Colombia took place in February 1925 for the Chivor Emerald Corporation¹⁶ and in July 1925 for the Colombia Emerald Development Corporation.¹⁷ The governor of Delaware subsequently repealed the charter of the Chivor Emerald Corporation in 1961 for failure to pay taxes.¹⁸

A number of the principal figures involved in leadership of the Colombia Emerald Development Corporation were associated with the Lewisohn group of companies, an American offshoot of the Lewisohn family mercantile business based originally in Hamburg, Germany.¹⁹ The brothers Leonard (1847–1902) and Adolph (1849–1938) Lewisohn had followed their older brother Julius in the second half of the 1860s from Hamburg to New York to assist with the American branch. Julius returned to Hamburg in 1872, and Leonard and Adolph went on to create one of the larger copper mining and processing empires in the United States between 1880 and 1900, operating as Lewisohn Brothers.²⁰ The German and American branches of the business formally separated in 1887.

By the time of the 1924 Chivor transaction, the Lewisohn group of companies had already been involved in mining activities in Colombia for several years. In 1916, the Lewisohn Brothers and Adolph Lewisohn & Sons formed the South American Gold and Platinum Company. After buying multiple mines in Colombia and merging with various other entities, this corporation had become the largest producer of noble metals (gold and platinum) in that country. Frederick Lewisohn (1881–1959), one of Leonard Lewisohn's sons, served as a vice president of the company.²¹ The Lewisohn group likely opted to take advantage of the low price at which the assets of the bankrupt Colombian Emerald Syndicate could be acquired (as compared to the £46,000, equivalent to US\$230,000, previously paid for the Chivor mines in 1919),²² to establish a new line of business in emerald mining.

The three listed incorporators of the Colombia Emerald Development Corporation all held roles (e.g., president, secretary, or director) in different mining companies associated with the Lewisohn group, especially the Seneca Copper Corporation and

the Santa Fe Gold & Copper Mining Company.²³ MacNamara, a mining engineer and entrepreneur having wide-ranging participation with Lewisohn Brothers entities, stepped in as president of the Colombia Emerald Development Corporation, a position that he would continue to fill in the years ahead.²⁴ After the transfer of assets of the Chivor Emerald Corporation to the new company, Frederick Lewisohn acquired between 40 and 50 percent of the authorized capital stock of the Colombia Emerald Development Corporation for a price in the range of 10 cents per share, or approximately \$50,000.²⁵ Shares were also being advertised to the American public by March 25, 1925, for a subscription price of \$2 per share.²⁶ As of May 19, 1926, the company was listed on the Boston Curb Exchange at \$1⅞ per share.²⁷

¹⁵For example, the reported addresses for the two companies during the late 1930s and early 1940s were identical, given as 32 Broadway, New York City. *Robert D. Fisher Manual of Valuable and Worthless Securities*, 6 (1938), p. 205; *Robert D. Fisher Manual of Valuable and Worthless Securities* (1944), p. 147.

¹⁶Escritura 344, February 16, 1925, Notaria 1, Archivo General de la Nación (Colombia).

¹⁷Escritura 1607, July 11, 1925, Notaria 1, Archivo General de la Nación (Colombia).

¹⁸State of Delaware, Executive Department, Chapter 465 Proclamation, January 16, 1961.

¹⁹*Engineering and Mining Journal*, 110, No. 15 (1920), p. 722; Albrecht, 2013.

²⁰*Engineering and Mining Journal*, 110, No. 15 (1920), p. 722; Albrecht, 2013.

²¹*The New York Times*, June 13, 1919; *The Economist*, 89 (1919), p. 39; *The Magazine of Wall Street*, 25 (1919), p. 57; *The New York Times*, July 5, 1959, p. 56.

²²Escritura 3084, December 27, 1919, Notaria 1, Archivo General de la Nación (Colombia).

²³*The Copper Handbook*, 10 (1911), pp. 1528–1529; *Trow's New York Copartnership and Corporation Directory*, 63 (1915), p. 912; *Trow's New York Copartnership and Corporation Directory*, 66 (1919), p. 1019; *The Copper Handbook*, 14 (1920), pp. 1256–1257; *Moody's Manual of Railroads and Corporation Securities*, 2, Part 1, Industrial Section (1921), pp. 1369–1370; *Engineering and Mining Journal*, 113, No. 9 (1922), p. 376.

²⁴*The Mines Handbook*, 12 (1916), p. 1005; *Mineral Resources of Michigan* (1917), p. 53; *Engineering and Mining Journal*, 122, No. 16 (1926), p. 602; *The New York Times*, August 7, 1926; *The New York Times*, August 10, 1926; *In re Idaho Copper Corporation*, Deposition of Keyes Winter, Deputy Attorney General, State of New York, Supreme Court of New York (Sept. 8, 1926); *The New York Times*, October 12, 1926; *Engineering and Mining Journal*, 123 (1927), p. 106; *Poor's Register of Directors of the United States* (1928), p. 918; *Poor's Register of Directors of the United States and Canada* (1932), p. 1291.

²⁵*The Brooklyn Daily Eagle*, January 6, 1927, p. 2; *Salt Lake Telegram*, January 13, 1927, p. 5; *The New York Times*, January 28, 1927.

²⁶*The News Journal* (Wilmington, Delaware), March 28, 1925, p. 17.

²⁷*The Anaconda Standard* (Anaconda, Montana), May 19, 1926, p. 12.



Figure 4. George Graham Rice was one of the most infamous financial manipulators in the United States during the first half of the twentieth century. In the late 1920s, his activities centered on aggressively promoting and selling shares in two entities, the Colombia Emerald Development Corporation, which owned the Chivor mining titles, and the Idaho Copper Company. He worked in cooperation with the president of the Colombia Emerald Development Corporation, Edmund J. MacNamara, and its largest shareholder, Frederick Lewisohn. The actions of Rice, MacNamara, and Lewisohn became the subject of court proceedings in New York that began in 1926 and were premised on allegations of fraud and stock market manipulation. Photo 1911, from *The Mining Investor*, Vol. 63, No. 1 (1911).

In the next stage of Chivor's history, the owning entity became entangled in a stock market scandal while operational activity was minimal. As to the latter, the first mining engineer sent to Chivor by the new mine owners was William Burns (1885–1962), who had already been working for the Lewisohn group in various functions (e.g., as manager of the Santa Fe Gold & Copper Mining Company or as secretary of the Rosemont Copper Company).²⁸ Burns reportedly had also performed development work in the 1920s at

Chivor for the former owner, the Colombian Emerald Syndicate.²⁹ During his tenure, Burns expended over \$40,000 on the Colombia Emerald Development Corporation's behalf on the property, but the resultant emeralds produced were not worth over \$4,000.³⁰ Burns later resigned, and he was succeeded by mining engineer Charles Mentzel (1881–1949), likewise previously associated with the Lewisohn-owned Santa Fe Gold & Copper Mining Company and having gained experience in Colombia in 1916 and 1917.³¹ Mentzel arrived at Chivor in late May 1926, and Burns returned to New York on June 13, 1926.³²

For operational purposes, materials published by the Colombia Emerald Development Corporation suggest that the company was only focusing on and/or asserting claims over the Chivor 1 and 2 mines, excluding the other three mines of the Chivor group.³³

Meanwhile, as to the stock market machinations, Frederick Lewisohn had transferred his package of shares to George Graham Rice (1870–1943, figure 4), either directly or through Rice's brother-in-law Frank J. Silva as a conduit, for a price of 75 cents per share.³⁴ Rice then began to market the shares via his weekly promotional circular the *Wall Street Iconoclast*,³⁵ which was sent to a mailing list of 600,000 recipients.³⁶ Rice was one of the most infamous financial manipulators of the era, having already spent time in prison on multiple occasions for various crimes of fraud and theft.³⁷

Rice's tactics are exemplified by two issues of the *Wall Street Iconoclast* we were able to locate from July and August 1926.³⁸ In those issues, Rice pro-

²⁸*Harvard Alumni Bulletin* 20 (1917), p. 440; *American Mining & Metallurgical Manual* (1920), p. 89.

²⁹Brock, 1929.

³⁰*ibid.*

³¹*Engineering and Mining Journal*, 101, No. 15 (1916), p. 663; *Engineering and Mining Journal*, 103, No. 11 (1917), p. 476; Brock, 1929.

³²File William Burns, List of United States Citizens Arriving at Port of New York, June 1926, Ancestry.com.

³³Colombia Emerald Development Corporation, *The Story of Emeralds* (Undated), 10 pp. The map included appears to be prepared after Canova (1921) but eliminates the other three mines shown on the original version.

³⁴*The Brooklyn Daily Eagle*, January 6, 1927, p. 2; *The New York Times*, January 6, 1927; *The New York Times*, January 28, 1927; *Engineering and Mining Journal*, 123 (1927), p. 635.

³⁵For example, *The Wall Street Iconoclast*, 5, No. 102, July 15, 1926; *The Wall Street Iconoclast*, 5, No. 105, August 5, 1926.

³⁶*The Pittsburgh Press*, February 28, 1928, p. 33.

³⁷Rice, 1913; *The Scranton Republican*, August 28, 1926, p. 15; Plazak, 2006; Thornton, 2015.

³⁸*The Wall Street Iconoclast*, 5, No. 102, July 15, 1926; *The Wall Street Iconoclast*, 5, No. 105, August 5, 1926.

moted the Colombia Emerald Development Corporation, as well as another Lewisohn entity sold on the Boston Curb Exchange, the Idaho Copper Company.³⁹ Rice aggressively recommended buying shares of the Lewisohn-controlled Colombia Emerald Development Corporation, reporting that the Lewisohn family had acquired the mines in the winter of 1924/1925. He also identified MacNamara as president of the company, emphasizing MacNamara's dual role as vice president of the Lewisohn Exploration & Development Corporation.⁴⁰ Rice likewise played upon the expertise of mining engineers Burns and Mentzel. Notably, it has been reported that Burns's resignation was prompted when he "learned that Rice was selling the stock and using his name as bait." Mentzel, prior to his departure for Colombia and without having seen the mine, had already written a report in the *Wall Street Iconoclast* that valued the property at \$5,000,000.⁴¹ One of Rice's strategies was thus to use the reputation of an industrial family well known in the mining business—Lewisohn—to incentivize investment.⁴²

An additional strategy was found in Rice's glowing portrayal of emerald production and valuation. The *Wall Street Iconoclast* reported extraordinarily rich finds such as 23,500 carats in June 1926⁴³ and calculated sensationally high values for the mining property and stock, claiming that a share "had a real value of between \$50 and \$75" and that the mines owned by the company "were valued at \$100,000,000 and were capable of producing an annual income for investors of between \$2,000,000 and \$5,000,000."⁴⁴ The stock of the Colombia Emerald Development Corporation rose over a period of 14 weeks from \$1 to \$17⁵/₈.⁴⁵ In reality, however, half of the 23,500 carats highlighted by Rice were worthless stones, and the remainder had an estimated value of 50 cents per carat.⁴⁶ The company reported a loss of \$57,000 for 1926.⁴⁷ As one mining engineer who worked under the Lewisohns at Chivor would later summarize: "I guess they [the Lewisohns] made more money on the stock market than mining."⁴⁸

Such discrepancies began to come to light as a result of actions beginning in 1926 by New York State Attorney General Albert Ottinger. Under the Martin Act (New York General Business Law, Article 23-A, Sections 352–353), he targeted the *Wall Street Iconoclast*, Rice, Silva, the Colombia Emerald Development Corporation, MacNamara, and Frederick Lewisohn.⁴⁹ In injunction proceedings, Ottinger claimed that "not over a spoonful of stones and only two of those salable, have ever been taken from the

mines."⁵⁰ A related investigation by Deputy Attorney General Keyes Winter led him to conclude "that the total value of the output of the mines for two years did not exceed \$13,000, and that many of the emeralds obtained were in an uncrystallized state and could not be marketed."⁵¹ Such numbers contrasted blatantly with claims proffered to promote sale of the stock, which indicated that emeralds of fabulous quality weighing between 28 and 80 carats, with a value between \$100 and \$500 per carat, had been found at Chivor.⁵²

A preliminary injunction restraining promotion, advertising, and sale of Colombia Emerald Development Corporation stock had been issued by early January 1927. It was then made permanent in a ruling handed down on or before February 19, 1927, in the New York Supreme Court (i.e., the trial-level state court).⁵³ Rice and associates were thereby restrained "from the sale of the stock of the emerald corporation unless complete information about the concern is furnished,"⁵⁴ and not a single share of the stock could be sold without giving a detailed explanation of the actual profit and losses from mining operations.⁵⁵ Al-

³⁹*The Wall Street Iconoclast*, 5, No. 102, July 15, 1926; *The Wall Street Iconoclast*, 5, No. 105, August 5, 1926. The Idaho Copper Company was also known as the Idaho Copper Corporation. Thornton, 2015.

⁴⁰Most likely a reference to the Lewisohn Exploration & Mining Co. or to the General Development Co.

⁴¹Brock, 1929.

⁴²*Engineering and Mining Journal*, 122, No. 16 (1926), p. 602.

⁴³*The Wall Street Iconoclast*, 5, No. 102, July 15, 1926; *The Wall Street Iconoclast*, 5, No. 105, August 5, 1926.

⁴⁴*The New York Times*, February 20, 1927; *Chicago Tribune*, February 27, 1927, p. 40.

⁴⁵*St. Louis Post-Dispatch*, January 6, 1927; *The Pittsburgh Press*, February 28, 1928.

⁴⁶Brock, 1929.

⁴⁷*The Cumulative Daily Digest of Corporation News*, No. 2 (1927), p. 165.

⁴⁸*The Billings Gazette*, May 16, 1954, p. 6.

⁴⁹*The New York Times*, August 7, 1926; *The New York Times*, October 12, 1926.

⁵⁰*The Brooklyn Daily Eagle*, January 6, 1927, p. 2.

⁵¹*The New York Times*, February 20, 1927; *Chicago Tribune*, February 27, 1927.

⁵²*The New York Times*, February 20, 1927; *Chicago Tribune*, February 27, 1927.

⁵³*The Brooklyn Daily Eagle*, January 6, 1927, p. 2; *The Brooklyn Daily Eagle*, January 9, 1927, p. 22; *The New York Times*, January 9, 1927; *The Bridgeport Telegram*, January 10, 1927, p. 5; *The Tribune* (Coshocton, Ohio), January 10, 1927, p. 4; *The New York Times*, January 28, 1927; *The New York Times*, February 20, 1927; *Jewelers' Circular*, 94, No. 4 (1927), p. 61; *Chicago Tribune*, February 27, 1927, p. 40.

⁵⁴*Chicago Tribune*, February 27, 1927.

⁵⁵*The New York Times*, February 20, 1927.



Figure 5. By 1927, South African mining engineer Peter W. Rainier had been hired to head operations at the Chivor emerald mine in Colombia, with the aim of turning the venture into a profitable one. However, a drastic loss generated in 1930, when mining costs far exceeded emerald sales, led to a directive in 1931 to close the mine. Photo from the Peter W. Rainier collection; courtesy of GIA.

though the injunction was later vacated in part to the extent that it applied to the Colombia Emerald Development Corporation, Frederick Lewisohn, and MacNamara, on account of insufficient evidence to establish the actual personal participation of Lewisohn and MacNamara in fraudulent practices, the restraint against the *Wall Street Iconoclast*, Rice, and Silva remained in force.⁵⁶

Rice ultimately avoided serious prosecution in connection with his dealings related to the Colombia Emerald Development Corporation. Still, matters pertaining to the Idaho Copper Company proceeded to trial and led to him being found guilty in 1928 and sentenced to four years in prison.⁵⁷ As an anecdotal footnote, while incarcerated at the federal penitentiary in Atlanta on those charges, Rice became a friend of another prominent inmate, Al Capone.⁵⁸

By the end of 1928, both the Colombia Emerald Development Corporation and the Idaho Copper Company had been delisted from the Boston Curb Exchange.⁵⁹

CHIVOR UNDER PETER W. RAINIER (1927–1931)

During late 1926 or early 1927, the president and directors of the Colombia Emerald Development Corporation decided to hire a new mining engineer to oversee on-site operations at the Chivor mine in Colombia, replacing Mentzel. The mine had been unprofitable for the preceding two years, but the ongoing legal proceedings in New York involving MacNamara and Frederick Lewisohn likely rendered

the alternative course of simply closing the mine inadvisable. The engineer selected as Mentzel's successor, apparently under an initial contract of six months,⁶⁰ was Rainier (figure 5). Born in Transvaal, South Africa, Rainier had obtained mining experience in countries such as Nigeria, Southern Rhodesia (Zimbabwe), and South West Africa (Namibia).⁶¹ At the time of his engagement, Rainier was living in the United States with his family. Mentzel did not, however, immediately leave Colombia and remained active in the country during 1928 and 1929, presumably still with the Colombia Emerald Development Corporation in some capacity.⁶²

Rainier began his work in Colombia in 1927, leaving his family behind in the United States when his son Peter W. Rainier, Jr. (born August 1926), was only a few months old.⁶³ His wife and children would later join him at Chivor in 1928. Efforts at the mine started with repairing the infrastructure, after which Rainier

⁵⁶*The New York Times*, May 7, 1927.

⁵⁷Plazak, 2006.

⁵⁸*Ibid.*

⁵⁹*Star Tribune* (Minneapolis), December 18, 1928.

⁶⁰Rainier, 1942.

⁶¹Weldon et al., 2016. Insofar as Weldon et al. (2016) chronicled Peter W. Rainier's account as presented in *Green Fire* (1942), the following discussion will focus more broadly on the chronology as it relates to independent documentation.

⁶²File Charles Mentzel, List or Manifest of United States Citizens Arriving at Port of New York, February 1928 and February 1929, Ancestry.com.

⁶³Rainier, 1942; Peter W. Rainier, Jr., pers. comm. 2017.

was able to improve the yield of operations and the quantity of facet-grade gem material. At that time, the traditional open-cast step-cutting technique (figures 6 and 7) continued to be employed. Small terraces or steps were cut in the extremely steep mountain surface, and the loose debris was washed away by a flood of previously collected water. Crystals were carefully removed by hand from the emerald-bearing veins or cavities within the host rock.

In 1929, Rainier published a study describing his mining operations at Chivor, and he traveled to New York to present the paper at a conference of the American Institute of Mining and Metallurgical Engineers in February 1930.⁶⁴ It is also logical to surmise that the trip to New York would have provided an opportunity to meet with his employer concerning the mining activities.

After Rainier returned to Colombia, he was joined at Chivor by geologist Verner A. Gilles (1886–1954) from April to August 1930 for geological mapping and evaluation of the mine.⁶⁵ Like many others sent to Chivor, Gilles had experience working for companies owned by the Lewisohn family.⁶⁶ His evaluation resulted in a report, dated September 20, 1930, that provided insight into the production and cost of mining.⁶⁷ In the period from 1925 to 1929, the mine yielded 137,000 carats in total, beginning from a low of 4,000 carats in 1925, the first year of mining oper-

Figure 6. In the late 1920s, mining operations at Chivor under Rainier still used the traditional open-cast step-cutting technique. Terraces or steps were cut into the surface of the extremely steep mountain slopes, and the debris was washed away via water previously collected in tanks. Photo from the Peter W. Rainier collection; courtesy of GIA.



Figure 7. The open-cast step-mining operations at Chivor under Rainier entailed manually excavating the terraces and then recovering crystals after exposure in the host rock. Photo from the Peter W. Rainier collection; courtesy of GIA.

ations under the Colombia Emerald Development Corporation, followed by a large quantity of low-grade stones in 1926. The costs of mining operations from 1926 to 1929 aggregated \$278,000, and it was noted that a maximum of 250 workers were on the payroll of the mine (figure 8). The total selling value of the emeralds produced from 1925 to 1929 was cal-

⁶⁴Rainier, 1929, 1931. The study was initially published in 1929 and was then reprinted in expanded form in 1931, incorporating comments generated during the discussion that followed oral presentation of the paper before the American Institute of Mining and Metallurgical Engineers in February 1930 in New York. A Spanish translation was published in 1934. Rainier, 1934. See also *The Wilkes-Barre Record*, March 21, 1930, p. 2.

⁶⁵Verner A. Gilles left Colombia on August 31 and returned to New York on September 10, 1930. File Verner Gilles, List of United States Citizens Arriving at Port of New York, September 1930, Ancestry.com.

⁶⁶*The Billings Gazette*, May 16, 1954, p. 6.

⁶⁷Gilles, 1930.



Figure 8. In the late 1920s to early 1930s, Rainier worked with several hundred miners at Chivor. Photo sent by Rainier to his sister, with a handwritten comment reading: “Indian miners drinking their Guarapo ration Sunday afternoon.” Prialx Rainier collection, Royal Academy of Music, London.

culated at \$274,000, indicating that the average price received per carat was approximately \$2. Such figures evidenced that the mine was not generally profitable, with mining costs versus emerald sales value roughly equal at best. The numbers also offered a counterpoint to the more optimistic estimation apparently held by Rainier, who would later opine that he handled “emeralds worth more than one million dollars” during his years of responsibility over the mine.⁶⁸

Gilles’s report further addressed geological aspects pertaining to the reserve of emerald-bearing rock at Chivor, concluding:⁶⁹

It is almost impossible to give an estimate of the value of this enormous deposit of emerald bearing rock. To sample the deposit is out of the question. Even drilling would not give an adequate idea of its value, due to the fact that the ratio between gangue rock and valuable mineral contents is so great. There is but one way to tell what the deposit is worth, and that is to work it out. Here is where the great hazard of emerald mining must be considered. Working out the emerald bearing formation now in reserve may mean a handsome profit and on the other hand it may mean a great loss. After all is said and done the question of profit in this case of mining is largely a matter of luck.

As previously noted, Gilles departed from Colombia in late August 1930, approximately concomitant with the arrival of American mining engineer Robert Elmer Sylvester (1904–1988, figure 9) to assist Rainier.⁷⁰ Sylvester’s contract had come through the Lewisohn group of companies,⁷¹ and a two-year stay in Colombia was planned.⁷² His tenure would actually end, however, by October 1931 when he returned to New York.⁷³

As these operational activities were taking place, in the background ownership and control of the Chivor mines had become the subject of a legal dispute, referred to as the *Joaquín Daza* case. Joaquín Daza B. submitted a petition dated December 27, 1929, to the Colombian government, claiming that the Chivor mine partly overlapped with his property and that mining operations were being conducted on his land.⁷⁴ He proposed that he be awarded financial compensation for the infringement. According to *Green Fire*, Rainier rejected such a proposal after Daza personally visited the mine with his demands.⁷⁵

In the more formal proceeding and at the request of the government, Rainier responded to Daza’s

⁶⁸Gilles, 1930.

⁶⁹Rainier, 1942.

⁷⁰Robert Elmer Sylvester received his degree from the School of Mines and Metallurgy, Institute of Technology, University of Minnesota, in 1927. He married in July 1930 and arrived at Chivor with his wife Josephine at the end of August 1930. Alumni Blue Book, School of Mines and Metallurgy, Institute of Technology, University of Minnesota (1950), 13, p. 135; Rebecca Toov, University of Minnesota Archives, pers. comm. 2018.

⁷¹*The Bismarck Tribune*, September 9, 1930, p. 3.

⁷²*The Billings Gazette*, July 20, 1930, p. 13; *Minnesota Chats*, January 2, 1931, p. 3.

⁷³File Robert Sylvester, List or Manifest of Alien Passengers for the United States Immigration Officer at the Port of Arrival, New York, October 1931, MyHeritage.com.

⁷⁴File “Joaquín Daza B.,” Volume “Propuestas Minas 99,” Ministerio de Industrias, Departamento de Minas y Petróleos, Archivo General de la Nación (Colombia).

⁷⁵Rainier, 1942.

claims via a letter dated August 4, 1930.⁷⁶ Therein, Rainier explained that he had no exact map of the mine boundaries, as no such document had been provided by his employer (figure 10). In connection with the case, the mine was inspected during the period from late January to early February 1931 by two government officials, i.e., the lawyer Alfonso Torres Barreto and the engineer Miguel Alvarez Uribe, together with Daza, Rainier, and Sylvester, and a report was issued on February 7, 1931. Yet no final resolution was reached, and ongoing consideration by the government was reflected in documents dated in 1934, 1935, and 1939.⁷⁷

The consideration apparently intensified in January 1941, when the mine was examined once again by Colombian officials. A report by engineer Nicolas

Figure 9. American mining engineer Robert Elmer Sylvester worked with Rainier at Chivor in 1930 and 1931. This photo was sent by Rainier to his sister, with a handwritten comment reading: "My American assistant R.E. Sylvester." Priaulx Rainier collection, Royal Academy of Music, London.

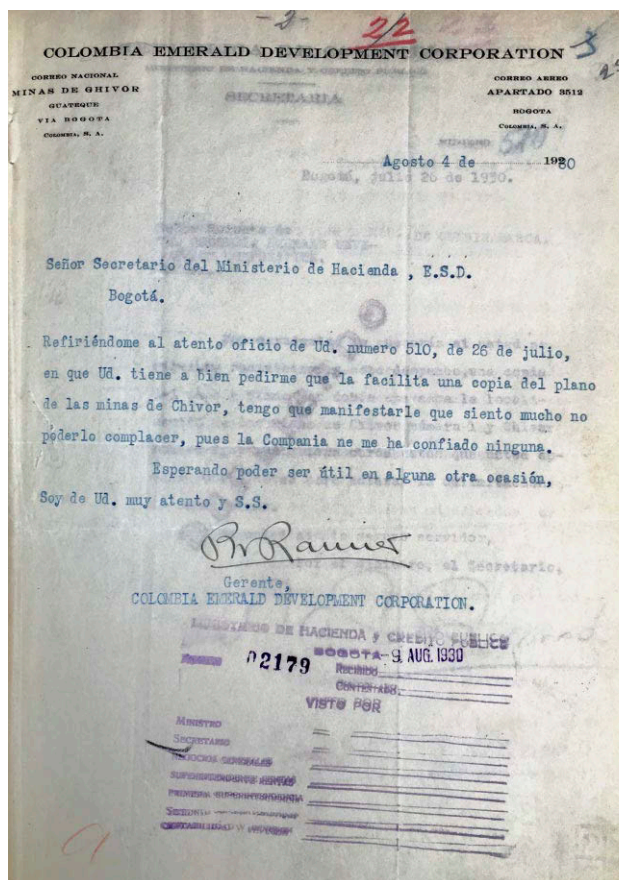
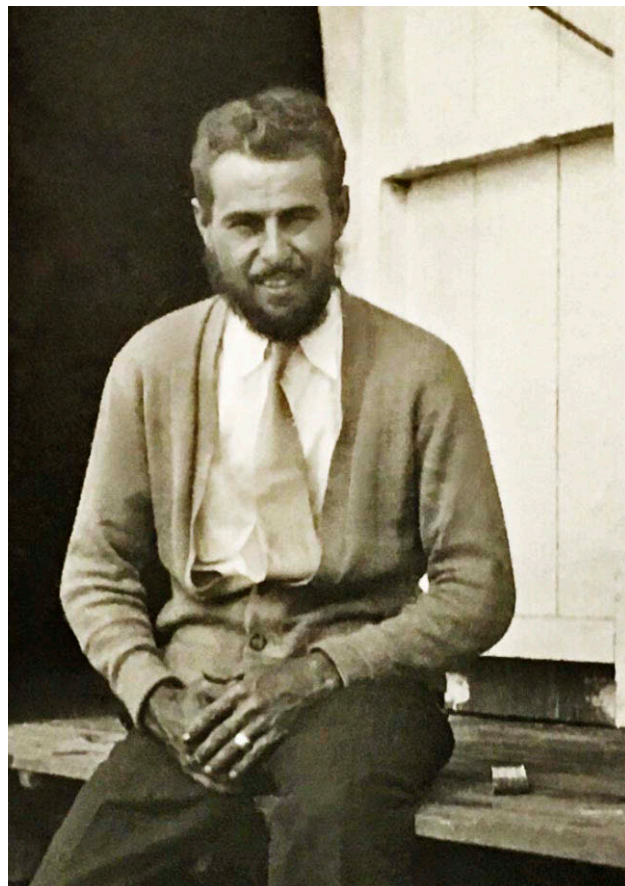


Figure 10. Letter dated August 4, 1930, written by Rainier to the Ministerio de Hacienda in Bogotá, indicating that he was not in possession of any maps depicting the exact boundaries of the Chivor mining claims. File "Joaquín Daza B.," Volume "Propuestas Minas 99," Ministerio de Industrias, Departamento de Minas y Petróleos, Archivo General de la Nación (Colombia).

Rosso, dated January 29, 1941,⁷⁸ incorporated a map showing currently mined sites, estimated mine boundaries, and relevant infrastructure (figure 11). Discussions between Rosso and Daza in Guateque had preceded the inspection, and Daza then reiterated his claims in letters submitted to the government dated from August to October 1941, wherein he also augmented his petition to request consideration of titles to the adjacent mines of Buenavista and Mundo Nuevo (figure 12; see also figure 25). Even

⁷⁶File "Joaquín Daza B.," Volume "Propuestas Minas 99," Ministerio de Industrias, Departamento de Minas y Petróleos, Archivo General de la Nación (Colombia).

⁷⁷Ibid.

⁷⁸Ibid.

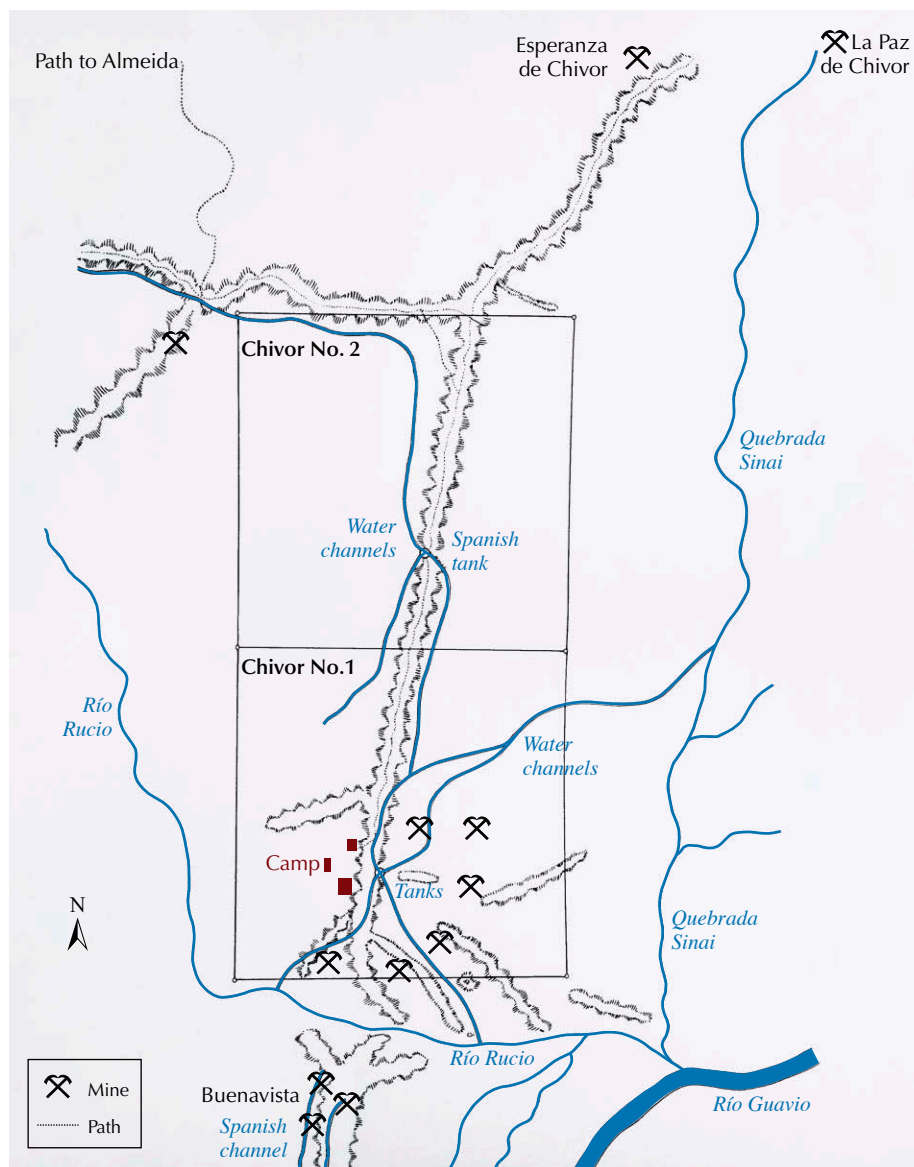


Figure 11. This map, which has been recreated based on the original hand-drawn map, shows the boundaries of the Chivor 1 and 2 mining claims registered in 1889, as well as the sites of the Esperanza de Chivor and La Paz de Chivor claims registered in 1904. These mines, referred to as part of the Chivor group, were all located between the Río Sinai and the Río Rucio (sometimes designated as Quebrada Sinai and Quebrada de las Minas, quebrada meaning gorge). The map also depicts workings, water channels, and tanks existing in 1941. South of the Río Rucio, operations at the Buenavista emerald mine are indicated. The map was incorporated in a report by the engineer Nicolas Rosso, dated January 29, 1941, to the Ministerio de Minas y Petróleos. File “Joaquín Daza B.,” Volume “Pro-puestas Minas 99,” Ministerio de Industrias, Departamento de Minas y Petróleos, Archivo General de la Nación (Colombia).

well into the 1950s, government documentation showed that the matter remained open, with the last recorded activity in the case dated to October 1958 and with no known definitive solution or final result.⁷⁹ Such a scenario contrasted markedly with Rainier’s recollection in *Green Fire*, where he represented that shortly after the 1931 examination of the mine’s boundaries, he received a telegram from the company’s agent in Bogotá declaring: “Government decided Joaquín’s claim groundless.”⁸⁰

Meanwhile, during the 1930 to 1931 period, both personal circumstances involving Rainier and hostilities at the mine property likely impacted operations, leading to possibly multiple temporary reductions or stoppages of work on behalf of the Colombia Emerald

Development Corporation. From a personal standpoint, Rainier and his wife Margaret acquired a hacienda known as “Las Cascadas” south of Río Rucio in the Departamento de Cundinamarca. The family moved there from Chivor in 1930 or 1931, when his son Peter W. Rainier, Jr., was four.⁸¹ Rainier was also

⁷⁹Diario Oficial (Colombia), 96, No. 30056 (1959), p. 597.

⁸⁰Rainier, 1942

⁸¹Peter W. Rainier, Jr., pers. comm. 2017 (“I moved to Chivor when I was two and my father was already there. I moved away from Chivor when I was four, so assume that the mine was shut down at that time. That was when my father started Las Cascadas.”). See also the interview of Peter W. Rainier Jr., by GIA staff, 2015, available at <https://www.gia.edu/gems-gemology/summer-2016-rainier-footsteps-journey-chivor-emerald-mine>.

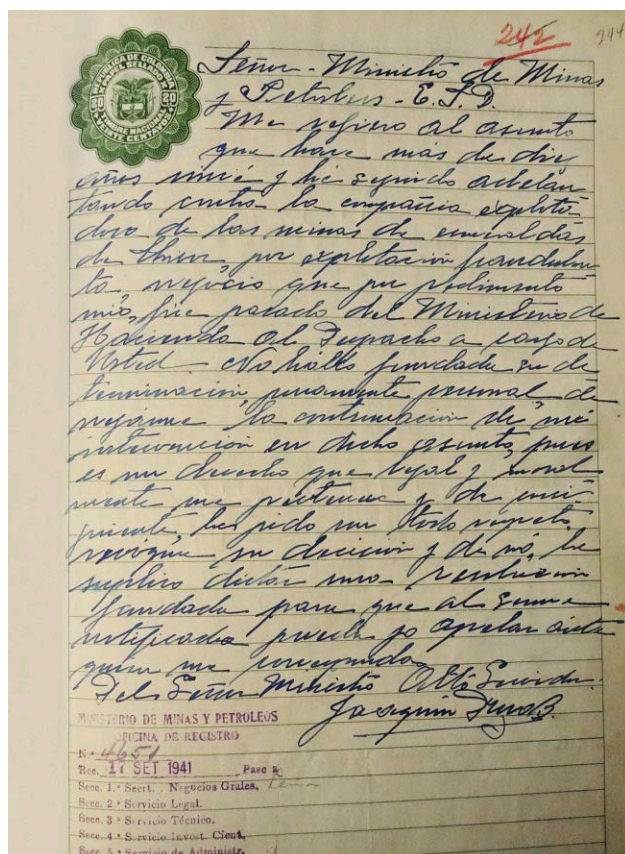


Figure 12. Letter from Joaquín Daza to the Ministro de Minas y Petróleos, dated September 1941, concerning his claims that the Chivor mine partly overlapped with his property and that mining operations were being conducted on his land. File “Joaquín Daza B.,” Volume “Propuestas Minas 99,” Ministerio de Industrias, Departamento de Minas y Petróleos, Archivo General de la Nación (Colombia).

involved, at least initially, in establishing operations at the hacienda. Nonetheless, he remained active as mine manager over Chivor, assisted by Sylvester, during the January and February 1931 developments in the Joaquín Daza case.⁸²

Regarding hostile conditions at the mine, security concerns would appear to have arisen at some point after the February 1931 inspection in the Joaquín Daza case, when the property became the target of repeated attacks from bandits. Peter W. Rainier, Jr., remembered: “After he [Peter W. Rainier, Sr.] got Las Cascadas in operation then he went back to Chivor and recaptured Chivor [from bandits] with his friends Chris Dixon and his sons and a couple of other guys and operated the mine for a while.”⁸³ Similarly, a photograph from that era showed Rainier, Christopher Ernest Dixon (figure 13), Dixon’s sons, and Sylvester



Figure 13. Christopher Ernest Dixon, business entrepreneur and emerald mining expert, worked in the 1890s for an English company then operating the Muzo emerald mine. In the first decade of the twentieth century, he became one of the shareholders in the Compañía de las Minas de Esmeraldas de Chivor that owned the mining titles for Chivor 1 and 2, and he also co-owned additional claims in the area. After Chivor was sold in 1919 to the US-based Colombian Emerald Syndicate, Ltd., he served as its official representative in Colombia in the early 1920s. Then, in the early 1930s, Dixon assisted Rainier in efforts to combat bandits at Chivor. Photo circa early 1930s; courtesy of Catalina and Melissa Dixon.

(figure 14)⁸⁴ and included a handwritten notation on the back (presumably by Rainier) that read: “Our gang

⁸²File “Joaquín Daza B.,” Volume “Propuestas Minas 99,” Ministerio de Industrias, Departamento de Minas y Petróleos, Archivo General de la Nación (Colombia).

⁸³Interview of Peter W. Rainier, Jr., by GIA staff, 2015, available at <https://www.gia.edu/gems-gemology/summer-2016-rainier-footsteps-journey-chivor-emerald-mine>.

⁸⁴Robert Elmer Sylvester was identified through assistance from Rebecca Toov, University of Minnesota Archives, pers. comm. 2018, and comparison with the photo of Sylvester, dated 1927, published in *The Gopher*, 40 (1927), p. 443 (electronic p. 463 at <https://umedia.lib.umn.edu/item/p16022coll339:27309/p16022coll339:27197>).



Figure 14. Robert Sylvester was hired in 1930 to assist Rainier in the operations at Chivor. Together with Rainier and Christopher Ernest Dixon, Sylvester was involved in the efforts to combat bandits who had invaded Chivor in 1931. Left: Detail of a photo from *The Gopher*, Vol. 40 (1927), p. 443 (electronic page 463 at <https://umedia.lib.umn.edu/item/p16022coll339:27309/p16022coll339:27197>); courtesy Rebecca Toov, University of Minnesota Archives, Minneapolis. Right: Photo with a handwritten comment (not shown) reading: “Our gang at Chivor during the bandit fighting days.” Shown from the left are Sylvester, MacFadden, Dixon (flanked by his sons), and Rainier. Photo from the Peter W. Rainier collection, courtesy of GIA.

at Chivor during the bandit fighting days.” That photo must have been taken before the close of October 1931, as that was when Sylvester left Colombia.⁸⁵

Final accounting had revealed a drastic loss of \$65,000 for the year 1930, calculated based on the actual costs of operations reduced by emerald sales worth only \$48,000.⁸⁶ Coupled with the negative assessment in the recently prepared report by Gilles, the leaders of the Colombia Emerald Development Corporation instructed Rainier to close the mine and to return to New York.⁸⁷ As directed, Rainier traveled to New York in October 1931 for consultation with the mine owners,⁸⁸ leaving his family at Las Cascadas.

According to Rainier in *Green Fire*, he returned to Colombia with preliminary permission from the company to continue mining operations at Chivor under his own responsibility.⁸⁹ He went on to recount that with the help of Dixon and his sons, the men “bombed out” the bandits who had overtaken the mine during Rainier’s absence. Rainier and Dixon then collaborated in mining the deposit for a few months, but the Colombia Emerald Development Corporation soon withdrew its permission and sent new staff to run the mine. Rainier and Dixon had to hand over operations to the new leaders sent by the owners and leave Chivor. Yet according to Rainier, the new operators again lost control of the mine after

a short period due to renewed hostilities from the bandits. Rainier’s account of this late 1931 to mid-1932 timeframe, however, has not been corroborated by independent evidence, and only the pre-October 1931 bandit fighting has been verified by the historical record.

In a report dated November 2, 1931, the United States Department of Commerce noted, “The Chivor emerald mine operated by American interests has been closed, owing to depressed prices.”⁹⁰ It was subsequently reported that Chivor was closed again in October 1932,⁹¹ but no documentation detailing the

⁸⁵File Robert Sylvester, List or Manifest of Alien Passengers for the United States Immigration Officer at the Port of Arrival, New York, October 1931, MyHeritage.com. To the extent that Rainier (1942) is susceptible to an interpretation that would place the bandit fighting solely after October 1931, such is not supported by the historical record.

⁸⁶*Engineering and Mining Journal*, 131 (1931), p. 485.

⁸⁷Rainier, 1942.

⁸⁸File Peter Rainier, List or Manifest of Alien Passengers for the United States Immigration Officer at the Port of Arrival, New York, October 1931, MyHeritage.com. The travel documentation gave Gachalá (interestingly not Chivor) as Rainier’s residence in Colombia and indicated that the purpose of the entry was to visit the Colombia Emerald Development Corporation for a planned stay of two months.

⁸⁹Rainier, 1942.

⁹⁰*Commerce Reports*, 4, No. 44 (1931), p. 247.

⁹¹*Mineral Trade Notes*, 2, No. 4 (1936), p. 18.

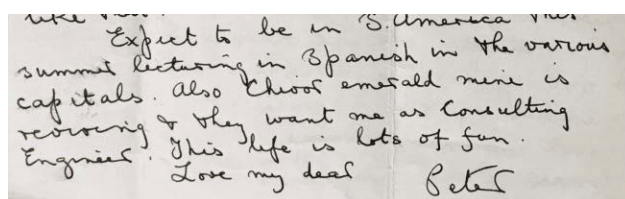


Figure 15. Detail from the final page of a letter dated April 1944 sent by Rainier to his sister Priaulx Rainier, discussing a possible return to Chivor as a consulting engineer. Priaulx Rainier collection, Royal Academy of Music, London.

mode of operation or the person(s) in charge of the mine in 1932 is available. Rainier remained in Colombia, working as a mining consultant, e.g., for the Colombian government at Muzo and Coscuez in 1933 and 1934.⁹² After the death of his wife Margaret in 1937, he left the country.⁹³

Rainier initially settled in Egypt for health reasons and then joined the British Eighth Army after the outbreak of World War II, serving from June 1940 to June 1943. During this period, Rainier was also engaged in writing several books, including *Green Fire* (1942), all in the genre of regaling readers with his adventures.⁹⁴ Following his retirement from the British Army, Rainier traveled in the United States, lecturing about his escapades fighting in Africa during the war. Speaking engagements in South America were planned as well, and he even considered taking a position as a consulting engineer at Chivor when contacted in 1944 by the mine owners about a potential attempt to reopen (figure 15).⁹⁵ Rainier died in a hotel fire in Ontario, Canada, in July 1945.⁹⁶

CHIVOR IN DORMANCY AND TRANSITION (1932–1947)

Following closure of the mine, Chivor entered a period of dormancy from an operational standpoint, at least insofar as concerned official work on behalf of the Colombia Emerald Development Corporation. Illegal mining and theft, however, remained a constant feature.⁹⁷ The interest of the press and public decreased and was only revived briefly by the release of *Green Fire* in 1942.⁹⁸

From a corporate and administrative perspective, documentation from the 1931 to 1932 period reflected that MacNamara remained president of the Colombia Emerald Development Corporation and that directors at the time included MacNamara, the banker Robert E. Henry, and the attorney Francis Philip Pace (1876–1957, figure 16).⁹⁹ On September

28, 1933, the name of the corporate entity was formally changed from Colombia Emerald Development Corporation to Chivor Emerald Mines, Inc.¹⁰⁰ The name change was registered in Colombia in November 1934.¹⁰¹ Corporate headquarters continued to be in New York City, and company information under the new name was officially filed with the New York State, Department of State, Division of Corporations, on November 23, 1935.¹⁰² Subsequent documentation from 1936 to 1940 showed that Henry was by then serving as president and Pace as secretary and/or treasurer.¹⁰³

In a renewed push to regain effective control, a national police squadron was dispatched to Chivor in 1936 to secure the mine pursuant to a contract between the government and Chivor Emerald Mines,

⁹²Rainier, 1933a, 1933b; *Minerals Yearbook* (1934), pp. 1095–1096; *Diario Oficial* (Colombia), 70, No. 22562 (1934), p. 140. Certain of these projects were undertaken in cooperation with Christopher Dixon.

⁹³Peter W. Rainier, Jr., pers. comm. 2017.

⁹⁴Published works included *African Hazard* (1940), *American Hazard* (1942), and *Pipeline to Battle: An Engineer's Adventures with the British Army* (1943). Additional book manuscripts remained unfinished. Letter by Peter Rainier, March 25, 1943, to his sister Priaulx Rainier, Priaulx Rainier collection, Royal Academy of Music, London.

⁹⁵Letter by Peter Rainier, April 25, 1944, to his sister Priaulx Rainier, Priaulx Rainier collection, Royal Academy of Music, London.

⁹⁶*The New York Times*, July 7, 1945.

⁹⁷*Diario Oficial* (Colombia), 69, No. 22208 (1933), p. 353.

⁹⁸Rainier, 1942; *The Ottawa Journal*, November 28, 1942, p. 21. Peter Rainier's story also provided the basis for a novel written by the Colombian author Torres Neira in 1967, using fictional characters styled after the real players (e.g., Rainier became Garnier).

⁹⁹*Poor's Financial Records, Industrial Manual*, New York (1931), p. 788; *Poor's Register of Directors of the United States and Canada* (1932), p. 257. Francis Philip Pace was born in Canada and moved with his parents to Buffalo, New York, in 1880. Pace was naturalized in 1890. Although his father was a stone cutter, Pace studied law and received a degree from the New York University School of Law. He went on to work in New York as a lawyer and was involved with multiple corporate boards. In his engagement with the Colombia Emerald Development Corporation and, after its renaming, Chivor Emerald Mines, Inc., Pace was supported for several years by his son Brice Pace (1915–2001), who held a degree in geology from New York University and sought to assist his father and the company as a member of the board of directors in the late 1930s. Tenth Census of the United States, 1880; *The Albany Law Journal*, 59 (1899), p. 484; *New York Herald*, August 5, 1916, p. 8; Fourteenth Census of the United States, 1920; Gregory, 1995.

¹⁰⁰State of Delaware, Department of State, Division of Corporations, Entity Details; *The Morning News*, September 29, 1933, p. 23; *The News Journal*, September 29, 1933, p. 29.

¹⁰¹Escritura 2045, November 17, 1934, Notaria 1, Archivo General de la Nación (Colombia).

¹⁰²New York State Department of State, Division of Corporations, Entity Information.

¹⁰³*The Newark Post*, November 26, 1936, p. 2; *Who's Who in New York City and State*, 10 (1938), p. 599; *Poor's Register of Directors and Executives, United States and Canada* (1940), p. 960.

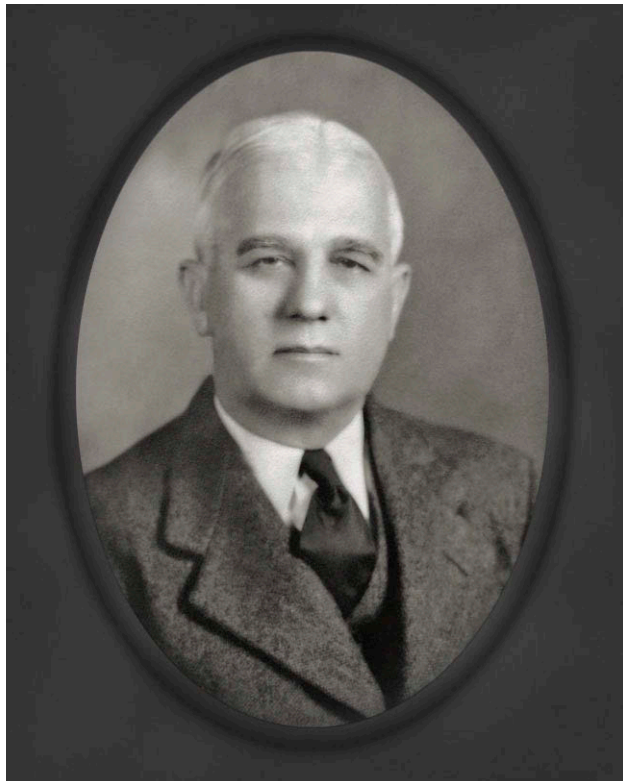


Figure 16. New York attorney Francis Philip Pace became associated with the Colombia Emerald Development Corporation by the early 1930s and continued to serve in multiple roles both under that name and as renamed Chivor Emerald Mines, Inc., in 1933. He initially filled positions as a member of the board of directors, treasurer, and secretary, eventually becoming one of the largest shareholders as well as president of the company in 1947. In the late 1940s, Pace traveled to Colombia to restart active mining operations, always in hopes of turning the company into a profitable enterprise. Photo circa 1930s; courtesy of Scott Pace.

Inc.¹⁰⁴ As a result, after several relatively quiet years with respect to mine operations, the mine was able to be leased from 1937 to 1940 (or even later) to the Compañía de Esmeraldas de Colombia, which employed about 100 workers.¹⁰⁵ In January 1941, the mine was being operated with Ernesto Fernández as the mine administrator.¹⁰⁶

Nonetheless, by 1943 the outlook of company leadership was not optimistic, with the financial press reporting: “Mr. Francis P. Pace, an attorney and treasurer of the company informed us on Oct. 29, 1943, that he has served the company for the last five years, and has received nothing for his services. He stated that he is the biggest stockholder and biggest creditor of the company. Mr. Pace considers the stock worth-

less.”¹⁰⁷ Later, as a consequence of the economic and political situation engendered by World War II, the mine again became inoperative until 1947,¹⁰⁸ with the exception of the ever-resilient illegal and uncontrolled mining, and even gun fighting, at the unguarded site.¹⁰⁹ Although the possibility of reopening may have been broached during the interim, such as by contacting Rainier in 1944 (again, see figure 15), such efforts went nowhere. After Walter J. Cowan served as corporate president in the early to mid-1940s,¹¹⁰ Pace took over that position in 1947.¹¹¹

CHIVOR UNDER RENEWED OPERATIONS (1947–1951)

After the hostilities of World War II drew to a close, the Chivor Emerald Mines, Inc., leadership endeavored to restart active mining operations. Pace always hoped that it would be possible to turn Chivor into a profitable mining site.¹¹² In service of that aim, and to address creditor issues, he traveled to Colombia at least three times, in 1947, 1948, and 1950.¹¹³ Operational control in Colombia was placed under a series of managers. James W. Raisbeck Jr., an American, began in July 1947,¹¹⁴ and was succeeded by Luis Salómon, an American, and Jacques Meyer, a Ger-

¹⁰⁴Diario Oficial (Colombia), 72, No. 23219 (1936), pp. 697–698.

¹⁰⁵*Minerals Yearbook* (1938), p. 1295; *Minerals Yearbook* (1939), p. 1393; *Minerals Yearbook* (1940), p. 1461; *Minerals Yearbook* (1941), p. 1409; Las Industrias Mineras y Manufactureras en Colombia, translation of Mining and Manufacturing Industries, United States Tariff Commission, Publication TC-250 (1949), pp. 30–31.

¹⁰⁶File “Joaquín Daza B.,” Volume “Propuestas Minas 99,” Ministerio de Industrias, Departamento de Minas y Petróleos, Archivo General de la Nación (Colombia).

¹⁰⁷Robert D. Fisher *Manual of Valuable and Worthless Securities* (1944), p. 147.

¹⁰⁸*Minerals Yearbook* (1949), p. 1579.

¹⁰⁹*Mineral Trade Notes*, 25, No. 2 (1947), pp. 28–29; Gaceta Judicial (Colombia), 72 (1952), pp. 282–290.

¹¹⁰Robert D. Fisher *Manual of Valuable and Worthless Securities*, 11 (1946), p. 149; Diario Oficial (Colombia), 83, No. 26422 (1947), pp. 454–456.

¹¹¹Diario Oficial (Colombia), 83, No. 26422 (1947), pp. 454–456; Diario Oficial (Colombia), 83, No. 26436 (1947), p. 657; Diario Oficial (Colombia), 83, No. 26672 (1948), p. 1132; Morello, 1956; Gaceta Judicial (Colombia), 97 (1961), pp. 138–145.

¹¹²Scott Pace (grandson of Francis Phillip Pace), pers. comm. 2018.

¹¹³File Francis P. Pace, Passenger Manifests of Airplanes Arriving at Miami, Florida, November 1947 and April 1948, Ancestry.com; Escritura 2204, July 12, 1950, Notaria 3a, Archivo General de la Nación (Colombia); Diario Oficial (Colombia), 87, No. 27372 (1950), pp. 367–368.

¹¹⁴Escritura 1353, April 28, 1947, Notaria 3a, Archivo General de la Nación (Colombia); Diario Oficial (Colombia), 83, No. 26422 (1947), pp. 454–456; Diario Oficial (Colombia), 83, No. 26436 (1947), p. 657.

man, in December 1947.¹¹⁵ Because of the limited funds available, the latter two instigated a contractor system under which contracted foremen hired and paid their own laborers.¹¹⁶ Salómon and Meyer were replaced by Eric G. Ramsay and Antonio C. Cosme, both United States citizens, in July 1950.¹¹⁷

Additional investment and involvement from Colombian parties had also been brought on board by 1950, as reported in the trade press:¹¹⁸

Present-day exploitation of the emerald deposits is directed by the two largest stockholders in the corporation, one of whom [Pace] has had many years' association with the firm and whose ceaseless efforts have salvaged a defunct corporation, with more or less worthless stock, and has placed it back into production, with the possibilities steadily increasing that the stockholders will at last begin to realize some return on their investment. The other of those two men [identity unknown to the authors] is a well-known Bogotá, Colombia, importer and exporter, who is in charge of the operations in Colombia. This man has himself invested large sums of money in the property, and, in his position on the spot, has been able to supervise the mining, appraisal, registration, and exportation of the gem stones.

Such efforts resulted in production of 5,400 carats in 1947, with yields increasing to 82,370 carats in 1948 and 91,656 carats in 1949.¹¹⁹ Although operations were impacted in late 1948 due to rioting and theft by local workers, the situation was brought under control after the company sent Carl (Carmine) Cavallo, an American civilian construction superintendent, to Colombia to restore order at the mine.¹²⁰

For a period extending approximately from the first to the third quarter of 1950, the New York owners employed American gem hunter Anderton



Figure 17. The American adventurer, gem dealer, and miner Russell W. Anderton took over mining operations at Chivor in the early months of 1950. After an initial term and a subsequent break, he returned to Colombia at the end of 1952. In the second half of the decade, Anderton shifted his attention to other exploration projects in the Chivor and Gachalá areas. Photo circa late 1950s; courtesy of Manuel J. Marcial.

¹¹⁵Escritura 4313, December 17, 1947, Notaria 3a, Archivo General de la Nación (Colombia); Diario Oficial (Colombia), 83, No. 26672 (1948), p. 1132.

¹¹⁶Wehrle, 1980.

¹¹⁷Escritura 2204, July 12, 1950, Notaria 3a, Archivo General de la Nación (Colombia); Diario Oficial (Colombia), 87, No. 27372 (1950), pp. 367–368.

¹¹⁸*Mineral Trade Notes*, 30, No. 1 (1950), pp. 29–38.

¹¹⁹*Minerals Yearbook* (1949), p. 1579; *Mineral Trade Notes*, 31, No. 1 (1950), pp. 31–32; *Minerals Yearbook* (1951), p. 551; *Minerals Yearbook* (1953), p. 556.

¹²⁰*Tampa Bay Times*, December 22, 1952, p. 5. Carl (Carmine) Cavallo apparently remained involved at Chivor in some capacity during periods in 1951 and 1952, but details of his role are vague. See also File Carmine Cavallo, Manifiesto de Pasajeros, Flight Bogotá – New York, December 21, 1951, MyHeritage.com.

¹²¹File Russell Anderton, List or Manifest of aliens employed on the vessel as members of crew, November 1949, MyHeritage.com.

¹²²Anderton, 1950–1951. See also Lentz, 1951; Spence, 1958a, 1958b.

(figure 17) to manage on-site operations at the mine. Anderton had just returned from gemstone ventures in Sri Lanka, having left Colombo on October 25, 1949, and having arrived in New York on November 21.¹²¹

During Anderton's tenure, mining methods differed from the practices under Klein and Rainier. According to Anderton,¹²² terraces were cut into the hillside only to the extent necessary to reveal the structures beneath the overgrowth. If promising veins were found, they were pursued exclusively by tunneling. The actual mining was still accomplished through the contractor system, with foreman hiring and paying their own laborers. The contractors identified the target areas they wished to tunnel and, upon approval from management, would organize the work. The emeralds found were (theoretically) turned over to the

mine administration, and the contractors received half the stones' value as compensation. Thievery, however, was rampant with this system.

Reported yield for 1950 amounted only to 7,177 carats,¹²³ and by late in the year tensions had arisen between the American and Colombian associates. As Anderton described in a report published in the winter of 1950–1951: “At the present writing Chivor, for all practical purposes, is closed.... The year was marked by a bitter struggle between the Colombian interests and the New York officers for control of the mine, a situation prevailing at the moment.”¹²⁴ By that point, in the midst of the mounting difficulties, Anderton had been dismissed from his management role at Chivor.¹²⁵

In the last months of 1950 and the first months of 1951, the dispute between the American and Colombian associates had intensified to the point that trade press reported: “The American group sent down a general representative to take charge of the operations. However matters became worse instead of improving, and subsequently chaos and complete lawlessness reigned the mine.”¹²⁶ The company was also in dire financial straits, owing more than 700,000 pesos (equivalent to about US\$280,000), and creditors had filed lawsuits. In August 1951, Chivor Emerald Mines, Inc., hired John M. McGrath to negotiate a financial settlement with the United States and Colombian creditors, but no resolution was achieved. Attempts by the American mine owners to sell the mine to the Colombian government were rejected as well.¹²⁷ Instead, the turmoil culminated by February 1952 in insolvency proceedings (*concurso de acreedores*) in civil court in Bogotá.¹²⁸ Efforts to sell the mine to the government were also reprised after the proceedings commenced, but the offers were rebuffed once again.

During the tumultuous period surrounding the insolvency, the entity apparently suspended mining operations from an official standpoint. Nonetheless, workers resumed some production in 1951, but all stones went into the black market.¹²⁹ With a degree of irony, a trade publication commented: “Despite this trouble, it was reported that a new vein was found at Chivor, and the emeralds produced were said to be the best quality ever taken from the mine.”¹³⁰

CHIVOR UNDER RECEIVERSHIP (1952–1970)

Once the insolvency proceedings had been instigated, Chivor operated under receivership.¹³¹ The historical record is unclear as to who first filled the role

of receiver (*síndico secuestre* or *síndico de concurso*), and details of the legal parameters governing the interaction between the receiver and company personnel are equally obscure. Anderton, however, did apparently return to the mine in a management capacity in 1952 to 1953, after writing *Tic-Polonga*.¹³² American press noted in 1952 that “Anderton is in New York now and plans to return to South America soon in another effort to control and operate these Mines.”¹³³ After that brief period, Anderton turned his attention to other prospecting and mining ventures in the Chivor and Gachalá regions. He remained in Colombia, but he gradually moved from mining operations to the gem trade in Bogotá.¹³⁴

From January 1955 to the end of September 1957, the position of receiver of Chivor Emerald Mines, Inc., in Bogotá was held by Walter de Freitas,¹³⁵ a Brazilian lawyer.¹³⁶ He was assisted by the Swiss mineralogist Dr. Jean (Juan) Stouvenel.¹³⁷ The mine inspector for Chivor throughout this period was Pedro Patiño Patiño (figure 18).¹³⁸ As receiver, Freitas's directive was to utilize company property for the benefit of creditors. Late in his term, however, he

¹²³*Mineral Trade Notes*, 33, No. 3 (1951), p. 36; *Mineral Trade Notes*, 35, No. 1 (1952), p. 35.

¹²⁴Anderton, 1950–1951.

¹²⁵The byline for the Anderton (1950–1951) article identified the author as “formerly Manager of Mines at Chivor,” thus indicating a term that had ended by the winter 1950–1951 quarter.

¹²⁶*Mineral Trade Notes*, 35, No. 1 (1952), p. 35.

¹²⁷Domínguez, 1965.

¹²⁸Memoria del Ministro de Minas y Petróleos al Congreso de 1960 (1960), pp. 20–21; *Gaceta Judicial* (Colombia), 97 (1961), pp. 138–145; Domínguez, 1965. The American mine owners were represented in Bogotá by Mauricio Makenzie.

¹²⁹*Mineral Trade Notes*, 35, No. 1 (1952), p. 35; *Minerals Yearbook* (1955), p. 440.

¹³⁰*Minerals Yearbook* (1954), p. 611.

¹³¹Anderton, 1955, 1957.

¹³²Anderton, 1965.

¹³³*The Tennessean*, November 9, 1952, p. 21.

¹³⁴Manuel J. Marcial de Gomar, pers. comm. 2017. Marcial de Gomar, a Florida-based jeweler, began working with Russell W. Anderton in Colombia in 1955 as an interpreter, and their cooperation continued in Anderton's later enterprises.

¹³⁵*Gaceta Judicial* (Colombia), 103–104 (1963), pp. 313–327.

¹³⁶Walter de Freitas studied law at the Universidade Federal de Minas Gerais in Belo Horizonte, Minas Gerais, Brazil, and received a degree in 1948. His ensuing career path saw him both working as a mining attorney and serving as an editor for the *Jurisprudência Mineira*, a Brazilian publication focused on the mining industry and prepared under the auspices of the judiciary in Minas Gerais.

¹³⁷Martínez Fontes and Parodiz, 1949; *Gaceta Judicial* (Colombia), 103–104 (1963), pp. 313–327.

¹³⁸*Gaceta Judicial* (Colombia), 127 (1968), pp. 5–8.



Figure 18. Pedro Patiño Patiño worked as a mine inspector at Chivor in the late 1950s, during the period when Walter de Freitas held the position of receiver of Chivor Emerald Mines, Inc., in Bogotá. Photo after 2000; courtesy of the Patiño family.

engaged in a transaction that would become mired in legal controversy. Freitas sold a portion of the emerald production near the end of September 1957 to Walter Maurer, a German gem merchant. A subsequent lawsuit questioned whether the sale had been properly conducted before his final day in office, while he was still authorized as receiver to dispose of company assets on behalf of creditors. The Corte Suprema de Justicia ultimately ruled in August 1961 that the transaction took place before Freitas left the position at the close of September 1957, and the decision cleared him of wrongdoing.¹³⁹

In October 1957, Freitas was succeeded by American Willis Frederick Bronkie (1912–1979, figure 19).¹⁴⁰ Bronkie filled dual roles as mining engineer over Chivor operations and receiver of Chivor Emerald Mines, Inc. One week after he took office, on October 8, 1957, Bronkie dismissed Patiño.¹⁴¹ Earlier that year, in February 1957, Pace had died, and records regarding the corporate leadership in New York become



Figure 19. Chivor was operated under the American Willis Frederick Bronkie for more than a decade, beginning in October 1957. During his tenure, he filled dual roles as mining engineer over Chivor and receiver of Chivor Emerald Mines, Inc. Insolvency proceedings instigated under Colombian law in 1952 led to a receivership that was eventually lifted in 1970. Shown on the left of Bronkie is Renata de Jara, who worked for him during the 1960s in the Bogotá office. Photo 1967; courtesy of Renata de Jara.

somewhat disjointed from that point. New York investment banker Oliver John Troster (1894–1976) served as a director and secretary from 1957,¹⁴² and by the very early 1960s (or even earlier than that), George

¹³⁹Gaceta Judicial (Colombia), 103–104 (1963), pp. 313–327.

¹⁴⁰Ibid.

¹⁴¹Gaceta Judicial (Colombia), 127 (1968), pp. 5–8. Pedro Patiño Patiño later challenged in a lawsuit whether he had been paid correctly.

¹⁴²*World Who's Who in Commerce and Industry*, 15th ed., 1967, published 1968/69, p. 1391; *Who's Who in Finance and Industry*, 16th ed., 1969, published 1970/71, p. 703; *Standard & Poor's Register of Corporations, Directors and Executives*, 2 (1975), p. 1426; *The New York Times*, October 5, 1976. Oliver John Troster had been a partner in the New York-based company Troster, Singer & Co. since 1920, and he apparently remained involved with Chivor Emerald Mines, Inc., until at least 1975.



Figure 20. In the 1960s, while Bronkie was leading operations at Chivor in Colombia, George Daniel Besler served as president of Chivor Emerald Mines, Inc., in New York. Besler held a degree in geology and throughout his career served a number of companies in various roles, focused primarily on the development of industrial technologies. Photo 1959; courtesy of Lynn G. Stewart.

Daniel Besler (1902–1994, figure 20)¹⁴³ of New York had stepped in as president of the company.¹⁴⁴

At the outset of his term, Bronkie faced substantial indebtedness to both Colombian and American creditors, as set forth in an accounting by the Corte Suprema de Justicia in 1961.¹⁴⁵ At that time, the Chivor mine was still accessible primarily by a one-day journey on horseback from Guateque, but a road to the mine from the towns Chivor and Almeida was constructed during Bronkie's tenure.¹⁴⁶

At the beginning, mining under Bronkie continued to employ the system of contractors who hired and paid their own local workers.¹⁴⁷ One inspector for each tunnel would be on the company's

payroll. The practice of using modern equipment such as an automatic compressor or bulldozers to remove the overburden, which had begun before he took office, was also continued.¹⁴⁸ Initially, work proceeded through simultaneous use of both step-cut terracing (i.e., an open-pit technique) and tunneling (i.e., an underground method following the emerald veins).¹⁴⁹ Step-cut terracing would be particularly useful in steep areas where a bulldozer was unable to operate. Tunneling work in the late 1950s involved eight separately named areas, each with a length of up to about 100 meters. For example, in April 1958, 96 men and nine contractors were working in two tunnel areas, one of which yielded gemstones worth over \$100,000 from approximately two meters of the emerald-bearing vein.¹⁵⁰ However, no new tunnels were dug, and from the mid-1960s to the end of the decade, exclusively open-pit work was performed.¹⁵¹

During that mid-1960s period, 125 miners were employed at Chivor,¹⁵² with a Spanish mine admin-

¹⁴³George Daniel Besler was the son of William George Besler (1865–1942), the general manager and president of the Central Railroad of New Jersey. George Daniel Besler received a degree in geology from Princeton University in 1926, but his subsequent career focused on industrial technology. He worked for the locomotive firm Davenport-Besler Corporation, and in the 1930s he and his brother William John Besler (1904–1985) developed high-pressure steam-powered engines for cars, locomotives, and the world's first steam-driven airplane. Throughout his life, Besler held roles in several companies. Family members recall that he was president of the company that owned the Chivor emerald mine in Colombia in the 1960s. *Who's Who in Commerce and Industry, International Edition*, 9 (1955), p. 99; Myers, 2000; Lynn G. Stewart, pers. comm. 2018.

¹⁴⁴Renata de Jara, pers. comm. 2018. Renata de Jara served as Willis Frederick Bronkie's secretary, typing and translating letters, and she recalls typing correspondence from Bronkie to George Daniel Besler as president from 1960 or 1961 onward. See also *The National Observer*, February 19, 1968, p. 8, which refers to George Besler as the president of Chivor Emerald Mines, Inc.

¹⁴⁵Gaceta Judicial (Colombia), 97 (1961), pp. 138–145.

¹⁴⁶Gonzalo Jara, pers. comm. 2018. In addition to improved physical access, Willis Frederick Bronkie apparently also sought to augment communications. He was represented in negotiations with the government for a radio transmission license by the Chivor Emerald Mines, Inc.'s legal agent in Colombia, Hernando Uribe Culla. *Diario Oficial (Colombia)*, 98, No. 30571 (1961), p. 286; *Diario Oficial (Colombia)*, 102, No. 31888 (1966), p. 495.

¹⁴⁷Johnson, 1959, 1961.

¹⁴⁸Anderton, 1957; Johnson, 1959, 1961.

¹⁴⁹Johnson, 1959, 1961.

¹⁵⁰In the late 1950s, the Colombian government also named several individuals Inspector of Emeralds in Chivor (Inspector de Esmeraldas en Chivor), always under renewable three-month contracts. *Diario Oficial (Colombia)*, 97, No. 30240 (1960), p. 581; *Diario Oficial (Colombia)*, 97, No. 30275 (1960), p. 116.

¹⁵¹Gonzalo Jara, pers. comm. 2018.

¹⁵²Anderton, 1965.



Figure 21. Sorting rough emeralds at the Chivor Emerald Mines, Inc., office in Bogotá. Photo circa 1965; courtesy of Renata de Jara.

istrator, Evaristo Muñoz.¹⁵³ Regardless of the methods used, success was extremely sporadic—mining could go on for months without production of a single emerald crystal of facetable quality.¹⁵⁴ The value of the emerald yield fluctuated on a yearly basis from as high as \$2,000,000 to as low as \$200,000.¹⁵⁵ In those years, the Colombian government oversaw the receivership and production largely through the inspector (Interventor de Salinas y Esmeraldas), Rafael A. Domínguez.¹⁵⁶

Bronkie, as both receiver of the company and mining engineer for Chivor, worked alternately in

the office in Bogotá and at the mine. He employed Alfredo Sierra as his so-called second in command and bodyguard. Life in that era was notoriously dangerous, and once Bronkie was even shot in the back at his house in Bogotá.¹⁵⁷

Between 1963 and 1968, Bronkie's business approach gradually transitioned from solely emerald mining to additional related enterprises. The broader focus incorporated dealing in and selling rough (figure 21) and cut (figure 22) stones to international buyers as well as opening jewelry shops (e.g., in Bogotá, Cartagena, Panama, Miami, and the Bahamas, figure 23).¹⁵⁸ The increased need for rough and especially cut emeralds to supply the jewelry stores was satisfied by purchasing rough and even faceted stones on the open market in Bogotá. As the 1960s drew to a close, the merchandising and retail business had overtaken the Chivor mining operations in prominence for the company.¹⁵⁹ By the end of the decade, the mine employed only 25 workers.¹⁶⁰

Given the reduced contribution from mining to the company's revenue-generating capacity, the leadership in New York began to contemplate "new methods to accelerate production."¹⁶¹ Specifically, in 1968 the press reported that Besler, as the company's president, had "sent an engineer to Bogota recently to convince Mr. Bronkie of the need to abandon eventually the laborious hand-picking method for a blasting-bulldozing operation that would increase the daily soil turnover by tenfold."¹⁶² Besler was quoted as saying: "After the receivership ends, we hope things will move along on a more progressive basis."¹⁶³

¹⁵³Alfonso Montenegro, pers. comm. 2018. Alfonso Montenegro, a miner, began working at Chivor in 1955 under Walter de Freitas, and he continued to serve under Willis Frederick Bronkie and mine administrator Evaristo Muñoz.

¹⁵⁴*The National Observer*, February 19, 1968, p. 8.

¹⁵⁵Cochrane, 1970.

¹⁵⁶Memoria del Ministro de Minas y Petróleos al Congreso de 1961 (1961), pp. 305–308; Memoria del Ministro de Minas y Petróleos al Congreso de 1963 (1963), pp. 28–31; Memoria del Ministro de Minas y Petróleos al Congreso de 1964 (1964), pp. 212–214; Memoria del Ministro de Minas y Petróleos al Congreso de 1965 (1966), pp. 195–197.

¹⁵⁷*The Morning Herald*, April 14, 1964, p. 3; Renata de Jara, Gonzalo Jara, and Robert E. Friedemann, pers. comms. 2018.

¹⁵⁸*The National Observer*, February 19, 1968, p. 8; Renata de Jara, pers. comm. 2018; Marcial, 2018.

¹⁵⁹Renata de Jara, pers. comm. 2018.

¹⁶⁰Robert E. Friedemann, pers. comm. 2018.

¹⁶¹*The National Observer*, February 19, 1968, p. 8.

¹⁶²*Ibid.*

¹⁶³*Ibid.*

Figure 22. Certificate for a faceted emerald from Chivor, signed in 1964 by Bronkie as Síndico Secuestre (receiver). Photo courtesy of Lyon & Turnbull Ltd., Fine Art, Antique & Jewellery Auctions.



Direct From the Chivor Mine to our Sales Office
in Freeport, Grand Bahama Island.

EMERALDS OF COLOMBIA LTD.
MERPORT BLDG.
FREEPORT, G.B.I.

BOGOTA

MOTEL CONTINENTAL
EDIFICIOS DE CHIVOR

CARRERA 5
CARRERA 7
CARRERA 8
CARRERA 9
CARRERA 10
CARRERA 13
CALLE 26
CALLE 15
CALLE 16
AVENIDA CARACAS

Hotel Tequendama

Main Lobby, Residencias Tequendama
Telephone - 34-25-01, Ext. 160.

Carrera 8 No. 15-46, Office No. 601
Telephones 43-59-53 and 42-91-52

Litho in U.S.A. - Litho Arts, Inc. - Miami
Airline Publications

CHIVOR EMERALD MINES INC.

EMERALDS MAKE DIAMONDS
GREEN WITH ENVY

The story of Colombian

EMERALDS

Figure 23. In the late 1960s, Bronkie's business approach gradually transitioned from solely mining at Chivor to entering the jewelry retail business. Flyer advertising shops in Freeport, Bahamas, undated; courtesy of Eduardo Restrepo Ortega.

The latter point, i.e., the end of the receivership, was apparently becoming a realistic possibility. The 1968 article noted that Bronkie had "paid the debts that forced the company into receivership 17 years ago" and that he expected "soon to file documents, asking a Colombian court to end the receivership, re-

turning control to the company's 3,000 American stockholders."¹⁶⁴ It was anticipated that when the receivership ended, Bronkie would turn over control to

¹⁶⁴Ibid.



Figure 24. A view from the campsite of the Buenavista mine, looking in a north-northeast direction to the southern bank of Río Rucio, shows the vicinity where the early indigenous tunnels were located, as well as the modern mining areas Los Gavilanes (1), Acuario (2), Calichal (3), San Gregorio (4), Milenio (5), Porvenir (6), Catedral (7), Klein & Cuatro (8), and El Pulpito (9), each represented by a mining symbol. Photo by G. Martayan, 2018.

a company representative recently sent to Colombia from New York.¹⁶⁵

That anticipation came to fruition two years later. In 1970, the Colombian court overseeing the insolvency proceedings ruled that the company's liabilities, aggregating \$330,000, had been satisfied. The receivership was lifted, and control of Chivor Emerald Mines, Inc., was returned to the entity's New York officials.¹⁶⁶ As of the year of the transition, Bronkie had been replaced by Richard S. Pastore, an American lawyer, as the final receiver; the Colombian attorney Luis E. Torres was representing the company; Noel R. Merriam, a United States citizen, was serving as general manager in Bogotá; and the Colombian Jose Rodriguez was filling the role of mine manager.¹⁶⁷ In terms of market value at that juncture, the stock was traded over the counter at 50 cents per share in 1970.¹⁶⁸ During his years in office, Bronkie had been paid, at least partly, in shares of the company, thereby becoming one of the larger shareholders.

CHIVOR POST-RECEIVERSHIP (1970–PRESENT)

With the termination of the receivership, the New York leadership regained control over mining operations at Chivor, and in 1971 the American management requested an inspector from the Colombian government to check the emerald production.¹⁶⁹

However, the Americans would soon step away from the Colombian emerald venture. Although the record as to details is beyond the scope of this study, Chivor was sold by Bronkie and/or the New York-based company representing the American shareholders in the early 1970s through a series of transactions.¹⁷⁰ Chivor was gradually taken over by Colombian interests.¹⁷¹

At present, the principal mines in the Chivor area are operated by two companies, Soescol Ltda. and San Francisco C.I.S.A., and/or their controlling shareholders Uvaldo Montenegro and Hernando Sánchez, respectively.¹⁷² Chivor is worked exclusively underground by tunneling, and open-pit emerald mining in the steep mountain range is no longer performed (figures 24 and 25). Currently,

¹⁶⁵Ibid.

¹⁶⁶*The New York Times*, May 16, 1970; Cochrane, 1970; Feininger, 1970.

¹⁶⁷Bancroft, 1971; Diario Oficial (Colombia), 108, No. 33382 (1971), p. 519; Gaceta Judicial (Colombia), 146 (1973), pp. 406–407.

¹⁶⁸*The National Monthly Stock Summary*, 117 (1970), p. 228.

¹⁶⁹*Latin America*, 5 (1971), p. 123.

¹⁷⁰Gonzalo Jara, pers. comms. 2017, 2018.

¹⁷¹Keller, 1981; Erazo Heufelder, 2005; Cepeda and Giraldo, 2012.

¹⁷²Fortaleché et al., 2017.



Figure 25. A view from the main campsite in Chivor, looking in a southwest direction, shows the steep mountain range with some small local mines and, on the other side of the valley (VR) of the Río Rucio (R), the mining areas Buenavista (1) and Mundo Nuevo (2), each represented by a mining symbol. Photo by G. Martayan, 2018.

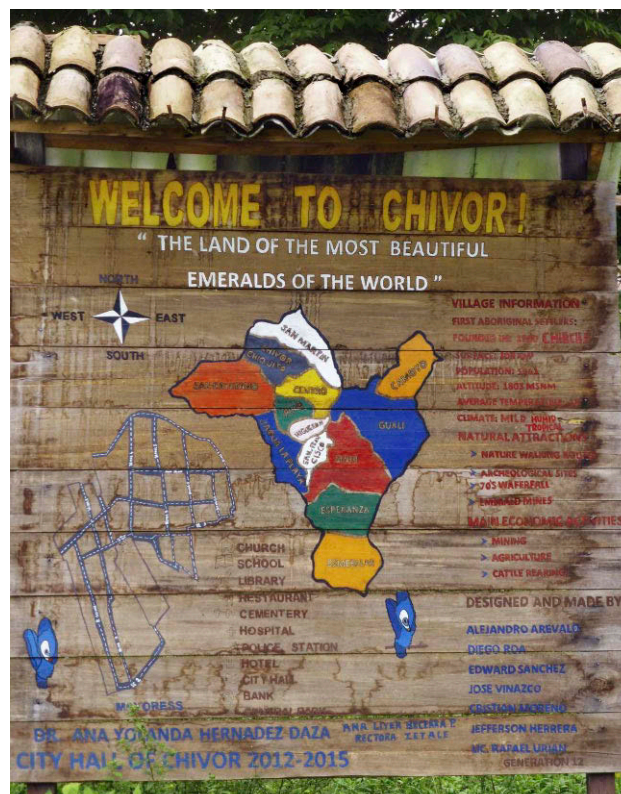
these primary operators are working numerous tunnels or mines on the different existing concessions—including San Pedro, San Gregorio, Manantial, Oriente, Piedra Chulo, Quebra Negra, Gualí, Dixon, and Tesoro.¹⁷³ Additional galleries known within the region are Gavilanes, San Judas, El Acuario, Mirador, Milenio, Porvenir, Palo Arañado, Calichal, Camoyo, Klein & Cuatro, Gualí, and El Pulpito. In the town of Chivor (figure 26), there is a small informal street market for faceted stones, specimens in matrix (figure 27), and rough emerald crystals (figure 28).

LEGENDS AND REALITY: RAINIER, ANDERTON, AND THE HISTORICAL RECORD

The view of Chivor's story from 1924 to 1970 has to date been largely guided by the accounts penned by Rainier and Anderton in *Green Fire* and *Tic-Polonga*, respectively. Both of those publications, however, are marked by notable absences. For instance, Rainier never mentioned the involvement of the corporate leadership in New York in the stock market manipulation controversy (Lewisohn, MacNamara, Rice), nor did he name either his predecessors in mine management (Burns, Mentzel) or his assistants in the work at Chivor (Gilles, Sylvester). Conversely, he dedicated a full chapter of his book to "Joaquin the Bandit," a character apparently inspired by Joa-

quín Daza with whom he was involved in a legal dispute. Yet Rainier's recitation contrasts strongly with

Figure 26. Sign welcoming visitors to the town of Chivor. Photo by G. Martayan, 2018.



¹⁷³Ibid.



Figure 27. At the local street market in the town of Chivor, miners offer emerald specimens in matrix. Photo by G. Martayan, 2018.

the detailed record found in the Archivo General de la Nación (Colombia) in Bogotá,¹⁷⁴ signaling an intent to offer an adventurous tale as opposed to an entirely factual text. Thus, a comparison of Rainier's narration in *Green Fire* with original documents preserved from the period shows that the book employed real events to establish a rough framework but that details were supplemented, embellished, and even rearranged chronologically to suit the genre. More mundane matters such as the facts from the late 1920s that led to his engagement by the mine owners and the colleagues cooperating at Chivor were omitted. With Anderton, the lack of nearly any dates to frame the events is particularly glaring. The difficulties are compounded by the fact that an untold number of individuals involved in admin-

¹⁷⁴ File "Joaquín Daza B.," Volume "Propuestas Minas 99," Ministerio de Industrias, Departamento de Minas y Petróleos, Archivo General de la Nación (Colombia).

istering or operating the mine from New York, Bogotá, or Chivor itself left few, if any, traces in publications or official records.

Nonetheless, by using independent contemporaneous materials in combination with and in restraint of the dramatized accounts, it has become possible to outline a more verifiable chronology of the period. The almost half-century in which Chivor was mainly owned and operated by the same American company saw numerous ups and downs in terms of productivity, emphasis, and financial fortunes.

In the first years after 1924, profit for the principal shareholders, in close cooperation with Rice, derived primarily from the United States stock market. Mining activities were comparatively minimal, and public interest centered on the scandals implicating company leaders Lewisohn and MacNamara. Then,

Figure 28. Rough emerald crystals are also offered by miners at the local street market in Chivor. Photo by G. Martayan, 2018.



under Rainer's mine management from the late 1920s into the beginning of the following decade, the situation shifted to a greater focus on the operational side. Before long, however, the scenario reversed again, with Chivor being closed and the company essentially withdrawing from operating the property to any significant degree until after World War II.

Yet another about-face in the late 1940s to early 1950s brought renewed operational efforts instigated by Pace on behalf of the company in New York and headed by Anderton at the mine. That era of productivity nonetheless shortly fell victim to controversy between American and Colombian associates and mounting debts. The result was insolvency proceedings instigated under Colombian law in 1952 and nearly two decades under receivership. Bronkie, as receiver and mining engineer, was eventually able to

restore a measure of financial health, and the receivership was lifted in 1970.

The American shareholders thereby regained full control over the mine, but within a few years, Chivor was sold, closing an era and paving the way for the increased local control and productivity existing today. While countless details remain fraught with mystery, particularly insofar as concerns the motivations incentivizing various decisions and any comprehensive accounting of mining costs versus emerald sales, the tale of Chivor, even as presently known, likely has few equals. One thing that is clear, however, is that Prof. Robert Scheibe's conclusion in September 1914 upon examining the mine's potential—positing a realistic "chance" for a successful venture but also an extremely high "risk" in buying the property—proved a prescient one.

ABOUT THE AUTHORS

Dr. Schmetzer is an independent researcher living in Petershausen, near Munich, Germany. Mr. Martayan is a senior geophysicist and longtime emerald aficionado residing in Paris, France. Miss Blake is a gemologist residing in Chevy Chase, Maryland.

ACKNOWLEDGMENTS

Documents, pictures, biographical data, and other information concerning the events of the years 1924 to 1970 described here have been provided by relatives of the persons involved, who have willingly reviewed their private records. Thanks are given especially to Ms. Catalina Dixon and Ms. Melissa Dixon (great-granddaughters of Christopher Ernest Dixon), Ms. Carola Kroll (granddaughter of Fritz Klein), Mr. Eduardo Restrepo Ortega

(grandson of Francisco Restrepo Escobar), Mr. Scott Pace (grandson of Francis Philip Pace), the Patiño family, Ms. Lynn G. Stewart (great-niece of George Daniel Besler), and to several individuals directly involved in events related to the history of Chivor such as Mr. Peter W. Rainier, Jr., Mr. Manuel J. Marcial, don Alfonso Montenegro, Ms. Renata de Jara, Mr. Gonzalo Jara, and Mr. Robert E. Friedmann. Mr. Dan Plazak and Mr. T.D. Thornton assisted with background concerning George Graham Rice. Ms. Rose Tozer and Ms. Judy Colbert at GIA's Richard T. Liddicoat Library in Carlsbad, California, helped with locating materials archived in the Institute's collections. Finally, countless other unnamed individuals and staff members at various United States university archives, libraries, and local administrations should also be thanked here for numerous details, references, addresses, and hints that contributed to completing the puzzle.

REFERENCES

- Albrecht H. (2013) *Adolph Lewisohn, Kupfermagnat im "Goldenen Zeitalter"*. Hamburg University Press, 148 pp.
- Anderton R.W. (1950-1951) Report on Chivor emerald mines. *G&G*, Vol. 6, No. 12, pp. 376-377, 379.
- (1953) *Tic-Polonga*. Doubleday & Company, Inc., New York, 254 pp.
- (1954) *Tic-Polonga*. Museum Press Limited, London, 224 pp.
- (1955) The new Gachalá emerald mine in Colombia. *G&G*, Vol. 8, No. 7, pp. 195-196.
- (1957) Emerald outlook in Colombia. *G&G*, Vol. 9, No. 2, pp. 60-61.
- (1965) The present status of Colombian emerald mining. *Lapidary Journal*, Vol. 19, No. 3, pp. 374-377.
- Bancroft P. (1971) The lure of Chivor. *Lapidary Journal*, Vol. 25, No. 1, pp. 128-131.
- Brock F.W. (1929) Investment pitfalls. *Oral Hygiene*, Vol. 19, pp. 789-795.
- Canova L.J. (1921) *Legend of the Discovery of Emeralds in the Colombian Andes*. Colombian Emerald Syndicate, Ltd., New York, 30 pp.
- Cepeda I., Javier Giraldo S.J. (2012) *Victor Carranza, alias "el Patrón"*. Grijalbo, Random House Mondadori, S.A., Bogotá, 162 pp.
- Cochrane R.S. (1970) U.S. owners regain Colombia gem mine. *Lapidary Journal*, Vol. 24, No. 5, p. 766.
- Domínguez R.A. (1965) *Historia de las Esmeraldas de Colombia*. Gráficas Ducal, Bogotá, 297 pp.
- Erazo Heufelder J. (2005) *Der Smaragdkönig*. Piper Verlag, München, 294 pp.
- Feininger T. (1970) Emerald mining in Colombia: History & geology. *The Mineralogical Record*, Vol. 1, No. 4, pp. 142-149.

- Fortaleché D., Lucas A., Muiyal J., Hsu T., Padua P. (2017) The Colombian emerald industry: Winds of change. *G&G*, Vol. 53, No. 3, pp. 332–358, <https://dx.doi.org/10.5741/GEMS.53.3.332>
- Gilles V.A. (1930) Geology of the Chivor emerald mine. In O. Buis and W.F. Bronkie, Eds., *Guide Book to the Geology of the Chivor Emerald Mine*. Colombian Society of Petroleum Geologists and Geophysicists, published 1966, pp. 5–18.
- Gregory E.I. (1995) *Incredible Stories of World War II Veterans*. Senior Publishers, Vineburg, California, pp. 54–57.
- Johnson P.W. (1959) The emeralds of Chivor today. *Lapidary Journal*, Vol. 13, No. 4, pp. 516–524.
- (1961) The Chivor emerald mine. *Journal of Gemmology*, Vol. 8, No. 4, pp. 126–152.
- Keller P.C. (1981) Emeralds of Colombia. *G&G*, Vol. 17, No. 2, pp. 80–92, <https://dx.doi.org/10.5741/GEMS.17.2.80>
- Klein F. (1941) *Smaragde unter dem Urwald*. Oswald Arnold Verlag, Berlin, 285 pp.
- (1951) *Smaragde unter dem Urwald*. Selbstverlag, Idar-Oberstein, 291 pp.
- Lentz M. (1951) Emeralds of Chivor. *Lapidary Journal*, Vol. 5, No. 3, pp. 172–176.
- Marcial M.J. (2018) *The Tears of Fura*. Outskirts Press, Denver, 293 pp.
- Martínez Fontes E., Parodiz J.J. (1949) *Guía de naturalistas sudamericanos*. Talleres Gráficos Lucania, Buenos Aires, 138 pp.
- Morello T. (1956) The gem of Colombia. *Américas*, Vol. 8, No. 10, pp. 21–24.
- Myers W.S. (2000) *Prominent Families of New Jersey*. Clearfield, Baltimore, Vol. 1, pp. 142–143 (reprint, originally published as *The Story of New Jersey*, 1945).
- Peretti A., Falise T. (2018) *Magnificent Green*. Second Edition, GRS Gemresearch Swisslab AG, Lucerne, 263 pp.
- Plazak D. (2006) *A Hole in the Ground with a Liar at the Top: Fraud and Deceit in the Golden Age of American Mining*. The University of Utah Press, Salt Lake City, Utah, 374 pp.
- Rainier P.W. (1929) The Chivor-Somondoco emerald mines of Colombia. The American Institute of Mining and Metallurgical Engineers, Technical Publication No. 258, 21 pp.
- (1931) The Chivor-Somondoco emerald mines of Colombia. *Transactions of the American Institute of Mining and Metallurgical Engineers AIME*, Vol. 96, pp. 204–223.
- (1933a) Las minas de esmeraldas de Muzo y Coscuez. Internal report, printed 1958 in *Boletín de Minas*, Vol. 5, Nos. 56–57, pp. 10–19.
- (1933b) Informe geológico de las minas de esmeraldas de Muzo. Internal report, printed 1965 in R.A. Domínguez, *Historia de las esmeraldas de Colombia*, Gráficas Ducal, Bogotá, pp. 237–240.
- (1934) Formación esmeraldífera de Chivor (Colombia-Sur América). *Minería*, Vol. 3, No. 28, pp. 1806–1815.
- (1942) *Green Fire*. Random House, New York, 296 pp.
- Rice G.G. (1913) *My Adventures with Your Money*. Richard G. Badger, Boston, 363 pp.
- Schmetzer K., Martayan G., Ortiz J.G. (2020) History of the Chivor emerald mine, Part I (1880–1925): From rediscovery to early production. *G&G*, Vol. 56, No. 1, pp. 66–109, <https://dx.doi.org/10.5741/GEMS.56.1.66>
- Spence G.H. (1958a) Emerald mining in Colombia. *The Gemmologist*, Vol. 27, No. 327, pp. 197–198.
- (1958b) Emerald mining in Colombia. *The Gemmologist*, Vol. 27, No. 328, pp. 215–218.
- Thornton T.D. (2015) *My Adventures with Your Money: George Graham Rice and the Golden Age of the Con Artist*. St. Martin's Press, New York, 298 pp.
- Torres Neira H. (1967) *Una gema y un destino*. Bogotá, 178 pp.
- Wehrle L. (1980) *Die Tränen des Mondes. Erlebtes aus Peru, Ecuador und Kolumbien*. Meyster Verlag, Wien–München, pp. 205–208.
- Weldon R., Ortiz J.G., Ottaway T. (2016) In Rainier's footsteps: Journey to the Chivor emerald mine. *G&G*, Vol. 52, No. 2, pp. 168–187, <https://dx.doi.org/10.5741/GEMS.52.2.168>
- Winkler M. (1928) *Investments of United States Capital in Latin America*. World Peace Foundation, Boston, p. 127.

For online access to all issues of GEMS & GEMOLOGY from 1934 to the present, visit:

gia.edu/gems-gemology



OPTICAL WHITENING AND BRIGHTENING OF PEARLS: A FLUORESCENCE SPECTROSCOPY STUDY

Chunhui Zhou, Tsung-Han Tsai, Nicholas Sturman, Nanthaporn Nilpetploy, Areeya Manustrong, and Kwanreun Lawanwong

White pearls and those with very light hues are routinely processed or treated by various methods after harvest, especially akoya and freshwater cultured pearls. Bleaching is the most prevalent and is often used in addition to *maeshori* treatment, an umbrella term for various types of luster enhancements. However, little reference has been made in the literature to the use of optical brighteners, the focus of this study, within the pearl trade. In this project, known samples of optically brightened akoya cultured pearls were studied and compared with their non-brightened counterparts and cultured pearls of various types. In addition, a South Sea cultured pearl was treated in-house with a commercial whitening product. Our preliminary results indicated that pearls treated by this method showed strong bluish fluorescence under long-wave ultraviolet (UV) excitation, and can be confidently separated from non-brightened pearls using fluorescence spectroscopy when a distinct fluorescence maximum at around 430 to 440 nm is observed.

Optical brightening agents (OBAs) are chemical compounds that can absorb light in the ultraviolet and violet region of the electromagnetic spectrum and emit light in the blue region as fluorescence, due to their extended conjugation and/or aromaticity. They are sometimes called fluorescent brightening agents or fluorescent whitening agents, and have been frequently used to enhance the appearance of fabric and paper (Lanter, 1966; Leaver and Milligan, 1984; Esteves et al., 2004; Bajpai, 2018). While many types of brighteners are listed in the Colour Index (<https://colour-index.com>), only a handful are commercially important. Some examples are shown in figure 1.

Photoluminescence is light emission from any form of matter after the absorption of photons. Fluorescence is a type of photoluminescence in which a molecule dissipates its absorbed energy through the rapid emission of a photon, while phosphorescence is the emission of radiation in a similar manner to fluorescence but on a longer timescale, so that emission continues after excitation ceases. Fluorescence

can be generated by exciting the substance via a range of energy sources. The molecule in the substance absorbs the source energy and once excited moves from a lower electronic state to a higher one. Immediately after absorbing energy, it loses the energy by emitting a photon; this process of photon emission is called luminescence. Typically, fluores-

In Brief

- Akoya and freshwater cultured pearls are routinely processed to improve their appearance.
- Long-wave UV radiation is a quick and useful tool to aid in the identification of some treatments.
- Optically brightened pearls appear white with the addition of agents, while bleaching makes pearls whiter by removing discoloration or pigmentation.
- Fluorescence spectroscopy is a quick and effective way of separating optically brightened pearls from bleached and untreated ones.

cence occurs at a lower energy than the absorbed radiation; this phenomenon is known as the Stokes shift (Lakowicz, 2006).

Fluorescence occurs widely in nature. For example, many kinds of gemstones such as rubies, emer-

See end of article for About the Authors and Acknowledgments.

GEMS & GEMOLOGY, Vol. 56, No. 2, pp. 258–265,

<http://dx.doi.org/10.5741/GEMS.56.2.258>

© 2020 Gemological Institute of America

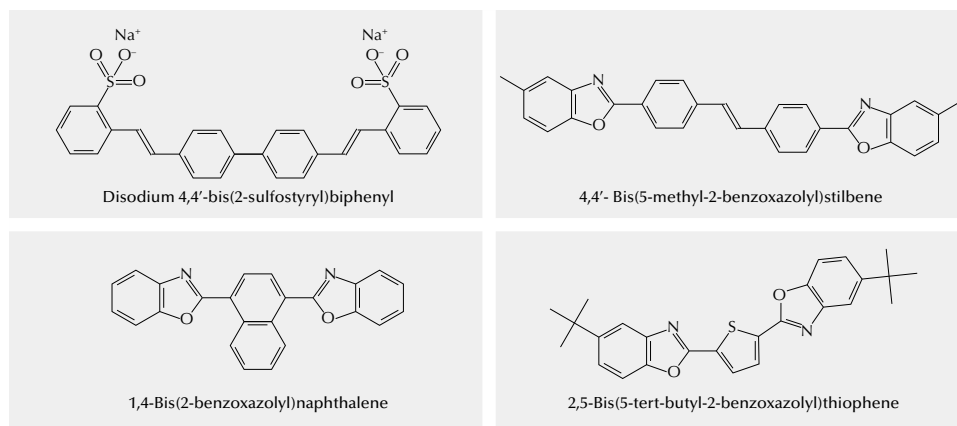


Figure 1. Chemical structures of commonly used optical brightening agents.

als, and diamonds can emit visible light when exposed to ultraviolet light. For research purposes, fluorescence can be measured by fluorescence spectroscopy. The emission signal from the sample is collected by a spectrometer to monitor the distribution in fluorescence intensity as a function of wavelength. Since fluorescence has a short lifetime, typically decaying within nanoseconds after the excitation, the sample must be constantly illuminated to maintain its fluorescence signal.

Fluorescence spectroscopy has been used extensively as a basic tool in a wide range of research fields, including chemistry, biology, mineralogy, and gemology (Lakowicz, 2006). For example, structural defects in minerals usually result in characteristic fluorescence. A typical application is to use fluorescence spectroscopy to distinguish natural diamond from its synthetic counterparts (Tsai and D'Haenens-Johansson, 2019). One important feature of fluorescence spectroscopy is its high sensitivity, which enables it to detect the luminescence signal from a near-zero background. Modern sensors make single-photon sensitivity possible. As a result, fluorescence spectroscopy is extremely sensitive, allowing for the detection of weak signals. Pearl, a biogenically originated material, inherits fluorescence characteristics typical of many organic materials, and the biogenic aragonite that constitutes the bulk of a pearl is well known for its fluorescence properties. These facts make fluorescence spectroscopy a potentially very useful tool for the identification of pearls from different species located in various areas.

Since both pearls and OBAs possess characteristic fluorescence features, the use of fluorescence spectroscopy makes it possible to easily detect pearls treated by such agents. The traditional way to observe pearl fluorescence is to use long-wave UV (LWUV) and short-wave UV (SWUV) lamps to excite

the sample and visually observe the fluorescence effect (color, intensity, distribution, etc.). Untreated white to cream-colored pearls generally show blue to greenish blue fluorescence under LWUV excitation. Akoya and freshwater cultured pearls, which are routinely processed, typically show strong bluish white fluorescence. Similar to these pearls, OBAs are also highly fluorescent. With exposure to UV radiation, a bright blue glow is visible from the OBA solution (an example is shown in figure 2). The use of fluorescence spectroscopy can easily separate the minor differences in fluorescence color exhibited by some pearls and the OBAs.

Figure 2. An example of blue fluorescence emitted by an OBA solution used in our in-house treatment experiment under LWUV radiation. Photo by Chunhui Zhou.



The use of OBAs in the cultured pearl industry is not unusual (Song and Fan, 1999; Japan Pearl Promotion Society, 2014), as they are sometimes routinely applied to cultured pearls post-harvest along with other types of processes such as bleaching or *maeshori* (which refers to various types of luster enhancement), but very little has been written in the gemological literature about the identification of this process (Shor, 2007). It is important to differentiate between the whitening effects due to bleaching and those produced by optical brightening, as they depend on two very different mechanisms: bleaching removes, or reduces the concentrations of, the color-causing pigmentations within pearls, while optical brighteners add an artificial optical effect to pearls, making them look less yellow by increasing the overall amount of blue light emitted due to these chemicals' blue fluorescence properties. The focus of this study is to use fluorescence spectroscopy as an easy method to detect the presence of OBAs. Such a technique would be of great practical interest to the trade and public in order to faithfully differentiate treated from untreated pearls.

MATERIALS AND METHODS

Two groups of mostly white-colored akoya bead cultured pearls ranging from 6.97×6.54 mm to 8.14×7.48 mm were supplied by Orient Pearl (Bangkok) Ltd. One group (139 pearls) was reportedly treated with unidentified OBAs in addition to the routine bleaching process, while the other group (150 pearls) was only bleached and not treated with OBAs (figure 3). In addition, three different types of white cultured pearls (akoya, freshwater, and South Sea) from GIA's research collection (figure 4), as well as samples from an untreated akoya strand reportedly cultured in Vietnam, also from GIA's research collection (figure 5), were included in the study.

One white South Sea cultured pearl was also treated in-house using a commercial laundry product (Rit Whitener & Brightener). According to the label, this product contained optical brighteners and sodium chloride. The pearl was immersed in the saturated brightener solution (approximately 1 g of brightener powder per 100 mL of water) for 3 hours at a slightly elevated temperature (about 40°C), with

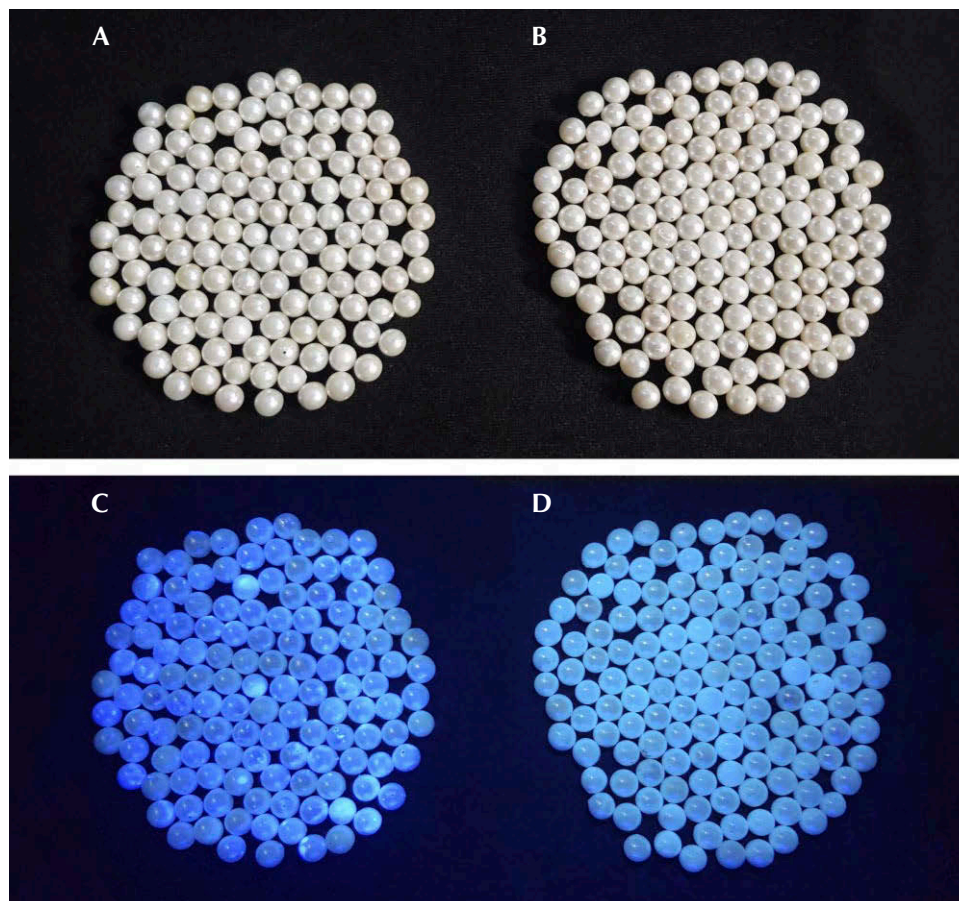


Figure 3. A group of optically brightened and bleached white akoya cultured pearls (A) and a group of bleached-only (no OBAs) akoya pearls (B) under normal daylight (A and B) and LWUV radiation (C and D). The samples exposed to OBAs exhibited a more intense bluish fluorescence reaction (C). Photos by Nanthaporn Nilpetploy.

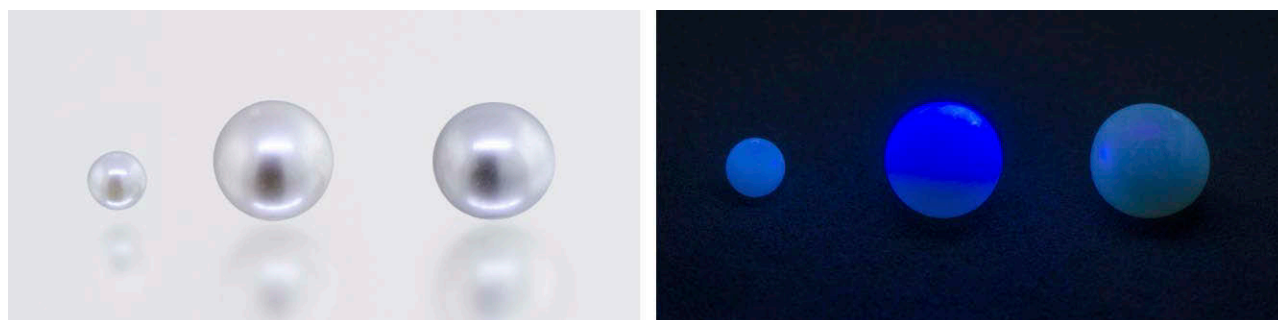


Figure 4. Three white cultured pearls—akoya (left), freshwater (middle), and South Sea (right)—shown in daylight (left photo) and exhibiting fluorescence under LWUV excitation (right photo). The freshwater pearl exhibited a distinctive blue fluorescence, which suggested it had been optically brightened. Photos by Sood Oil (Judy) Chia.

occasional stirring. It was subsequently rinsed with tap water and air-dried before further examination.

All the samples were initially examined using various standard gemological techniques, including a gemological microscope, ultraviolet-visible (UV-Vis) reflectance spectroscopy, and Fourier-transform (FTIR) reflectance spectroscopy. Because these tests cannot consistently identify optical brighteners, the results are not shown here. For the purpose of this particular project, a fluorescence spectroscopy unit was designed to measure pearl fluorescence with the aim of detecting OBAs. The fluorescence spectroscopy unit included a 385 nm UV light-emitting diode (LED) as the excitation light source, a spectrometer for monitoring the visible light region as the fluorescence sensor, and a bi-fabricated fiber-optic probe that guided the excitation light to the sample

and transmitted the collected fluorescence signal from the sample to the detector. The spectrometer was configured to monitor the spectrum from 400 to 700 nm, which covers the fluorescence range needed to analyze reactions from untreated pearls and OBAs. Two optical filters were used to isolate the pearl fluorescence from the UV LED in order to avoid the excitation light overwhelming the sensor, as well as to enhance the sensitivity of the system. A 390 nm short-pass filter was positioned behind the UV LED, and a 410 nm long-pass filter was positioned in front of the detector.

In addition to fluorescence spectroscopy, visual observation of the fluorescence reactions was performed under a conventional 5-watt LWUV (365 nm) lamp or a GIA-designed LWUV unit incorporating a narrow-band 365 nm UV LED source.

Figure 5. A strand of non-bleached and non-brightened akoya cultured pearls of various colors (left) and their varied fluorescence reactions under LWUV radiation (right). Photos by Sood Oil (Judy) Chia.



RESULTS

The two groups of akoya cultured pearls exhibited similar external appearances in terms of their size, color, shape, luster, and surface condition. The group that had been bleached and treated with OBAs appeared to be slightly whiter and more lustrous than the non-brightened group, although this could be due to the individual differences among the samples. No systematic before and after comparison on the appearances of the treated group was available. Under LWUV radiation, the group treated with OBAs showed a more consistent and stronger bluish reaction (again, see figure 3). Some of the OBA-treated pearls (especially the cream samples) showed spotty and uneven reactions under LWUV, indicating the treatment concentrated in surface areas where blemishes existed. This was confirmed by microscopy since the surface condition of the nacre was not perfect given the lower grade of akoya used in the experiment. In order to see if OBAs were detectable, fluorescence spectroscopy was applied to selected samples from each group, and the results are shown in figure 6. All bleached-only samples tested showed broad fluorescence maxima at around 480 to 490 nm, while the bleached and OBA-treated samples showed narrower fluorescence maxima at around 430 to 434 nm with an additional shoulder around 470 nm. The

Figure 6. Fluorescence spectra of bleached and optically brightened (red) and bleached and non-brightened (blue) akoya pearls. The non-brightened pearls show a broad fluorescence maximum at around 480 to 490 nm, whereas the OBA-treated samples exhibit a narrower fluorescence maximum at around 430 to 434 nm with a shoulder at around 470 nm.

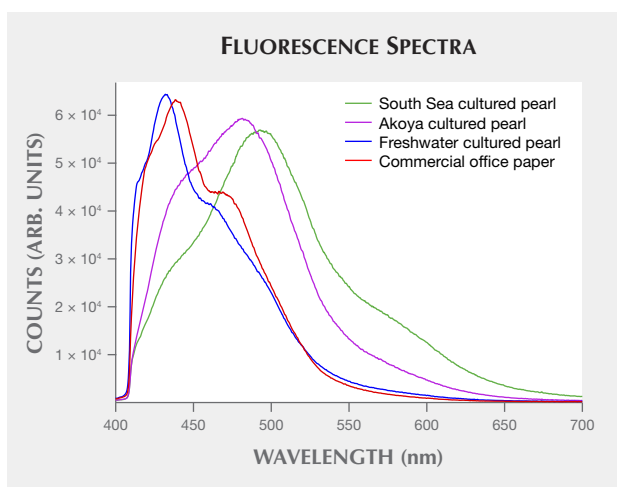
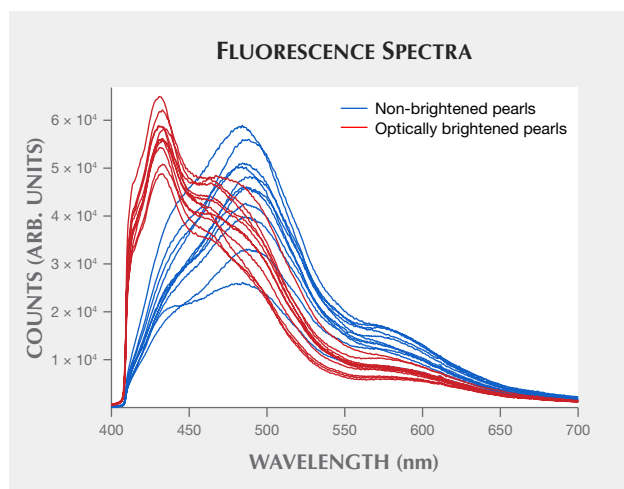


Figure 7. The fluorescence spectra of a white South Sea cultured pearl (green), white akoya cultured pearl (purple), white freshwater cultured pearl (blue), and white commercial office paper (red). The freshwater pearl tested in this study and the white paper show fluorescence results consistent with those expected for OBAs.

shifted fluorescence maxima are consistent with the fluorescence characteristics of commercially available OBAs (Lawson-Wood and Evans, 2018).

The three white cultured pearl samples from GIA's collection showed various fluorescence reactions under LWUV (figure 4, right photo). The South Sea cultured pearl showed a moderate greenish reaction and the akoya cultured pearl a slightly bluish reaction, while the freshwater pearl exhibited the most distinctive and strongest bluish reaction. These observations indicated that the South Sea cultured pearl was most likely not treated, the akoya cultured pearl was most likely traditionally processed with bleaching, and this particular freshwater pearl was also processed. Its UV fluorescence reaction looked very similar to the optically brightened akoya samples we studied. The fluorescence spectra of these three pearls confirmed these predictions (figure 7). The South Sea cultured pearl showed a fluorescence maximum at around 494 nm, the akoya cultured pearl at around 482 nm, and the freshwater pearl at around 432 nm with a shoulder at around 465 nm. The fluorescence reaction and the spectrum of the freshwater pearl matched well with the OBA-treated akoya samples discussed earlier.

Additionally, a piece of standard commercial white office paper was tested. Its fluorescence reaction under LWUV was found to be strong blue, and its fluorescence spectrum exhibited a maximum at around 439 nm with a shoulder at around 474 nm, similar to the

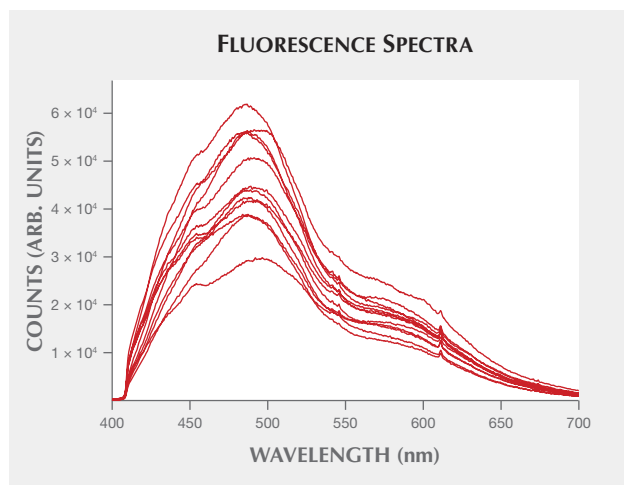


Figure 8. Fluorescence spectra of variously colored untreated akoya pearls, showing fluorescence maxima ranging from around 480 to 500 nm. The small sharp peaks shown near 540 and 610 nm are due to the ambient environment (room light and computer monitor light reflection).

OBA-treated pearls studied. It was no surprise to see such features since optical brighteners are routinely applied to commercial white paper (Bajpai, 2018).

In order to verify the results, several non-bleached and non-brightened akoya cultured pearls of various colors that included cream, light yellow, silver, and light gray were tested with the same fluorescence spectroscopy method. Untreated akoya pearls can ex-

hibit this same wide range of bodycolors when routine processing is not carried out (Otter et al., 2017). These pearls showed a variety of weak fluorescence reactions under LWUV radiation, with the weaker reactions the result of fluorescence quenching by their bodycolors (figure 5, right).

Spectroscopic results showed that in keeping with bleached akoya pearls, these samples exhibited a fluorescence maximum ranging between 480 and 500 nm (figure 8). These results and additional tests (data not shown) on GIA akoya and South Sea cultured pearls (master samples), as well as on untreated freshwater pearls of various colors from the GIA research collection, confirmed that non-brightened pearls fluoresce a weaker blue (cyan) color (480 to 500 nm), while OBA-processed pearls exhibit more intense blue and violet colors (430 to 440 nm).

Finally, one white South Sea cultured pearl was treated in-house using a commercial laundry product (Rit Whitener & Brightener) containing OBAs and sodium chloride, as indicated on its label. The main ingredient listed on the manufacturer's website for this type of product is linear alkylbenzene sulfonate (CAS No. 25155-30-0). The simple method described in the Materials and Methods section resulted in an increased bluish fluorescence under LWUV, and also a slightly higher luster and whiter appearance for the pearl (figure 9). Its fluorescence changed to shorter wavelengths from around 500 nm to around 443 and 478 nm as expected, similar to the fluorescence results

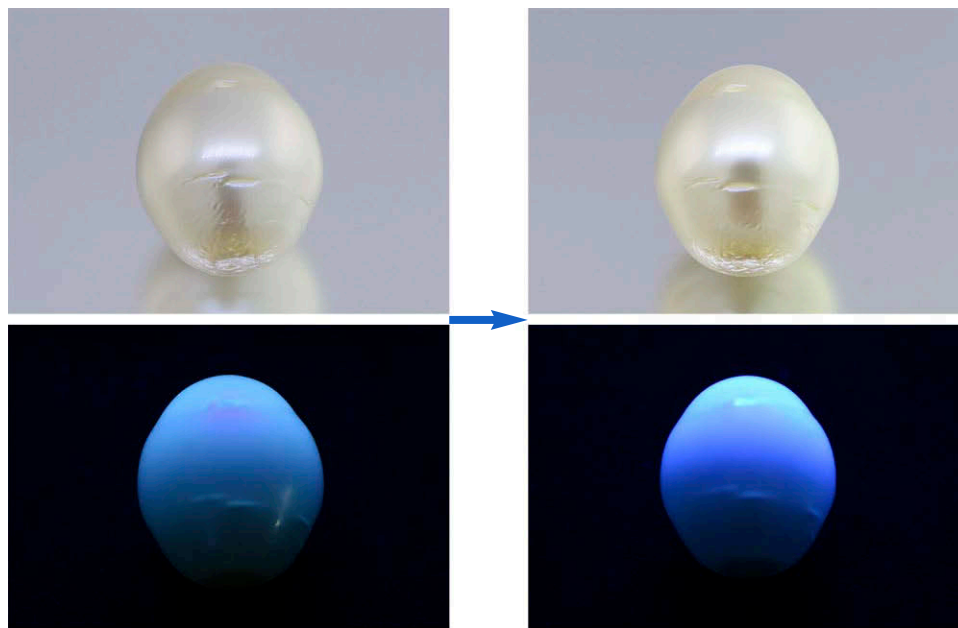


Figure 9. External appearances and fluorescence reactions under LWUV of a white South Sea cultured pearl before (left) and after (right) in-house treatment using a commercial brightener. Photos by Sood Oil (Judy) Chia.

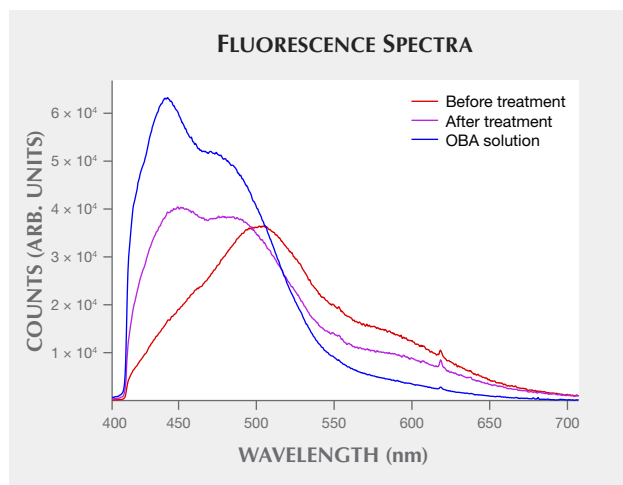


Figure 10. Fluorescence spectra of the white South Sea cultured pearl before (red) and after (purple) in-house brightening treatment. The OBA solution's spectrum is also shown in blue.

obtained for the OBA solution itself (figure 10). However, the exact OBAs applied for routine pearl treatment in the trade are most likely different from the one applied in the in-house experiment, and the actual methods are probably much more sophisticated and time sensitive. This likely explains why the fluorescence maximum of the pearl treated in-house differs from the treated samples obtained from the trade.

DISCUSSION

The application of OBAs to pearls is not new in the pearl trade, but it is sometimes not regarded as a treatment (Japan Pearl Promotion Society, 2014). OBAs are usually applied in conjunction with bleaching and are thus considered part of routine processing. Little has been discussed in the gemological literature on the identification of this process, even though optical brightening and bleaching utilize two different mechanisms to enhance the appearances of pearls. In this study, the authors focused on the identification of this process using fluorescence spectroscopy in combination with visual fluorescence observations under LWUV radiation. Both methods proved useful, but the spectroscopic method has the advantage of accurately distinguishing OBA-processed pearls from routinely processed pearls, regardless of their colors, which might affect the visual appearance and intensity of their UV fluorescence. While bleaching may make their fluorescence inten-

sities stronger, OBAs often change the fluorescence properties of the pearls more dramatically for both the fluorescence hues and intensities. These changes are consistent with the original fluorescence properties of the OBAs (shifting the fluorescence maxima to shorter wavelengths in the blue and violet range). Since there are many different types of OBAs in the market and the exact process is unknown, the effects of OBAs are not within the scope of this study, although we observed a slight increase in luster and white appearance for the South Sea cultured pearl treated in-house. With more sophisticated methods and better chemicals, these effects could be more prominent. The extent of such a process used in the trade is also not clear; the authors have heard some sources in the trade say it is used less often than it was many years ago. Similarly, the stability of such a process also requires better sample comparison and prolonged observation, which has not been fully addressed in this study.

In addition to the detection of OBAs in pearls, fluorescence spectroscopy could potentially have applications in the detection of other color treatments used on pearls (Tsai and Zhou, 2020). Furthermore, differences in the fluorescence characteristics of various types of pearls may also be used to separate pearls from different host mollusk species, as previously reported (Ju et al., 2011). While the optimal UV excitation wavelength for pearls has not been fully investigated, the excitation source used in this particular study has proved quite effective. The full potential of this advanced technique for pearls and other gemstone identification scenarios warrants greater attention.

CONCLUSIONS

This study proves that fluorescence spectroscopy, in combination with visual fluorescence observation, may provide a quick and easy way to detect the presence of different optical brighteners that have been applied to various nacreous pearls. The samples examined generally showed a strong fluorescence peak at around 430–440 due to OBAs, while non-brightened pearls usually exhibited a fluorescence peak at around 480–500 nm. While cultured pearls may be subject to routine processes involving various types of chemical agents, it is important for the trade to be aware of this particular component and its identification criteria.

HYDROGEN AND OXYGEN STABLE ISOTOPE RATIOS OF DOLOMITE-RELATED NEPHRITE: RELEVANCE FOR ITS GEOGRAPHIC ORIGIN AND GEOLOGICAL SIGNIFICANCE

Kong Gao, Ting Fang, Taijin Lu, Yan Lan, Yong Zhang, Yuanyuan Wang, and Yayun Chang

Hydrogen and oxygen stable isotope ratios of dolomite-related nephrites around the world were studied using data from the literature ($n = 120$). These isotope ratios are highly effective for discriminating dolomite-related nephrites from the four most important origins worldwide. Nephrite from Vitim in Russia has the lowest isotope ratio values reflected in $\delta^2\text{H}$ and $\delta^{18}\text{O}$ values, followed by Chuncheon in South Korea and then Xinjiang Uyghur Autonomous Region in China. Nephrite from Sanchakou in the Qinghai Province of China has the highest values. Other occurrences are characterized by high $\delta^{18}\text{O}$ values similar to or higher than those of samples from Sanchakou. The differences are derived mainly from the ore-forming fluids. Vitim and Chuncheon isotope ratio values were mainly affected by meteoric water (rainwater, lake water, seawater, river water, glacial water, and shallow groundwater). Xinjiang nephrite-forming fluids were mixtures of magmatic hydrothermal fluids (able to be modified by metamorphism) and meteoric water. The hydrothermal fluids forming the Qinghai, Luodian, Dahua, and Xiuyan nephrites underwent some metamorphic alteration or regional metamorphism.

Nephrite is a near-monomineralic rock composed of tremolite-actinolite, $\text{Ca}_2(\text{Mg,Fe})_5\text{Si}_8\text{O}_{22}(\text{OH})_2$. It occurs worldwide (figure 1) and is classified as dolomite-related or serpentine-related according to the different parent rocks and ore-hosting rocks, and both types form by metasomatism (Yui et al., 1988; Tang et al., 1994; Yang and Abduriyim, 1994; Harlow and Sorensen, 2005; Burtseva et al., 2015). The large and well-known dolomite-related nephrite deposits are distributed in the Xinjiang Uyghur Autonomous Region (hereafter abbreviated as Xinjiang) of China, Qinghai Province of China, Siberia in Russia, and Chuncheon in South Korea (figure 1). Data from smaller-scale deposits such as Val Malenco in Italy and Złoty Stok in Poland are also used in this study (figure 1). The rest of the data were collected from nephrites produced at multiple small-scale

sources in China: Xiuyan, Tanghe, Dahua, and Luodian (figure 2).

With nephrite jade, a premium is placed on geographic origin since the gem's cultural significance differs by location. It is possible to have an opinion

In Brief

- Geographic origin can have a significant impact on the value of nephrite.
- Hydrogen and oxygen stable isotope ratios, particularly the latter, provide a robust tool for origin determination.
- Dolomite-related nephrites from Vitim, Chuncheon, Xinjiang, and Qinghai differ from one another by distinct hydrogen and oxygen stable isotope ratios.
- Differences in hydrogen and oxygen stable isotope ratios for nephrite are related to ore-forming fluids.

on the origin of a small amount of nephrite by simple visual examination, since some varieties with unique

See end of article for About the Authors and Acknowledgments.

GEMS & GEMOLOGY, Vol. 56, No. 2, pp. 266–280,
<http://dx.doi.org/10.5741/GEMS.56.2.266>

© 2020 Gemological Institute of America

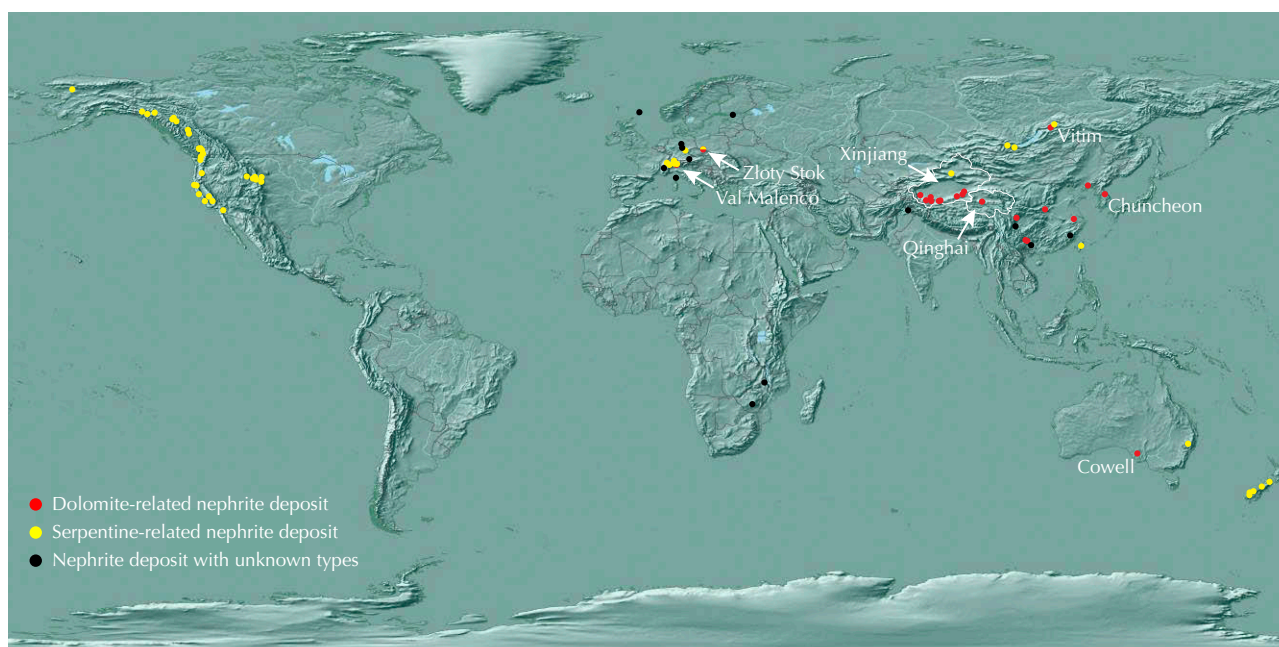


Figure 1. Distribution map of reported nephrite deposits worldwide. The four most important dolomite-related nephrite sources are Vitim in Russia, Chuncheon in South Korea, and Xinjiang and Qinghai in China. From @naturalearthdata.com.

gemological characteristics such as color, luster, and transparency have mainly occurred in specific deposits. In Xinjiang, for example, high-quality white primary nephrite occurs in Qiemo County.¹ There it is commonly associated with brown nephrite (figure 3A, rough with white core and very thick brown rind). The brown is a color seldom found in nephrite from other deposits in Xinjiang. The highest-quality white primary nephrite (figure 3B, white plate) mostly comes from the Hetian region and Qiemo County. Placer nephrite (figures 3C and 3D, pendants with figures carved out of brownish red skin) occurs in the Yulongkashi River and Kalakashi River basins. A considerable quantity of primary nephrite from Ruoqiang County features a yellow color component (figure 3E, greenish yellow fish) that is absent from other samples. Black nephrite (figure 3F, bangle bracelet) colored by graphite, on the other hand, mainly occurs in the Hetian region and has not been found in Qiemo County or Ruoqiang County. However, the origin determination of a tremendous amount of dolomite-related nephrite cannot be solved by this simple observation. Previous researchers used trace elements combined with appearance to identify geographic origin and obtained some

informative results (Zhong et al., 2013; Luo et al., 2015). Unfortunately, rigorous and scientific determination of geographic origin is still not available.

Hydrogen and oxygen isotope ratio values (see box A), which might vary for the same gemstone from different regions due to diverse ore-forming environments and models, can be used for geographic origin determi-

TABLE 1. Location names expressed in Chinese *pinyin* and their English equivalents.

Chinese <i>pinyin</i>	English
A'erjishan	Altyn Tagh
Alamasi	Alamas
Bayinguoleng region	Bayingholin region
Hetian	Hoten/Hotan
Kalakashi, Hetian	Qaraqash, Hoten
Kashi region	Kashkar region
Keliya River	Keriye/Keriya River
Qiemo County, Bayinguoleng	Cherchen County, Bayingholin
Ruoqiang County, Bayinguoleng	Chaqliq County, Bayingholin
Takelamagan Desert	Taklimakan Desert
Tashiku'ergan County	Taxkorgan/Tashkurghan County
Yecheng County, Kashi	Qaghiliq County, Kashkar
Yulongkashi, Hetian	Yurungqash, Hoten
Yutian County	Keriye County, Hoten

¹This paper uses Chinese *pinyin* to express all Chinese location names involved, and the corresponding commonly used English names are listed in table 1.



Figure 2. The distribution of main dolomite-related nephrite deposits of China. Primary and placer nephrite occur at Xiuyan, but the latter is not plotted in the map.

nation (Giuliani et al., 1998, 2000, 2005, 2007). A mass spectrometer is needed to determine the isotope ratio values (see box B). The spot produced by secondary ion mass spectrometry (SIMS), laser ablation-inductively coupled plasma-mass spectrometry (LA-ICP-MS), and laser ablation inductively coupled plasma time-of-

flight mass spectrometry (LA-ICP-TOF-MS) for stable isotope analysis of gemstones can be restricted to craters of 10–100 μm in diameter and a few angstroms to microns deep (Giuliani et al., 2000, 2005; Abduriyim and Kitawaki, 2006; Wang et al., 2016, 2018). The craters produced are very small, to the point of not

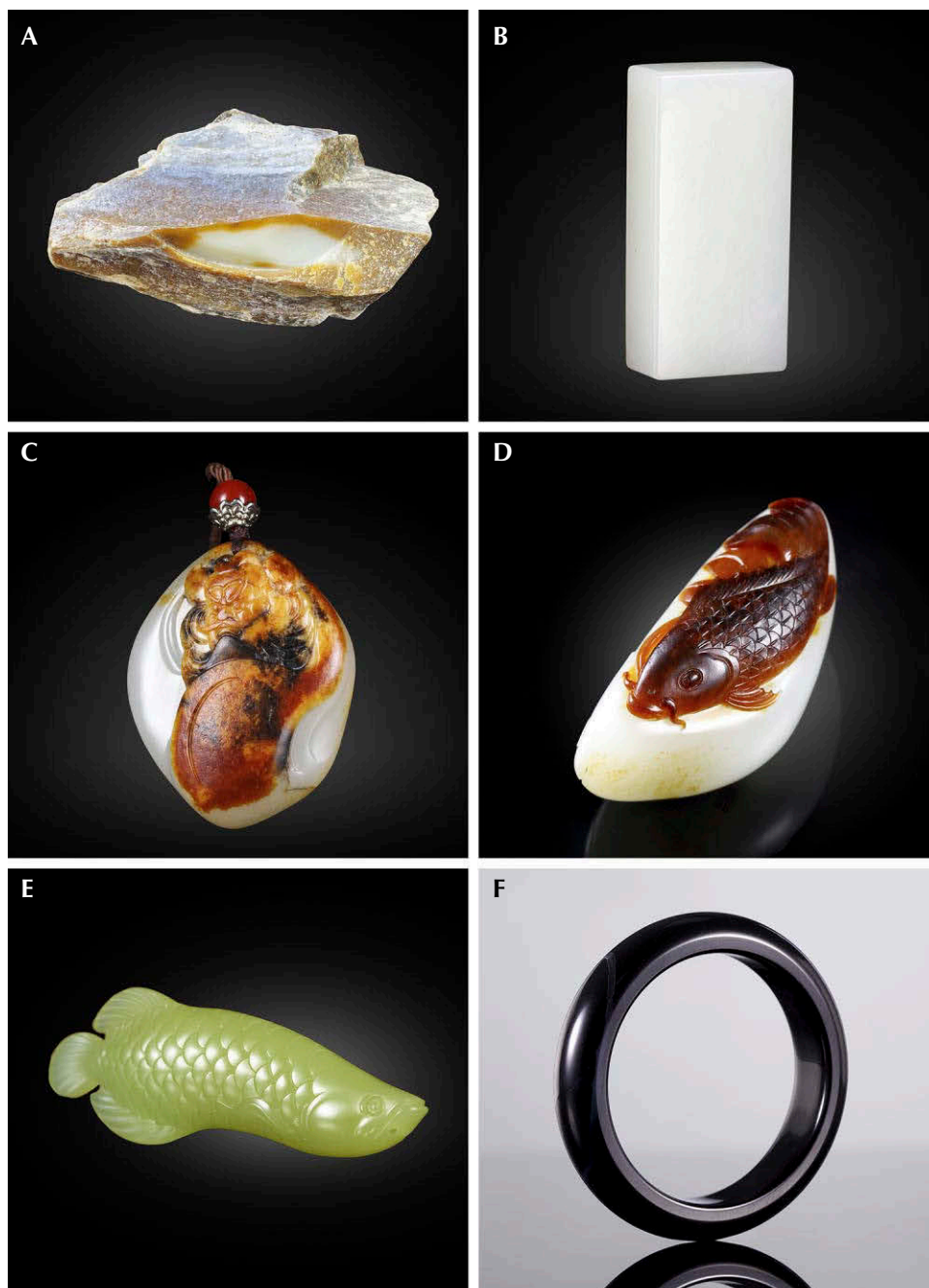


Figure 3. Nephrites from different localities of Xinjiang showing distinct appearances. A: The rough is a typical piece of white-brown nephrite from Qiemo County. B: The white plate is primary nephrite of the highest quality, which occurs in both the Hetian region and Qiemo County. C and D: Two pendants carved from placer nephrite collected in the Hetian region feature brownish red skin sculpted into different figures. E: The greenish yellow fish features a yellow color component of primary nephrite from Ruoqiang. F: Black nephrite like that of the bangle bracelet mainly occurs in the Hetian region. Photos by Dong He; courtesy of Elegant China.

being noticeable without magnification. This permits the method to be applied to gemstones and historical antiques (Giuliani et al., 2000, 2005).

Geographic origin discrimination of nephrite by isotopes is seldom reported, even though many hydrogen and oxygen isotope ratio studies on this material have been carried out (table 2). By summarizing and analyzing all available hydrogen and oxygen isotopic data of dolomite-related nephrites worldwide from published references, this study discusses the geographic origin discrimination based on the rela-

tionship between the characteristics of nephrite and its formation environment.

WHY DO ISOTOPE RATIOS MATTER TO GEMOLOGISTS?

The application of isotopes has gradually attracted the attention of gemologists (Wang et al., 2016). In addition to hydrogen and oxygen isotope ratios, which can help determine the geographical origins of corundum and emerald (Giuliani et al., 1998, 2000, 2005, 2007; Wang

BOX A: INTRODUCTION TO OXYGEN AND HYDROGEN STABLE ISOTOPE RATIOS

Atoms with an equivalent atomic number (i.e., atoms of the same element) can differ from one another in their number of neutrons. For example, ^{18}O has 8 protons and 10 neutrons, and ^{16}O has 8 protons and 8 neutrons; ^2H , also known as deuterium (D), has 1 proton and 1 neutron, while ^1H has 1 proton and no neutrons. Such atoms with the same number of protons but different numbers of neutrons are defined as isotopes.

The mass difference inherent from divergent neutrons causes isotopic fractionation, which occurs as the isotopes of an element are distributed between two substances or phases in differing ratios in a given system. This process can be affected by temperature, equilibrium or kinetic processes, and other physiochemical processes. The isotope fractionation will reach and maintain equilibrium unless conditions change. Therefore, isotope abundance can be used as a tracer to reveal certain geochemical processes in geological bodies.

Isotope ratio, defined as the measured relative abundance of a heavy isotope to its lighter counterpart (e.g., $^{18}\text{O}/^{16}\text{O}$ and $^2\text{H}/^1\text{H}$), is typically used rather than the isotope abundance itself. The isotopic fractionation factor (α) is introduced to represent the extent of fractionation of isotopes between two phases. It is defined as the ratio of isotope ratios in one phase to the other coexisting phase. For example, in a system consisting of phase A and phase B, the oxygen isotope fractionation factor can be defined as

$$\alpha_{\text{A-B}} = \frac{(^{18}\text{O}/^{16}\text{O})_{\text{A}}}{(^{18}\text{O}/^{16}\text{O})_{\text{B}}}$$

et al., 2019), carbon isotopes are considered useful in identifying natural and synthetic diamonds (Wang et al., 2014), and radioactive isotopes have also been used to determine the ages of gemstones (Link, 2015).

Traditional methods using the parameters of inclusions, optical characteristics, and trace elements are often not enough to solve the problems of geographic origin determination of nephrite. Isotopic analysis has provided geochemical and chronological information for all sorts of geological samples: Stable isotopes can be used to study gemstone origin (source materials, formation process, and geographical localities), whereas radioactive isotopes can be utilized to determine the formation ages. The stable isotope study of dolomite-related nephrite in our works, together with previous studies on corundum and emerald (Giuliani et al., 1998, 2000, 2005, 2007; Wang et al., 2019), show that the geographic origin characteristics of isotopes in gemstones can be explained from their formation environment and formation process.

The isotopic fractionation factor is always a function of temperature, which can be obtained by theoretical calculation or experiment (Graham et al., 1984; Zheng, 1993, 1995).

Both oxygen and hydrogen isotope ratios are also reported in so-called delta notation given in terms of per mil (‰). In other words, the delta value

$$\delta^{18}\text{O} = \frac{(^{18}\text{O}/^{16}\text{O})_{\text{sample}} - (^{18}\text{O}/^{16}\text{O})_{\text{standard}}}{(^{18}\text{O}/^{16}\text{O})_{\text{standard}}} \times 1000\text{‰}$$

and

$$\delta^2\text{H} = \frac{(^2\text{H}/^1\text{H})_{\text{sample}} - (^2\text{H}/^1\text{H})_{\text{standard}}}{(^2\text{H}/^1\text{H})_{\text{standard}}} \times 1000\text{‰}$$

in which $^{18}\text{O}/^{16}\text{O}$ and $^2\text{H}/^1\text{H}$ are the isotope ratios defined above. Values of delta > 0 indicate that relative to the standard samples, the tested sample has a higher heavy isotope abundance, and a negative delta value indicates a higher light isotope abundance.

International general isotope standards are issued by the International Atomic Energy Agency (IAEA) and the U.S. National Institute of Standards and Technology (NIST). The delta values of hydrogen and oxygen isotopes are calculated using the value for Standard Mean Ocean Water (SMOW), which has $^2\text{H}/^1\text{H}$ of $(155.76 \pm 0.10) \times 10^{-6}$, $^{18}\text{O}/^{16}\text{O}$ of $(2005.20 \pm 0.43) \times 10^{-6}$, and $^{17}\text{O}/^{16}\text{O}$ of $(373 \pm 15) \times 10^{-6}$. Other hydrogen isotope standard samples include SLAP, GISP, NBS-22, and NBS-30.

Thus, relative isotopic abundances are reliable parameters for determining geographic origin and offer a sound complement to traditional methods.

DATA AND CALCULATION

In all, 120 sets of hydrogen and oxygen isotope data (some lacking hydrogen data) for dolomite-related nephrites were collected from all known related published studies, from a variety of researchers (table 2 and figure 4), to illustrate geographic origin discrimination with stable isotopic ratios.

Hydrogen and oxygen isotope delta values of nephrite can be used to calculate the corresponding values of its formation fluids. Hydrogen isotope fractionation of tremolite relative to water is not affected by temperature in the approximate range of 350° to 650°C (Graham et al., 1984), and thus

$$10^3 \ln \alpha_{\text{Tr-H}_2\text{O}} = -21.7 \pm 2 \quad (1)$$

while oxygen isotope fractionation (Zheng, 1993, 1995) can be expressed as

$$10^3 \ln \alpha_{\text{Tr-H}_2\text{O}} = (3.95 \times 10^6 / T^2) - (8.28 \times 10^3 / T) + 2.38 \quad (2)$$

In both equations, $\alpha_{\text{Tr-H}_2\text{O}}$ is the isotopic fractionation factor (see box A) between the nephrite and its formation fluid, and T is the absolute temperature (K) of the nephrite-forming system. The nephrite formation temperature is confined to approximately 223°–425°C, especially near 350°C (Tang et al., 1994; Yui and Kwon, 2002; Chen et al., 2014; Liu et al., 2016), by methods using the homogenization temperatures of tremolite fluid inclusions (Liu et al., 2011a; Chen et al., 2014), the combination of the pyrite decrepitation temperature and calcite homogenization temperature (Wang et al., 2007; Xu and Wang, 2016), the mineral assemblage (Yang, 2013), and isotopes (Yui et al., 1988). Thus, the value of 350°C was used to calculate the isotopes of fluids from which nephrite forms.

Both the isotope fractionation factor $\alpha_{\text{Tr-H}_2\text{O}}$ and delta values ($\delta^{18}\text{O}$, $\delta^2\text{H}$) are defined after isotope ratios ($^{18}\text{O}/^{16}\text{O}$, $^2\text{H}/^1\text{H}$) of nephrite and its formation fluids (see box A). Thus, the delta values of the nephrite-forming fluids ($\delta^{18}\text{O}_{\text{Tr-H}_2\text{O}}$, $\delta^2\text{H}_{\text{Tr-H}_2\text{O}}$; table 2) can be cal-

culated from the delta values of corresponding nephrite, which is acquired by isotope determination (see box B).

GEOGRAPHIC ORIGIN CHARACTERISTICS

Vitim in Russia, Chuncheon in South Korea, and Xinjiang and Qinghai in China are the four most important dolomite-related nephrite source areas. The relative abundances of the hydrogen and oxygen isotopes of nephrites from these regions differ significantly (figure 4). In particular, oxygen isotope $\delta^{18}\text{O}$ values (see figure 4 and table 2) range from -20.0‰ to -14.6‰, -9.9‰ to -8.2‰, 0.5‰ to 7.9‰, and 11.4‰ to 12.6‰, respectively, without any overlap. Cowell in Australia is considered another large dolomite-related nephrite deposit but is seldom studied. The only $\delta^2\text{H}$ - $\delta^{18}\text{O}$ data (see figure 4 and table 2) fall within the range of Xinjiang placer nephrite; nevertheless, the $\delta^2\text{H}$ values are significantly higher than those of Xinjiang primary nephrite.

The nephrites from Xinjiang, distributed in a belt longer than 1300 km, show convergent hydrogen and oxygen isotopic characteristics. The isotope delta values of their primary dolomite-related nephrites are covered by placer ones (figure 4).

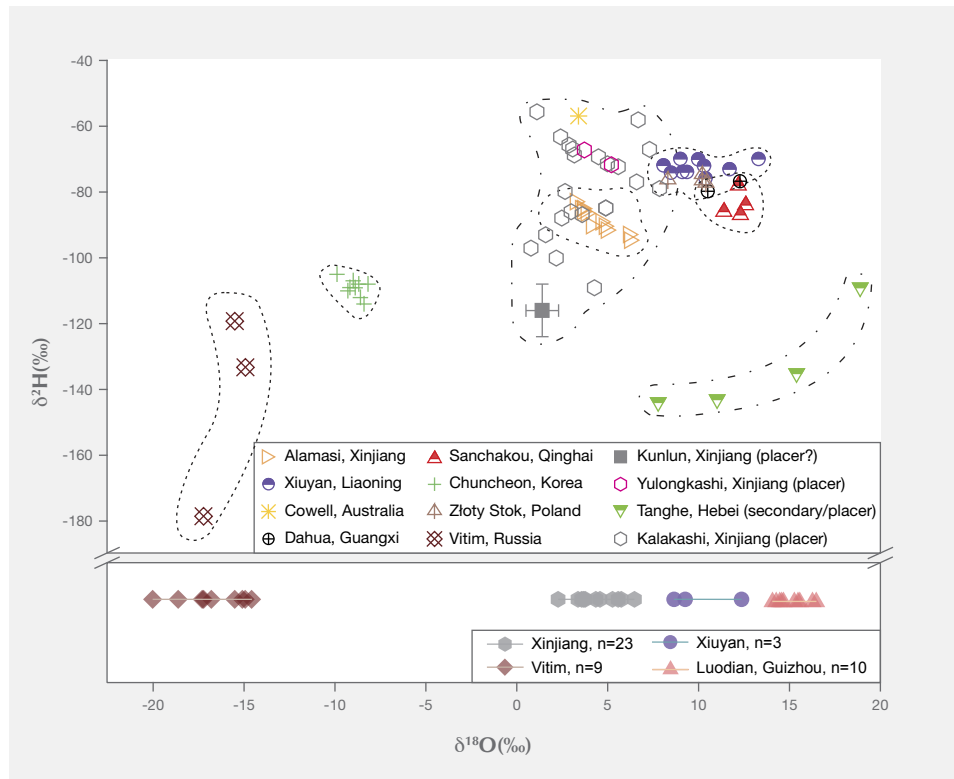


Figure 4. Hydrogen and oxygen isotopic compositions (top), and oxygen isotopic composition only (bottom), of dolomite-related nephrites around the world.

BOX B: ANALYTICAL METHODS FOR DETERMINING OXYGEN AND HYDROGEN ISOTOPE CONCENTRATIONS

Isotope concentrations are commonly measured with a mass spectrometer operating on the principle that the degree of deflection of charged particles in a magnetic field is inversely proportional to the mass-to-charge ratio (m/z) (figure B-1). Generally, mass spectrometers can be divided into four parts: the sampling system, the ion source, the mass analyzer, and the detector.

Stable isotope analysis has advanced from macroanalysis to microanalysis and now includes methods of static mass spectrometry, laser ablation (multi-collector)-inductively coupled plasma-mass spectrometry (LA-(MC)-ICP-MS), and secondary ion mass spectrometry (SIMS). High accuracy and low sample loss make these technologies suitable for isotopic analysis of gemstones.

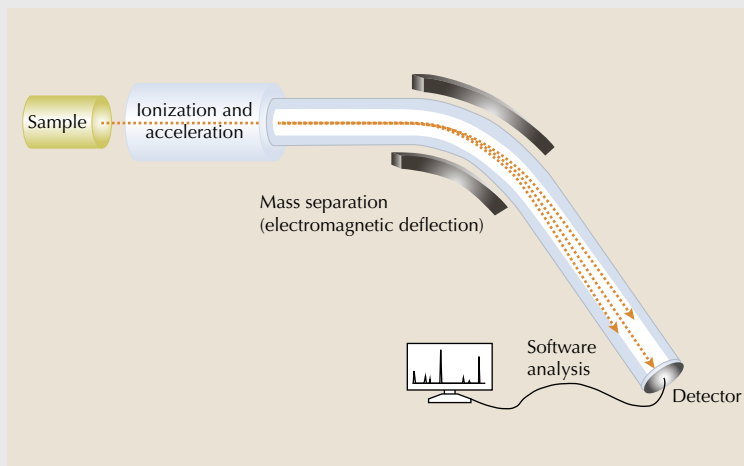


Figure B-1. The basic schematic of mass spectrometry. Modified from chem.libretexts.org.

Samples from some relatively small deposits such as Xiuyan in Liaoning Province, Złoty Stok in Poland, and Dahua in Guangxi Province (figure 4) show slightly higher $\delta^2\text{H}$ values than those of Qinghai nephrite and Xinjiang primary nephrite. Their ranges of $\delta^{18}\text{O}$ values cover that of Sanchakou samples but do not overlap with Xinjiang primary nephrite. Fortunately, nephrites from these three regions typically have their own distinct appearances. Luodian nephrite from Guizhou has notably higher $\delta^{18}\text{O}$ values than the others (no $\delta^2\text{H}$ value data have been collected). In recent years, secondary nephrite has been found in the Tanghe River in Hebei Province. It is speculated to be a dolomite-related nephrite according to the regional geology, field observation, and petrographic analysis (Chen et al., 2014). Its hydrogen and oxygen isotope ratios are completely isolated from others in the plot of $\delta^2\text{H}$ - $\delta^{18}\text{O}$ (figure 4) by low $\delta^2\text{H}$ and high $\delta^{18}\text{O}$ values.

NEPHRITE-FORMING FLUIDS FROM MAGMATIC WATER AND METEORIC WATER

Fluids containing gases, liquids, and silicate compositions always occur as the most active parts of geological processes. They are composed mainly of H_2O , CO_2 , NaCl, metal components, silicate compositions, and organic matter. The fluids that correspond to nephrite formation are hydrothermal fluids, which refer to gas-liquid two-phase systems having their own temperatures and pressures. Hydrothermal flu-

ids are released from magma (magmatic fluids) or metamorphism (metamorphic fluids) due to changes in temperature and pressure. They also can be meteoric waters (including rainwater, lake water, seawater, river water, glacial water, and shallow groundwater) heated by geological processes.

The original characteristics of the hydrogen and oxygen isotopes of nephrite mainly result from the ore-forming fluids. The calculated $\delta^2\text{H}_{\text{Tr-H}_2\text{O}}$ and $\delta^{18}\text{O}_{\text{H}_2\text{O}}$ values of hydrothermal fluids forming the Vitim and Chuncheon nephrites plot near the Craig line² (figure 5), indicating that their predominant ore-forming fluids were meteoric waters in an environment with a high fluid/rock ratio (Yui and Kwon, 2002; Burtseva et al., 2015).

For the Xinjiang nephrite, magmatic fluid, meteoric water, and metamorphic water are all possible candidates for the ore-forming fluids (figure 5), and a low fluid/rock ratio is indicated (Yui and Kwon, 2002; Liu et al., 2011a, 2011b, 2016). The $\delta^{18}\text{O}_{\text{H}_2\text{O}}$ values of the nephrite-forming fluids for Alamas nephrite, which occurs in granite-dolomite contact zones (Liu et al., 2010, 2011a), decrease in the con-

²The Craig line, also referred to as the meteoric water line, represents the relationship between $\delta^2\text{H}$ and $\delta^{18}\text{O}$ of meteoric water—i.e., $\delta^2\text{H} = 8\delta^{18}\text{O} + 10$ (Craig, 1961). The kaolinite line (Zheng and Chen, 2000) shown in figure 5 represents the relationship between $\delta^2\text{H}$ and $\delta^{18}\text{O}$ of kaolinite in weathering profile (i.e., $\delta^2\text{H} = 7.5\delta^{18}\text{O} - 220$). Most of the soil samples in nature fall on or near the kaolinite line.

tact zone in the order of granite → nephrite → wall rock. The $\delta^{18}\text{O}_{\text{H}_2\text{O}}$ values of magmatic fluids, seldom influenced by crustal rocks during intrusion, should equal the high values of the Xinjiang nephrite-forming fluids (figure 5). The $\delta^{18}\text{O}_{\text{dol}}$ values of wall rock are far lower than those of common carbonates of sedimentary origin, at only 6.1‰ (Wan et al., 2002). Then, the $\delta^{18}\text{O}_{\text{H}_2\text{O}}$ value for the water in equilibrium with wall rock is 1.6‰ ($1000 \ln \alpha_{\text{dol-H}_2\text{O}} = 3.06 \times 10^6/T^2 - 3.24$ after Zheng and Chen (2000), assuming that the temperature for the wall rock during nephrite formation was between 252° and 295°C). This value is lower than those of the fluids in equilibrium with most of the Xinjiang nephrite (figure 5). In addition, considering the characteristics of the chemical zoning (Liu et al., 2010), the higher $\delta^{18}\text{O}_{\text{H}_2\text{O}}$

values for green nephrite fluids than for white ones in the Alamasí deposit (Wan et al., 2002) provide another indicator that oxygen isotopes decrease from granite to wall rock. However, the $\delta^{18}\text{O}_{\text{H}_2\text{O}}$ value should have increased gradually if water unilaterally diffused from the granite to the wall rock, since water in equilibrium with nephrite is enriched or slightly depleted in ^{18}O (depending on the temperature, calculated according to Equation 2 with T around 350°C). Considering that the $\delta^2\text{H}$ value of the Alamasí nephrite is negatively related to the $\delta^{18}\text{O}$ value (figure 4), the conflict can be explained by dualistic fluid sources. One is post-magmatic hydrothermal fluids provided by the granite forming the nephrite, while the other must be the meteoric water from the dolomite marble.

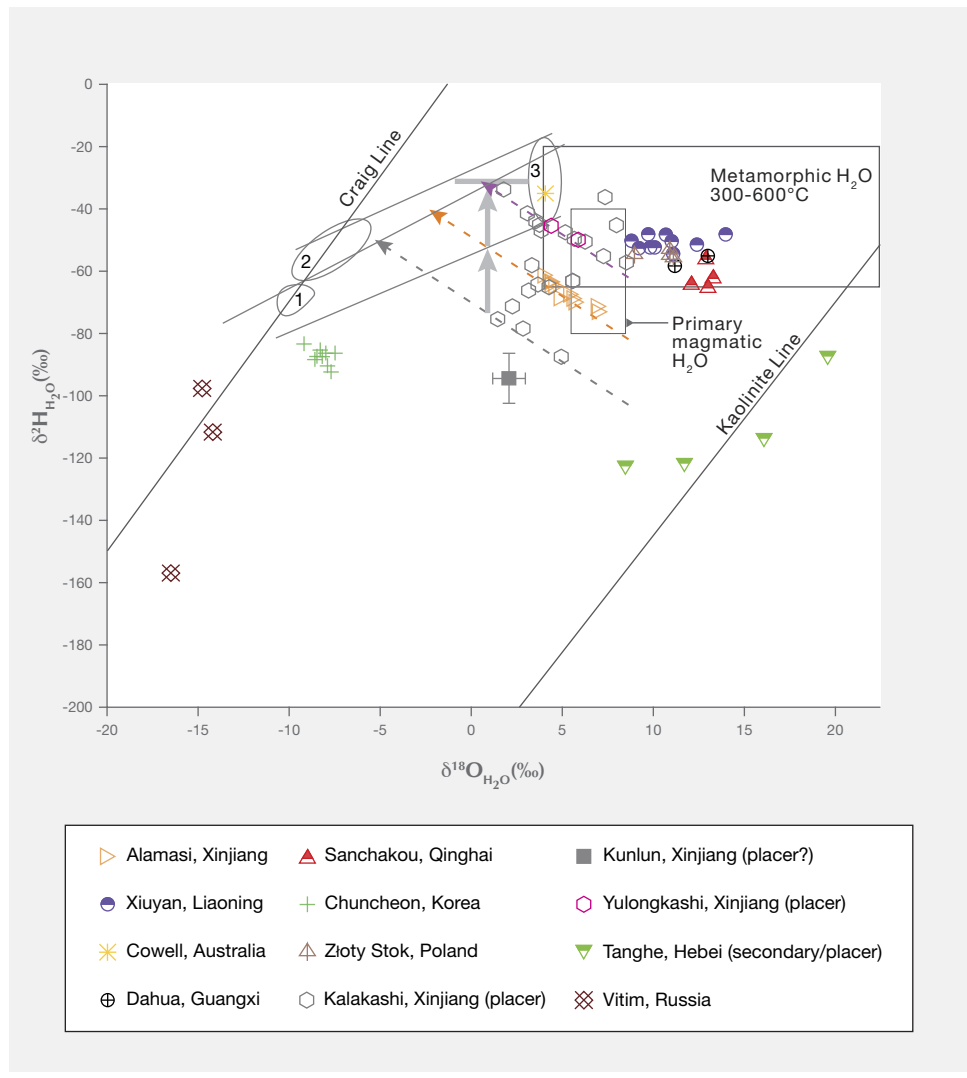


Figure 5. $\delta^2\text{H}_{\text{H}_2\text{O}}$ and $\delta^{18}\text{O}_{\text{H}_2\text{O}}$ data of dolomite-related nephrite-forming fluids at 350°C. Nephrites from Alamasí, Yulongkashi, and Kalakashi show a trend marked by a set of arrows from the bottom right to the top left, which can be explained as dualistic fluid sources. Compared with the primary nephrite from Alamasí, the hydrogen isotope of placer nephrite changes greatly (indicated by the vertical arrow) without distinct $\delta^{18}\text{O}_{\text{H}_2\text{O}}$ variations, which are caused by fluid-rock reaction possibly. The ellipses represent hydrogen and oxygen isotopes of water from (1) the Qiemo River basin (Wang et al., 2013), covering the A'erjishan region; (2) the Hetian River basin and Keliya River basin, covering the Alamasí, Agejugai, and Hetian regions; and (3) a pond in the Taklimakan Desert hinterland (Li et al., 2006).

TABLE 2. Hydrogen and oxygen isotope delta values of dolomite-related nephrites.

No.	$\delta^{18}\text{O}$ (‰)	$\delta^2\text{H}$ (‰)	$\delta^{18}\text{O}_{\text{H}_2\text{O}}$ (350°C) (‰)	$\delta^2\text{H}_{\text{H}_2\text{O}}$ (350°C) (‰)	Locality	Description	Mass spectrometer	Reference
1	3.8	-86.7	4.5	-65		White		
2	3.2	-83	3.9	-61.3		White		
3	6.1	-93.1	6.8	-71.4		White-green		
4	4.6	-89	5.3	-67.3		White-green		
5	3.5	-85.1	4.2	-63.4		White-green		
6	3.6	-85.9	4.3	-64.2	Alamasi, Yutian County, Hetian (Xinjiang, China) ^a	White-green	MAT-252	Liu et al. (2011a)
7	6.2	-94.7	6.9	-73		White-green		
8	4.1	-90.2	4.8	-68.5		Green		
9	3.6	-85	4.3	-63.3		Green		
10	4.9	-91.6	5.6	-69.9		Green		
11	4.8	-90.4	5.5	-68.7		Green		
12	3.8	-86.2	4.5	-64.5		Green		
13	3.8		4.5			White		
14	3.7		4.4			White-green		Wan et al. (2002)
15	3.6		4.3			Green		
16	2.3		3.0			Mutton-fat		
17	5.8		6.5		Agejugai, Hetian County, Hetian (Xinjiang, China)	White		Wan et al. (2002)
18	5.6		6.3			White-green		
19	6.5		7.2			Green ^b		
20	5.3		6.0		Yecheng County, Kashi (Xinjiang, China)	Green		Wan et al. (2002)
21	4.6		5.3		Datong, Tashiku'ergan County, Kashi (Xinjiang, China)	Green		Wan et al. (2002)
22	4.4		5.1		Ruoqiang County, Bayinguoleng (Xinjiang, China)	White-green		Wan et al. (2002)
23	3.4		4.1		Qiemo County, Bayinguoleng (Xinjiang, China)	White-green		Wan et al. (2002)
24	3.9		4.6			Light brown		
25	4.8		5.5			Brown		
26	4.7		5.4			Brown		
27	5.6		6.3			White-green		
28	4.6		5.3			Green		
29	3		3.7			Green		
30	3.6		4.3		Tashisayi Qiemo County, Bayinguoleng (Xinjiang, China)	Green	MAT-252	Wu (2016) ^c
31	3.7		4.4			Green		
32	3.1		3.8					
33	3.9		4.6			Green		
34	4		4.7			Light brown		
35	4.6		5.3					
36	4.8		5.5					
37	5.2	-71.8	5.9	-50.1	Yulongkashi, Hetian (Xinjiang, China)	White, placer	MAT-252	Liu et al. (2011b)
38	3.7	-67.3	4.4	-45.6		White, placer		
39	5.6	-72.4	6.3	-50.7		White-green, placer		
40	1.1	-55.7	1.8	-34	Kalakashi, Hetian (Xinjiang, China)	White-green, placer	MAT-252	Liu et al. (2011b)
41	5	-71.4	5.7	-49.7		White-green, placer		
42	2.9	-65.7	3.6	-44		White-green, placer		

No.	$\delta^{18}\text{O}$ (‰)	$\delta^2\text{H}$ (‰)	$\delta^{18}\text{O}_{\text{H}_2\text{O}}$ (350°C) (‰)	$\delta^2\text{H}_{\text{H}_2\text{O}}$ (350°C) (‰)	Locality	Description	Mass spectrometer	Reference	
43	3.2	-68.7	3.9	-47	Kalakashi, Hetian (Xinjiang, China)	Black, placer	MAT-252	Liu et al. (2011b)	
44	2.4	-63.3	3.1	-41.6		Black, placer			
45	4.5	-69.3	5.2	-47.6		Black, placer			
46	3.1	-67.1	3.8	-45.4		Black, placer			
47	0.8	-97	1.5	-75.3		Green, placer			
48	7.3	-67	8.0	-45.3		Black, placer			
49	2.7	-80	3.4	-58.3		Black, placer			
50	6.6	-77	7.3	-55.3		Black, placer			
51	3.6	-87	4.3	-65.3		Green, placer			
52	6.7	-58	7.4	-36.3		Black, placer			
53	3	-86	3.7	-64.3		Black, placer	MAT-252	Liu et al. (2016) ^d	
54	4.9	-85	5.6	-63.3		Green, placer			
55	2.2	-100	2.9	-78.3		Black, placer			
56	7.9	-79	8.6	-57.3		Black, placer			
57	2.5	-88	3.2	-66.3		Green, placer			
58	4.3	-109	5.0	-87.3		Green, placer			
59	1.6	-93	2.3	-71.3		Green, placer			
60	0.5 to 2.3	-108 to -124	1.24 to 3.04	-86.3 to -102.3		Kunlun (Xinjiang, China)	Primary or placer unknown		Yui and Kwon (2002)
61	12.3	-76.9	13.0	-55.2		Dahua (Guangxi, China)			Xu and Wang (2016)
62	10.5	-79.8	11.2	-58.1					
63	-8.7	-108	-8.0	-86.3	Chuncheon (South Korea)			Yui and Kwon (2002)	
64	-8.4	-114	-7.7	-92.3					
65	-9.9	-105	-9.2	-83.3					
66	-9	-107	-8.3	-85.3					
67	-8.2	-108	-7.5	-86.3					
68	-8.6	-112	-7.9	-90.3					
69	-8.9	-109	-8.2	-87.3					
70	-9.3	-110	-8.6	-88.3					
71	-9.2	-109	-8.5	-87.3					
72	3.4	-57	4.1	-35.3	Cowell, South Australia (Australia)			Yui and Kwon (2002)	
73	-15.52	-119.3	-14.8	-97.6	Vitim area, Buryatia (Russia)		MAT-253	Burtseva et al. (2015)	
74	-16.8		-16.1						
75	-17.24	-178.5	-16.5	-156.8					
76	-15.51		-14.8						
77	-14.95		-14.2						
78	-14.93	-133.2	-14.2	-111.5					
79	-15.1		-14.4						
80	-14.58		-13.8						
81	-18.63		-17.9						
82	-17.33		-16.6			Semi-nephrite with prismatic coarse-grained tremolite			
83	-20.02		-19.3			Semi-nephrite with prismatic coarse-grained tremolite			MAT-253
84	-17.24		-16.5		Semi-nephrite with prismatic coarse-grained tremolite				

TABLE 2 (continued). Hydrogen and oxygen isotope delta values of dolomite-related nephrites.

No.	$\delta^{18}\text{O}$ (‰)	$\delta^2\text{H}$ (‰)	$\delta^{18}\text{O}_{\text{H}_2\text{O}}$ (350°C) (‰)	$\delta^2\text{H}_{\text{H}_2\text{O}}$ (350°C) (‰)	Locality	Description	Mass spectrometer	Reference
85	10.2	-76.4 (2) ^e	10.9	-54.7	Złoty Stok, Lower Silesian (Poland)		MAT-253	Gil et al. (2015a)
86	8.3	-76.2 (3)	9.0	-54.5				
87	10.4	-77.2 (3)	11.1	-55.5				
88	10.2	-74.6 (3)	10.9	-52.9				
89		-113 ± 4.8		-91.3	Val Malenco, Sondrio (Italy)			Adamo and Bocchio (2013)
90	10	-70	10.7	-48.3	Xiuyan (Liaoning, China)			Wang et al. (2007)
91	9.3	-74	10.0	-52.3				
92	8.5	-74	9.2	-52.3				
93	8.1	-72	8.8	-50.3				
94	13.3	-70	14.0	-48.3				
95	11.7	-73	12.4	-51.3				
96	10.4	-76	11.1	-54.3				
97	10.3	-72	11.0	-50.3				
98	9.1	-74	9.8	-52.3				
99	9	-70	9.7	-48.3				
100	12.4		13.1			White	Wan et al. (2002)	
101	9.3		10.0			Yellow-white		
102	8.7		9.4			Yellow		
103	11.4	-86	12.1	-64.3	Sanchakou (Qinghai, China)	Green	MAT-251EM	Zhou (2006)
104	12.3	-87	13.0	-65.3		Green-white		
105	12.2	-78	12.9	-56.3		White		
106	12.6	-84	13.3	-62.3		"Water line" in white nephrite ^f		
107	7.8	-144	8.5	-122.3	Tanghe (Hebei, China)	Placer/secondary		Chen et al. (2014)
108	15.4	-135	16.1	-113.3		Placer/secondary		
109	18.9	-109	19.6	-87.3		Placer/secondary		
110	11	-143	11.7	-121.3		Placer/secondary		
111	15.3		16.0		Luodian (Guizhou, China)	Green-white	MAT-251EM	Yang (2013)
112	14.3		15.0			Green		
113	15.6		16.3					
114	16.5		17.2					
115	14.7		15.4			White		
116	14.5		15.2			White		
117	14.1		14.8			White		
118	14.6		15.3					
119	15.5		16.2			Green-white		
120	16.3		17.0					

^aThe deposits in Hetian and Kashi are counted in the West Kunlun region, while those in Bayinguoleng are counted in the A'erjinshan region.

^bThe sample is marked as "Bi yu" in Chinese in the original reference, which mostly equates with serpentine-related nephrite. However, we tend to believe the original authors meant a nephrite with dark green color.

^cAuthors Kong Gao, Ting Fang, and Yuanyuan Wang once participated in the research project sponsoring the thesis. Therefore, we can supplement the content of the original literature, which is not detailed enough.

^dOnly those tremolite contents higher than 99 wt.% are chosen from Liu et al. (2016). However, it is not ruled out that individual samples may be serpentine-related since their Fe contents can be high.

^eThe figure in parentheses is the number of samples tested. The number before the parentheses is the average value.

^fA "water line" refers to the band in nephrite that is more transparent than the matrix. It is composed of prismatic coarse-grained tremolite crystals parallel to each other.

NEPHRITE-FORMING FLUIDS MODIFIED BY METAMORPHISM OR METASOMATISM

The hydrogen and oxygen isotopes of nephrites from Xiuyan (Duan and Wang, 2002; Wan et al., 2002; Wang et al., 2007) and Złoty Stok (Gil et al., 2015a) overlap with each other to some extent (figure 4). Their calculated fluid isotopes plot in the regional metamorphic water field (figure 5), which is in accordance with their geological environment. The Xiuyan nephrite occurs not far from the famed serpentine jade deposit formed from metamorphic hydrothermal fluids (Wu et al., 2014). Silicon isotope studies support the interpretation that the formation of the Xiuyan nephrite was related to metamorphic fluids (Duan and Wang, 2002; Wu et al., 2014). At Złoty Stok, some geological bodies related to serpentine occur not far from the dolomite-related nephrite deposit (Gil et al., 2015a,b).

Like the nephrite-forming fluids of Xiuyan and Złoty Stok, those of Dahua and Sanchakou plot in the metamorphic water field (figure 5). The $\delta^{18}\text{O}$ values of the Dahua, Sanchakou, and Luodian nephrites are higher than others (with the exception of Tanghe), and these deposits are related to basic igneous rocks of diabase or gabbro (Zhou et al., 2006; Yang et al., 2012; Li et al., 2014; Zhang et al., 2015; Xu and Wang, 2016), which is distinct from other dolomite-related nephrites. The presence of siliceous components in the wall rocks is another common feature for these three deposits. The wall rock for Dahua nephrite is a suite of interbedded layers of calcirudite, calcarenite, and micrite mixed with laminar siliceous rocks and paramoudra (Xu and Wang, 2016). Yang et al. (2013) discussed the relationship between nephrite formation and siliceous veins in the Sanchakou deposit. The country rocks around the Luodian nephrite are siliceous clayey micrites and cherty limestones (Yang et al., 2012; Li et al., 2014). These silicalites compensate for the Si shortage during the formation of nephrite from basic rocks. For Luodian nephrite, this is supported by the $\delta^{18}\text{O}$ equilibrium between quartz and nephrite. The $\delta^{18}\text{O}_{\text{Qz}}$ value of the quartz from the deposit is 22.4‰ (Yang, 2013). Thus, the calculated $\delta^{18}\text{O}_{\text{Tr}}$ value for tremolite by the quartz-tremolite fractionation equation $10^3 \ln \alpha_{\text{Qz-Tr}} = 2.25 \times 10^6/T^2 + 0.46$ (Zheng, 1995) at 350°C equals 16.15‰, which is in the range of its nephrite $\delta^{18}\text{O}$ value = 14.1‰–16.5‰ (Yang, 2013). The speculation of compensation is also supported by the Si isotope accordance between the nephrite and the siliceous veins, paramoudra, and silicalites ($\delta^{30}\text{Si} = 1.1\text{‰}$ – 1.7‰ ; Yang, 2013). These values, in combination with field

observations, indicate that the hydrothermal fluid forming Luodian nephrite derived from either diabase intrusion (Yang et al., 2012; Zhang et al., 2015) or seawater circulation driven by diabase intrusion (Li et al., 2014). A comparable process occurred at Sanchakou: The water in the sediments convected with magmatic hydrothermal fluids (Zhou, 2006), or the acidic magmatic hydrothermal fluids that extracted Mg from gabbro (Yang et al., 2013) reacted with wall rocks and formed nephrite. Obviously, the hydrothermal fluids that formed these nephrites were no longer the original magmatic hydrothermal fluids, but rather the fluids that had been modified by metasomatism.

XINJIANG PLACER NEPHRITE ISOTOPES AND FLUID-ROCK REACTION

The Xinjiang placer nephrites, which are mainly dug out from paleo river beds flowing through the Taklamagan Desert, differ from the primary ones by their wide ranges of hydrogen and oxygen isotope ratios, especially $\delta^2\text{H}$ (figure 4). There are four factors potentially influencing this difference:

- **Impurities:** Impurities may induce a conspicuously high $\delta^2\text{H}$ value (Liu et al., 2016), as well as a wide range of variation.
- **Compositional effect:** Most of the placer nephrite tested featured high Fe (Liu et al., 2011b, 2016), which can result in a compositional effect on hydrogen isotope fractionations in a tremolite- H_2O system (Vennemann and O'Neil, 1996).
- **Complicated derivations:** Since several primary deposits occur in the upper reaches of the Yulongkashi and Kalakashi Rivers, the placer nephrite might come from different primary deposits, even including serpentine-related nephrite (Liu et al., 2016).
- **Fluid-rock reaction:** The $\delta^2\text{H}$ – $\delta^{18}\text{O}$ trends of some of the Xinjiang placer nephrites are similar to those of the Alamasi nephrite (figure 4). The $\delta^{18}\text{O}$ value, which is mainly controlled by the nephrite itself (Yui et al., 1990), has remained nearly constant after nephrite formation due to its high closure temperature of 424°C (Brady, 1995).

The closure temperature can be understood as the lowest temperature of isotope diffusion or loss. That is, the $\delta^{18}\text{O}$ value of the placer nephrite is almost equal to that of the primary nephrites. The $\delta^2\text{H}$ value

of the placer nephrite, however, can be enhanced by the reaction between meteoric water (desert water that has been fractionated by evaporation; figure 5) and rock (nephrite).

The hydrogen in hydrous minerals diffuses rapidly and shows a closure temperature, below which it will no longer diffuse and change its composition, in cooling metamorphic rocks far below the formation temperature of the mineral assemblages (Graham, 1981). The closure temperature (T_c) for hydrogen isotope volume diffusion can be expressed as (Dodson, 1973):

$$T_c = R/[E \ln(\frac{A\tau D_0}{a^2})] \quad (3)$$

where the time constant is

$$\tau = -RT^2/(\frac{EdT}{dt}) \quad (4)$$

in which the activation energy for tremolite $E = 71.5$ kJ/mol (Graham et al., 1984; Farver, 2010); the gas constant $R = 8.314$ J/mol/K; the anisotropic factor for cylinder case $A = 27$ (Dodson, 1973); the pre-exponential factor in the Arrhenius relationship $D_0 = 1.21 \times 10^{-8}$ m²/s, calculated from figure 5 of Graham et al. (1984). Thus, the closure temperature can be as low as 61°C (calculated by grain radius $a = 0.5$ μm, cooling rate $dT/dt = -10^\circ\text{C/d}$) to 123°C (calculated by $a = 1$ μm, $dT/dt = -50^\circ\text{C/d}$). Since the radius of nephrite tremolite can be smaller, the calculated closure temperature will decrease. Furthermore, an experiment showed that tremolite can dissolve at a pH of 6.9 at a low temperature of 37°C (Diedrich et al., 2014). Grapes and Sun (2010) suggested that higher porosity created by actinolite dissolution results in an exponential increase in weathering. Tremolite fibers, with

lower iron concentration than actinolite, have high chemical reactivity as well (Pacella et al., 2015). Thus, the hydrogen isotope ratio can re-equilibrate at low temperature between the placer nephrite and meteoric water, enhancing the $\delta^2\text{H}$ value of the former.

CONCLUSIONS

On the basis of formation environment and formation process, hydrogen and oxygen isotope ratios of nephrites from around the world can be analyzed. These isotope ratios, even for oxygen alone, appear to be discrimination criteria for the geographic origin determination of dolomite-related nephrites, especially those from Vitim (Russia), Chuncheon (South Korea) and the Xinjiang Uyghur Autonomous Region and Qinghai Province of China. However, the nephrite $\delta^{18}\text{O}$ values from Xiuyan, Dahua, and Złoty Stok overlap. The isotopic ratio differences are mainly derived from the ore-forming fluids. The isotopes of dolomite-related nephrites from Russia, South Korea, Xinjiang, and Qinghai Province increase in sequence, and the ore-forming fluids vary in the order of meteoric water → mixture of magmatic water and meteoric water → mixed water that experienced metamorphism to some extent or is even dominated by metamorphic fluid. Furthermore, the hydrogen isotope of the placer nephrite from the Hetian region of Xinjiang could have been modified by meteoric water when it was buried in paleo river beds flowing through the desert.

Based on this limited data set, we show that isotope ratio analysis is a new gem origin identification tool for gemologists studying nephrite (similar to what other researchers have shown for emerald and corundum). However, we point out with caution that more data is needed to optimize our findings.

ABOUT THE AUTHORS

Dr. Gao is a research group leader of the National Gems & Jewellery Technology Administrative Center (NGTC) and director of the application R&D department at the Shenzhen Research Institute, NGTC. Ms. Fang is a postgraduate at the University of Science and Technology Beijing. Dr. Lu is chief scientist of NGTC. Mr. Lan is principal instrument researcher of NGTC, director of Shenzhen Research Institute, and vice director of Shenzhen Lab, NGTC. Mr. Zhang is a research group leader of NGTC and vice director of Shenzhen Lab, NGTC. Ms. Wang is an analytical technician, and Mr. Chang is an engineer, at the China Hetian Jade Product Quality Supervision Testing Center (Xinjiang).

ACKNOWLEDGMENTS

The authors wish to express their gratitude for reviewers Dr. Yunbin Guan at Caltech, Dr. Andy Shen, Dr. George Rossman, and Dr. Ahmadjan Abduriyim for their thorough reviews of this manuscript and helpful comments and criticism. We thank technical editors Jennifer Stone-Sundberg and Tao Z. Hsu for their elaborate work handling the manuscript. We also appreciate Professor Guanghai Shi for his constructive suggestions.

REFERENCES

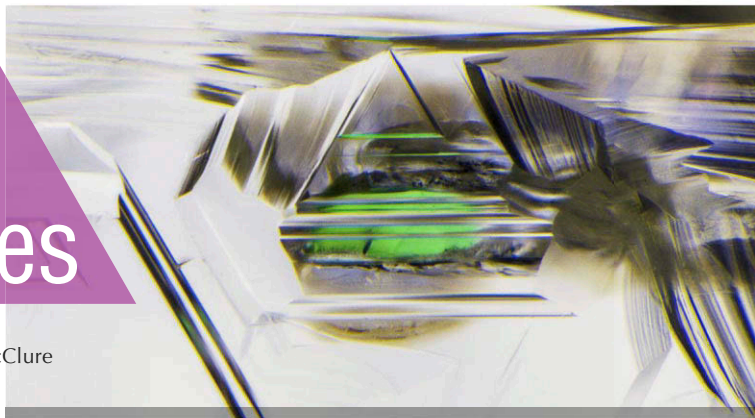
- Abduriyim A., Kitawaki H. (2006) Applications of laser ablation-inductively coupled plasma-mass spectrometry (LA-ICP-MS) to gemology. *G&G*, Vol. 42, No. 2, pp. 98–118, <http://dx.doi.org/10.5741/GEMS.42.2.98>
- Adamo I., Bocchio R. (2013) Nephrite jade from Val Malenco, Italy: Review and update. *G&G*, Vol. 49, No. 2, pp. 2–10, <http://dx.doi.org/10.5741/GEMS.49.2.98>
- Brady J.B. (1995) *Diffusion Data for Silicate Minerals, Glasses, and Liquids*. American Geophysical Union, Washington, DC.
- Burtseva M.V., Ripp G.S., Posokhov V.F., Murzintseva A.E. (2015) Nephrites of East Siberia: Geochemical features and problems of genesis. *Russian Geology and Geophysics*, Vol. 56, No. 3, pp. 402–410, <http://dx.doi.org/10.1016/j.rgg.2015.02.003>
- Chen C., Yu X.J., Wang S.Q. (2014) Study on gemmological characteristics and ore genesis of nephrite from Tanghe, Hebei Province. *Journal of Gems and Gemmology*, Vol. 16, No. 3, pp. 1–11 (in Chinese with English abstract), <http://dx.doi.org/10.15964/j.cnki.027jgg.2014.03.001>
- Craig H. (1961) Isotopic variations in meteoric waters. *Science*, Vol. 133, No. 3465, pp. 1702–1703, <http://dx.doi.org/10.1126/science.133.3465.1702>
- Diedrich T., Schott J., Oelkers E.H. (2014) An experimental study of tremolite dissolution rates as a function of pH and temperature: Implications for tremolite toxicity and its use in carbon storage. *Mineralogical Magazine*, Vol. 78, No. 6, pp. 1449–1464, <http://dx.doi.org/10.1180/minmag.2014.078.6.12>
- Dodson M.H. (1973) Closure temperature in cooling geochronological and petrological systems. *Contributions to Mineralogy and Petrology*, Vol. 40, No. 3, pp. 259–274, <http://dx.doi.org/10.1007/BF00373790>
- Duan T.Y., Wang S.Q. (2002) Study on stable isotopes of Xiuyan nephrite (tremolite). *Acta Petrologica et Mineralogica*, Vol. 21, No. S1, pp. 115–119 (in Chinese with English abstract).
- Farver J.R. (2010) Oxygen and hydrogen diffusion in minerals. *Reviews in Mineralogy and Geochemistry*, Vol. 72, No. 1, pp. 447–507, <http://dx.doi.org/10.2138/rmg.2010.72.10>
- Gil G., Barnes J.D., Boschi C., Gunia P., Raczynski P., Szakmány G., Bendő Z., Péterdi B. (2015a) Nephrite from Złoty Stok (Sudetes, SW Poland): Petrological, geochemical, and isotopic evidence for a dolomite-related origin. *The Canadian Mineralogist*, Vol. 53, No. 3, pp. 533–556, <http://dx.doi.org/10.3749/canmin.1500018>
- Gil G., Barnes J.D., Boschi C., Gunia P., Szakmány G., Bendő Z., Raczynski P., Péterdi B. (2015b) Origin of serpentinite-related nephrite from Jordanów and adjacent areas (SW Poland) and its comparison with selected nephrite occurrences. *Geological Quarterly*, Vol. 59, No. 3, pp. 457–472, <http://dx.doi.org/10.7306/gq.1228>
- Giuliani G., France-Lanord C., Coget P., Schwarz D., Cheilletz A., Branquet Y., Giard D., Martin-Izard A., Alexandrov P., Piat D.H. (1998) Oxygen isotope systematics of emerald: Relevance for its origin and geological significance. *Mineralium Deposita*, Vol. 33, No. 5, pp. 513–519, <http://dx.doi.org/10.1007/s001260050166>
- Giuliani G., Chaussidon M., Schubnel H., Piat D.H., Rollion-Bard C., France-Lanord C., Giard D., de Narvaez D., Rondeau B. (2000) Oxygen isotopes and emerald trade routes since antiquity. *Science*, Vol. 287, No. 5453, pp. 631–633, <http://dx.doi.org/10.1126/science.287.5453.631>
- Giuliani G., Fallick A.E., Garnier V., France-Lanord C., Ohnenstetter D., Schwarz D. (2005) Oxygen isotope composition as a tracer for the origins of rubies and sapphires. *Geology*, Vol. 33, No. 4, pp. 249–252, <http://dx.doi.org/10.1130/G21261.1>
- Giuliani G., Fallick A.E., Rakotondrzafy M., Ohnenstetter D., Andriamamonjy A., Ralantoarison T., Rakotosamizanany S., Tseheno M.R., Offant Y., Garnier V., Dunaigre C., Schwarz D., Mercier A., Rattrimo V., Ralison B. (2007) Oxygen isotope systematics of gem corundum deposits in Madagascar: Relevance for their geological origin. *Mineralium Deposita*, Vol. 42, No. 3, pp. 251–270, <http://dx.doi.org/10.1007/s00126-006-0105-3>
- Graham C.M. (1981) Experimental hydrogen isotope studies III: Diffusion of hydrogen in hydrous minerals, and stable isotope exchange in metamorphic rocks. *Contributions to Mineralogy and Petrology*, Vol. 76, No. 2, pp. 216–228, <http://dx.doi.org/10.1007/BF00371961>
- Graham C.M., Harmon R.S., Sheppard S.M.F. (1984) Experimental hydrogen isotope studies: Hydrogen isotope exchange between amphibole and water. *American Mineralogist*, Vol. 69, No. 1–2, pp. 128–138.
- Grapes R.H., Yun S.T. (2010) Geochemistry of a New Zealand nephrite weathering rind. *New Zealand Journal of Geology and Geophysics*, Vol. 53, No. 4, pp. 413–426.
- Harlow G.E., Sorensen S.S. (2005) Jade (nephrite and jadeite) and serpentinite: Metasomatic connections. *International Geology Review*, Vol. 47, No. 2, pp. 113–146, <http://dx.doi.org/10.2747/0020-6814.47.2.113>
- Li K.X., Jiang T.L., Xing L.C., Zhou M.Z., Luo T.Y. (2014) A preliminary study on mineralogy and ore deposits genetical model of luodian nephrite jade, Luodian, Guizhou Province, China. *Acta Mineralogica Sinica*, Vol. 34, No. 2, pp. 223–233 (in Chinese with English abstract), <http://dx.doi.org/10.16461/j.cnki.1000-4734.2014.02.013>
- Li W.P., Hao A.B., Zheng Y.J., Liu B., Yu D.S. (2006) Regional environmental isotopic features of groundwater and their hydrogeological explanation in the Tarim Basin. *Earth Science Frontiers*, Vol. 13, No. 1, pp. 191–198 (in Chinese with English abstract), <http://dx.doi.org/10.3321/j.issn:1005-2321.2006.01.025>
- Link K. (2015) Age determination of zircon inclusions in faceted sapphires. *Journal of Gemmology*, Vol. 34, No. 8, pp. 692–700.
- Liu Y., Deng J., Shi G.H., Lu T.J., He H.Y., Ng Y.N., Shen C.H., Yang L.Q., Wang Q.F. (2010) Chemical zone of nephrite in Alamas, Xinjiang, China. *Resource Geology*, Vol. 60, No. 3, pp. 249–259, <http://dx.doi.org/10.1111/j.1751-3928.2010.00135.x>
- Liu Y., Deng J., Shi G.H., Yui T.F., Zhang G.B., Abuduwayiti M., Yang L.Q., Sun X. (2011a) Geochemistry and petrology of nephrite from Alamas, Xinjiang, NW China. *Journal of Asian Earth Sciences*, Vol. 42, No. 3, pp. 440–451, <http://dx.doi.org/10.1016/j.jseae.2011.05.012>
- Liu Y., Deng J., Shi G.H., Sun X., Yang L.Q. (2011b) Geochemistry and petrogenesis of placer nephrite from Hetian, Xinjiang, Northwest China. *Ore Geology Reviews*, Vol. 41, No. 1, pp. 122–132, <http://dx.doi.org/10.1016/j.oregeorev.2011.07.004>
- Liu Y., Zhang R.Q., Abuduwayiti M., Wang C., Zhang S.P., Shen C.H., Zhang Z.Y., He M.Y., Zhang Y., Yang X.D. (2016) SHRIMP U-Pb zircon ages, mineral compositions and geochemistry of placer nephrite in the Yurungkash and Karakash River deposits, West Kunlun, Xinjiang, northwest China: Implication for a magnesium skarn. *Ore Geology Reviews*, Vol. 72, pp. 699–727, <http://dx.doi.org/10.1016/j.oregeorev.2015.08.023>
- Luo Z.M., Yang M.X., Shen A.H. (2015) Origin determination of dolomite-related white nephrite through iterative-binary linear discriminant analysis. *G&G*, Vol. 51, No. 3, pp. 300–311, <http://dx.doi.org/10.5741/GEMS.51.3.300>
- Pacella A., Fantauzzi M., Turci F., Cremisini C., Montereali M.R., Nardi E., Atzei D., Rossi A., Andreozzi G.B. (2015) Surface alteration mechanism and topochemistry of iron in tremolite asbestos: A step toward understanding the potential hazard of amphibole asbestos. *Chemical Geology*, Vol. 405, pp. 28–38, <http://dx.doi.org/10.1016/j.chemgeo.2015.03.028>
- Tang Y.L., Chen B.Z., Jiang R.H. (1994) *Chinese Hetian Nephrite*. Xinjiang People's Publishing House, Xinjiang (in Chinese).
- Vennemann T.W., O'Neil J.R. (1996) Hydrogen isotope exchange reactions between hydrous minerals and molecular hydrogen: I. A new approach for the determination of hydrogen isotope fractionation at moderate temperatures. *Geochimica et Cos-*

- mochimica Acta*, Vol. 60, No. 13, pp. 2437–2451, [https://dx.doi.org/10.1016/0016-7037\(96\)00103-2](https://dx.doi.org/10.1016/0016-7037(96)00103-2)
- Wan D.F., Wang H.P., Zou T.R. (2002) Silicon and oxygen isotopic compositions of Hetian jade, Manasi green jade and Xiuyan old jade (tremolite). *Acta Petrologica et Mineralogica*, Vol. 21, No. S1, pp. 110–114 (in Chinese with English abstract).
- Wang H.A.O., Krzemnicki M.S., Chalain J. (2016) Simultaneous high sensitivity trace-element and isotopic analysis of gemstones using laser ablation inductively coupled plasma time-of-flight mass spectrometry. *Journal of Gemmology*, Vol. 35, No. 3, pp. 212–223.
- Wang H.A.O., Cartier L.E., Baumgartner L.P., et al (2018) A preliminary SIMS study using carbon isotopes to separate natural from synthetic diamonds. *Journal of Gemmology*, Vol. 36, No. 1, pp. 38–43.
- Wang K., Graham I., Martin L., Voudouris P., Giuliani G., Lay A., Harris S., Fallick A. (2019) Fingerprinting Paraneostri rubies through oxygen isotopes. *Minerals*, Vol. 9, No. 2, pp. 91, <http://dx.doi.org/10.3390/min9020091>
- Wang S.Q., Zhao C.H., Yu G., Yuan X.M., Duan T.Y. (2007) *Xiuyan Jades in China*. Science Press, Beijing (in Chinese).
- Wang W.X., Wang R.J., Li W.P., Yin X.L., Liu C.L. (2013) Analysis of stable isotopes and hydrochemistry of rivers in Tarim Basin. *Hydrogeology & Engineering Geology*, Vol. 40, No. 4, pp. 29–35 (in Chinese with English abstract), <http://dx.doi.org/10.16030/j.cnki.issn.1000-3665.2013.04.020>
- Wang W.Y., D'Haenens-Johansson U., Smit K., Breeding C.M., Stern R. (2014) Carbon isotope analysis of CVD synthetic gem diamonds. In 2014 *GSA Annual Meeting* in Vancouver, British Columbia.
- Wu L.J. (2016) Study on gemological and mineralogical characteristics and genesis of nephrite in Tiantai, Qiemo, Xinjiang. Master's thesis. China University of Geosciences, Beijing.
- Wu Z.Y., Wang S.Q., Ling X.X. (2014) Characteristics and origin of nephrite from Sangpiyu, Xiuyan County, Liaoning Province. *Acta Petrologica et Mineralogica*, Vol. 33, No. S2, pp. 15–24 (in Chinese with English abstract).
- Xu L.G., Wang S.Q. (2016) Gemological characteristics and genesis of Dahua nephrite. *Acta Petrologica et Mineralogica*, Vol. 35, No. S1, pp. 1–11 (in Chinese with English abstract).
- Yang F.X., Abduriyim A. (1994) Honten jade and its marketing. *Journal of China Gemstone*, Vol. 1, pp. 81–84.
- Yang L. (2013) Study on petro-mineral features and genetic mechanism of Luodian jade, Guizhou Province. Ph.D. thesis. Chengdu University of Technology, Chengdu.
- Yang L., Lin J.H., Wang L., Tan J., Wang B. (2012) Petrochemical characteristics and genetic significance of Luodian jade from Guizhou. *Journal of Mineralogy and Petrology*, Vol. 32, No. 2, pp. 12–19 (in Chinese with English abstract), <http://dx.doi.org/10.3969/j.issn.1001-6872.2012.02.003>
- Yang T.X., Yang M.X., Liu H.L., Wu Y., Li J. (2013) New understanding for Sanchahe nephrite deposit in East Kunlun. *Journal of Guilin University of Technology*, Vol. 33, No. 2, pp. 239–245 (in Chinese with English abstract), <http://dx.doi.org/10.3969/j.issn.1674-9057.2013.02.007>
- Yui T.F., Kwon S.T. (2002) Origin of a dolomite-related jade deposit at Chuncheon, Korea. *Economic Geology*, Vol. 97, No. 3, pp. 593–601, <http://dx.doi.org/10.2113/97.3.593>
- Yui T.F., Yeh H.W., Lee C.W. (1988) Stable isotope studies of nephrite deposits from Fengtien, Taiwan. *Geochimica et Cosmochimica Acta*, Vol. 52, No. 3, pp. 593–602, [https://dx.doi.org/10.1016/0016-7037\(88\)90321-3](https://dx.doi.org/10.1016/0016-7037(88)90321-3)
- (1990) A stable isotope study of serpentinization in the Fengtien ophiolite, Taiwan. *Geochimica et Cosmochimica Acta*, Vol. 54, No. 5, pp. 1417–1426, [https://dx.doi.org/10.1016/0016-7037\(90\)90165-H](https://dx.doi.org/10.1016/0016-7037(90)90165-H)
- Zhang Y.D., Yang R.D., Gao J.B., Chen J., Liu Y.N., Zhou Z.R. (2015) Geochemical characteristics of nephrite from Luodian County, Guizhou Province, China. *Acta Mineralogica Sinica*, Vol. 35, No. 1, pp. 56–64 (in Chinese with English abstract), <http://dx.doi.org/10.16461/j.cnki.1000-4734.2015.01.009>
- Zheng Y.F. (1993) Calculation of oxygen isotope fractionation in hydroxyl-bearing silicates. *Earth and Planetary Science Letters*, Vol. 120, No. 3–4, pp. 247–263, [http://dx.doi.org/10.1016/0012-821X\(93\)90243-3](http://dx.doi.org/10.1016/0012-821X(93)90243-3)
- (1995) Oxygen isotope fractionation in amphiboles. *Science Geologica Sinica*, Vol. 30, No. 1, pp. 1–11 (in Chinese with English abstract).
- Zheng Y.F., Chen J.F. (2000) *Stable Isotope Geochemistry*. Science Press, Beijing (in Chinese).
- Zhong Y.P., Qiu Z.L., Li L.F., Gu X.Z., Luo H., Chen Y., Jiang Q.Y. (2013) REE composition of nephrite jades from major mines in China and their significance for indicating origin. *Journal of the Chinese Society of Rare Earths*, Vol. 31, No. 6, pp. 738–748 (in Chinese with English abstract).
- Zhou Z.Y. (2006) Study on ore-forming tectonic setting and mechanism of Sanchakou nephrite (tremolite Jade), East Kunlun. Ph.D. thesis, Tongji University, Shanghai.
- Zhou Z.Y., Liao Z.T., Ma T.T., Yuan Y. (2006) Study on the genetic mechanism and material source of Sanchakou nephrite deposit in East Kunlun. *Contributions to Geology and Mineral Resources Research*, Vol. 21, No. 3, pp. 195–198, 202 (in Chinese with English abstract), <http://dx.doi.org/10.3969/j.issn.1001-1412.2006.03.010>

Lab Notes

Editors

Thomas M. Moses | Shane F. McClure



Cat's-Eye ANDRADITE

The Carlsbad laboratory received a 49.65 ct semitranslucent to opaque brownish yellow oval cabochon (figure 1) for identification. The stone's most notable feature was its display of cat's-eye phenomenon across the dome. It had a refractive index over the limit of the refractometer and a hydrostatic specific gravity of 3.74.

Raman spectroscopy was used to assist with the identification, and the data collected (figure 2) were matched with andradite garnet from the GIA reference database. Analysis by energy-dispersive X-ray fluorescence (EDXRF) showed a composition consistent with andradite garnet, $\text{Ca}_3\text{Fe}_2(\text{SiO}_4)_3$, further proof of the stone's identity.

Internally, the stone is host to very fine and tightly packed needle-like inclusions running parallel to the base. With the stone cut as an oval cabochon, light is reflected off the inclusions, creating a rolling eye across the dome. This phenomenon is common in many gemstone species, and the demantoid variety of andradite garnet has been known to display cat's-eye phenomenon (Spring 2018 Lab Notes, pp. 58–59). This stone is a larger example of cat's-eye andradite garnet.

Nicole Ahline

Editors' note: All items were written by staff members of GIA laboratories.

GEMS & GEMOLOGY, Vol. 56, No. 2, pp. 281–291.

© 2020 Gemological Institute of America



Figure 1. A 49.65 ct brownish yellow andradite cabochon with chatoyancy across the dome.

Quench-Cracked Dyed Blue CHALCEDONY Resembling Larimar

Recently, GIA's Tokyo laboratory examined five round beads that were

semitransparent to opaque and showed blue to greenish blue body-colors with a network-like structure of whitish zones (figures 3 and 4). These beads were acquired at an ornamental gem material shop in Tokyo and were sold as "sea-blue chalcedony," but the resemblance to Larimar led to our investigation.

The beads were identified as chalcedony based on spot RI readings of 1.53 to 1.54, SG values ranging from 2.48 to 2.65, and microscopic features such as parallel curved bands (figure 4B). Raman spectroscopic features (figure 5) also suggested that the beads were mainly composed of quartz crystals and matched chalcedony (e.g., D. Pop et al., "Raman spectroscopy on gem-quality microcrystalline and

Figure 2. Raman spectrum of the cat's-eye andradite compared to the known reference. Spectra are offset vertically for clarity.

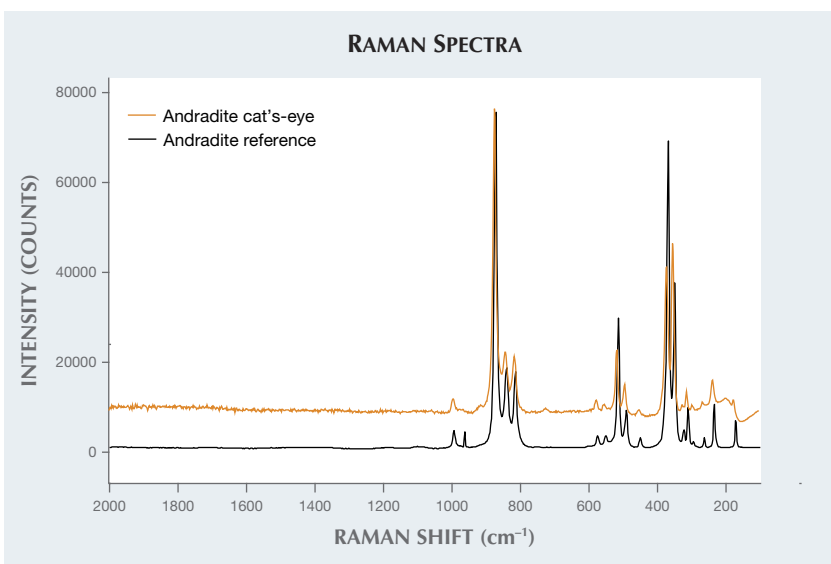




Figure 3. Two of five round beads of quench-crackled dyed chalcedony and a pear-shaped Larimar cabochon. The bottom bead is 10.25 mm in diameter.

amorphous silica varieties from Romania," *Studia Universitatis Babeş-Bolyai, Geologia*, Vol. 49, 2004, pp. 41–52). Raman spectra of the beads showed no characteristics of chrysocolla (Spring 2020 Gem News International, pp. 188–189). Qualitative EDXRF analysis detected peaks related to Si, Fe, and Cu, indicating that Cu was likely the color-causing element. Ultraviolet-visible (UV-Vis) spectra also showed a broad band from 500 to 1000 nm that corresponded with Cu. There was no polymer detected by Fourier-transform infrared (FTIR) spectroscopy and no reaction when

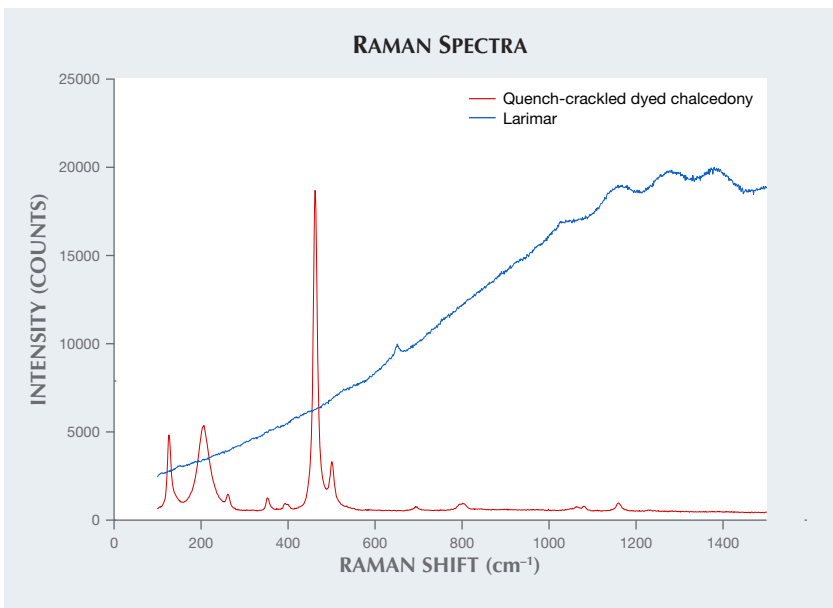


Figure 5. Raman spectra of quench-crackled dyed blue chalcedony (red trace) and Larimar (blue trace). The dyed chalcedony Raman peaks match those of chalcedony and not Larimar.

touched with a hot point. Under a gemological microscope, the stones revealed whitish zones following fractures. In order to consider the overall structure of such fractures, we cut them in half. Cross sections of the beads showed that the fractures with whitish zones were concentrated on the surface (figure 6). Such a structure is a known characteristic of quench-crackled dyed chalcedony and was reported previously (see Winter 2009 Lab Notes, p. 288). These beads probably represent a new color variety.

These quench-crackled dyed chalcedonies resemble Larimar in color

and appearance. Larimar is a rare blue variety of pectolite with the ideal chemical formula of $\text{NaCa}_2\text{Si}_3\text{O}_8(\text{OH})$ that displays white, green, and pale to sky blue colors. Blue color seen in Larimar is believed to be caused by the presence of small amounts of Cu^{2+} within its structure (e.g., R.E. Woodruff and E. Fritsch, "Blue pectolite from the Dominican Republic,"

Figure 4. A: A quench-crackled dyed chalcedony bead containing whitish zones following fractures; field of view 11.80 mm. B: Another bead showing a curved banding structure; field of view 12.80 mm. C: A pear-shaped Larimar cabochon (also shown in figure 3); field of view 16.20 mm. Note that it has a mottled blue and white color and contains other mineral inclusions.

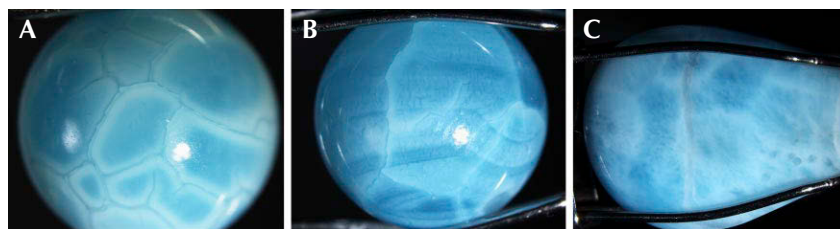
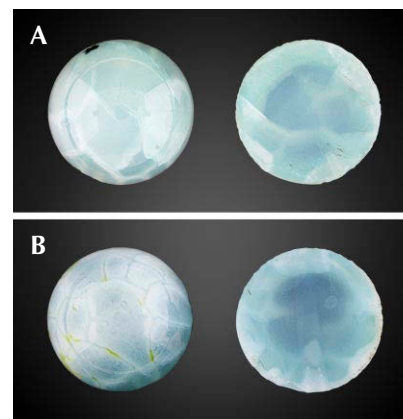


Figure 6. Cross sections of two round beads of quench-crackled dyed chalcedony, 10.25 mm in diameter. Note that the white color is concentrated on the surface and along internal fractures.



Winter 1989 *G&G*, pp. 216–225). We compared these beads with Larimar (the pear cabochon on the right in figure 3) to reveal their differences. The Larimar cabochon showed a mottled blue and white color with network-like whitish zones and other natural mineral inclusions (figure 4C) (again, see Woodruff and Fritsch, 1989). It had a spot RI reading of 1.60 and an SG of around 2.80. On the other hand, the quench-crackled dyed blue chalcedony beads had whitish zones following a network of fractures (figure 4B) and no other mineral inclusions.

This material can easily be separated from Larimar using standard gemological testing such as RI and SG. Advanced testing is useful in confirming the cause of blue color and the presence of polymer treatment.

Makoto Miura

DIAMOND

Irradiated Blue Diamond with Interesting DiamondView Image

We often receive lab-irradiated diamonds at the laboratory that have either natural or laboratory-grown origins (e.g., Summer 2018 Lab Notes, pp. 215–216). However, we recently received a 1.00 ct Fancy Deep greenish blue irradiated diamond (figure 7) with some unusual gemological features. The diamond's spectra and imaging showed that it had received artificial irradiation likely followed by annealing, which created unusually high concentrations of nitrogen vacancy (NV) centers.

As with most lab-irradiated diamonds, it was irradiated with the table side down; thus, the culet facing the beam received the highest dose of irradiation while much of the table facet was comparatively protected. The irradiated pavilion shows orange fluorescence due to a high concentration of NV centers (figure 8, left). Irradiated diamonds are often subjected to some low-temperature annealing after irradiation in order to “stabilize” the defects (e.g., Spring 2018 Gem News International, pp. 105–107); however, we generally do not see evi-

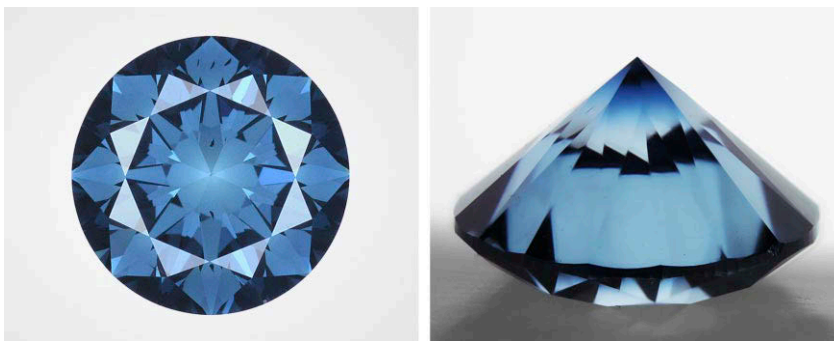


Figure 7. This 1.00 ct Fancy Deep greenish blue diamond (left) owes its color to artificial irradiation, which is also evidenced by the color concentration at the culet (right).

dence of NV centers forming from that low-temperature heating.

Here we see a combination of treatment conditions that generated an NV-related fluorescence on the pavilion and the crown; however, the original blue fluorescence of the natural, pre-irradiated diamond persists on the table, which was “shielded” during the irradiation (figure 8, right). The table experienced a lower radiation dose, fewer NV centers formed as a result, and we observe a transition from the orange NV fluorescence to the intrinsic blue fluorescence. Thus, the DiamondView fluorescence collected from the table creates an intriguing image.

The combination of the intrinsic defect concentrations along with the specific irradiation dose and subse-

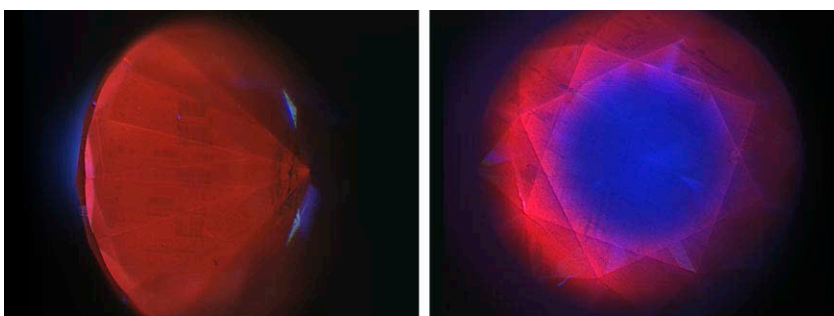
quent annealing conditions created an unusual treated diamond for scientific study and an interesting reinterpretation of a “nailhead” diamond—a term often applied to a poorly cut stone that is dark on the table. Here, this effect can only be revealed under UV illumination.

Sally Eaton-Magaña

Multiple Radiation Stains Suggest Interesting Geological Residency

A rough diamond crystal weighing 4.05 ct was observed with radiation staining on its surface. Radiation staining is thought to occur when radioactive fluids or minerals are adjacent to a diamond crystal in the earth. The radiation imparts damage to the

Figure 8. The DiamondView fluorescence images of the irradiated diamond collected from the pavilion (left) show a high concentration of NV centers creating the orange fluorescence. On the table (right), the NV concentration has decreased sufficiently so that the NV-related orange fluorescence transitions to the diamond's intrinsic blue fluorescence.



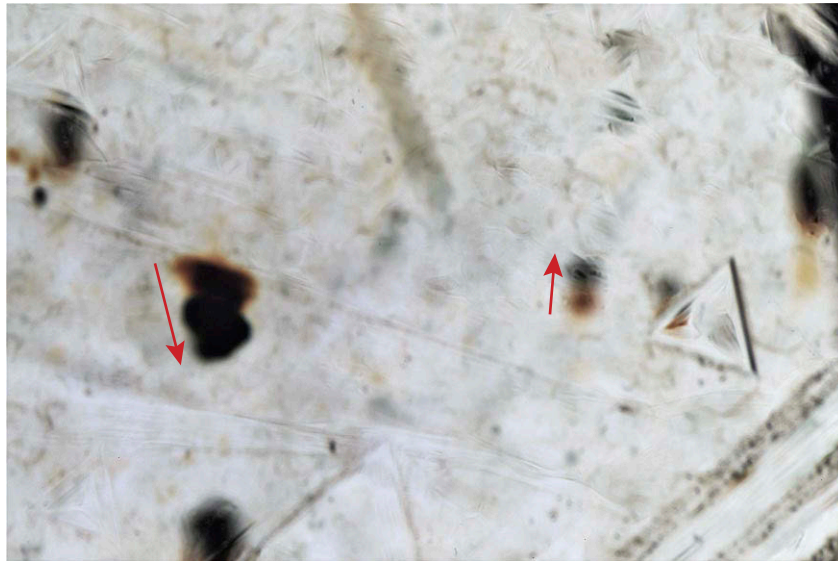
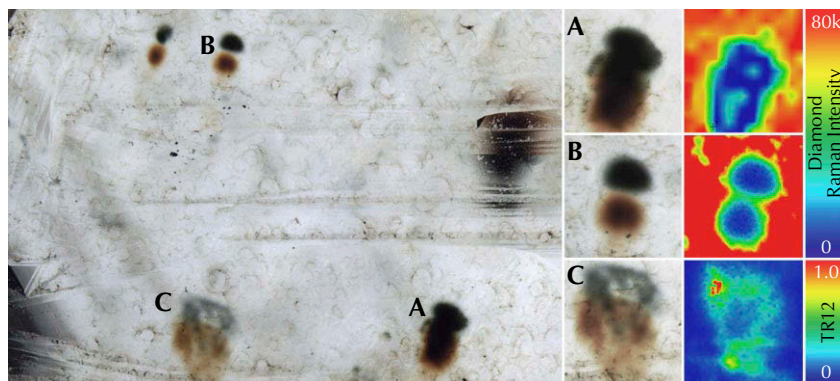


Figure 9. Radiation staining is visible on opposite sides of the rough diamond crystal. On the upper surface the green stain is closer to the bottom of the image, whereas on the lower surface the green stain is closer to the top of the image. The arrows indicate the direction of displacement, which are in opposite directions on opposite sides of the rough crystal. Field of view 2 mm.

diamond lattice, leaving behind vacancies and interstitial carbon atoms.

When initially formed, these stains are green or greenish in color. If they

Figure 10. A portion of one side of the 4.05 ct rough diamond (left; field of view 3 mm) shows the relative placement of several radiation stains that are detailed with PL mapping at right. A: The photographed image of a very dark radiation stain and the corresponding PL map of diamond Raman intensity. B: The image of a brown radiation stain separated from its green counterpart and the corresponding PL map of its diamond Raman intensity. C: An image of a light radiation stain. Its PL map plots the TR12 intensity, instead of Raman intensity as in A and B, which was much higher within the radiation stain than within the colorless section. The PL maps in A and B were collected with 532 nm excitation and plot the diamond Raman peak area at 573 nm, while the map in C with 455 nm excitation plots the TR12 peak area at 470 nm and normalized to the diamond Raman peak area.



are subjected to heat, the stains will turn to a brownish color. This particular diamond had both green and brown radiation stains on the surface. Nearly all of the stains existed in pairs, one brown and one green, and were of the same shape. This has been reported previously (C.M. Breeding et al., "Natural-color green diamonds: A beautiful conundrum," Spring 2018 *G&G*, pp. 2–27), and the proposed mechanism is that the diamond crystal is adjacent to a radioactive substance that imparts a green stain. When the diamond crystal is shifted slightly, the radioactive minerals create a new stain of the same shape but slightly displaced. The diamond was heated before the second set of stains had formed, which turned the initial set of stains brown.

In this rough crystal, the stain pairs are on opposite sides and in opposite directions (figure 9). The shift must have occurred in the direction from brown to green, which means this crystal most likely rotated with respect to its environment. The other explanation is that the host material on either side shifted in opposite directions by roughly the same amount.

To examine the spectroscopic differences between the green and brown radiation stains, we collected photoluminescence (PL) maps using 532 and 455 nm excitation in confocal mode. We collected data on several of the radiation stains but will focus this discussion on three of them (figure 10). Figure 10A has dark, almost black coloration in the center with dark green and brown color around the periphery. Figure 10B shows green and brown radiation stains but with a colorless section between them, and figure 10C has very light radiation staining.

In the radiation stain imaged in figure 10A, the diamond Raman peak was quite broad and distorted within the radiation stain compared to the surrounding diamond (figure 11, inset). The broadened and distorted Raman peaks are indicators of the radiation damage brought upon these areas and are consistent with prior observations of other very dark radiation stains (e.g., S. Eaton-Magaña and K.S.

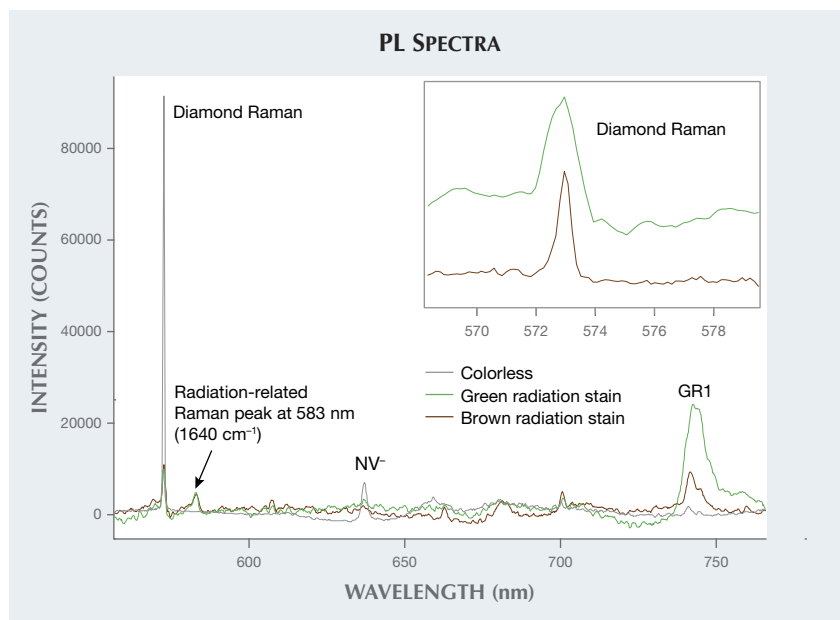


Figure 11. These 532 nm excitation spectra show differences in features between the brown and green radiation stains imaged in figure 10A and a nearby colorless portion of the diamond. In the colorless diamond, the Raman peak is much larger and shows the NV⁻ peak and a weak GR1. The brown and green stains show much lower diamond Raman intensity, and the peak width is greater within the green stain (inset). Both the green and brown radiation stains also show a radiation-related Raman peak at 1640 cm⁻¹ (583 nm; Eaton-Magaña and Moe, 2016) and comparatively pronounced GR1 peaks. Other unknown and intrinsic features are also present in these spectra.

Moe, "Temperature effects on radiation stains in natural diamonds," *Diamond and Related Materials*, Vol. 64, 2016, pp. 130–142). The average Raman peak FWHM (full width at half maximum) within the green portion of the radiation stain was ~1.6 nm, while the average width within the brown portion of the radiation stain was ~1.1 nm. For comparison, the Raman width in the colorless sections was ~0.5 nm. The detected Raman intensity was also much lower than that of the surrounding colorless diamond (figures 10A and 11). Natural diamond and irradiation-related features such as TR12 (470 nm), H3 (503.2 nm), and NV⁻ (637 nm) were not detected within this heavily damaged radiation stain. The GR1 peak was detected, though with higher intensity within the green radiation stain (figure 11).

In figure 10B, the PL map is consistent with the visual image and

shows the area between the green and brown radiation stains approaching the features of the surrounding colorless diamond. Both figures 10B and 10C show indications of less radiation damage compared to figure 10A. The TR12, H3, and NV⁻ features were detected in both the green and brown radiation stains, and the natural diamond features of H3 and NV⁻ showed higher intensity in the brown. The GR1 and TR12 were slightly higher in the green radiation stains than in their brown counterparts and greater still than in the surrounding colorless diamond (figure 10C). For the radiation stains pictured in figures 10B and 10C, the diamond Raman widths were generally equivalent to those of the surrounding diamond. The PL maps also demonstrated that the boundary of the high GR1 intensity extended laterally ~30 μm beyond the colored radiation stain and into the surrounding colorless diamond;

this is consistent with prior estimates of alpha radiation penetration (Eaton-Magaña and Moe, 2016).

In the radiation stains shown in figure 10, the brown portions of the radiation stains displayed features closer to the intrinsic diamond (lower diamond Raman width of the radiation stain shown in figure 10A and its corresponding spectra shown in figure 11, along with higher intensities of H3 and NV⁻ of radiations stains shown in figures 10B and 10C; spectra not shown). These features suggest that the time and temperature that created the transition from green to brown as the diamond shifted to a new position also brought some "healing" from the localized radiation effects detected within the green radiation stains. This sample was interesting scientifically, as it allowed some direct comparison of radiation stain features created by the same point sources.

Troy Ardon and Sally Eaton-Magaña

HEMIMORPHITE Resembling Paraíba Tourmaline

A 5.61 ct semitransparent blue cabochon (figure 12) was submitted to the New York laboratory for a Paraíba tourmaline origin report because of its electric blue color and its similar RI and internal features. Microscopic observation revealed parallel tubes,

Figure 12. This 5.61 ct electric blue cabochon was identified as hemimorphite.



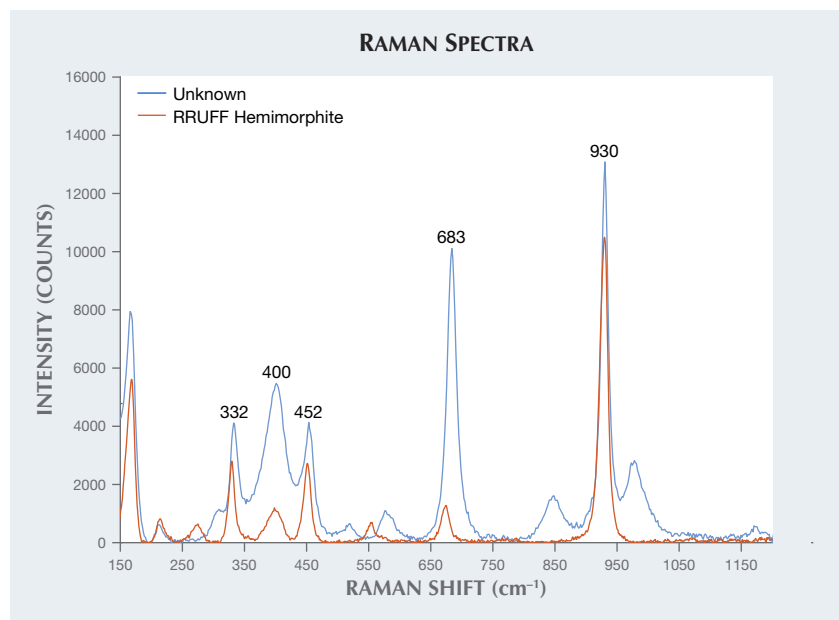


Figure 13. Raman spectra of a 5.61 ct semitransparent blue cabochon that matched with hemimorphite in the RRUFF database (no. R070536).

fluid inclusions, and white granular flake-like inclusions. The stone's optic character could not be determined due to the cabochon shape and abundance of inclusions, and only an approximate RI of 1.61–1.63 with a birefringence of 0.02 could be obtained. Specific gravity was 3.45, which is inconsistent with tourmaline, and the fluorescence reaction was medium blue under short-wave and inert under long-wave UV radiation. We confirmed its identity by Raman spectroscopy, which showed a match with hemimorphite (<https://rruff.info/Hemimorphite/R070536>), as shown in figure 13.

Hemimorphite is a zinc silicate, $Zn_4Si_2O_7(OH)_2 \cdot H_2O$; the purest form is white or colorless. Impurities cause different colors, such as copper (Cu^{2+}) for a bluish and greenish tint, ferrous iron (Fe^{2+}) for green, and ferric iron (Fe^{3+}) for brown. Laser ablation–inductively coupled plasma–mass spectrometry (LA-ICP-MS) composition analysis revealed that this stone contained no iron but did contain copper, which produced the electric blue color.

Sudarat Saeseaw

SAPPHIRE

Exceptional Purple Montana Sapphire

The Carlsbad laboratory recently received a 10.47 ct purple octagonal modified brilliant-cut sapphire (figure

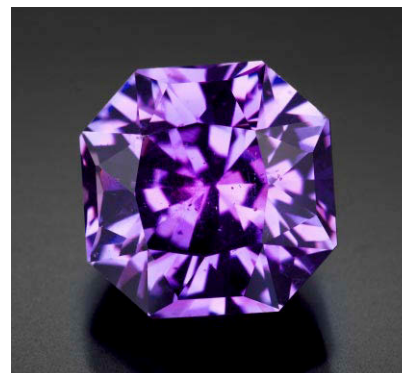
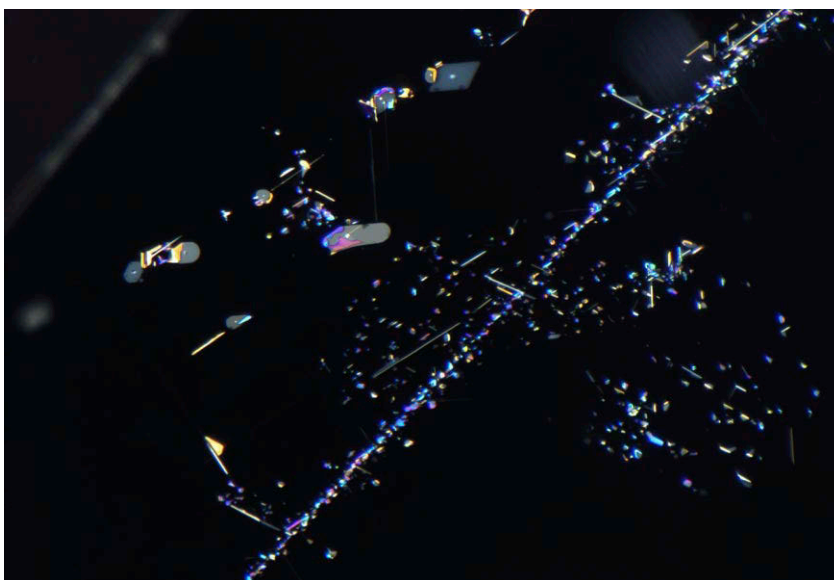


Figure 14. This 10.47 ct sapphire is notable as a large, unheated purple sapphire from Montana.

14) for an identification and origin report. Standard gemological testing gave a 1.762 to 1.770 refractive index, indicating corundum, and a hydrostatic specific gravity (SG) of 4.00. The stone displayed no fluorescence under long-wave and short-wave UV.

Microscopic examination showed an interesting combination of inclusions, including an iridescent healed fissure surrounding a crystal, particulate clouds with intact and unaltered rutile needles/silk, flaky stringers, and twinning with intersection tubules

Figure 15. Flaky particles and stringers of colorful rutile silk seen in the 10.47 ct purple Montana sapphire. Field of view 1.58 mm.



(figure 15). This inclusion scene is consistent with unheated corundum from Montana (Winter 2018 Lab Notes, pp. 434–435).

Laser ablation–inductively coupled plasma–mass spectrometry (LA-ICP-MS) was used to conclusively determine the stone’s trace element chemistry, and the results were compared to corundum samples from GIA’s colored stone reference collection. Trace element measurements indicated ranges of 13.6–15.0 ppma Mg, 13.1–15.0 ppma Ti, 7.76–8.36 ppma V, 38.3–39.4 ppma Cr, 1560–1600 ppma Fe, and 16.5–17.0 ppma Ga. The chemistry matched well with reference stones GIA has collected from Montana’s secondary deposits. With a combination of microscopic observation, advanced testing, and GIA’s reference collection, we were able to confirm the geographic origin of this sapphire.

Of all North American corundum localities, Montana reigns supreme. While rubies are only rarely found, facet-quality sapphire is mined at a number of different locations. Fine blue and purple gems have been mined at Yogo Gulch in central Montana, but cut gems over one carat are rare. Fancy sapphires are found associated with the placers of Missouri River and at Dry Cottonwood Creek and Rock Creek. These deposits produce larger material, but the colors tend to be pale. The successful development of heat treatment technology there has renewed interest in Montana sapphire.

This particular gem is consistent with those found in Montana’s secondary deposits. It is a particularly fine example due to its saturated purple color, large size, and absence of heat treatment.

Maryam Mastery Salimi and
Nathan Renfro

Negative Crystal Containing a Mobile CO₂ Bubble in Blue Sapphire Heated with Pressure

Among the common inclusions seen in almost every mineral are primary

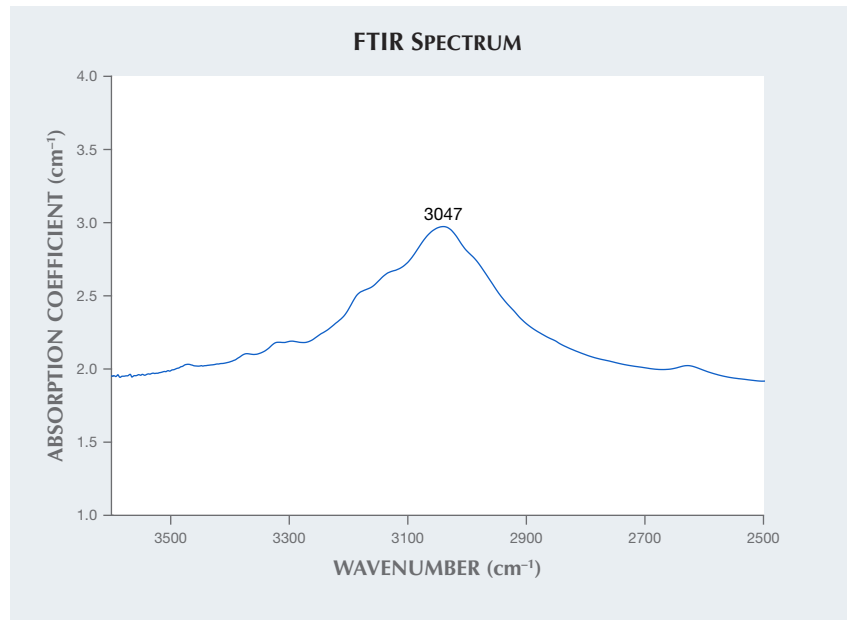


Figure 16. The blue sapphire’s FTIR spectrum shows a strong absorption band centered around 3047 cm⁻¹, suggesting treatment with heat and pressure.

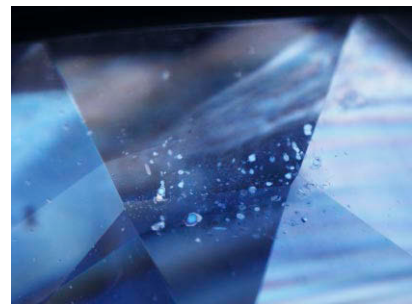
cavities, or negative crystals. Negative crystals in sapphire are usually filled with liquid and gaseous carbon dioxide (CO₂) and may also contain solids such as diaspore or graphite.

At GIA’s Bangkok laboratory, the author recently examined a 6.41 ct transparent blue faceted sapphire. It had a refractive index of 1.760–1.768, and its fluorescence reaction was inert under long- and short-wave UV radiation. Fourier-transform infrared (FTIR) spectroscopy is a useful technique to determine heat treatment in corundum. The sample’s FTIR spectrum (figure 16) showed a broad band centered around 3047 cm⁻¹ that has been reported in sapphires treated with heat and pressure (M.S. Krzemnicki et al., “Sapphires heated with pressure – A research update,” Spring 2019 *InColor*, pp. 86–90).

Microscopic observation revealed altered growth tubes, dissolved particles, melted crystals with altered fingerprints, and small birefringent crystals in a low-relief partially healed fissure (figure 17), proof of high-temperature heat treatment with pressure (Winter 2018 *Gem News International*, p. 458). When the sapphire was

gently heated by the microscope bulb, the gas bubble became smaller and disappeared as the gas and liquid homogenized. The presence of CO₂ fluid inclusions in negative crystals is important evidence of natural origin and the absence of thermal enhancement (J.I. Koivula, “Carbon dioxide fluid inclusions as proof of natural-colored corundum,” Fall 1986 *G&G*, pp. 152–155). Interestingly, this sample exhibited a rounded bubble in a negative

Figure 17. When the sapphire was viewed under cross-polarized light, a plane of small birefringent crystals was observed in a partially healed fissure. Field of view 4.10 mm.



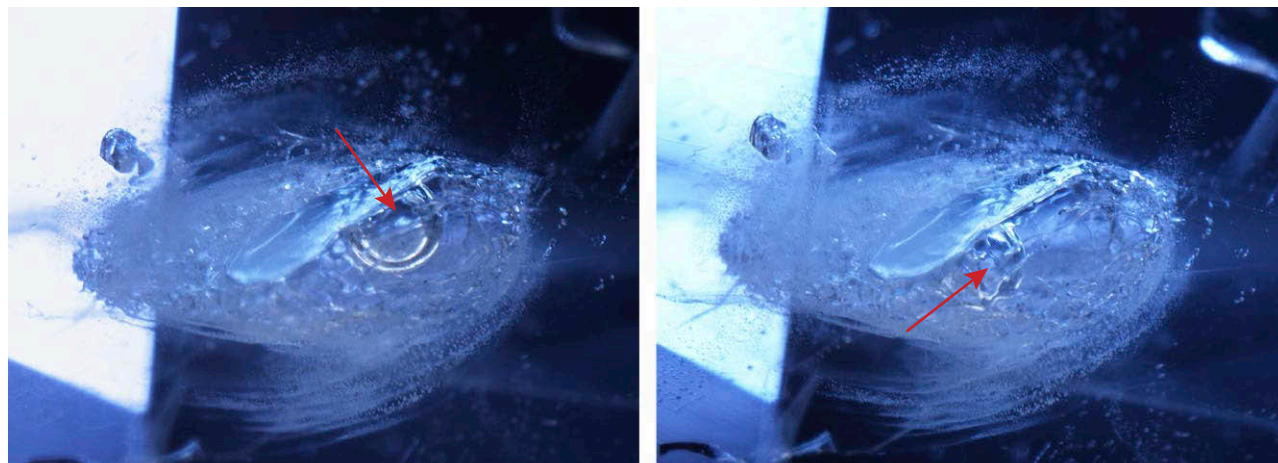


Figure 18. A negative crystal with a mobile CO₂ bubble in the blue sapphire heated with pressure. Field of view 2 mm.

crystal that moved and was still observed when gently heated with a hot point (figure 18). Raman spectroscopy confirmed the bubble as carbon dioxide (CO₂). To our knowledge, a mobile CO₂ bubble in a negative crystal has not been reported in a sapphire heated with pressure.

Nattida Ng-Pooresatien

Figure 19. An 11.16 ct pink sapphire from Mozambique.



Pink Mozambique Sapphire

Recently, GIA's Carlsbad lab received an 11.16 ct pink sapphire (figure 19) for a colored stone identification and origin report. Standard gemological testing was consistent with sapphire, giving a refractive index of 1.759–1.769 and a hydrostatic specific gravity of 4.00.

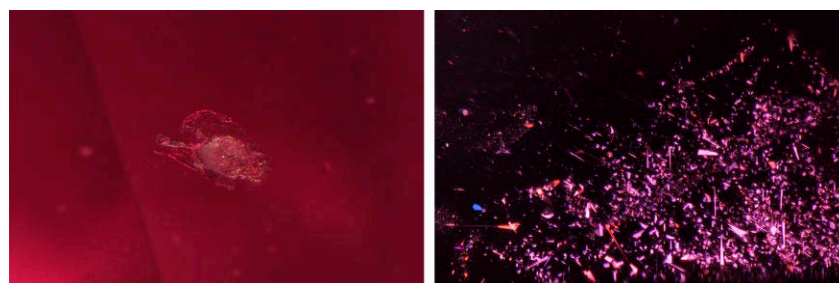
The sapphire contained various inclusions (figure 20) such as negative crystals and transparent colorless crystals. These inclusions showed no indication of thermal alteration, suggesting the stone was unheated. Bands of silk arranged in a hexagonal formation with irregularly shaped thin films intermixed with particle clouds could be seen throughout the stone. This suite of inclusions was consistent with a Mozambique origin.

Advanced testing confirmed that the sapphire was unheated and from Mozambique. Infrared spectroscopy produced a spectrum consistent with unheated sapphire. The spectra showed a single peak at 3309 cm⁻¹ with no secondary peak at 3232 cm⁻¹ (Summer 2019 Gem News International, pp. 290–291). Laser ablation–inductively coupled plasma–mass spectrometry (LA-ICP-MS) confirmed the stone's chemical composition of a higher iron and lower vanadium content, which is typical of Mozambique sapphires.

Mozambique is known for rubies that are saturated in color. With its 11.16 ct size and pure pink hue, this unheated Mozambique sapphire was a unique encounter.

Nicole Ahline

Figure 20. A negative crystal (left; field of view 1.79 mm) and a cluster of silk (right; field of view 2.57 mm) that could be seen throughout the pink sapphire.



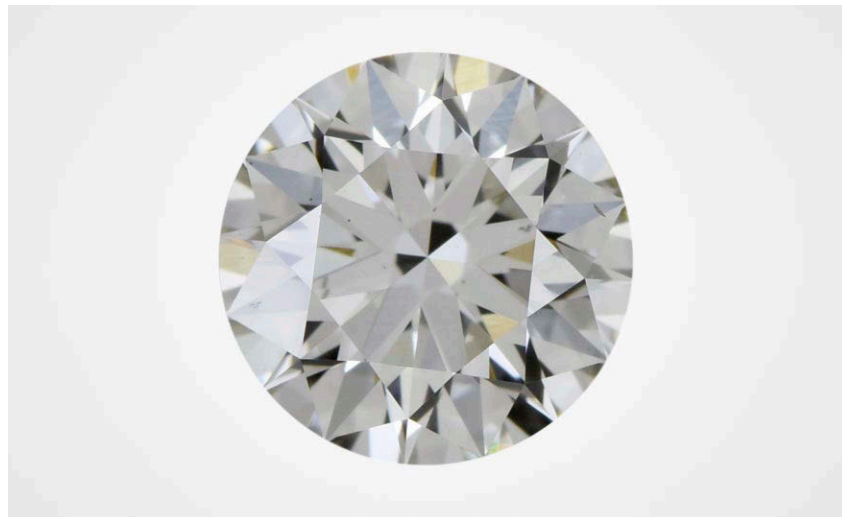


Figure 21. Face-up image of one of the HPHT-processed CVD laboratory-grown diamonds submitted to the Antwerp lab. This 1.02 ct round brilliant synthetic diamond has J-equivalent color and VS₂ clarity.

SYNTHETIC DIAMOND

HPHT-Processed CVD Laboratory-Grown Diamonds with Low Color Grades

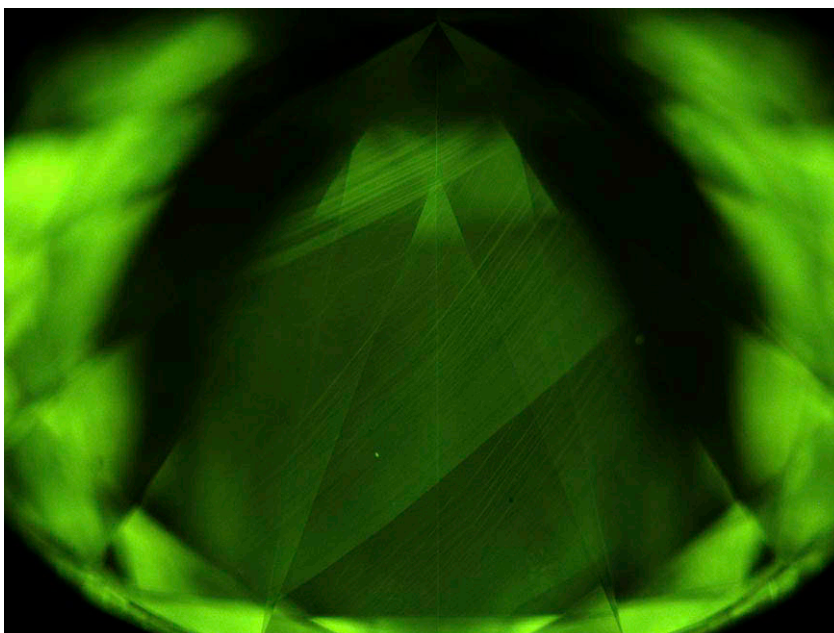
When CVD-produced diamonds are grown with nitrogen added to the gas mixture, or when the growth rate is relatively high, the as-grown crystal ends up having an undesirable brown color. In order to improve this color, CVD-grown diamonds are often treated at high-pressure, high-temperature (HPHT) conditions after their growth. The Antwerp laboratory recently received 11 CVD laboratory-grown diamonds that had been subjected to HPHT treatment after growth but still had a relatively uniform low color grade (J-equivalent, figure 21).

The samples were round brilliants with weights ranging from 1.02 ct to 1.33 ct and clarity grades in the VS range. Commonly observed clarity characteristics were crystals, needles, and pinpoints along with feathers. They were classified as type IIa diamonds with weak additional absorption peaks at 1332, 1344, 2947, and 3031 cm⁻¹. Four showed a weak absorption peak at 3107 cm⁻¹ (N3VH). None of them showed the CVD-spe-

cific NVH⁰ band at 3123 cm⁻¹ (P.M. Martineau et al., "Identification of synthetic diamond grown using chemical vapor deposition [CVD]," Spring 2004 *G&G*, pp. 2–25). UV-vis-

ible absorption spectra taken at liquid nitrogen temperature revealed the presence of the SiV⁻ center, a defect commonly observed in CVD synthetic diamonds. Photoluminescence (PL) spectra taken with various excitation wavelengths and at liquid nitrogen temperature showed the presence of a strong SiV⁻ doublet (736.6/736.9 nm), strong NV^{0/-} (575 and 637 nm) centers, numerous peaks in the 520–550 nm region, and a strong H3 (503.2 nm) center. Furthermore, all the spectra showed an absence of the SiV⁰ (946 nm) and 596/597 nm centers. This last center is commonly observed in as-grown CVD synthetic diamonds but is removed by post-growth HPHT treatment. A weak H2 center (986 nm) was observed in six stones. Weak Ni-related absorption peaks were detected in 830 nm PL spectra of all the samples, but at higher wavelengths than expected (884–885 nm, potentially attributed to high strain). Microscopic analysis using crossed polarizing plates confirmed the presence of strain throughout the stones.

Figure 22. DiamondView image of one of the 11 CVD samples shows green fluorescence and clear linear growth striations. The layers indicate stop-start growth.



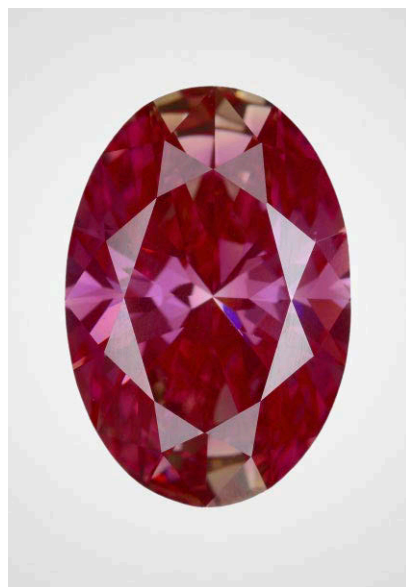


Figure 23. This 3.02 ct HPHT-grown diamond with color equivalent to Fancy Vivid pink had an unstable color.

DiamondView images showed green luminescence (linked to the strong H3 center revealed by PL spectra) and a weak bluish green phosphorescence. All samples showed clear linear growth striations. Some revealed a multilayer stop-start growth. The orientation of the growth layers gives an indication of the angle at which the stone is cut from the rough plate (figure 22).

Based on all the observations, we conclude that the analyzed CVD laboratory-grown diamonds underwent HPHT treatment after growth. Their relatively low color grades are believed to be linked to the duration of the treatment. More efficient treatment would likely result in a higher color grade.

Ellen Barrie

HPHT Laboratory-Grown Pink Diamond with Unstable Color

While rare, it is not uncommon for certain types of diamond to change color when exposed to different lighting or thermal conditions. Consider, for example, chameleon-type diamonds, which can change color from



Figure 24. Left: Strong color zoning observed under natural lighting conditions. Right: The fluorescence pattern follows this zoning, as observed in the DiamondView image (strong short-wave UV).

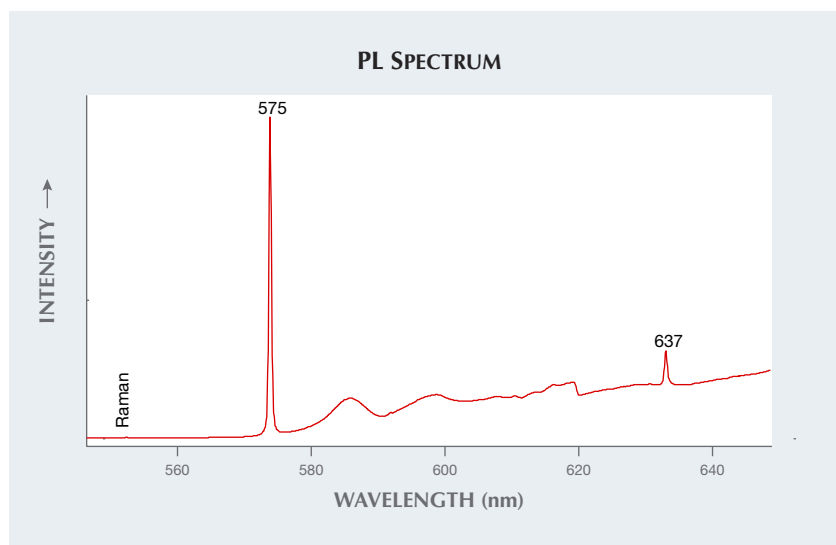
yellowish green to orangy yellow when heated or concealed in the dark for long periods of time.

Recently submitted to GIA's New York laboratory for examination was a 3.02 ct laboratory-grown diamond with the equivalent color grade of Fancy Vivid pink (figure 23). Typical of an HPHT-grown laboratory-grown diamond, it exhibited strong color zoning (figure 24, left) related to its typical hourglass synthetic growth structure. Of note, it exhibited very strong orange fluorescence when exposed to ultra-short-wave ultraviolet radiation (figure 24, right). This is of note as it is

indicative of post-growth treatment to create the desirable pink color.

This diamond was grown with a very carefully controlled nitrogen content that produced approximately 1.6 ppm of type Ib single substituted nitrogen (post treatment). The nitrogen content was calculated from a normalized mid-infrared spectrum. Post-growth treatment of irradiation/annealing generated very strong absorption from the nitrogen vacancy (NV) centers that are responsible for both the pink bodycolor and the very strong orange-red fluorescence (see the PL spectrum in figure 25).

Figure 25. 514 nm (green) photoluminescence spectrum showing strong NV (nitrogen vacancy) centers at 575 and 637 nm. These are responsible for the very strong bodycolor and orange-red fluorescence.



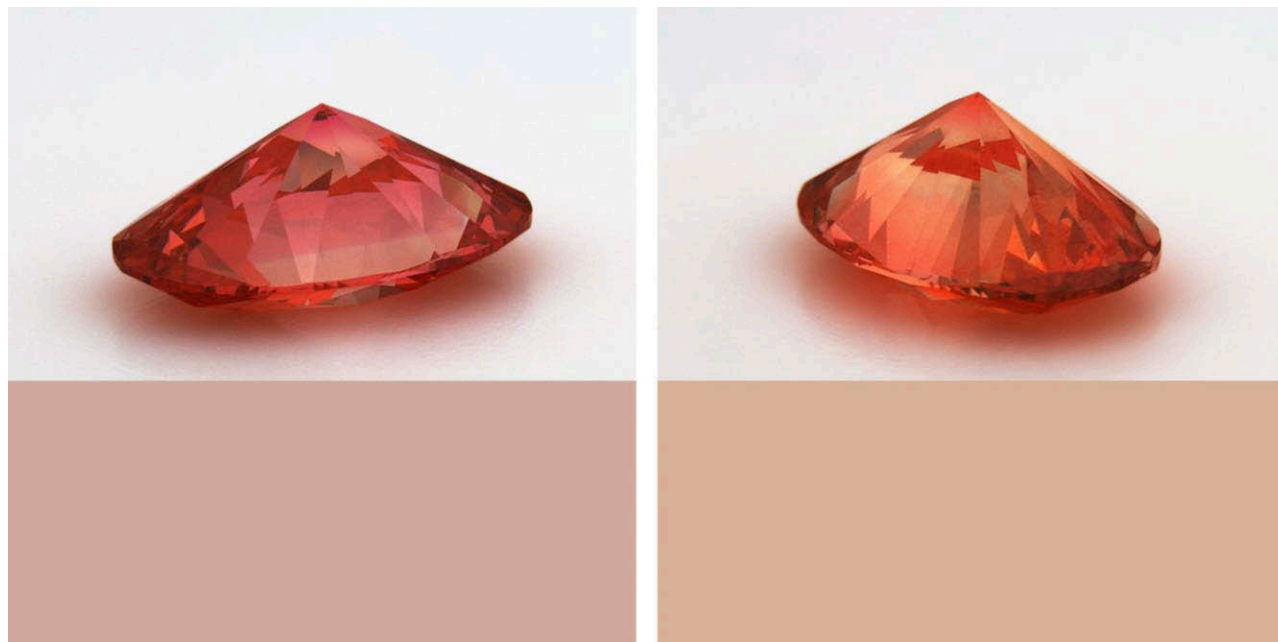


Figure 26. A dramatic hue shift from pink to orange was observed when the synthetic diamond was exposed to short-wave UV radiation. Color swatches (bottom) were generated from recorded LCH values both before and after UV bleaching. The two images (top) were taken using standard lighting in the GIA colorimeter, which recorded the LCH values.

When excited by short-wave UV radiation, the nitrogen vacancy color-causing centers are bleached and desaturated, resulting in a hue shift to orange (figure 26). This is a temporary color change, and within minutes the diamond will revert to its stable pink color under normal daylight conditions.

Using LCH (lightness, chroma, and hue) values, color swatches (fig-

ure 26, bottom) were generated that accurately represent the color change observed. The images in figure 26 (top) were captured using a GIA-built colorimeter with standard lighting conditions.

With the recent influx of laboratory-grown fancy-color diamond into the market, these phenomena are of note to consumers.

Kaitlyn Mack and Paul Johnson

PHOTO CREDITS

Diego Sanchez—1, 7 (left), 14; Shunsuke Nagai—3, 6; Makoto Miura—4; Sally Eaton-Magaña—7 (right), 8, 10; Troy Ardon—9; Nuttapol Kitdee—12; Aaron Palke—15; Nattida Ng-Pooresatien—17, 18; Robison McMurtry—19; Nathan Renfro—20; Ellen Barrie—21; Michaela Harinová—22; Jian Xin (Jae) Liao—23; Paul Johnson—24 (right)



Böhmite in Corundum

Gemologists at Bangkok's Lotus Gemology laboratory recently examined a large lot of rubies believed to originate from the Montepuez area of Mozambique. Microscopic examination confirmed that assessment. Many of these stones displayed features in their infrared spectra that are typical for böhmite, with a characteristic "twin peak" spectrum at ~ 3309 and 3089 cm^{-1} (figure 1).

One of the stones showed a large area cut through on a pavilion facet that appeared to be a foreign substance. A similar substance was seen in many of the fissures in the stone (figure 2). Judicious use of the hot point under the micro-

Figure 1. "Twin peak" infrared spectrum of böhmite in the Mozambique ruby, with prominent peaks at ~ 3309 and 3089 cm^{-1} .

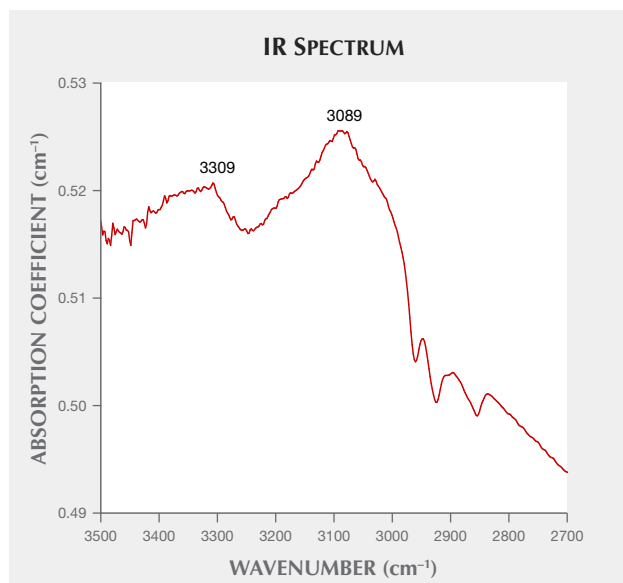


Figure 2. A large area of a foreign substance cut through on the surface of a ruby from the Montepuez area of Mozambique. This substance infilled not only this cavity but also many narrow fissures in the stone. Micro-Raman analysis identified it as böhmite. Dark-field + diffuse overhead illumination. Photomicrograph by Richard W. Hughes; field of view 3 mm.

scope produced no reaction. We then moved to analyze the substance via micro-Raman. The result was böhmite, which neatly confirmed the results from the infrared spectrum.

About the banner: This plate of muscovite mica from Brazil contains an interesting frond of tourmaline that shows vibrant color using polarized light. Photomicrograph by Nathan Renfro; field of view 15.67 mm.

Editors' note: Interested contributors should contact Nathan Renfro at nrenfro@gia.edu and Stuart Overlin at soverlin@gia.edu for submission information.

GEMS & GEMOLOGY, VOL. 56, No. 2, pp. 292–297.

© 2020 Gemological Institute of America

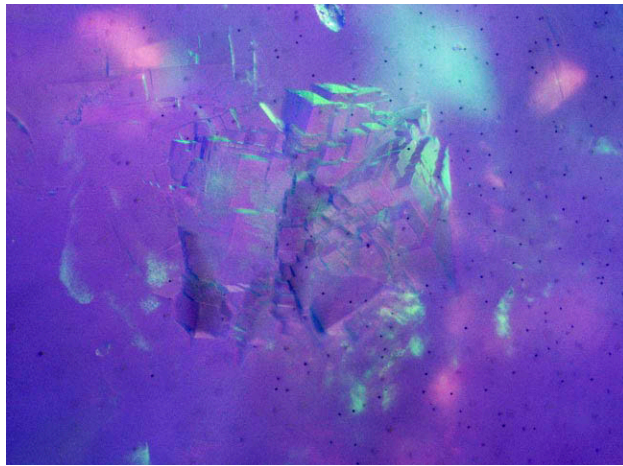


Figure 3. Chabazite inclusion in an Ethiopian opal. Photomicrograph by Aurélien Delaunay; field of view 1.42 mm.

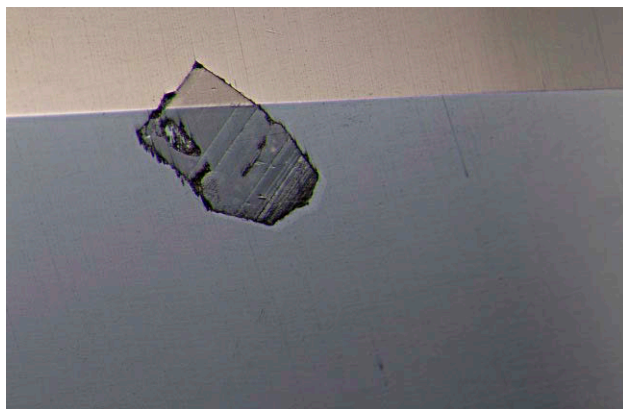
Böhmite, $\text{AlO}(\text{OH})$, is a polymorph of diasporé. In corundum it is generally a secondary mineral, infilling surface-reaching openings after the host corundum has grown.

Richard W. Hughes
Lotus Gemology, Bangkok

Rare Inclusion of Chabazite in a Precious Opal From Ethiopia

An opal received for analysis at the Laboratoire Français de Gemmologie (LFG) in Paris was classified as a light opal, with a bodycolor that matched to neutral gray N8 on the Munsell scale. The play-of-color was divided into sections with well-defined outlines that fit together or were rounded off in the form of digits (B. Rondeau et al., "On the origin of digit patterns in gem opal," Fall 2013 *G&G*, pp. 138–146).

Figure 4. This crystal broke the surface of a dark red spinel believed to be from Mogok. It had a lower luster than the spinel, and undercutting indicated a lower hardness. Photomicrograph by Richard W. Hughes, diffuse overhead illumination; field of view 2.5 mm.



The drilled bead weighed 12.02 ct and measured 13.4 mm in diameter. It contained small black inclusions of pyrite but also a crystalline inclusion in the form of aggregated pseudocubes (figure 3). This inclusion was identified as chabazite via Raman analysis. The pseudocubes were in fact near-cubic rhombohedra.

While this mineral has already been documented in veins and opal nodules from Ethiopia, it is rarely seen in cut stones (B. Chauviré, "Genèse de silice supergène sur Terre et implications sur Mars," PhD thesis, University of Nantes, 2015; N.D. Renfro and S.F. McClure, "Dyed purple hydrophane opal," Winter 2011 *G&G*, pp. 260–270). Chabazite, $\text{CaAl}_2\text{Si}_4\text{O}_{12}\cdot 6\text{H}_2\text{O}$, is a member of the zeolite family. This mineral is formed in gaseous cavities of extrusive volcanic rocks, which is similar to how opals from Ethiopia form. This inclusion is also proof of the Ethiopian geographic origin of this gem, as it has not been described in opal from other localities.

Aurélien Delaunay and Ugo Hennebois
Laboratoire Français de Gemmologie

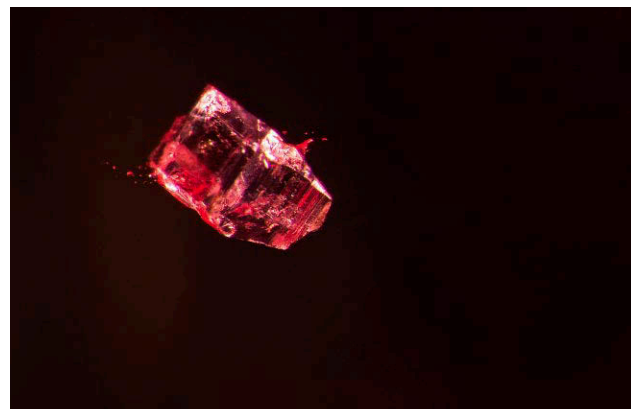
Emmanuel Fritsch
Université de Nantes, France

Fluorophlogopite in Burmese Spinel

Lotus Gemology in Bangkok received a large parcel of dark red spinels for identification. Their colors, inclusion features, and trace element chemistry suggested that they originated from Myanmar's Mogok Stone Tract.

In one faceted specimen, a crystal was found breaking the surface (figure 4). The crystal's surface luster suggested a refractive index below that of the host spinel, and undercutting suggested it was also significantly lower in hardness. The inclusion's interior also displayed signs of

Figure 5. In darkfield illumination, cleavage was visible inside the crystal. Micro-Raman analysis showed it to be fluorophlogopite. Photomicrograph by Richard W. Hughes, darkfield illumination; field of view 2.5 mm.



cleavage (figure 5). Thinking it was possibly a carbonate, we proceeded to do micro-Raman analysis on the crystal. To our surprise, the result was fluorophlogopite.

Fluorophlogopite, $\text{KMg}_3(\text{AlSi}_3\text{O}_{10})(\text{F,OH})_2$, is a species in the mica group and a member of the trioctahedral mica subgroup. To the best of our knowledge, this is the first reported instance of this species in spinel. Nor are we aware of it having been found included in any gem mineral to date.

Richard W. Hughes

Unusually Shaped Rutile Crystal Inclusions in Russian Emerald

Russian emeralds have been mined since the mid-nineteenth century near Yekaterinburg in the Ural Mountains. They are classified as schist-related emeralds, meaning they formed in the reaction zone of a pegmatite intruding into schists. Similar emeralds are found in Zambia, Brazil, and Ethiopia. All of these deposits can show a similar inclusion scene (S. Saeseaw et al., "Geographic origin determination of emerald," Winter 2019 *GeJG*, pp. 614–646).

A 1.489 ct Russian emerald crystal collected by GIA at the Mariinsky Priisk mine showed several interesting included crystals. The crystals appeared as long yellowish brown rods (figure 6). In some cases, they appeared as a group of disordered coarse needles (figure 7). They were identified by Raman spectroscopy as rutile. Although rutile crystal inclusions are common in schist-related emeralds, this crystal morphology is unusual and has not previously been mentioned in the literature. Therefore, this inclusion might be unique and different from the other schist-related emerald sources. These unusual patterns could potentially be an indicator of Russian origin.

Charuwan Khowpong
GIA, Bangkok

A Sapphire with a Negative Crystal Containing a Mobile Graphite Daughter Crystal

Mineral and fluid phases within negative crystals in metamorphic sapphires provide us with general information on the sapphire and the trapped fluid itself. Such inclusions indicate a stone has not been heated when intact negative crystals are observed containing carbon dioxide (e.g., Fall 1986 Lab Notes, pp. 152–155). The author recently had an opportunity to identify a natural star sapphire containing a unique daughter crystal phase within a negative crystal.

This stone, which measured $22.20 \times 18.00 \times 14.05$ mm with an estimated weight of 62 ct, was set in a ring. It displayed a six-rayed asterism due to light reflection from numerous long intersecting needles. Gemological observation and properties confirmed that this stone was a natural sapphire. The presence of unaltered mineral crystals and the chromophore cannibalization pattern around

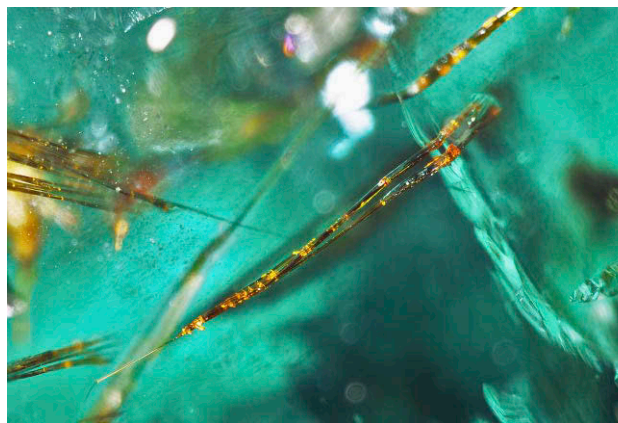
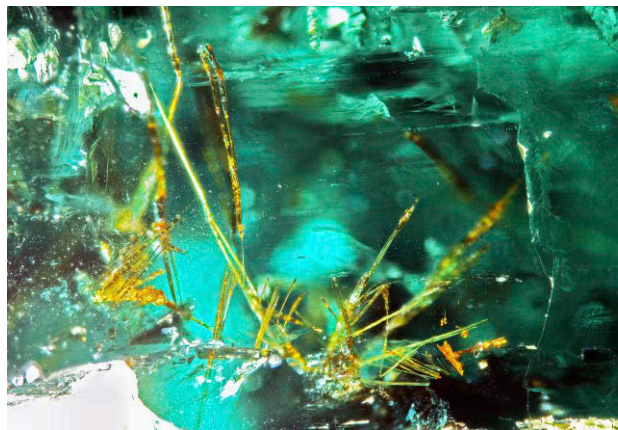


Figure 6. This long yellowish brown rod was identified by Raman spectroscopy as rutile. Photomicrograph by Charuwan Khowpong; field of view 1.75 mm.

dense clouds of needles indicated the stone had not been heat treated (J.I. Koivula, "Internal diffusion," *Journal of Gemmology*, Vol. 20, No. 7/8, 1987, pp. 474–477). Notably, this stone had one large negative crystal containing an opaque hexagonal crystal (figure 8). The hexagonal daughter crystal was free to move within the negative crystal when the stone was rocked and tilted. Careful infrared spectroscopic measurements suggested that this negative crystal was mainly filled with water and CO_2 based on water-related peaks at 3706 and 3605 cm^{-1} and a large CO_2 broad band at 2340 cm^{-1} . However, the opaque daughter crystal was not identified by Raman spectroscopy because the negative crystal containing this daughter phase was located in a deeper section of the stone. Its hexagonal crystal shape and appearance suggested that the mobile hexagonal

Figure 7. The group of disordered coarse needles of rutile. Photomicrograph by Charuwan Khowpong; field of view 3.65 mm.



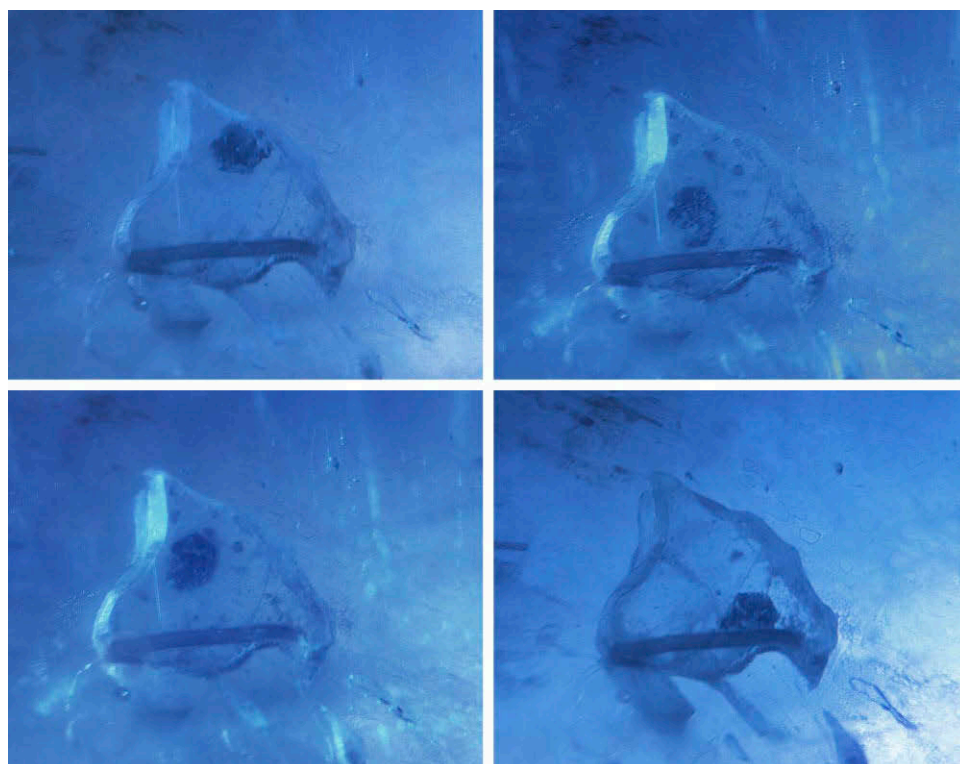


Figure 8. This opaque hexagonal daughter crystal, of what is likely graphite, moves within the large negative crystal in the metamorphic star sapphire. Photomicrographs by Makoto Miura; field of view 4.0 mm.

daughter crystal was graphite, which has been previously documented (E.J. Gübelin and J.I. Koivula, *Photoatlas of Inclusions in Gemstones*, Vol. 3, Opinio Verlag, Basel, Switzerland, 2008, p. 268). This is the first example of a negative crystal with a mobile solid phase in corundum that the author has encountered.

Makoto Miura
GIA, Tokyo

Windmills in Rare Mineral Sphalerite

Sphalerite is a rare gem mineral that crystallizes in the cubic crystal system and consists largely of zinc sulfide formed with variable iron, with the chemical formula of (Zn,Fe)S. Its color is usually yellow, brown, red, or gray to gray-black with high dispersion and high adamantine luster. The author recently examined a high-quality faceted orange sphalerite weighing 47.56 ct that revealed three-ray structures reminiscent of windmills with each propeller arm separated by 120°. Additionally, the orange color was concentrated in the immediate region of the three radial arms of each propeller-like structure (figure 9). Other typical internal characteristics of sphalerite such as strong angular internal growth with orange color zoning, particulate clouds, tiny crystals, and fingerprints, were also observed. This distinctive structure resembling windmills is the first such feature the author has encountered in sphalerite.

Ungkhana Atikarnsakul
GIA, Bangkok

Trapiche-Like Pattern in an Emerald from Pakistan

GIA's colored stone research collection contains many unique samples. The emerald sample shown in figure 10 was mined at Swat Valley in the Khyber Pakhtunkhwa region of Pakistan and fabricated by polishing two parallel windows perpendicular to the c-axis of the hexagonal crystal in order to show its inclusions. The sample weighed 0.47 ct prior to fabrication and 0.36 ct after processing.

Figure 9. A group of windmill-like inclusions with orange color concentrations observed in sphalerite. Photomicrograph by Ungkhana Atikarnsakul; field of view 3.1 mm.



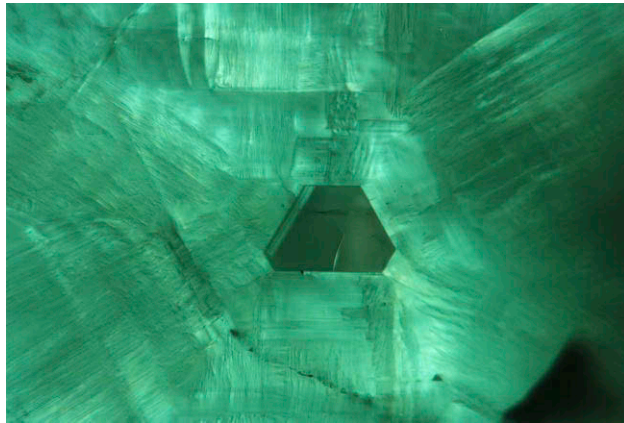


Figure 10. A distinct near-colorless hexagonal core with radiating fibrous arms is evident in this Pakistani emerald from Swat Valley. Photomicrograph by Charuwan Khowpong; field of view 1.40 mm.

At first glance, nothing unusual was noted in this sample, but when correctly illuminated under the microscope it revealed a pattern that could easily pass for trapiche. The stone showed radiating zones of turbid growth with six-fold symmetry. This makes it a trapiche-like stone rather than a true trapiche, which has distinct arms that separate the growth zones. While classic trapiche patterns are mostly associated with Colombian emeralds, the Swat region also produces emeralds with radiating black intergrowths. Still, this structure was very different from the

trapiche structure previously documented in some emeralds from Pakistan (Fall 2019 Gem News International, "Trapiche emerald from Swat Valley, Pakistan," pp. 441–442). In this case, the distinct growth feature consisted of a colorless hexagonal core from which six-rayed fibrous arms extended. Lighting was an important consideration in maximizing the color in this stone, and the features were fully observed using brightfield illumination. This was a wonderful example of a pattern rarely encountered in emeralds.

*Piradee Siritheerakul and Charuwan (Gibb) Khowpong
GIA, Bangkok*

Quarterly Crystal: Pyrite in Quartz

Pyrite and quartz are two relatively common minerals. Transparent colorless quartz, known as rock crystal, is host to a wide variety of mineral and fluid inclusions, more so than any other gem mineral. While pyrite and rock crystal are both common, finding a good example of crystalline pyrite inside of rock crystal quartz is a gem mineral collector's prize.

Known for its fine emeralds, the Chivor mine in Colombia is also a mineralogical source of both pyrite and colorless quartz. On occasion, crystals of Colombian quartz are known to host pyrite. As shown in figure 11 (opposite page), we recently had the opportunity to examine one such specimen, which hosted numerous bright metallic brassy yellow modified octahedrons of pyrite (figure 12). The inclusions were not randomly scattered throughout the 466.27 ct quartz, but instead were situated neatly just

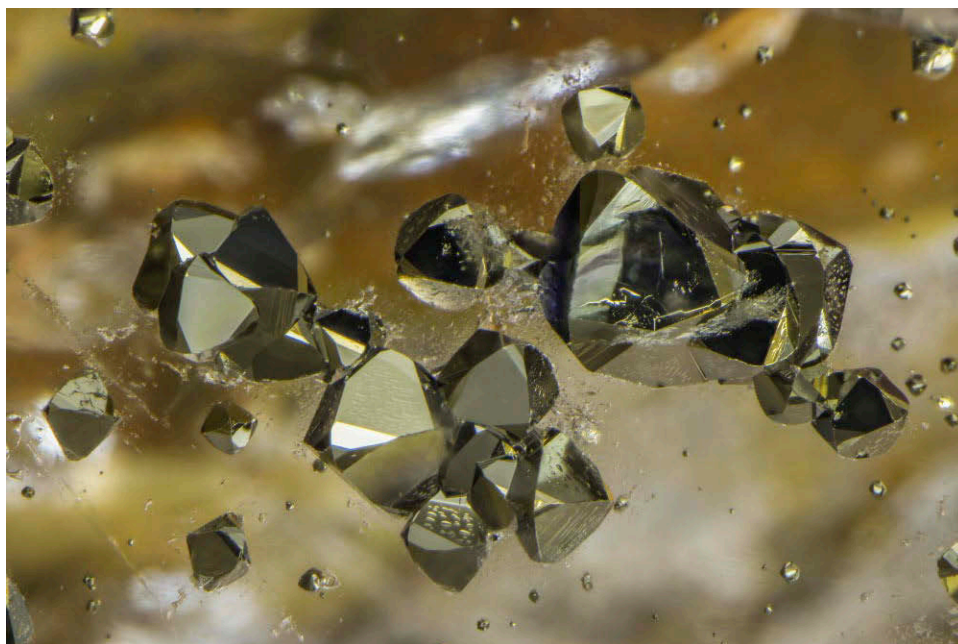


Figure 12. These modified octahedrons of pyrite were deposited along one prism face of their quartz host. Photomicrograph by Nathan Renfro; field of view 7.62 mm.



Figure 11. This example of Colombian pyrite-containing rock crystal weighs 466.27 ct and measures 61.90 mm in length. Photo by Diego Sanchez.

under the surface of one of the prism faces. Another interesting feature was that all of the pyrite inclusions were present in a range of sizes with well-defined crystal faces, suggesting that the pyrite crystals precipitated syngeneti-

cally (at the same time) from a directional fluid rich in pyrite forming iron sulfide.

*John I. Koivula and Nathan Renfro
GIA, Carlsbad*

Gem News International

Contributing Editors

Emmanuel Fritsch, *University of Nantes, CNRS, Team 6502, Institut des Matériaux Jean Rouxel (IMN), Nantes, France* (fritsch@cnsr-immn.fr)

Gagan Choudhary, *Gem Testing Laboratory, Jaipur, India* (gagan@gjepcindia.com)

Christopher M. Breeding, *GIA, Carlsbad* (christopher.breeding@gia.edu)

COLORED STONES AND ORGANIC MATERIALS

Purplish pink diaspore reportedly from Afghanistan. Diaspore, an orthorhombic aluminum oxide hydroxide mineral with the formula $AlO(OH)$, is a relative newcomer to the jewelry scene, with some stones possessing a captivating ability to change color between pale green, yellow, pink, and purple when viewed in different sources of light (C. Shen and R. Lu, "The color origin of gem diaspore: Correlation to corundum," Winter 2018 *G&G*, pp. 394–403). Here we document a new find of purplish pink gem diaspore reportedly from Nangarhar Province, Afghanistan (figure 1).

Previously, transparent crystals of diaspore in sizes suitable for jewelry purposes were only recovered from mining operations on Ilbir Mountain near the village of Pinarçik,

Figure 1. This purplish pink diaspore is reportedly from a new deposit in Afghanistan, discovered in February 2020. The faceted stones weigh 0.57 to 1.60 ct; courtesy of Donald Hofler. The rough stones range from 4.15 to 17.52 ct; courtesy of Salman Khan. Photo by Diego Sanchez.



Milas District, Muğla Province, Turkey (M. Hatipoğlu and S. Chamberlain, "A gem diaspore occurrence near Pinarçik, Muğla, Turkey," *Rocks & Minerals*, Vol. 86, No. 3, pp. 242–249). Gem diaspore from Turkey has been reported since the late 1970s (K. Scarratt, "Faceted diaspore," *Journal of Gemmology*, Vol. 17, No. 3, 1980, pp. 145–148), but it was not until commercial mining began in 2005 that a consistent supply became available and was subsequently marketed under various trade names including Zultanite and Csarite (S. Kotlowski and L. Rosen, "A short history of diaspore and its trade names Zultanite and Csarite," *International Gem Society*, www.gemsociety.org/article/short-history-diaspore-trade-names-zultanite-csarite). Additionally, alluvial deposits in Myanmar near Mong Hsu have yielded limited amounts of chromium-colored gem-quality crystals in small sizes since 2004 (U Hla Kyi and K.K. Win, "A new deposit of gem quality colour-change diaspore from Mōng Hsu, Myanmar," *Australian Gemmologist*, Vol. 22, No. 4, pp. 169–170).

Dealers Salman Khan (ARSAA Gems & Minerals) and Noshad (Noshad Gems Enterprises), both based in Peshawar, Pakistan, reported that in March 2020, a purplish pink diaspore from a new deposit had reached the gem market. The new material was reportedly coming from the Goshta district of Nangarhar Province near the village of Ragha. The authors obtained several samples from Salman Khan and Donald Hofler, a gem dealer in Texas, to perform gemological and advanced testing to characterize this material. These samples would be classified as F-type samples (collected in the international market) according to the classi-

Editors' note: Interested contributors should send information and illustrations to Stuart Overlin at soverlin@gia.edu or GIA, The Robert Mouawad Campus, 5345 Armada Drive, Carlsbad, CA 92008.

GEMS & GEMOLOGY, VOL. 56, No. 2, pp. 298–316.

© 2020 Gemological Institute of America

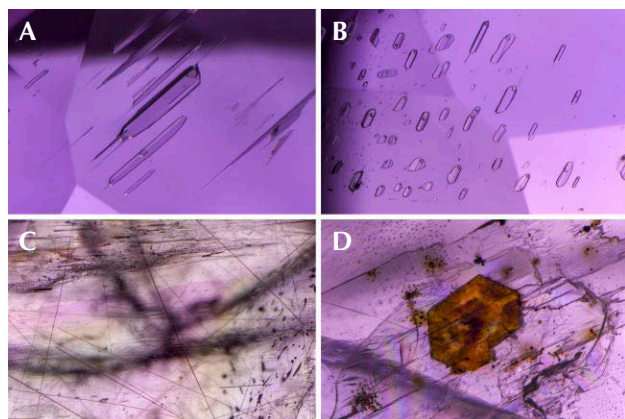


Figure 2. Microscopic examination of the diaspore revealed numerous elongate fluid inclusions (A) and planes of fluid inclusions (B). Also observed in two rough samples were fine black rutile needles (C), and one stone contained an unidentified brown hexagonal crystal (D). Photomicrographs by Nathan Renfro; field of view 1.88 mm (A), 1.44 mm (B), 4.47 mm (C), and 1.41 mm (D).

fication scheme used by GIA's field gemology department (W. Vertriest et al., "Field gemology: Building a research collection and understanding the development of gem deposits," Winter 2019 *G&G*, pp. 490–511). It was also reported by the Peshawar-based dealers that preliminary experiments with gamma irradiation resulted in samples becoming an undesirable dark brownish orange color, but this was not tested further by the authors.

Microscopic examination showed that the dominant type of micro feature in the material is fluid inclusions, typically consisting of a gas bubble, liquid, and occasionally a solid phase. Fine curved black rutile needles were also observed in two of the samples (confirmed by Raman analysis), while one diaspore crystal contained a brown hexagonal crystal that the authors were unable to identify (figure 2). Brown epigenetic staining and cleavage cracks were observed in several samples. Strong doubling from birefringence was also characteristic of the material.

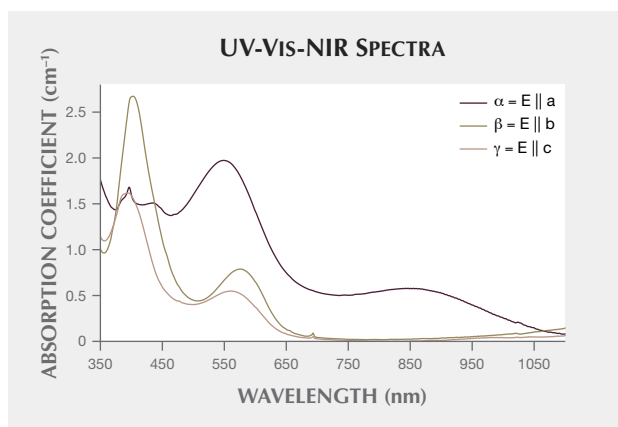
Gemological testing revealed a biaxial positive mineral with refractive indices of $n_\alpha = 1.700$, $n_\beta = 1.721$, and $n_\gamma = 1.749$, and a specific gravity of 3.38. The maximum birefringence observed was 0.049. Examination with a dichroscope showed three distinct pleochroic colors, consistent with a biaxial mineral: dark purplish pink, pale yellow, and pale pink. The diaspore showed a very weak red fluorescence under long-wave ultraviolet light and an irregular chalky yellow fluorescence reaction under short-wave UV. When the samples were examined with daylight-equivalent illumination and compared to incandescent illumination, a slight color shift was observed. The samples appeared less purplish, going from purplish pink in daylight-equivalent lighting to a nearly pure pink hue in

incandescent lighting, but no distinct color change of the dominant hue was observed in the faceted samples.

Advanced spectroscopic instrumentation was used to further characterize the new diaspore material. One sample was optically oriented into a polished cube with parallel faces polished perpendicular to the crystallographic axes (T. Thomas et al., "Device and method of optically orienting biaxial crystals for sample preparation," *Review of Scientific Instruments*, Vol. 85, No. 9, 2014, 093105). The ultraviolet/visible/near-infrared (UV-Vis-NIR) absorption spectra of the polished cube revealed broad absorption bands centered in the range of 560 and 580 nm for alpha, beta, and gamma polarizations (figure 3). Under daylight-equivalent lighting, the saturated purple-pink color was consistent with the alpha vibration direction, pale greenish yellow for the beta direction, and light purplish pink for the gamma direction. Under incandescent light, the pleochroic colors were saturated purple-pink for the alpha color, orange-pink for the beta color, and light pink for the gamma color. Color swatches were calculated using the measured spectra to produce a representative color for each pleochroic color and also to show how the colors mix relative to their crystallographic axes (figure 4).

Observations under the microscope showed the cleavage direction in the faceted stones to be nearly parallel to the table (it is inclined slightly, presumably to avoid cleaving when polishing the table facet). This orientation places the b-axis approximately perpendicular to the table facet, which will facilitate the best color face-up, composed primarily of a mixture of the alpha and gamma rays.

Figure 3. UV-Vis-NIR spectra were collected from an optically oriented sample to resolve the alpha, beta, and gamma vibrational directions in the Afghan diaspore. All three spectra showed a broad absorption band centered between 560 and 580 nm resulting primarily from vanadium and chromium. In this sample, the average concentrations were 57 ppma vanadium, 20 ppma chromium, 205 ppma iron, and 84 ppma titanium.



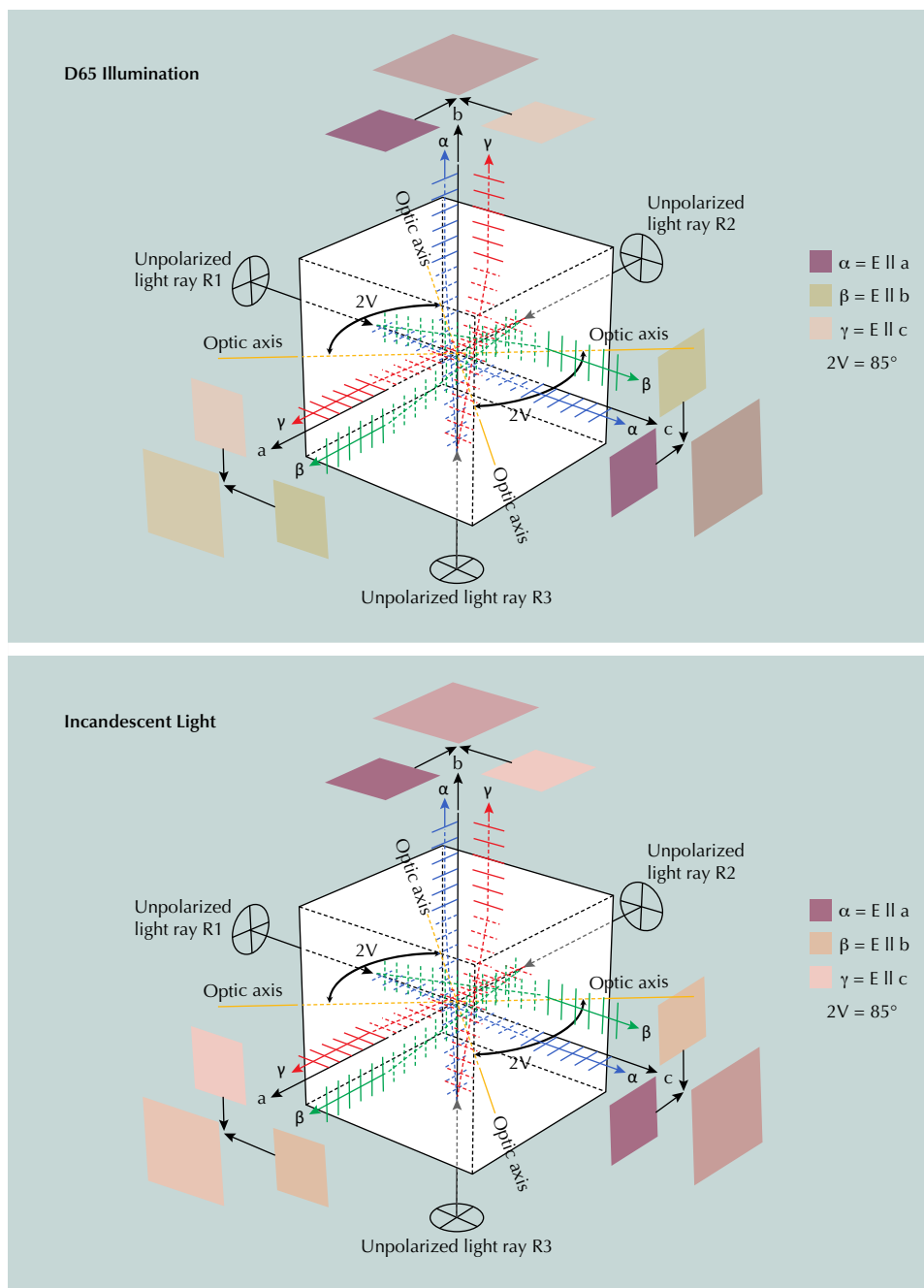


Figure 4. One diaspore sample was fabricated into a crystallographically oriented block in order to measure the polarized spectra, which were used to analyze the color. This figure shows the relationship of the polarized spectra measured parallel to each crystal axis and the resulting colors produced when the polarized spectra are mixed together under daylight (top) and incandescent (bottom) conditions, which is what the viewer would observe using unpolarized light transmitted through the sample normalized to a 1 cm path length. Under daylight-equivalent lighting, the alpha color was saturated purple-pink, the beta color was light greenish yellow, and the gamma color was light pink. Under incandescent light, the alpha color was a saturated purple-pink, the beta color was orange-pink, and the gamma color was light pink. The acute $2V$ angle, or angle between the two optic axes, was measured as 85° in this sample. Both axes lie in the optic plane that is perpendicular to the b crystal axis.

Raman analysis confirmed the material's identity as diaspore (figure 5, left). Fourier-transform infrared (FTIR) spectroscopy showed absorption features at approximately 2115 and 1990 cm^{-1} and broad absorption bands at approximately 4080 and 3000 cm^{-1} , all of which are consistent with diaspore (figure 5, right). Chemical analysis of seven samples showed a bulk composition consistent with that of diaspore, and average notable trace element concentrations showed 27 ppma chromium (ranging from 14 to 48 ppma), 31 ppma vanadium (from 14 to 59 ppma), 213 ppma titanium (from 67 to 428 ppma), and 252 ppma iron (from 137 to 350 ppma).

This exciting discovery of purplish pink diaspore from Afghanistan may prove to be a significant new deposit. While production volume is currently unknown, several kilograms of material have been reported and large faceted stones of nearly 50 ct have been described on social media (Mark Smith, @thailankagems). The color of this diaspore can be attributed mainly to trace element concentrations of chromium and vanadium. The concentrations of these elements are generally different from those in Turkish diaspore, which has significantly lower vanadium, and those in Burmese material, which

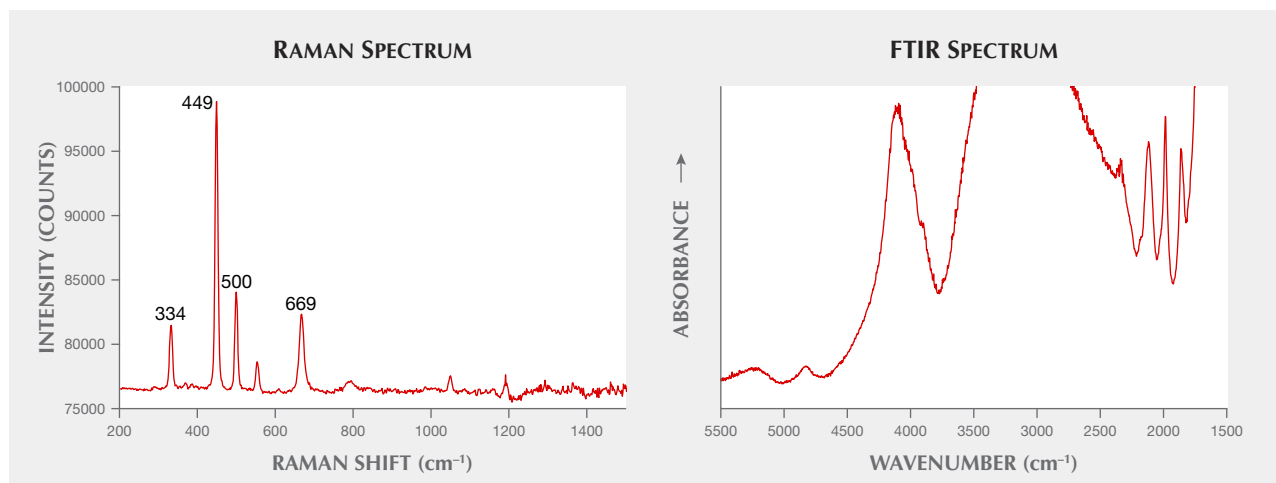


Figure 5. The purplish pink gem material from Afghanistan showed a Raman spectrum (left) that matched diaspore, with a dominant peak at 449 cm^{-1} and smaller peaks at 334 , 500 , and 669 cm^{-1} . Its FTIR spectrum (right) was consistent with diaspore, with absorption features at approximately 2115 and 1990 cm^{-1} and broad absorption bands at approximately 4080 and 3000 cm^{-1} .

generally has much higher chromium. This new attractive color of gem-quality diaspore will certainly be a welcome addition to the gem trade.

Ian Nicastro
San Diego, California
Wim Vertriest
GIA, Bangkok

Nathan Renfro, Ziyin Sun, Aaron Palke, and Paul Mattlin
GIA, Carlsbad

Fossil ivory update with Lee Downey. Lee Downey, owner of Artifactual (Tucson, Arizona), spoke with us in early 2020 about his 35 years in the fossil ivory carving trade and the impact of ivory bans on his business. Until recently Downey carved fossil ivory from mammoth and walrus tusks thousands of years old; he has never used elephant

ivory. But legislative measures banning all ivory in response to the poaching of African elephants have diminished ivory demand.

Downey got his start in silver and turquoise and established Artifactual in the late seventies. Since then, he has lived and worked in an ivory carving village in Bali with artisans he calls “the most talented carvers in the world.” When he first arrived in Bali, they were carving bone and coconut shell. His task was to carve animals and animal skulls out of fossil ivory. “We created a trade,” he said. He showed us two of Artifactual’s current offerings (figure 6). “But now the material has become flat-out illegal in eight states.”

Since 2014, California, Hawaii, Illinois, Nevada, New Hampshire, New Jersey, New York, and the District of Columbia have enacted prohibitions against trade in ivory. (Two other states, Oregon and Washington, have banned



Figure 6. Fossil walrus ivory carvings by Artifactual. The base of the octopus carving is chalcociderite. Photos by Kevin Schumacher.



Figure 7. A mammoth tusk carved with sea life by Lee Downey. Photo by Kevin Schumacher.

only ivory from living elephants.) Downey said that Hawaii's ban in particular "tanked" the trade. Customers even in states where ivory remains legal are reluctant to purchase fossil ivory, he said.

"I understand why they're doing it," Downey told us. "I'd rather save all wildlife if there was a way." But he said the effect of the bans on his business has forced him to prepare to exit the fossil ivory trade. He is selling his current ivory inventory at lower prices and not buying additional material.

Downey showed us a mammoth tusk carved with sea life (figure 7) as well as two belt buckles featuring mammoth ivory (figure 8). All of them use material sourced from Alaska. "This washes up on beaches and comes out of gold mines," he said. "It's highly sought after by the knife makers. It's got colors that elephant ivories will



Figure 8. A selection from Artifactual's inventory of fossil ivory. Clockwise from top left: belt buckle with mammoth ivory, knife with mammoth tooth handle, belt buckle with mammoth ivory, and frog carving of fossil walrus ivory. Photo by Kevin Schumacher.

never have. It just keeps weathering out of the dirt." Downey added that this ivory is at least 10,000 years old.

Mammoth ivory can be differentiated from elephant ivory by a simple field test to observe its natural grain lines. But there is no test to determine whether a specimen of walrus ivory comes from a fossil or a modern animal. According to Downey, this is a problem in the trade.

Artifactual uses fossil walrus ivory from St. Lawrence Island, Alaska. This ivory is 500 to 15,000 years old and dug by the native Yupik people. "It's part of their income, and they own the island," he said. "For us it's a legitimate and ethical trade."

Downey added that the legislation on ivory also prohibits mammoth tooth because it comes from an ivory-bearing animal. He showed us a knife with a carved mammoth tooth handle (figure 8). Knife makers are some of the biggest buyers of mammoth tooth, he said, and the bans have dramatically impacted their business.

As a result of the decreased demand for ivory, Artifactual is moving its business to other materials, including jet, natural American turquoise and variscite, steel (figure 9, left), and meteorite. "Gaia" (figure 9, right) is carved from a piece of the Gibeon iron-nickel meteorite, which landed in prehistoric times in Namibia and is believed to be around four billion years old. The company also does a lot of business in silver.

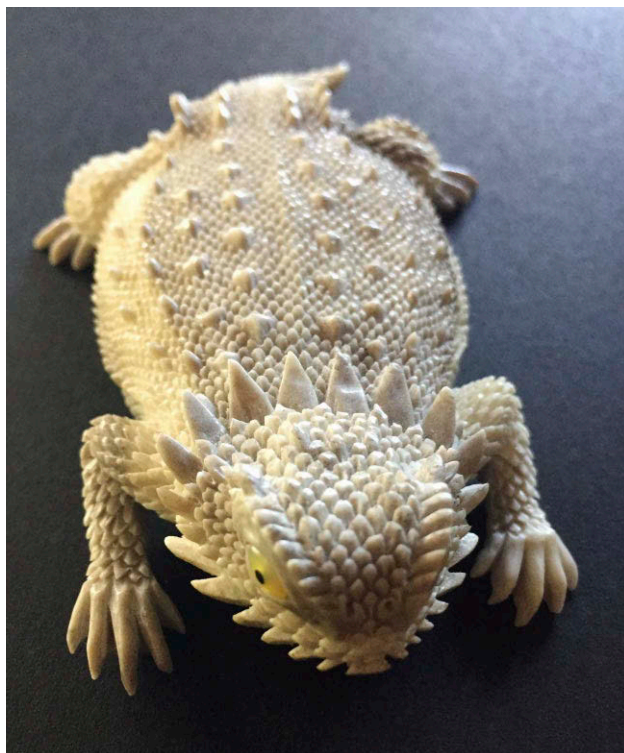
Downey has also sought out materials similar to ivory but without the ethical and legal challenges. He has begun



Figure 9. Left: “Alpha,” a stainless steel foundry-cast skull by Artifactual, one of six in a series. Right: “Gaia,” the second skull Downey carved from a piece of the Gibeon meteorite, has a tridymite crystal inclusion in the forehead. The geometric pattern on its surface was caused by the slow process of cooling as the meteor moved through space. Photos by Kevin Schumacher.

carving moose antlers naturally shed by the animals (figure 10). “The moose antler has been a really good substitute

Figure 10. A moose antler carving of a horned toad by Lee Downey. Photo by Duncan Pay.



for the ivory,” he said. He also recently began carving vintage billiard balls. “We’ll carve anything that’s carvable,” he said.

For our video interview with Lee Downey, visit <https://www.gia.edu/gems-gemology/summer-2020-gem-news-fossil-ivory-update>.

Erin Hogarth and Duncan Pay
GIA, Carlsbad

The “Fragility of the Eternal” kunzite: Origin, cutting, and identification. Lapidary, the art of colored stone fashioning, is an art that requires a keen eye, talent, and great patience. Different gem materials have their particular quirks that must be considered when planning the various steps required to reach the ultimate goal of obtaining the most aesthetic stone while usually also optimizing weight yield.

Spodumene is known to challenge even the most experienced cutter owing to its high fragility, perfect cleavage planes, and unpredictability in different cutting directions. This is further magnified when the rough is exceptionally large and the cutter’s goal is to produce the largest faceted kunzite in the world.

This was author VT’s aim as he prepared to work on a piece of rough spodumene that weighed 2,950 g. The untreated crystal (figure 11) originated from Kunar Province in Afghanistan. Although a wide crack was visible at one end and about 30% of the opposite end contained numerous inclusions, the removal of both sections still left more than 1.5 kg of relatively clean rough after 20 hours of wire sawing (the safest method under the circumstances). Since the rough was oversized, some of the routine cutting ac-

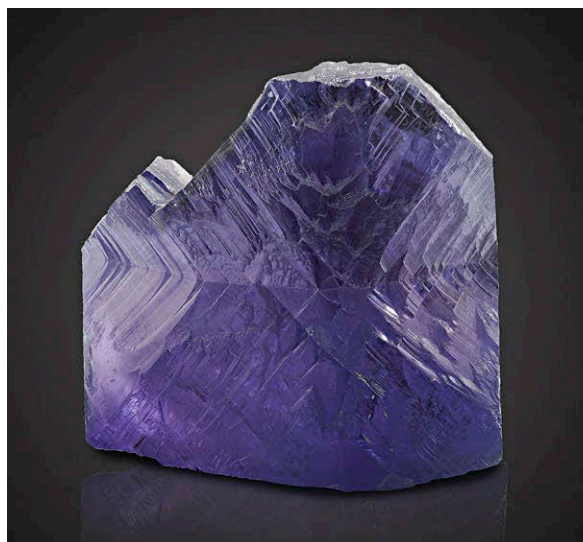


Figure 11. The pronounced pleochroism of the rough spodumene crystal weighing 2,950 grams, seen here in two orientations, was one of the properties that had to be considered during fashioning. Photos by Arjuna Irsutti.

cessories such as dops and transfer holders, as well as the cutting tactics, had to be adapted for the job.

Prior to the start of the process came the design element. No journey can be completed without knowing the destination, and so rather than playing it safe and opting for a simple design, the artist, VT, chose a truly challenging facet pattern of his own design that incorporated 914 facets. The “Fragility of the Eternal” design is based on the stained glass window of the iconic Notre Dame cathedral in Paris. The stone is the fifth in a series of six cut designs that fall under VT’s “World Heritage” project.

VT would also have to revise his usual strategy due to the size. So instead of cutting the pavilion first, followed by the girdle, crown, and finally the table facet, it was necessary to start with the table facet for this masterpiece. This presented its own challenges since the faceting required specialized equipment belonging to a friend in Moscow. The choice of equipment was also dictated by the material’s fragility and perfect cleavage, which prevented the use of coarse laps. This combined to make the work time-consuming, especially since large facets were the order of the day.

The next step required the rough to be rounded in order to achieve the basic outline of the stone in its face-up position. This meant that sufficient pressure had to be applied to the 1.5 kg preform using both hands. Eventually the correct shape resulted. The diameter measured approximately 85 mm, while the table facet came in at 65 mm. This allowed the final weight to be approximated using formulas and the facet plan shown in figure 12. The result, between 2,500 and 3,000 ct, indicated that it would supersede the largest known faceted spodumene, an 1,800 ct green spodumene cut by John Sinkankas in 1959 that was destined for the Royal Ontario Museum in Toronto.

Although the rest of the preforming could not be done traditionally by hand, VT managed to use his faceting unit

with custom-made dops provided by his friend and former student Danial Hu. The pre-faceting step took considerable time to complete because the goal was to create an important piece of art and each facet needed to be cut in a pattern that matched the stained glass window in the Notre Dame cathedral with a precision of tenths of a millimeter. Perhaps the most complex part of the process was creating 16 mains and 16 additional lines extending from the center (culet) to the girdle, each containing eight (main) and five (additional) parallel-sided facets, continuous with one another. An equally challenging task was ensuring the proportions were correct while cutting 18 rows of facets of different sizes and shapes, where one often does not depend on another, and finally making the last row of facets correspond exactly with the girdle, which was already pre-shaped. It was impossible to change the width of the final facets without breaking the pattern, which meant that the pavilion had to finish precisely where the girdle started. In other words, the width of all 18 rows had to be exactly proportional to the diagram. Another look at figure 12 is enough to show that the girdle does not simply separate the crown from pavilion as in traditional faceted stones: It is an essential element of the design.

Many chances for something to go awry existed during the cutting process. Only a slight error in judgment or calculation would result in disaster. For example, if the rows of facets were just a bit too wide, there would not have been enough space for the design and the pavilion would have required a complete recut. If some were too narrow, the girdle would have needed recutting, resulting in a smaller stone, which would also have meant recutting the table facet. Fortunately, the final facet positions aligned perfectly around the girdle, and the stone’s final diameter (83.7 mm) was off by just over 1.0 mm from the initial calculations.

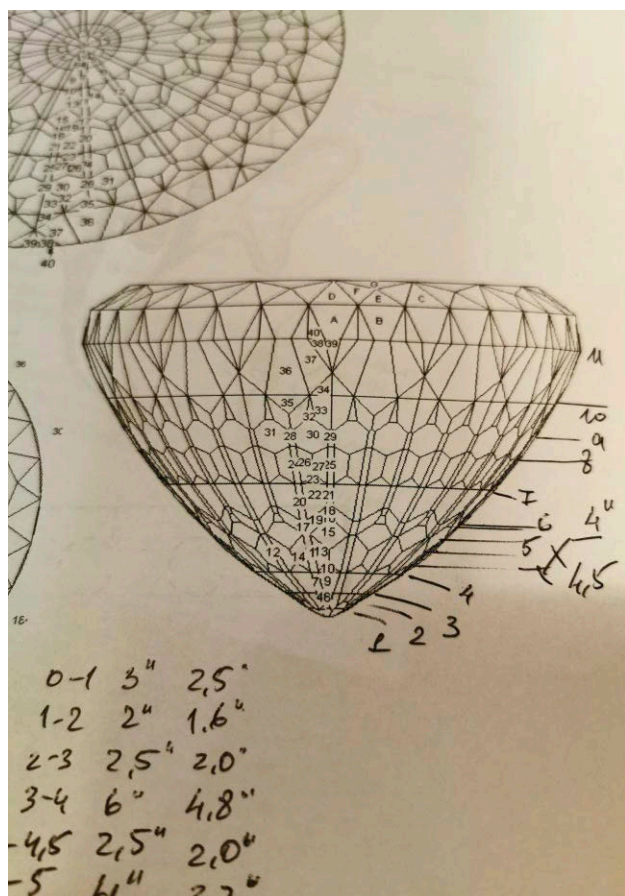


Figure 12. A working diagram showing the facet positions. These helped estimate the final weight of the finished stone before work began on the rough. Photo by Victor Tuzlukov.

The next steps, pre-polishing and polishing of the pavilion facets (figure 13), were straightforward in comparison. Yet, as mentioned previously, the sheer size meant that the vertical pressure had to be applied equally over the whole stone during pre-polishing, requiring modification of the technique used for routine work on smaller stones. If too much force was applied to the left or right side, or back and forth, the facets would become too large and the pattern would be broken. To overcome this, the stone's own weight provided sufficient force on the rotating lap so that the pressure was always equally distributed.

After more than two months of daily work, the pavilion was polished. The next step was transferring the stone to a new dop to polish the crown. Unlike traditional lapidary procedures, directly heating the stone as part of the transfer was not an option, as the process could crack the stone along the twin plane in the direction it needed to be doped, and because the size was once again a factor when it came to how evenly the heat warmed the stone. This resulted in the application of a technique that the late Jeff Ford from Michigan shared with VT in 2006, using a com-

bination of wax and superglue. The wax is placed on the hot dop, which is softened by the heat. The cold stone is then placed, pavilion first, in contact with the wax, and an impression of the surface is made in it. One drop of superglue is enough to secure the stone firmly in position, and it can be removed by reapplying a little heat to warm the wax again.

After three months of work, the final polishing step was completed. The gem's removal from the dop was an exciting moment, and it was wonderful to finally see the end product in all its glory (figure 14). The finished piece weighed 3,051 ct, very close to the maximum estimated weight of 3,000 ct.

The final step in the stone's journey was its submission to GIA's Bangkok laboratory for examination and a report. The gemologists were excited to study such a large kunzite, although the size, 83.75–83.79 × 65.00 mm, presented challenges that limited the testing equipment that could be used. Hence, basic gemological techniques came to the fore, with Raman spectroscopy the only advanced technique used as a final confirmation. The stone was found to be anisotropic with a loupe and microscopic observation

Figure 13. The polishing step on the stone's pavilion begins to show the intricate optical effects of the completed piece. Photo by Victor Tuzlukov.





Figure 14. The 3,051 ct “Fragility of the Eternal,” containing 914 facets, is believed to be the world’s largest cut kunzite. Photo by Adisorn Wattanavanich.



Figure 15. Marble polar bear with silver fish on a petrified opalized wood stand. Photo by Svetlana Kulenko; courtesy of Anton Akulenko.

up to 70× magnification, and this property was also apparent in terms of the strong pleochroism that could be easily seen as the stone was turned. The same purple and green colors are also clearly evident in figure 11.

The RI readings of 1.660–1.676 (birefringence of 0.016) together with the trichroic colors seen through a dichroscope showed it was optically biaxial. Inclusions such as growth tubes, transparent crystals, negative crystal fingerprints, and a “natural” retained on the girdle all proved the stone was natural. Combined with the weak and moderate orange zoned long-wave ultraviolet fluorescence reaction, the data were consistent with spodumene, kunzite variety.

Since the stone was cut and submitted by VT with a series of photographs documenting this fact, the GIA report (dated May 27, 2020) also mentioned that it was represented as cut by him. Since it was the largest known faceted kunzite examined by GIA at the time, and indeed the largest faceted example of its kind known to exist, a GIA Notable Letter was issued to accompany the report.

Victor Tuzlukov
Bangkok

Patcharee Kaewchaijaroenkit and Nicholas Sturman
GIA, Bangkok

Occurrence of petrified woods in the Russian Far East: Gemology and origin. Petrified woods are used all over the world as an excellent material for souvenirs, jewelry, and spectacular collectible pieces. A new occurrence of petrified wood was discovered in 2014 in the Primorsky Krai region of the Russian Far East, near the village of Kiparisovo. The fossils were found in the northwestern part of a sand and gravel quarry, at the contact of rhyolitic volcanic ash tuffs and basalts overlapping them. The sample sizes varied from several centimeters to two meters.

Local jewelers started using the wood fossils as stands for souvenirs (figure 15) and polished collectible samples. The petrified wood appeared in regional jewelry stores and attracted Chinese tourists’ attention, creating demand for the raw material from China’s market.

More than a hundred samples were studied at the Analytical Center of the Far Eastern Geological Institute of the Far Eastern Branch of the Russian Academy of Sciences (FEGI FEB RAS). We examined the mineral composition, structure, and gemological characteristics using standard gemological equipment, a Nikon E100 POL optical microscope, and a MiniFlex2 X-ray diffractometer (XRD). Several examples of petrified wood were found: white, yellowish, marble-like, chalcedony-like, banded, banded chalcedony-

Figure 16. Cabochons of petrified wood from the Russian Far East. Photo by Dmitrii G. Fedoseev.



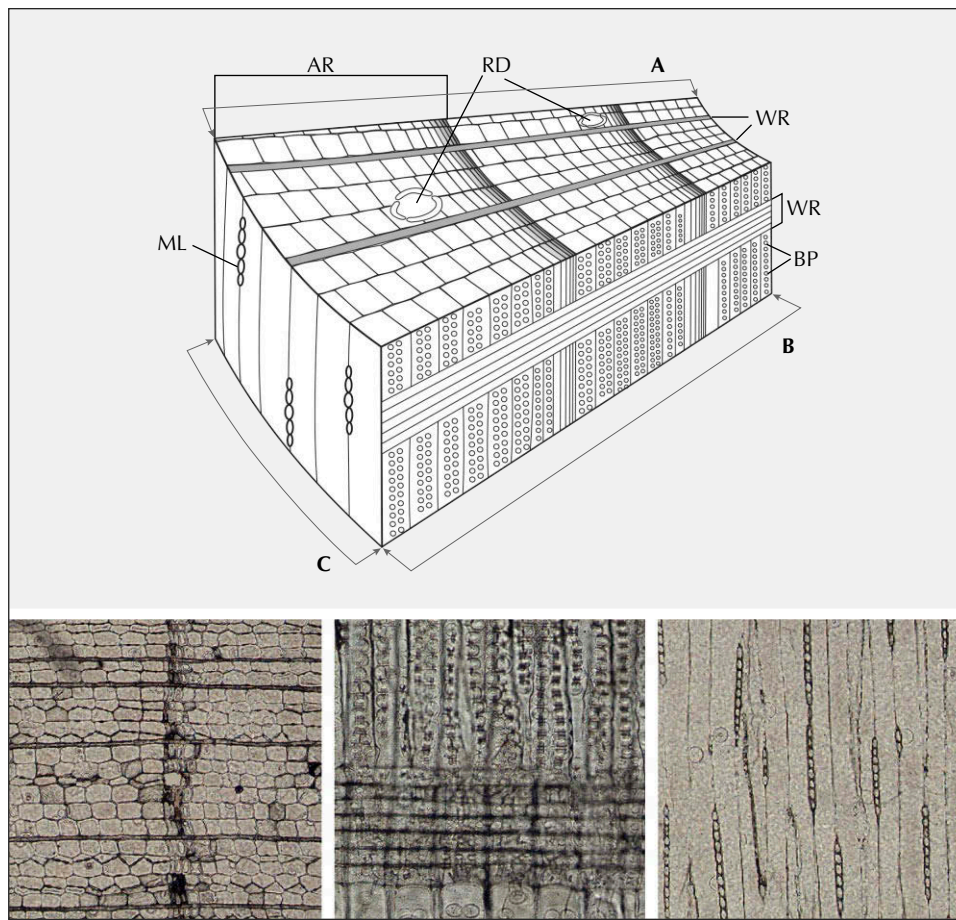


Figure 17. Top: Schematic cross section of a conifer's trunk showing the transection (A), radial section (B), tangential section (C), annual ring (AR), resin ducts (RD), wood rays (WR), bordered pits (BP), and middle lamellae (ML). Bottom left: Transection of petrified wood with wood rays (horizontal lines), resin ducts, and annual ring; field of view 5.5 mm. Bottom center: Radial section of petrified wood with wood rays (horizontal lines) and tracheids with bordered pits (round-shaped); field of view 2.7 mm. Bottom right: Tangential section of petrified wood with chains of middle lamellae; field of view 5.5 mm. Photomicrographs by Dmitrii G. Fedoseev.

like with brownish growth rings, partially carbonized, and black coalified (figure 16).

The refractive indices of polished plates ranged from 1.40 to 1.54 in different areas and corresponded to chalcedony, opal, and quartz. Luminescence was weak bluish or greenish under short-wave UV; most samples were inert under long-wave UV. Samples had a fibrous cellular structure. The shape of the cells (tracheids) was angular, rectangular, and sometimes subsquare (figure 17, bottom left). The transections of the samples showed very narrow single-row horizontal wood rays. Vertical resin ducts that looked like white dots were located in the latewood area of the annual rings (vertical dark band) (figure 17, bottom left). On the radial sections of the samples, we observed wood rays (horizontal lines) and bordered pits (round-shaped pores) (figure 17, bottom center). Middle lamellae (chains-like cells) were seen on a tangential section of petrified wood (figure 17, bottom right).

The absence of vessels, the unique type of wood rays and tracheids with bordered pits, the character of the middle lamellae, and the presence of vertical resin ducts indicated that these samples belonged to coniferous plants. X-ray diffraction analysis showed that all the varieties of petrified wood had an opal-cristobalite-tridymite composition.

The geology of the area allowed us to imagine the formation conditions. As a result of catastrophic volcanic eruptions of rhyolitic magmas as glowing ash clouds, and late effusions of mantle magmas, thick layers of volcanic ash and overlapping basalt flows were formed. The basalt lava flows outpoured into the water basin with a temperature exceeding 1000°C. Lavas overlapped the flooded trunks and thick bottom sediments of ash silts. When the basalt melt came into contact with water, the surface of the lava flow instantly quenched with the formation of pillow lavas. The space between the pillow lavas was filled with clastic glassy rocks known as hyaloclastites.

Thus, the flooded trees were under the hyaloclastites and pillow lavas. Some trees, under the weight of a lava flow, had taken a vertical position. Some trunks that sunk in hyaloclasts were charred, while trunks in ash silts remained unchanged. During silicification, the charred parts of the trunks acquired a black color and the uncharred parts became white, light yellow, to brownish (figure 18). Buried trees underwent strong deformation with flattening of the trunks, splitting, and fragmentation of wood.

The main source of silica when replacing the cells of trees by quartz or opal was ash silts. This was promoted by a low-alkaline water-saturated volcanic ash with a high SiO₂ content (over 72 wt.%). The silicon-containing



Figure 18. Left: Part of a petrified wood. Right: Opalized petrified wood sample with play-of-color. Photos by Dmitrii G. Fedoseev.

aqueous solutions penetrated woods that, under anaerobic conditions, represented local geochemical barriers where precipitation of free silica replacing plant cells occurred. Depending on the concentration of silicon in the solution in plant cells, the deposition of opal, chalcedony, or quartz occurred. The foregoing description allows us to imagine a majestic picture of how Nature created this wonderful combination of the worlds of plants and stones.

Vera Pakhomova, Valentina Solyanik, Dmitrii Fedoseev,
Svetlana Y. Kulenko (s_buravleva@yahoo.com), and
Vitaliya B. Tishkina
Far East Geological Institute (FEGI FEB RAS)
Vladivostok, Russia
Valeriya S. Gusarova
Far Eastern Federal University (FEFU), Vladivostok

Portrait of a Paraíba rough: Challenging gems in hard times. The impact of COVID-19 on the global gem trade is unquestionable. Traditional sales and services in most consuming countries came to a grinding halt. But the effects of lockdowns are also deeply felt in distant trade centers that rely on a steady supply of rough gemstones to feed their cutting, treating, and manufacturing industries.

Many of the brokers that take care of the transfer from producing countries to manufacturing hubs were

suddenly unable to perform their vital role in the gemstone supply chain. Without a constant flow of new rough material, the wheels that drive the entire industry stop turning.

When a crisis like this happens, people are forced to turn to other sources. In the trading center of Chanthaburi, Thailand, the most obvious source of rough is easily overlooked: the back of the safe. Over the years, rough parcels of varying qualities have been kept for a rainy day, and in some cases material has been held back for years to keep prices buoyant via artificial scarcity.

Difficult times have seen many established businesses releasing some of these old parcels, sometimes of material not seen in volume for years (or even decades), such as Kenyan rubies from the John Saul mine or spessartine “Fanta” garnet from Nigeria.

Both authors had the privilege to handle one of the unique pieces that came from the back of someone’s safe into the market.

When SBL first saw this piece, his immediate reaction was that it was tanzanite. Several other colleagues and knowledgeable friends had the same first impression. It was difficult to imagine the true identity of this crystal, which was the size of a duck’s egg.

This was an 85 g, 427 ct piece of unheated cuprian or Paraíba-type tourmaline rough from Mozambique (figure 19; see also the video at www.gia.edu/gems-gemology/summer-

Figure 19. This 85 g Mozambican cuprian tourmaline was released in the Chanthaburi market in May 2020. While everyone can agree that this is a unique and valuable piece, there is no agreement on the price that can be put on it. Photo by Simon Bruce-Lockhart.



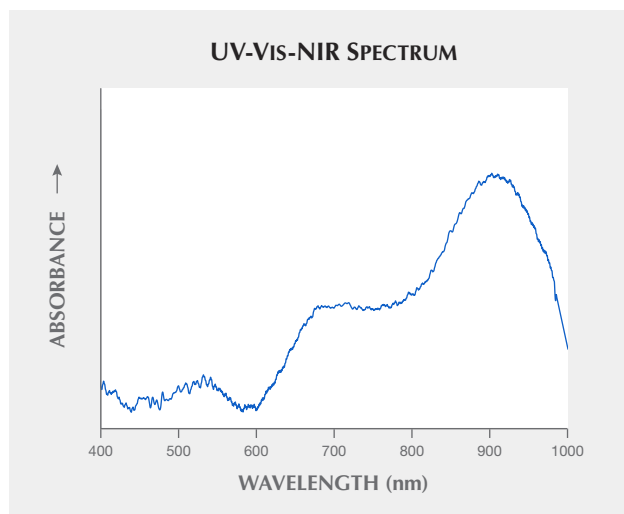


Figure 20. The UV-Vis-NIR spectrum shows clear absorption peaks at 660 and 900 nm that are typical for cuprian tourmaline.

2020-gemnews-mozambique-paraiba-rough). The stone was shown in the rough gem trading circuit of Chanthaburi near the end of May 2020. The GIA laboratory in Bangkok was able to do some limited testing on the stone, confirming that it was indeed a cuprian tourmaline (figure 20).

Large crystals of copper-bearing tourmaline were seen a decade ago at the advent of the Mavuco mines, but nothing of this size and quality has been seen on the open market for some time. For more on this material, see B.M. Laurs et al., “Copper-bearing (Paraíba-type) tourmaline from Mozambique,” Spring 2008 *G&G*, pp. 4–30.

There is little doubt that such a large, prestigious piece attracts attention. After that, the consensus stops. While it is undeniable that this stone is very valuable, no one can agree on precisely how valuable it is.

The decisions of how to heat and cut it to open up that coveted blue-green color produced by copper are critical to the value-adding process. The results of heat treating Mozambican cuprian tourmaline can be seen in figure 22 of Laurs et al. (2008).

The unheated Paraíba gem was taken to the handful of factories in Chanthaburi and Bangkok capable of buying and value-adding such a piece. Factoring in cracks, internal stress, and the orientation of some inclusions, all the factories determined that the stone should be cut into several pieces.

But everyone had a different opinion of exactly how to manufacture this piece. And this is where the dreams of Paraíba profits get smashed on the anvil of market reality.

A well-saturated large crystal will, when cut into numerous smaller pieces, exhibit a paler saturation of the original hue. Given that the market will pay much more per carat for larger Paraibas of intense color than for smaller paler Paraibas, the range of potential value outcomes regarding the number of pieces to cut is dizzying.

Furthermore, heat treatment of any stone is unpredictable, but tourmaline is a notoriously fickle gem to heat. Would you simply remove the frosted surface and heat it before sawing and preforming? This carries the risk that the gem will shatter uncontrollably during heating, but also the possibility of producing a single Paraíba tourmaline of spectacular size and a coveted deeper color. Or would you play it safe by cutting and grinding it into several smaller preforms and heating the many pieces? This mitigates some of the risks, but sacrifices the potential for capitalizing on the size of the rough.

Even if you play it safe, there is still no guarantee that minor unintended cracking will not require the resizing and re-orientating of preforms before faceting, which could significantly reduce the final color and weight yet again.

The transformative yet risky process of slicing, preforming, heating, and faceting is in some ways a gamble. The reality is that neither buyer nor vendor actually knows what will happen, and there is an element of chance layered on top of the manufacturer’s skill. The coveted “Paraíba” hue and saturation after heating are not guaranteed, and cases of “overcooking” cuprian tourmalines until only a pale pink color remains are not unheard of. These many variables create unknowable outcomes.

The most prudent buyers calculate their offers based on the risk of as many as six or more paler pieces, and offer much lower than expected when seeing this magnificent piece of rough. The vendors optimistically hold to their dream of a higher value based upon two or three larger, well-saturated pieces—and with such a wide disparity in value-outcome consensus, rough gems like this take time to sell. In the case of this piece, no agreement was reached after several rounds of back-and-forth between the different parties, and the stone was returned to its owner.

While this story is not unique, it highlights many aspects of the gem trade that most people throughout the supply chain are unfamiliar with. In these tough COVID times, it becomes especially important to realize how many hands have handled the gems we are seeing and which challenges every single one faces.

*Simon Bruce-Lockhart
Chanthaburi, Thailand*

*Wim Vertriest
GIA, Bangkok*

A new deposit of pink natrolite from Indonesia. In early 2020, a parcel of stones representing some unique material found in early 2020 from the island of Nusa Kambangan, Central Java, Indonesia, was sent to Taiwan Union Lab of Gem Research (TULAB) for certification service. At the beginning, wholesalers claimed that the gemstone was thomsonite. Because its texture was very similar to the green-blue pectolite variety Larimar produced in the Dominican Republic, the stone was also misrepresented with the trade name “pink Larimar.”



Figure 21. Rough stones and polished cabochons of pink natrolite. The heart-shaped cabochon is 35.6 mm wide. Photo by Yu-Ho Li.

By observing the rough stones with host rocks provided by the supplier, the occurrence was found to be vein-filling or cavity-filling within basalt. These stones had orange-pink to brownish pink color with white zoning and showed a botryoidal or radial crystal habit (figure 21).

The average specific gravity of this parcel of gemstones was 2.24, and the spot RI was 1.49. With the owner's consent, the parcel of polycrystalline material was tested with a Vickers hardness tester. The values were converted to Mohs hardness and ranged from 4.4 to 4.6. The samples' Raman spectra were analyzed and compared to the RRUFF mineral spectral database; unexpectedly, the results were consistent with published

spectra of natrolite ($\text{Na}_2\text{Al}_2\text{Si}_3\text{O}_{10}\cdot 2\text{H}_2\text{O}$) instead of thomsonite ($\text{NaCa}_2\text{Al}_5\text{Si}_5\text{O}_{20}\cdot 6\text{H}_2\text{O}$) (figure 22). The UV-Vis spectra revealed that the pink natrolite stones had a wide absorption band at 400–570 nm (figure 23). The EDXRF results also indicated that the pink gemstone was natrolite and contained a trace iron component. On the basis of EDXRF and UV-Vis results, the orange-pink to brownish pink color appeared to have been caused by Fe^{3+} ; however, this presumption still needs further verification.

This natrolite from Indonesia has a unique rose pink color and Larimar-like texture on polished surfaces, which is not common in natrolite from other localities. Although initially misrepresented by the merchant as thomsonite or

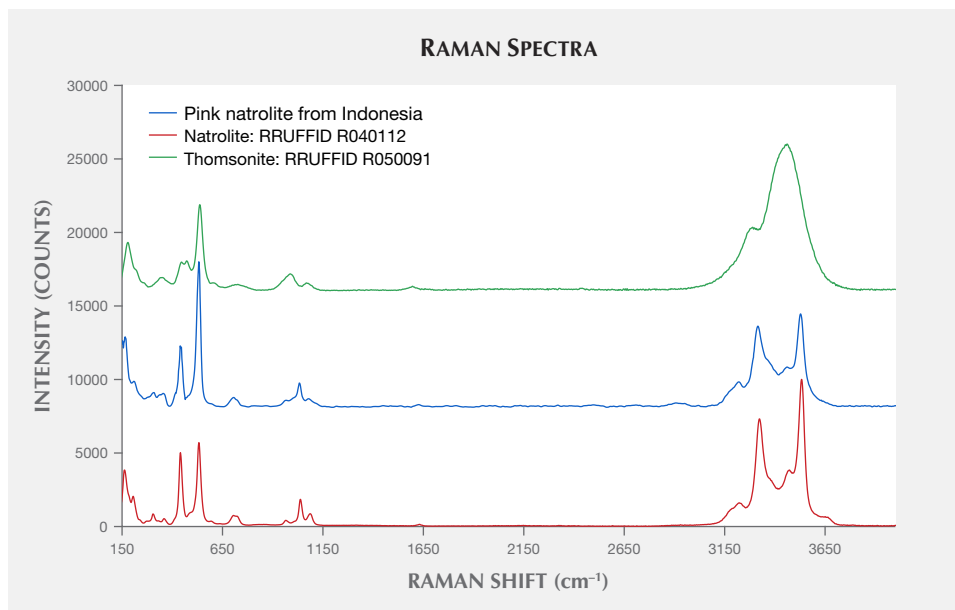


Figure 22. Stacked Raman spectra of the pink natrolite from Indonesia compared to those of natrolite and thomsonite published in the RRUFF database; all spectra are normalized and baseline corrected.

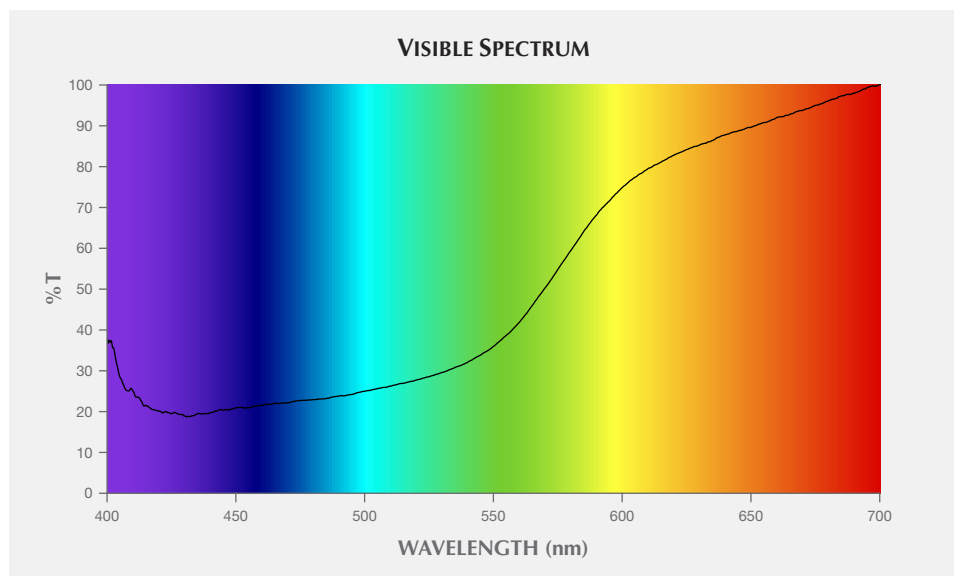


Figure 23. The normalized visible-light transmission spectrum of pink natrolite shows a wide absorption band at 400–570 nm that results in a brownish pink to orange-pink color.

pink Larimar, its beautiful appearance and durability are indeed comparable to Larimar. Subsequently, a new trade name “rhodatrolite,” meaning “rose natrolite,” was developed by the merchant for marketing this gemstone because of its color and texture. With enough mine production, pink natrolite from Indonesia has the potential to become a popular gemstone on the market.

Yu-Ho Li

*Institute of Earth Sciences
National Taiwan Ocean University, Keelung*

Huei-Fen Chen

*Institute of Earth Sciences and
Center of Excellence for Oceans
National Taiwan Ocean University*

Shu-Hong Lin

*Institute of Earth Sciences
National Taiwan Ocean University
Taiwan Union Lab of Gem Research, Taipei*

DIAMONDS

Finders, keepers: Field trip to Crater of Diamonds, USA.

There’s only one place on earth where the general public can prospect for diamonds directly from a primary kimberlite pipe: Crater of Diamonds State Park. This park is nestled among the pines, 100 miles off the interstate near the town of Murfreesboro, Arkansas. It boasts a network of scenic walking trails, picnic sites, and campsites. At its Diamond Discovery Center, visitors can learn about the local geology. Staff are also on hand to identify any minerals that are taken home, per their “finders, keepers” policy. The park is an ideal spot for a field trip. The state also hosts many other unusual igneous rocks, including carbonatite, lamprophyre, and lamproite. With this in mind, our university petrology class piled into a van to visit Arkansas

and learn about mantle-derived magmas and associated volcanism. As a side quest, we wanted to try prospecting.

The park’s main attraction is diamonds, but there are also olivine, pyrope, almandine, and amethyst to be found. Most of the diamonds recovered there are small (approximately 0.20 ct or less); see figure 24. Rarely, prospectors have found stones larger than 1 carat, including the famous Uncle Sam, a whopping 40.23 ct. The park’s diamond-bearing rocks are comprised of hypabyssal olivine lamproite and phlogopite-rich tuffs and breccias, characterized by

Figure 24. These diamonds from Crater of Diamonds State Park were mined previously by other prospectors. They range up to approximately 0.06 ct. Photo by Roy Bassoo.





Figure 25. Prospecting for diamonds at the Mauney mine, now Crater of Diamonds State Park, circa 1908. Photo courtesy of the Crater of Diamonds Archives.

high Mg# values (atomic ratio of Mg to Fe in an igneous rock) and K_2O content (E. Walker, "Petrogenesis of the Prairie Creek, Arkansas, diamondiferous olivine lamproite," PhD thesis, University of Western Ontario, Ontario, Canada, 1991). The deposit grades between 0.01 and 1.25 carats per 100 tons (D.P. Dunn, "Xenolith mineralogy and geology of the Prairie Creek lamproite province, Arkansas," PhD thesis, University of Texas, Austin, 2002). In the early twentieth century, when the richest material was mined, there was a brief diamond rush in the area (figure

25). After a string of ownership changes and failed business ventures, visions of a South African-style diamond district never materialized. In 1972 the state of Arkansas purchased the land and opened it to public prospecting. Since then, visitors have found more than 33,000 diamonds (www.arkansasstateparks.com).

After a couple of days learning about the igneous rocks in the area, it was time to test our luck at treasure hunting. We gathered buckets, shovels, and sieves from park headquarters for a small rental fee and headed out to 15 hectares

Figure 26. A local prospector digging for diamond ore and demonstrating sieving technique. Photos courtesy of Glenn Worthington.

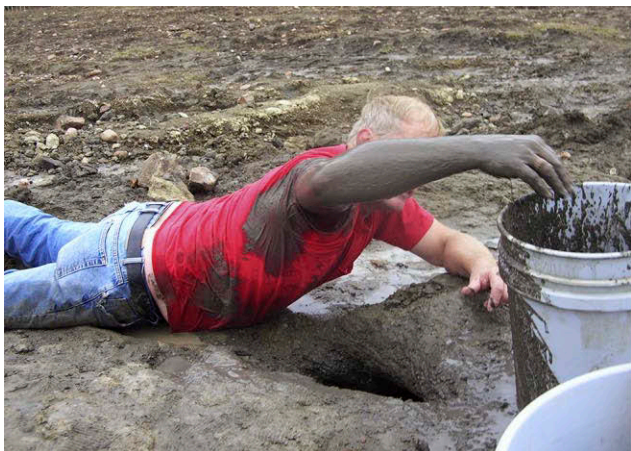




Figure 27. Three of the diamonds the authors collected from Crater of Diamonds State Park (approximately 0.01–0.05 ct). Note the irregular and fragmented morphology and brown to yellow colors. Photos by Roy Bassoo.

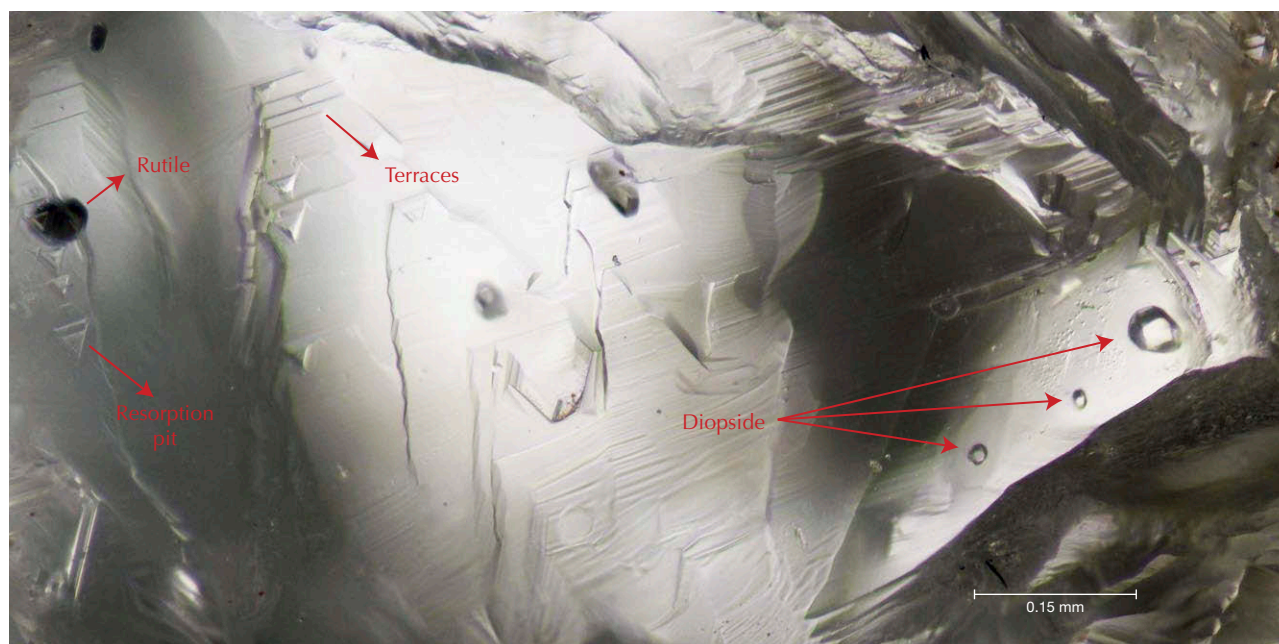
of routinely plowed “blue ground.” We chose a spot, shoveled soil into buckets, and carried these heavy parcels of dirt to the wash station for sieving (figure 26). The trick is to shake the sieve back and forth just beneath the water in the horizontal plane, then rotate and repeat. This motion should concentrate the heavy minerals in the center and bottom of the sieve. Then, like a master chef, the prospector flips the entire mineral concentrate upside down and examines the heavies that sink to the bottom.

In three hours, we found a small collection of diamonds! Granted, they were also very small in size, ranging from 0.01 to 0.05 ct (figure 27). Most prospectors at Crater of Diamonds miss stones this small, but as trained mineralogists we were attentive to small crystals. The diamonds were predominantly colorless, although a couple were yellow to brown. Their dominant morphology was

octahedral with uncommon dodecahedrons and macles. Resorption pits and terraced surfaces were pervasive. The diamonds were also fragmented, likely due to the explosive nature of the diatreme crater.

Treasure in hand, we then turned to the science. Back in our lab, we ground and polished the diamonds into wafers to examine their composition and crystal interiors. Raman spectroscopy determined that inclusions of rutile and diopside were common (figure 28). N contents, measured with Fourier-transform infrared spectroscopy, ranged from trace amounts (type IIa) to 1250 ppm (type IaAB). Cathodoluminescence imagery showed blue to turquoise response colors, typical of diamonds mined from primary deposits worldwide. They also feature fascinating patterns of growth banding and resorption truncations, which indicate a complex mantle crystallization history (figure 29).

Figure 28. Terraced dissolution surface textures and inclusions of rutile and diopside embedded within the diamond. The diopside inclusions are aligned along a growth band. Photomicrograph by Roy Bassoo.



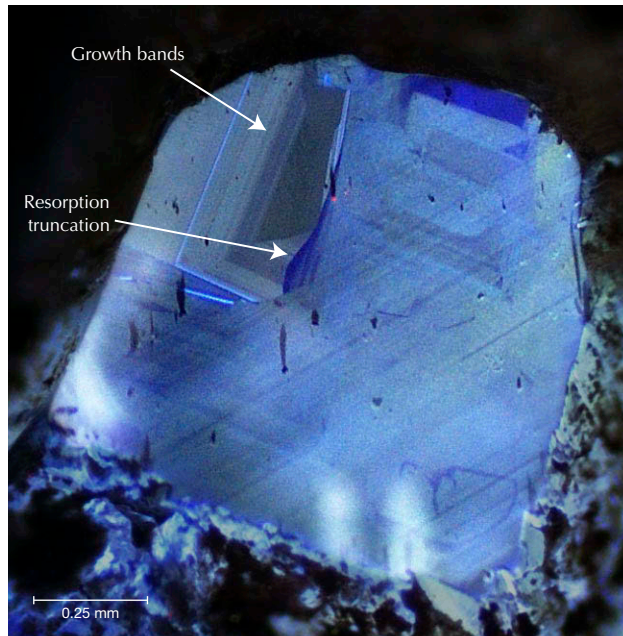


Figure 29. Cathodoluminescence image of a polished diamond wafer, showing complex banding and truncations that highlight different diamond growth conditions. Image by Roy Bassoo.

We found Crater of Diamonds to be a thoroughly enjoyable treasure hunting adventure. Our visit gave us hands-on experience with diamond-bearing igneous rocks and challenged us to imagine how diamonds formed beneath the North American craton. We have new appreciation for the back-aching labor required by the artisanal miners worldwide who are the foundation of the gem trade. Scientific understanding and trade awareness were the substance of our visit, highlighted by moments of joyful discovery. We encourage readers to put Crater of Diamonds State Park on their gemology “bucket list” to hunt for their very own American diamond.

Roy Bassoo and Kenneth S. Befus
Department of Geosciences, Baylor University
Waco, Texas

SYNTHETICS AND SIMULANTS

Greenish blue glass imitating gem silica. Gem silica, also known as “chrysocolla chalcedony,” is considered the most valuable variety of chalcedony. Its attractive blue to bluish green color is generated by finely disseminated minute inclusions of chrysocolla. The main sources include Taiwan, the United States, Mexico, Peru, and Indonesia. For years, gem silica has been especially popular in Taiwan. Due to the pleasing saturated blue color of Taiwanese material, which is among the world’s finest, it commands a premium price.

At the same time, the current lack of production in Taiwan is driving prices substantially higher. Thus, imitations and treatments are gradually emerging in the marketplace, confusing customers. Recently we obtained three polished specimens from a gift shop in Taidong County, Taiwan (near the locality of the gem silica mine), that appeared to have good quality of color and transparency (figure 30). The merchant claimed they were gem silica mined in Taiwan, but they were subsequently identified as glass imitations.

Standard gemological tests showed the following properties of the three samples: color—uniform greenish blue; diaphaneity—translucent; spot RI—1.48; SG—2.48 to approximately 2.57; fluorescence—inert to long-wave UV radiation, weak greenish white to short-wave UV radiation. Actual gem silica, meanwhile, has the following properties: color—commonly uneven; spot RI—1.54; SG—approximately 2.63. Examination with a gemological microscope revealed numerous obvious gas bubbles of different sizes (figure 31, left). In the case of the marquise sample, numerous gas bubbles led to a relatively low specific gravity. When viewed with oblique incident light, many small dimples were visible on the polished surface (figure 31, right). In addition, there were some small conchoidal fractures along the bottom edges of samples. In order to gain a more thorough understanding, further advanced analysis was carried out.

FTIR reflectance spectroscopy showed a main reflected band at approximately 1065 cm^{-1} (figure 32), consistent with the characteristic spectrum of glass (see Fall 2019 GNI, p. 443–445; T.B. Wang et al., “Relationship between the frequency of the main LO mode of silica glass and angle of incidence,” *Journal of Chemical Physics*, Vol. 119, No. 1, 2003, pp. 505–508). Chemical analysis by LA-ICP-MS detected multiple elements: Si (averaging 617000 ppmw), Na (averaging 151000 ppmw), Al (averaging 101000 ppmw), Ca (averaging 24900 ppmw), K (averaging 19600 ppmw), Ba (aver-

Figure 30. Two oval and one marquise cabochon of greenish blue glass samples ranging from 2.17 to 2.60 ct. Photo by Min Ye.



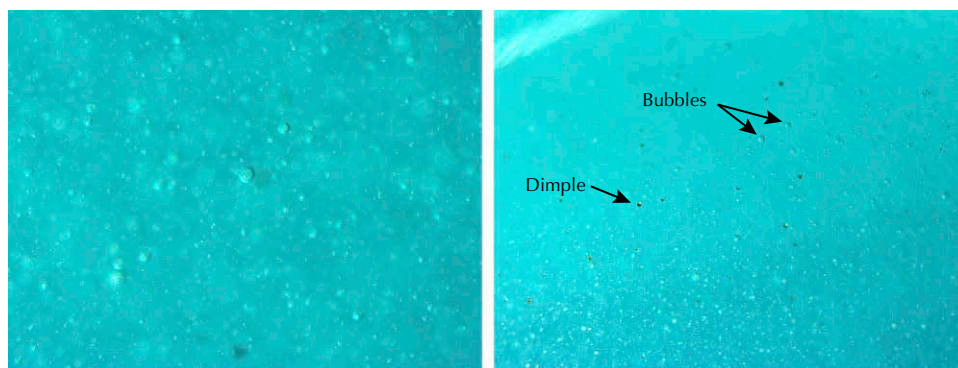
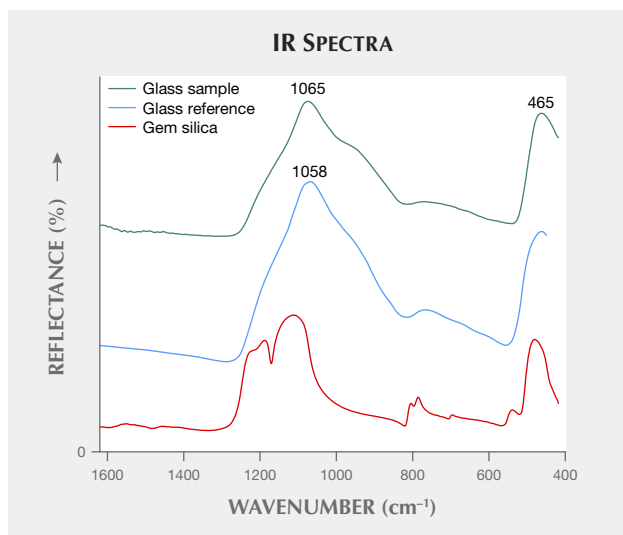


Figure 31. Left: Numerous gas bubbles of various sizes were typical internal features of the three samples; field of view 1.28 mm. Right: Many small dimples could be found on the polished surface; field of view 3.70 mm. Photomicrographs by Min Ye in overhead lighting (left) and oblique illumination (right).

aging 17800 ppmw), Pb (averaging 3840 ppmw), Mg (averaging 2580 ppmw), Fe (averaging 1620 ppmw), Cu (averaging 5940 ppmw), and Cr (averaging 716 ppmw). This composition identified the three samples as silicate glass, which is decidedly different from gem silica (whose majority component is silica and chrysocolla, a copper silicate). UV-Vis-NIR spectra of the specimens presented a strong broad absorption band around 760 nm (figure 33), revealing Cu^{2+} as the coloring agent. In addition, two weak absorption bands at 424 and 439 nm might have been related to trace amounts of Fe^{3+} , while the 690 nm band was possibly due to the existence of Cr^{3+} (see W. Thiemson et al., "Redox ratio and optical absorption of polyvalent ions in industrial glasses," *Bulletin of Materials Science*, Vol. 30, 2007, pp. 487–495; V. Vercamer, "Spectroscopic and structural properties of iron in silicate glasses," PhD thesis, Université Pierre et Marie Curie-Paris VI, 2016, pp. 97–145).

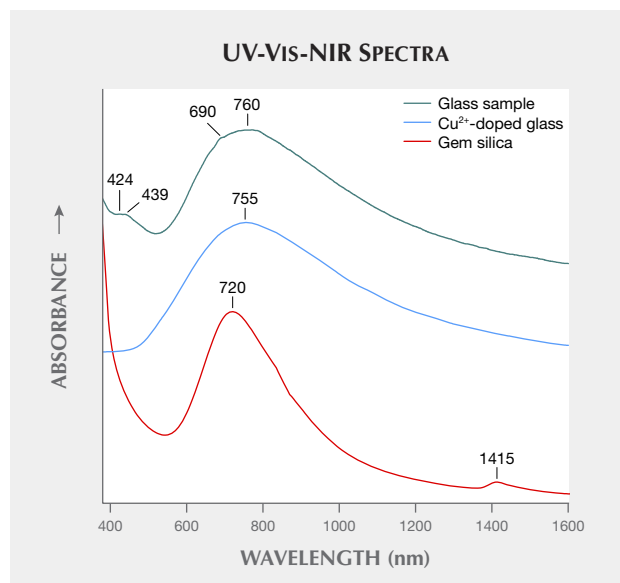
Figure 32. Representative infrared reflectance spectra of the three samples (green trace) were compared with the reference spectra for glass (blue trace) and natural gem silica (red trace, collected by the author). The diagnostic reflected peak of the glass sample is near 1065 cm^{-1} , quite different from the gem silica peaks. The spectra are offset for clarity.



Combining all the evidence, the three greenish blue samples were confirmed to be artificial glass colored by an unknown copper additive. Gas bubble inclusions were the diagnostic feature for identification, and FTIR spectra were also helpful. This case is a reminder that customers need to be cautious when purchasing gemstones, even near the geographic source.

Min Ye and Andy H. Shen (shenxt@cug.edu.cn)
Gemmological Institute
China University of Geosciences, Wuhan

Figure 33. Typical UV-Vis-NIR absorption spectra of the three samples (green trace) were compared with those of Cu^{2+} -doped glass (blue trace) and natural greenish blue gem silica (red trace, collected by the author). In the typical plot for the glass samples, the absorption band around 760 nm is assigned to Cu^{2+} . Two weak absorption bands in the glass imitation at 424 and 439 nm might be related to trace amounts of iron, while the 690 nm band is possibly due to the presence of chromium. The spectra are offset for clarity.



Marble imitation of jadeite rough. In recent decades, jadeite prices have risen dramatically. Driven by profit, a variety of imitations are found in the jadeite jewelry market. Meanwhile, imitations such as quartzite are fixtures in the rough jadeite market. Recently, our research group received for testing a 30 kg stone that resembled jadeite rough and was submitted as such. The stone had a yellow weathered skin with a grainy texture, similar to jadeite. There was a narrow “window” (figure 34) that showed the green color of the material underneath the skin. For identification purposes, the authors exposed another area on the surface of the rough and then ground it for testing.

Due to the weight, some standard gemological testing methods could not be used, such as measurement of refractive index and specific gravity. Therefore, the sample was studied by visual and 10× loupe observation, hardness testing, chemical reagent detection, and infrared spectroscopy.

Scratch testing revealed a Mohs hardness between 2 and 5, lower than jadeite’s hardness of 6–7. The surface was yellow,

Figure 34. This 30 kg stone was submitted as a piece of jadeite rough. A narrow window (in the red circle) opened on the surface of the rough reveals a green material underneath the skin. Photo by Huang Jing.

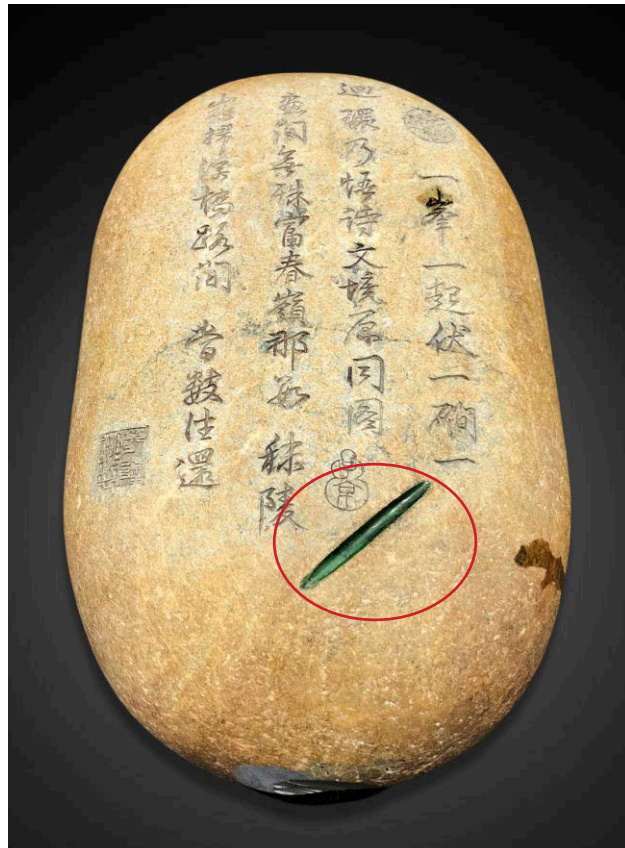


Figure 35. The newly exposed part of the rough stone was identified as marble. Photo by Huang Jing.

low, just like the weathered skin of jadeite rough, and the narrow window in figure 34 revealed green color below the skin. Scrubbing the window with alcohol removed the green color, indicating that the window had been dyed. To test the material, diluted hydrochloric acid was dropped on the newly exposed portion in figure 35. The acid foamed continuously, showing that the sample contained carbonate (Z. Hanli et al., “Study on acid polishing of carbonate white jade,” *Journal of Gems and Gemmology*, Vol. 5, No. 4, 2003, pp. 24–27). The acid testing combined with visible observations and hardness testing identified the sample as marble. The jadeite granular structure came from the marble’s cleavage planes.

Testing of the exposed part by infrared spectrometry revealed 1525, 1432, 1080, 883, 670, 553, and 483 cm^{-1} absorbance peaks, characteristic of serpentinized marble.

The serpentinized marble’s yellow weathered skin and grainy texture could have easily been mistaken for jadeite rough. This serves as an alert to the industry to be careful even when examining rough, as imitations are showing up.

Huang Jing, Yan Shuyu, and Chen Shuxiang (corresponding author, kedachenshuxiang@163.com)

*School of Materials Science and Engineering
Qilu University of Technology
(Shandong Academy of Sciences)
Shandong, China*

*Cheng Youfa
National Gold and Diamond Testing Centre of China
Shandong*

ERRATUM

The Spring 2020 Lab Note “Solid carved dark gray diamond ring” (pp. 132–133) erroneously stated that the 13.15 ct ring was carved from a 20 ct piece of rough. The correct rough weight was 196 ct.